A Lin's method approach to Heteroclinic Connections involving Periodic Orbits – Analysis and Numerics

Dissertation

zur Erlangung des akademischen Grades

Dr. rer. nat.

vorgelegt von

Dipl.-Math. Thorsten Rieß

am 28. Januar 2008 eingereicht bei der Fakultät für Mathematik und Naturwissenschaften der Technischen Universität Ilmenau

Tag der öffentlichen Verteidigung: 16. Mai 2008

Betreuer: PD Dr. Jürgen Knobloch und Prof. Dr. Bernd Krauskopf

Gutachter: Prof. Dr. Bernd Krauskopf (University of Bristol)
Prof. Dr. Bernd Marx (Technische Universität Ilmenau)
Prof. Dr. Eusebius Doedel (Concordia University Montréal)

urn:nbn:de:gbv:ilm1-2007000415

Mind the gap.

CONTENTS

CHAPTER 1

Introduction

This chapter gives background information about the topic of this thesis, both historical references and recent research areas, and it gives a short overview of articles that influenced the chosen approach. We also introduce the general setting that is used throughout the thesis and point out important properties of the considered system and the involved objects.

1.1 General background

The qualitative analysis of dynamical systems is an active field of research in modern mathematics. The roots of this type of analysis reach back as far as the 1890 article [Poi90] by mathematician and physicist H. Poincaré, who discovered complicated dynamics in an otherwise deterministic model system for the three-body problem. This is widely believed to be the beginning of the qualitative analysis of dynamical systems which aims at the understanding of the long-term behaviour of given systems (such as models of physical, biological or chemical systems) and how this behaviour depends on the change of external parameters. This understanding requires knowledge of global and characteristic features of such a system, for example steady state solutions or periodic solutions. Typically, one is interested in the location of invariant (stable or unstable) manifolds of these objects, as these manifolds give insight into the global dynamics. The analysis of the change of the dynamics (in the sense of a change of the interaction of the special objects and their corresponding manifolds) by means of analytical, geometrical or statistical methods is now known as *bifurcation theory*.
For dynamical systems theory and bifurcation theory, see textbooks such as [GH83, Kuz98, Str94, Rob99, Wig90] as entry points into the extensive literature. In recent years, the qualitative analysis of the dynamics near connecting cycles (such as homoclinic orbits connecting an equilibrium point to itself or heteroclinic cycles connecting two equilibrium points) has drawn much attention. These objects act as 'organising centers' for the nearby dynamics and therefore understanding the dynamics near connecting cycles gives insight into global dynamical features.

The analysis of the dynamics near homoclinic and heteroclinic orbits to equilibrium points is now a widely used tool, both theoretically and numerically in practical model systems. For a long time, the analytical treatment of the dynamics near connecting cycles was dominated by the 'Shilnikov group', for an overview of their results and methods we refer to [SSTC98, SSTC01], and to [Kuz98] for further bibliographical notes. The main tool for studying the dynamics with this more geometrical approach is a Poincaré map, which is constructed for the connecting cycle. However, more recently X.-B. Lin proposed a new method for the theoretical analysis of this kind of 'recurrent' dynamics in his article [Lin90], which proved to be more appropriate to detect particular orbits or even shift dynamics in certain geometrically complicated constellations. Many contributions to this method have been made since then, most notably by B. Sandstede and J. Knobloch [San93, Kno04]. So far, it has been used for orbits connecting hyperbolic equilibria, recently an extension to non-hyperbolic equilibria has been made by J. Klaus and J. Knobloch [KK03, Kla06]. Lin's method is also the basis of the recent analytical considerations by J. Rademacher [Rad04, Rad05], he uses the method to describe homoclinic bifurcations from heteroclinic cycles between equilibria and periodic orbits.

On the practical side, numerical methods for the analysis of connecting cycles are well-established and widely used for the bifurcation analysis of model equations. This analysis allows conclusions about the dynamics of a system, even if theoretical considerations are not possible or not yet done; it often even gives new ideas what phenomena to look out for theoretically. Single homoclinic or heteroclinic orbits connecting equilibria are numerically described by boundary value problems that use projection boundary conditions near the equilibria. To solve this kind of boundary value problem, standard algorithms can be used. The software package AUTO by E. Doedel *et al.* [DPC+00, DPC+06] is a commonly used programme, that provides many routines for bifurcation analysis and the solution of boundary value problems. In [OCK03] a numerical method for homoclinic branch switching that uses Lin's method is proposed; this is a good example of how Lin's method can be utilised numerically.

In this thesis we introduce an extension of Lin's method for heteroclinic cycles connecting a hyperbolic equilibrium and a hyperbolic periodic orbit (or *EtoP heteroclinic cycle* for short), but we use a different approach than in [Rad05]. The idea in our approach is to use the Poincaré map to describe the dynamics near the periodic orbit and then to consider the hybrid system consisting of the original continuous system and the discrete system. This has the advantage that many known results for Lin's method for discrete dynamical systems can be used. Moreover, we develop general estimates which allow us to formulate a wide range of bifurcation equations in the given setting.

Further, we use the theory based on our extension of Lin's method to develop a new numerical method to find and to continue a heteroclinic orbit connecting a hyperbolic equilibrium and a hyperbolic periodic orbit. We denote such a connection by *EtoP connection*, regardless of the direction of the flow. Such an EtoP connection may not be robust, but of codimension $d \geq 1$, meaning that it generically exists at isolated points in d-dimensional parameter space. Due to the codimension and the global nature of this type of orbit, advanced numerical methods are necessary to find it.

1.2 Setting

In this thesis we deal with a setting situated in $\mathbb{R}^n$, $n \geq 3$. We consider a family of dynamical systems generated by the ODE

$$\dot{x} = f(x, \lambda), \quad x \in \mathbb{R}^n, \lambda \in \mathbb{R}^m \tag{1.2.1}$$

and throughout we assume that f is sufficiently smooth.
We assume that in a suitable neighbourhood Λ of a critical parameter value $\lambda = \lambda^*$, the system (1.2.1) has a hyperbolic equilibrium p and a hyperbolic periodic orbit Υ (we do not indicate their dependence on λ in the notation). Without loss of generality, we set $\lambda^* = 0$ for the analytical considerations in Chapter 2, but return to the λ^* notation in Chapter 3. The (λ-dependent) stable and unstable manifolds of p and Υ are denoted by $W^{s/u}_\lambda(p)$ and $W^{s/u}_\lambda(\Upsilon)$, respectively (for $\lambda = \lambda^*$ we omit the subscript λ and only write $W^{s/u}(p)$ and $W^{s/u}(\Upsilon)$, respectively).
For our analytical considerations that use an extension of Lin's method, we assume that there exists a complete heteroclinic EtoP cycle for $\lambda = \lambda^*$. However, for the development of a numerical method to find and continue single EtoP connections, we generally only assume that one EtoP connection is present.
More precisely, we assume that for $\lambda = \lambda^*$ the system (1.2.1) has the following properties:

(C1) There is a hyperbolic equilibrium p; its unstable manifold $W^u(p)$ is of dimension k: $\dim W^u(p) = k$.

(C2) There is a hyperbolic periodic orbit Υ; its stable manifold $W^s(\Upsilon)$ is of dimension l: $\dim W^s(\Upsilon) = l$.

(C3) The dimensions of $W^u(p)$ and $W^s(\Upsilon)$ at most add up to the space dimension n: $k+l \leq n$.

(C4) The manifolds $W^u(p)$ and $W^s(\Upsilon)$ intersect in an isolated EtoP connecting orbit $\Gamma_1 \subset W^u(p) \cap W^s(\Upsilon)$. Moreover, the non-degeneracity condition

$$T_g W^u(p) \cap T_g W^s(\Upsilon) = f(g, \lambda^*) \tag{1.2.2}$$

holds for each point $g \in \Gamma_1$.

(C5) There exists a neighbourhood Λ of λ^* such that the extended manifolds

$$W^u_\Lambda(p) := \bigcup_{\lambda \in \Lambda} W^u_\lambda(p) \times \{\lambda\} \text{ and } W^s_\Lambda(\Upsilon) := \bigcup_{\lambda \in \Lambda} W^s_\lambda(\Upsilon) \times \{\lambda\}$$

intersect transversally (in $\mathbb{R}^{n+m}$) at (g, λ^*) for all $g \in \Gamma_1$, that means

$$\dim \left(T_{(g,\lambda^*)} W^u_\Lambda(p) + T_{(g,\lambda^*)} W^s_\Lambda(\Upsilon) \right) = n + m \tag{1.2.3}$$

for all $g \in \Gamma_1$.

Consider system (1.2.1) and let Conditions (C1)–(C5) hold. Then we define the value

$$d := n + 1 - k - l \geq 1. \tag{1.2.4}$$

Conditions (C1)–(C5) describe the existence and non-degeneracity of one EtoP connection Γ_1.
As already mentioned, for the analytical considerations we need another EtoP connection Γ_2 that connects the periodic orbit back to the equilibrium; if both EtoP connections exist, we speak of a heteroclinic EtoP cycle. The analysis of recurrent dynamics requires to have an EtoP cycle.
We assume that the following non-degeneracy condition holds for Γ_2:

(C6) $W^u(\Upsilon)$ and $W^s(p)$ intersect in an EtoP connection Γ_2: $\Gamma_2 \subset W^u(\Upsilon) \cap W^s(p)$. We demand the following minimal intersection condition for the intersection of $W^u(\Upsilon)$ and $W^s(p)$:

$$\dim\left(T_g W^s(p) \cap T_g W^u(\Upsilon)\right) = d \text{ for all } g \in \Gamma_2. \tag{1.2.5}$$

Condition (C6) means that $W^u(\Upsilon)$ and $W^s(p)$ intersect in a robust heteroclinic EtoP connection $\Gamma_2 \subset W^s(p) \cap W^u(\Upsilon)$ which is not isolated if $d > 1$.
Alternatively, instead of Condition (C6), we also consider the situation where the intersection of $W^u(\Upsilon)$ and $W^s(p)$ is degenerate:

(C6') There is a heteroclinic EtoP connection Γ_2 in the intersection of $W^u(\Upsilon)$ and $W^s(p)$: $\Gamma_2 \subset W^s(p) \cap W^u(\Upsilon)$;

$$\dim\left(T_g W^s(p) \cap T_g W^u(\Upsilon)\right) = d + 1 \tag{1.2.6}$$

holds for all $g \in \Gamma_2$.

Definition 1.2.1 *Consider system* (1.2.1) *and let Conditions* (C1)–(C5) *hold. We say that the EtoP connection* Γ_1 *is of* codimension d. *If additionally Condition* (C6) *is satisfied, we say that the complete heteroclinic EtoP cycle is of codimension* d.
If Condition (C1)–(C5) *and Condition* (C6') *are satisfied and we assume a 'quadratic tangency' (see below), then the codimension of the EtoP cycle is* $d + 1$.

Condition (C3) means that (generically) the EtoP connection Γ_1 is not robust and indeed Condition (C5) tells us that Γ_1 breaks as the manifolds $W^u_\lambda(p)$ and $W^s_\lambda(\Upsilon)$ split up with nonzero velocity for $\lambda \neq \lambda^*$. For Γ_2 on the other hand, Condition (C6) implies that $\dim(W^s(p) \cap W^u(\Upsilon)) = d$, thus Γ_2 is robust, see Section A.2 for details. For the implications of Condition (C6'), we restrict to the case $n = 3$. In accordance with our assumptions $\dim W^s(p) = \dim W^u(\Upsilon) = 2$ and $d = 1$ and thus Γ_2 is isolated. However, due to Condition (C6'), the traces of $W^u(\Upsilon)$ and $W^s(p)$ in any cross-section of Γ_2 have a common tangent. In Section 2.4 we assume that this tangency is quadratic, meaning that the distance of the traces of the manifolds can be expressed as quadratic functions along the common tangent, cf. Figure 2.4 below for a draft of the situation in the cross-section.

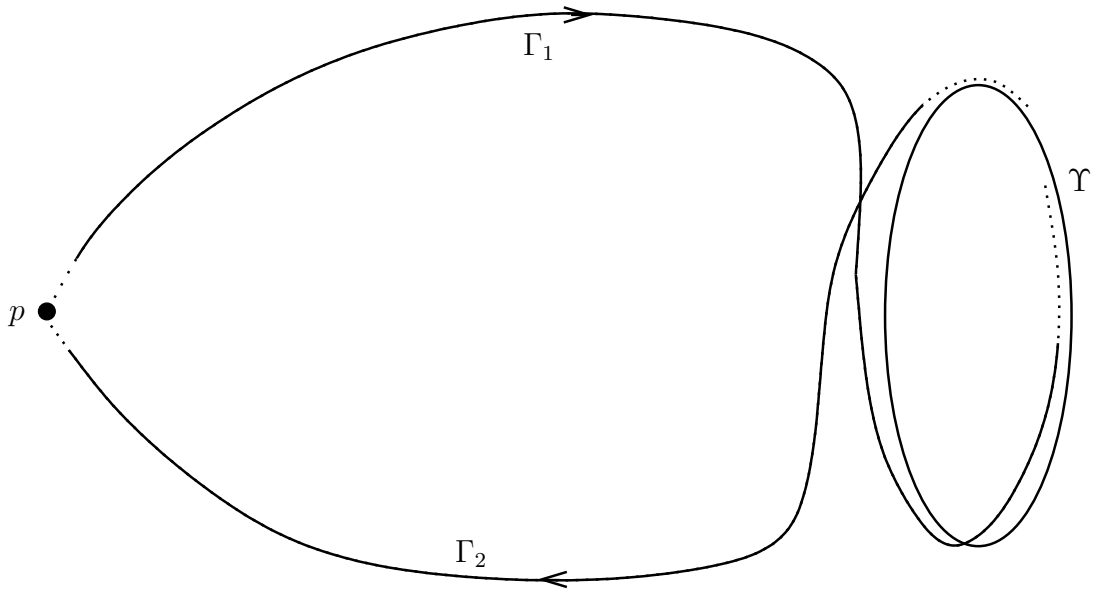

Figure 1.1: Draft of the general setting. Shown are the hyperbolic equilibrium p, the hyperbolic periodic orbit Υ and the heteroclinic cycle consisting of $\Gamma_1 \subset W^u(p) \cap W^s(\Upsilon)$ and $\Gamma_2 \subset W^u(\Upsilon) \cap W^s(p)$.

By excluding all other degeneracities (see Conditions (C4) and (C5)), it follows from (1.2.2) and (1.2.3) that

$$\begin{aligned} n + m &\leq \dim T_{(g,\lambda^*)} W^u_\Lambda(p) + \dim T_{(g,\lambda^*)} W^s_\Lambda(\Upsilon) - 1 \\ m &\geq n + 1 - k - l = d. \end{aligned}$$

So it turns out that the number of parameters m needs to be at least d to unfold the bifurcation of Γ_1; this justifies Definition 1.2.1 which states that Γ_1 is of codimension d.

Remark 1.2.2 *It is important to note that there are two different notation schemes used in this thesis. The first part (Chapter 2) is devoted to the analysis and an extension of Lin's method, therefore we try to keep the standard notation in this context. The second part (Chapter 3) deals with the numerical application, and here we also try to use the standard notation. To avoid confusion, we try to keep both notation schemes congruent where possible and we refer to the Table of notations for an overview of the used symbols and their respective meanings.*

This thesis is organized as follows: In Chapter 2 the full setting above (C1)–(C6)/(C6') is analysed using an extension and adaptation of Lin's method which is explained in detail. A hybrid system consisting of a discrete dynamical system and a continuous dynamical system is used to construct a sequence of partial orbits that stay near the heteroclinic cycle for all times. Two consecutive partial orbits may only have jumps in certain prescribed subspaces in cross-sections of the EtoP cycle. Moreover, estimates for the jump functions are derived. Using these estimates, bifurcation equations for various types of solutions near the heteroclinic

cycle are developed and discussed. The existence of homoclinic orbits to p and homoclinic orbits to Υ is discussed and references to our numerical results in Chapter 3 are given.
In Chapter 3 we introduce a novel numerical method to find and to continue a heteroclinic EtoP connection as described by Conditions (C1)–(C5). The method is based on the theoretical results of Chapter 2 and uses the well-established continuation package AUTO to numerically solve the arising boundary value problems. The performance of the method is demonstrated by three examples, also showing how to use the numerical data of a complete heteroclinic EtoP cycle as starting data for the continuation of other types of orbits nearby. Numerical evidence that supports the analytical results is found in the examples, and also a new accumulation phenomenon of an EtoP connection to itself is discovered. Finally, the method is extended to finding periodic-to-periodic (PtoP) heteroclinic connections and demonstrated on a codimension-zero PtoP connection.
In Chapter 4 conclusions are drawn and avenues for future research are given.

CHAPTER 2

Lin's method for EtoP cycles

In this chapter we introduce the analytical tools to deal with heteroclinic cycles between hyperbolic equilibria and hyperbolic periodic orbits (*EtoP cycles* for short). We give a short overview of the classical application of Lin's method, which is commonly used to analyse the dynamics near connecting cycles between hyperbolic equilibria, and we present the idea and the main result of our approach in the first section. The second section is dedicated to the details of an adaptation of Lin's method to the setting presented in Section 1.2. In the third section, the jump estimates are derived that are finally used in the fourth section to discuss bifurcation equations for different types of objects near the heteroclinic cycle.

2.1 Idea and main result

In this section the main idea and results of the analytical considerations regarding the application of Lin's method for heteroclinic EtoP cycles are presented. The basic idea is to use a method that is inspired by the 'classical' usage of Lin's method which we briefly summarise. For a related setting that consists of a heteroclinic cycle connecting two equilibria (with one heteroclinic connection being robust and the other non-robust) and the application of Lin's method in this so-called T-point setting, see [KLW07] and references therein ([GS86, FSFRL02]).
We assume that for the critical parameter value λ^* a heteroclinic cycle exists and we introduce two cross-sections Σ_1 and Σ_2 to the heteroclinic connections. The idea is then to construct a so-called *Lin orbit* (see also Definition 2.1.2 below) that consists of a sequence of partial orbits (i.e. orbits that are only considered on a subinterval of their respective maximal domain) that stay close to the heteroclinic cycle. Each such partial orbit provides a transition either from Σ_1 to Σ_2 or from Σ_2 to Σ_1, and the Lin orbit is constructed such that two consecutive partial orbits provide a single 'loop' around the heteroclinic cycle. Moreover, two consecutive partial orbits may only have a jump in Σ_1 or in Σ_2 and this jump is only allowed parallel to certain prescribed directions Z_1 and Z_2, respectively. One main conclusion of Lin's method

is that for given transition times for each of the consecutive loops, such a Lin orbit does exist and it is unique. The procedure to construct a Lin orbit usually consists of two steps, one of which describes the 'splitting of the manifolds' and the other the 'transition to finite time'.
In the first step, the original heteroclinic solutions (at the critical parameter value) $\gamma_1(\cdot)$ and $\gamma_2(\cdot)$ are perturbed such that – for each $\lambda \neq \lambda^*$ – solutions $\gamma_1^{\pm}$ and $\gamma_2^{\pm}$ within the stable and unstable manifolds of p and Υ are constructed. γ_1^+ approaches Υ for increasing time while γ_1^- approaches p for decreasing time; the solutions $\gamma_2^{\pm}$ provide the connection in the opposite direction.
In the second step, the solutions $\gamma_1^{\pm}$ and $\gamma_2^{\pm}$ are perturbed further and thus a sequence of partial orbits X_i^{12} and X_i^{21} is constructed (i denotes the number of the revolution along the EtoP cycle). These partial orbits connect the cross-sections Σ_1 and Σ_2 and follow the respective solutions $\gamma_{1/2}^{\pm}$; the key point here is that they are coupled near the equilibrium point and near the periodic orbit, respectively, see also Figure 2.1. The main difference of the approach presented here and the 'classical' application of Lin's method (and also the approach in [Rad05]) is how the solutions are coupled near the periodic orbit. In our approach we use a discrete dynamical system implied by the Poincaré map to describe the dynamics near the periodic orbit and partial orbits of this system to do the actual coupling, see below for details.
We start with the notation for a neighbourhood of the EtoP cycle that is used throughout this chapter.

Notation 2.1.1 *We denote a neighbourhood of the heteroclinic cycle* $\Gamma = \Gamma_1 \cup \Gamma_2$ *by* $\mathcal{U}_\Gamma$. *This neighbourhood is usually considered being small with the exact extent given by the analysis.*

Similar to the procedure in the classical application of Lin's method, we introduce cross-sections Σ_1 and Σ_2 of Γ_1 and Γ_2, respectively. These sections are assumed to intersect the heteroclinic orbits Γ_1 and Γ_2 at the points $\gamma_1(0)$ and $\gamma_2(0)$, respectively:

$$\begin{aligned} \Sigma_1 &:= \gamma_1(0) + Y_1, \\ \Sigma_2 &:= \gamma_2(0) + Y_2 \end{aligned}$$

where Y_1 and Y_2 are $(n-1)$-dimensional linear subspaces. Within the linear subspace Y_1 we define a linear subspace Z_1 such that

$$\mathbb{R}^n = Z_1 \oplus (T_{\gamma_1(0)} W^u(p) + T_{\gamma_1(0)} W^s(\Upsilon)).$$

Within Y_2 we define linear subspaces Z_2 and U such that

$$\operatorname{span}\{f(\gamma_2(0), 0)\} \oplus U = T_{\gamma_2(0)} W^u(\Upsilon) \cap T_{\gamma_2(0)} W^s(p)$$

and

$$\mathbb{R}^n = Z_2 \oplus (T_{\gamma_2(0)} W^u(\Upsilon) + T_{\gamma_2(0)} W^s(p)).$$

In Section 2.2 we give some more details about the involved linear subspaces and how they are chosen, but for now it is sufficient to observe that we introduce a subspace Z_1 within Y_1 that is not contained in the tangent spaces of $W^u(p)$ and $W^s(\Upsilon)$ at $\gamma_1(0)$, and a subspace Z_2 within Y_2 that is not contained in the tangent spaces of $W^u(\Upsilon)$ and $W^s(p)$ at $\gamma_2(0)$ (note

that $\dim Z_2 = 0$ and $\dim U = d-1$ if Condition (C6) applies and $\dim Z_2 = 1$ and $\dim U = d$ if Condition (C6') applies).
First we define what we refer to as a Lin orbit (see Figure 2.1 for a sketch) which plays an important role in the bifurcation analysis of the introduced setting.

Definition 2.1.2 *A sequence $\boldsymbol{X} = (X_i^{12}, X_i^{21})_{i\in\mathbb{Z}}$ of partial orbits (i.e. orbits that are only considered on a subinterval of the maximal domain) X_i^{12} and X_i^{21} that are inside a neighbourhood $\mathcal{U}_\Gamma$ of the heteroclinic cycle $\Gamma := \{\Gamma_1, \Gamma_2\}$ is called* Lin orbit *(with respect to $\mathcal{U}_\Gamma$) if it satisfies the following conditions:*

(i) Each partial orbit X_i^{12} starts at $\underline{X_i^{12}} \in \Sigma_1$ and follows Γ_1 to Υ, then follows Γ_2 and hits Σ_2 in a point $\overline{X_i^{12}}$. Similarly, each partial orbit X_i^{21} starts at $\underline{X_i^{21}} \in \Sigma_2$, follows Γ_2 to p and finally follows again Γ_1 until it ends at $\overline{X_i^{21}} \in \Sigma_1$.

(ii) The starting point of X_{i+1}^{12} and the end point of X_i^{21} in Σ_1 may only have a jump parallel to Z_1, the starting point of X_i^{21} and the end point of X_i^{12} in Σ_2 may only have a jump parallel to Z_2:

$$\overline{X_i^{21}} - \underline{X_{i+1}^{12}} \in Z_1 \text{ and } \overline{X_i^{12}} - \underline{X_i^{21}} \in Z_2.$$

Let $2\omega_i$ be the transition time of the partial orbit X_i^{21} from Σ_2 to Σ_1, and let ν_i be the number of revolutions for which X_i^{12} stays inside a fixed neighbourhood $\mathcal{U}_\Upsilon$ of Υ, cf. Figure 2.1. Then a complete Lin orbit of (1.2.1) is characterized by the sequences $\boldsymbol{\omega} = (\omega_i)_{i\in\mathbb{Z}}$ and $\boldsymbol{\nu} = (\nu_i)_{i\in\mathbb{Z}}$ along with parameters $\boldsymbol{\vartheta} = (\vartheta_i)_{i\in\mathbb{Z}}$, $\vartheta_i \in U$, and $\lambda \in \mathbb{R}^m$, see Theorem 2.1.4. This gives rise to the notation $\boldsymbol{X}(\boldsymbol{\omega}, \boldsymbol{\nu}, \boldsymbol{\vartheta}, \lambda)$. The neighbourhood $\mathcal{U}_\Gamma$ is given by the analysis. If it follows from the context, we use the short notation *Lin orbit*.
The analysis in Section 2.2 is entirely devoted to the proof of the existence and uniqueness of a Lin orbit for given transition times and revolutions.

Notation 2.1.3 *Bold letters denote sequences. $\boldsymbol{\omega} > \Omega$ means that the sequence $\boldsymbol{\omega} = (\omega_i)_{i\in\mathbb{Z}}$, $\omega_i \in \mathbb{R}^+$, is such that $\omega_i > \Omega$ for all $i \in \mathbb{Z}$. Similarly, $\boldsymbol{\nu} > 2N$ means that the sequence $\boldsymbol{\nu} = (\nu_i)_{i\in\mathbb{Z}}$, $\nu_i \in \mathbb{N}$, is such that $\nu_i > 2N$ for all $i \in \mathbb{Z}$. The symbol $\boldsymbol{\vartheta}$ denotes the sequence $\boldsymbol{\vartheta} = (\vartheta_i)_{i\in\mathbb{Z}}$ with $\vartheta_i \in U$.*

The following main theorem guarantees the existence and uniqueness of Lin orbits for given transition times and revolutions near Υ:

Theorem 2.1.4 *Consider system* (1.2.1) *and Conditions* (C1)–(C5) *together with* (C6) *or* (C6').
There are constants $N \in \mathbb{N}$ and $\Omega, c > 0$ such that for all $\boldsymbol{\omega} > \Omega$, $\boldsymbol{\nu} > 2N$ and $\boldsymbol{\vartheta}$, $\vartheta_i \in U$, and $\lambda \in \mathbb{R}^m$ with $\|\boldsymbol{\vartheta}\|, \|\lambda\| < c$, there is a unique Lin orbit $\boldsymbol{X}(\boldsymbol{\omega}, \boldsymbol{\nu}, \boldsymbol{\vartheta}, \lambda)$.

To prove Theorem 2.1.4 we use an extension of Lin's method (see above and [Lin90, San93, Kno04]). The idea is to split the system into two parts, a continuous part that describes the dynamics everywhere except in a certain neighbourhood of Υ, and a discrete part that describes the dynamics near the periodic orbit by means of a Poincaré map with respect

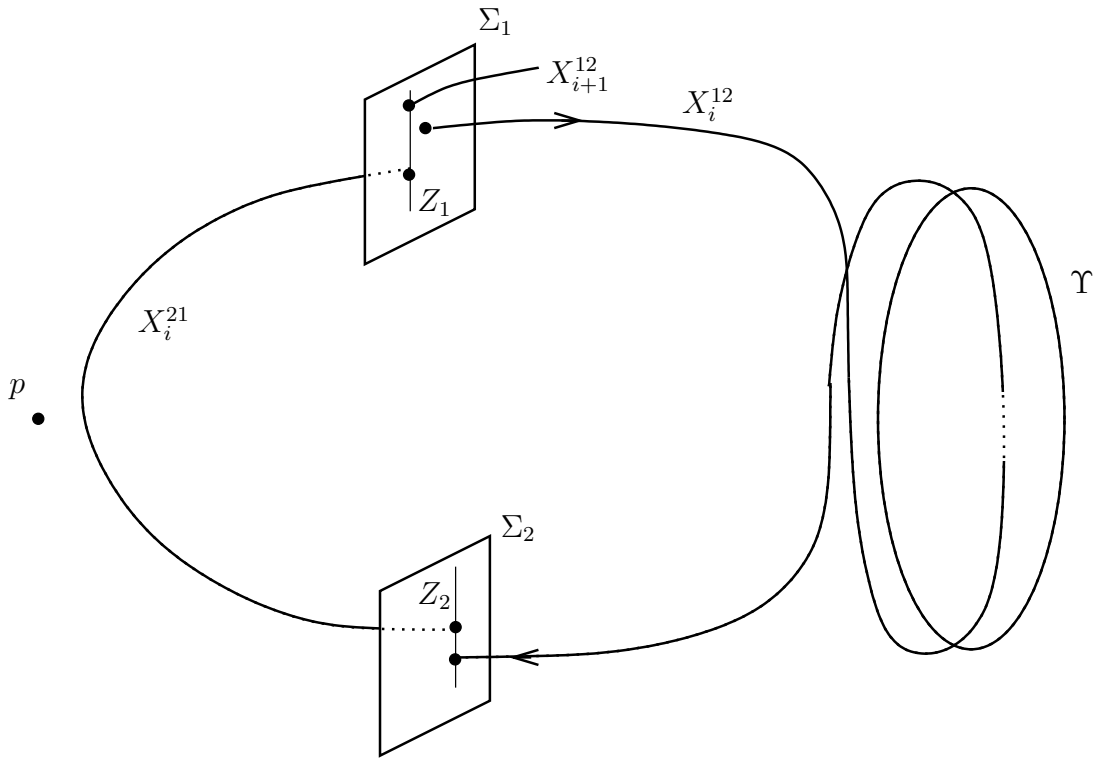

Figure 2.1: Part of a Lin orbit $\boldsymbol{X}$ in the described setting. The partial orbit X_i^{12} starts in Σ_1, follows Γ_1 to Υ, then follows Γ_2 until it ends in Σ_2. The partial orbit X_i^{21} starts in Σ_2, follows Γ_2 to p, then follows Γ_1 until it ends in Σ_1. The end point of X_i^{21} and the start point of X_{i+1}^{12} have a jump parallel to Z_1 (inside Σ_1), the end point of X_i^{12} and the start point of X_i^{21} have a jump parallel to Z_2 (inside Σ_2).

to a Poincaré section Σ_Υ. For the continuous system we prove the existence of 'partial Lin orbits' connecting Σ_Υ with itself while satisfying certain boundary conditions in Σ_Υ. Here, by 'partial Lin orbit' we mean a 'discontinuous orbit' with jumps only in Σ_1 and Σ_2 parallel to Z_1 and Z_2, respectively. Further, we prove that there are partial orbits of the discrete system satisfying boundary conditions as they are known from the theory of Shilnikov variables (cf. [Kno04] and references therein). Then we prove that the respective boundary conditions can be adjusted such that it is possible to match the end point of a partial Lin orbit with the start point of a partial orbit of the discrete system and the end point of this partial orbit with the start point of the next partial Lin orbit. This leads to an alternating sequence of partial Lin orbits and partial orbits of the discrete system that finally defines the sought-after Lin orbit.
The detailed proof of Theorem 2.1.4 is the main subject of the first part of this thesis and is carried out in detail in Section 2.2.
The next step in the analysis of the described setting is the construction of bifurcation equations for special solutions near the heteroclinic cycle. To derive these equations, it is important to know estimates of the sizes of the jumps that arise in the constructed Lin orbit. Here we only consider Condition (C6) (i.e. there are only jumps in Σ_1 and no jumps in Σ_2) and define the so-called jump function $\boldsymbol{\Xi} = (\Xi_i)_{i\in\mathbb{Z}}$ by

$$\Xi_i(\boldsymbol{\omega}, \boldsymbol{\nu}, \lambda) := \overline{X_i^{21}}(\boldsymbol{\omega}, \boldsymbol{\nu}, \boldsymbol{\vartheta}, \lambda) - \underline{X_{i+1}^{12}}(\boldsymbol{\omega}, \boldsymbol{\nu}, \boldsymbol{\vartheta}, \lambda).$$

Recall that $\overline{X_i^{21}}(\boldsymbol{\omega}, \boldsymbol{\nu}, \boldsymbol{\vartheta}, \lambda)$ denotes the end point of $X_i^{21}(\boldsymbol{\omega}, \boldsymbol{\nu}, \boldsymbol{\vartheta}, \lambda)$ within Σ_1 near Γ_1, and $\underline{X_{i+1}^{12}}(\boldsymbol{\omega}, \boldsymbol{\nu}, \boldsymbol{\vartheta}, \lambda)$ denotes the start point of $X_{i+1}^{12}(\boldsymbol{\omega}, \boldsymbol{\nu}, \boldsymbol{\vartheta}, \lambda)$ within Σ_1 near Γ_1. Note that, although technically Ξ_i also depends on a sequence $\boldsymbol{\vartheta}$, we do not express that dependence in the notation. The reason is that we only consider Condition (C6) and therefore the sequence $\boldsymbol{\vartheta}$ does not contribute to the dynamics, the ϑ_i are only used to select which of the (infinitely many) heteroclinic connections in $W^u(\Upsilon) \cap W^s(p)$ the partial orbits X_i^{12} and X_i^{21} follow. In Section 2.4.1 we briefly discuss the case where we assume Condition (C6') and thus consider additional jumps in Σ_2. In this case the dependence on $\boldsymbol{\vartheta}$ is indeed crucial to the jump estimates.
To estimate the leading terms of the jump function, it is necessary to make assumptions on the leading eigenvalues. Here, μ^s denotes the leading stable eigenvalue of the linearisation at p, μ_Υ^u denotes the leading unstable eigenvalue of the linearisation of the equilibrium $q := \Sigma_\Upsilon \cap \Upsilon$ of the discrete dynamical system implied by the Poincaré map (note that this value is the leading unstable Floquet multiplier of Υ). By 'leading eigenvalue' we refer to the eigenvalue that is closest to the imaginary axis in the continuous case and closest to the unit circle in the discrete case.
We consider two different cases of eigenvalue constellations:

(H 2.1) The leading stable and unstable Floquet multipliers of Υ, denoted by $\mu^s_\Upsilon(\lambda)$ and $\mu^u_\Upsilon(\lambda)$, are simple and real. There are constants $\bar{\mu}^{ss}_\Upsilon$, $\bar{\mu}^{uu}_\Upsilon$, $\bar{\mu}^s_\Upsilon$ and $\bar{\mu}^u_\Upsilon$ such that

$$0 < |\mu^{ss}_\Upsilon| < \bar{\mu}^{ss}_\Upsilon < |\mu^s_\Upsilon(\lambda)| < \bar{\mu}^s_\Upsilon < 1 < \bar{\mu}^u_\Upsilon < |\mu^u_\Upsilon(\lambda)| < \bar{\mu}^{uu}_\Upsilon < |\mu^{uu}_\Upsilon|$$

holds for all remaining stable and unstable Floquet multipliers μ^{ss}_Υ and μ^{uu}_Υ.
Moreover, we demand that for the leading Floquet multipliers

$$|\mu^u_\Upsilon(\lambda)|^{-2} < |\mu^s_\Upsilon(\lambda)| < |\mu^u_\Upsilon(\lambda)|^{-\frac{1}{2}}$$

holds.
The leading stable and unstable eigenvalues $\mu^s(\lambda)$ and $\mu^u(\lambda)$ of the linearisation at p are simple and real. There are constants $\bar{\mu}^{ss}$, $\bar{\mu}^{uu}$, $\bar{\mu}^s$ and $\bar{\mu}^u$ such that

$$\mathrm{Re}\mu^{ss} < \bar{\mu}^{ss} < \mu^s(\lambda) < \bar{\mu}^s < 0 < \bar{\mu}^u < \mu^u(\lambda) < \bar{\mu}^{uu} < \mathrm{Re}\mu^{uu}$$

holds for all remaining stable and unstable eigenvalues μ^{ss} and μ^{uu}.
Moreover, we demand that for the leading eigenvalues

$$2\mu^s(\lambda) < -\mu^u(\lambda) < \frac{\mu^s}{2}$$

holds.

(H 2.2) Let $\mu^s_\Upsilon(\lambda)$ and $\mu^u_\Upsilon(\lambda)$ be as in Hypothesis (H 2.1). The leading stable and unstable eigenvalues $\mu^s(\lambda)$ and $\mu^u(\lambda)$ are simple and complex (non-real). There are constants $\bar{\mu}^{ss}$, $\bar{\mu}^{uu}$, $\bar{\mu}^s$ and $\bar{\mu}^u$ such that

$$\mathrm{Re}\mu^{ss} < \bar{\mu}^{ss} < \mathrm{Re}\mu^s(\lambda) < \bar{\mu}^s < 0 < \bar{\mu}^u < \mathrm{Re}\mu^u(\lambda) < \bar{\mu}^{uu} < \mathrm{Re}\mu^{uu}$$

holds for all remaining stable and unstable eigenvalues μ^{ss} and μ^{uu}.
Moreover, we demand that for the leading eigenvalues

$$2\mathrm{Re}\mu^s(\lambda) < -\mathrm{Re}\mu^u(\lambda) < \frac{\mathrm{Re}\mu^s}{2}$$

holds.

The following Hypothesis guarantees that the heteroclinic connections Γ_1 and Γ_2 approach p and Υ generically, that is, they do not approach in the strong stable/unstable directions. This is also known as a non-orbit-flip condition. To formulate the assumptions, we need some notation that is properly introduced later in this thesis. Let Σ_Υ denote a Poincaré section of Υ and Π the Poincaré map with respect to Σ_Υ. Then we consider the discrete dynamical system given by the Poincaré map (cf. (2.2.43)) and denote the saddle equilibrium $\Upsilon \cap \Sigma_\Upsilon$ by q. Further, we denote the orbit in $W^s(q)$ that is given by the intersection points of Γ_1 with Σ_Υ by Γ^+ and we denote the orbit in $W^u(q)$ that is given by the intersection points of Γ_2 with Σ_Υ by Γ^-. The notation $W^{ss/uu}$ refers to the strong stable/unstable manifold.

(H 2.3) The connecting orbits do not approach p and Υ in the strong stable and unstable manifolds:

$$\Gamma_1 \not\subset W^{uu}(p) \text{ and } \Gamma^+ \not\subset W^{ss}(q);$$
$$\Gamma^- \not\subset W^{uu}(q) \text{ and } \Gamma_2 \not\subset W^{ss}(p).$$

For the following assumption we need some additional notation, cf. Section 2.3. We consider the adjoint variational equation along Γ_1 (with respect to the scalar product used in (2.3.6) below)

$$\dot{x} = -\left(D_1 f(\gamma_1(t), 0)\right)^T x$$

and denote the transition matrix by $\Psi(\cdot,\cdot)$ and the stable subspace for $t \to \infty$ at $t = 0$ by $E_1^s(0)$ (and the respective subspace for $t \to -\infty$ at $t = 0$ by $E_1^u(0)$, accordingly). Then by construction, $Z_1 \subset E_1^s(0) \cap E_1^u(0)$. Let ϖ^+ denote the transition time from Σ_1 to Σ_Υ (see Hypothesis (H 2.8) below) and let $\tilde{Z}_1 := \Psi(\varpi^+, 0)Z_1$. For the discrete dynamical system as introduced above, we consider the adjoint variational equation along Γ^+ and define in a similar manner the subspaces $E_{1,d}^{s/u}(0)$. Analogously we define the subspaces concerning the adjoint variational equation along Γ_2 and Γ^-, respectively. We denote the associated strong stable/unstable subspace (that is, all stable/unstable directions except the weakest direction) by $E_{1/2}^{ss/uu}(0)$.
We assume the following hypothesis for Z_1, $\tilde{Z}_1$,Z_2 and $\tilde{Z}_2$ holds:

(H 2.4) $Z_1 \not\subset E_1^{uu}(0)$ and $\tilde{Z}_1 \not\subset E_{1,d}^{ss}(0)$. $Z_2 \not\subset E_2^{ss}(0)$ and $\tilde{Z}_2 \not\subset E_{2,d}^{uu}(0)$.

Geometrically, this is the so-called non-inclination-flip condition. It means (for Γ_1) that the stable manifold $W^s(\Upsilon)$ intersects the manifold $W_{loc}^{cu}(p)$ transversally and an analogous condition for Γ_2. Here, the manifold denoted by W_{loc}^{cu} is such that its tangent space $T_p W_{loc}^{cu}$ consists of all unstable and the weakest stable direction. Note that in general this manifold is not determined uniquely, however, in this case the tangent spaces along Γ_1 are uniquely defined. See also [Kno04], Section 2.3.2, for a deeper discussion of the geometrical implications.
Under either of the eigenvalue hypotheses we can now show the following properties of the jump function which can then be used to formulate bifurcation equations; therefore the two following theorems are the main results of this chapter. First we consider the real leading eigenvalue case.

Theorem 2.1.5 *Consider system* (1.2.1) *and let Conditions* (C1)–(C6)*, Hypothesis* (H 2.3) *and Hypothesis* (H 2.4) *hold. Assume that the leading eigenvalues are as stated in Hypothesis* (H 2.1)*.*
Let $\Omega, N, \boldsymbol{\omega}, \boldsymbol{\nu}$ *be according to Theorem* 2.1.4*. Then the structure of the jump function* $\boldsymbol{\Xi} = (\Xi_i)_{i\in\mathbb{Z}}$ *is as follows:*

$$\begin{aligned}\Xi_i(\boldsymbol{\omega}, \boldsymbol{\nu}, \lambda) = \lambda + c_1(\lambda) e^{2\mu^s(\lambda)\omega_i} + c_2(\lambda)\left(\mu_\Upsilon^u(\lambda)\right)^{-\nu_{i+1}} \\ + o\left(e^{2\mu^s(\lambda)\Omega}\right) + o\left(\left(\mu_\Upsilon^u(\lambda)\right)^{-2N}\right) + \mathcal{R}(\Omega, N)\end{aligned} \tag{2.1.1}$$

with $\mathcal{R}(\Omega, N) = O\left(\left(\mu_\Upsilon^u(\lambda)\right)^{-N} e^{2\mu^s(\lambda)\Omega}\right)$.

The functions $c_{1,2} : \mathbb{R}^m \to \mathbb{R}^{\dim Z_1}$ *are continuous and* $c_{1,2}(0) \neq 0$ *holds. The o-terms and the O-term are valid for* Ω *and* N *tending to infinity. Moreover, the jump function* $\boldsymbol{\Xi}$ *depends smoothly on* $\boldsymbol{\omega}$ *and* λ*.*

For the complex leading eigenvalue case we get a similar result:

Theorem 2.1.6 *Consider system* (1.2.1) *and let Conditions* (C1)–(C6)*, Hypothesis* (H 2.3) *and Hypothesis* (H 2.4) *hold. Assume that the leading eigenvalues are as stated in Hypothesis* (H 2.2)*.*
Let $\Omega, N, \boldsymbol{\omega}, \boldsymbol{\nu}$ *be according to Theorem* 2.1.4*. Then there is a constant* $\phi^s \in \mathbb{R}$ *such that the structure of the jump function* $\boldsymbol{\Xi} = (\Xi_i)_{i\in\mathbb{Z}}$ *is as follows:*

$$\begin{aligned}\Xi_i(\boldsymbol{\omega}, \boldsymbol{\nu}, \lambda) = \lambda + c_1(\lambda) \sin\left(2\mathrm{Im}\mu^s(\lambda)\omega_i + \phi^s\right) e^{2\mathrm{Re}\mu^s(\lambda)\omega_i} + c_2(\lambda) \left(\mu^u_\Upsilon(\lambda)\right)^{-\nu_{i+1}} \\ + o\left(e^{2\mathrm{Re}\mu^s(\lambda)\Omega}\right) + o\left(\left(\mu^u_\Upsilon(\lambda)\right)^{-2N}\right) + \mathcal{R}(\Omega, N)\end{aligned} \tag{2.1.2}$$

with $\mathcal{R}(\Omega, N) = O\left(\left(\mu^u_\Upsilon(\lambda)\right)^{-N} e^{2\mathrm{Re}\mu^s(\lambda)\Omega}\right)$*.*
The functions $c_{1,2} : \mathbb{R}^m \to \mathbb{R}^{\dim Z_1}$ *are continuous and* $c_{1,2}(0) \neq 0$ *holds. The o-terms and the O-term are valid for* Ω *and* N *tending to infinity. Moreover, the jump function* $\boldsymbol{\Xi}$ *depends smoothly on* $\boldsymbol{\omega}$ *and* λ*.*

Remark 2.1.7 *Due to the construction, all the statements in Theorem* 2.1.4*, Theorem* 2.1.5 *and Theorem* 2.1.6 *remain valid for* $\Omega \to \infty$ *or* $N \to \infty$*.*

The proof of these estimates (exemplarily for Theorem 2.1.5) can be found in Section 2.3.
In Section 2.4 we use the jump estimates stated in Theorem 2.1.5 and Theorem 2.1.6 to construct and discuss bifurcation equations for various types of orbits near the heteroclinic EtoP cycle. The main results are stated in the following theorems.
We start with homoclinic orbits to p that stay near the heteroclinic EtoP cycle:

Theorem 2.1.8 *Consider system* (1.2.1) *and let Conditions* (C1)–(C6)*, Hypothesis* (H 2.3) *and Hypothesis* (H 2.4) *hold. Additionally, assume that the eigenvalue situation Hypothesis* (H 2.1) *or Hypothesis* (H 2.2) *holds.*
Then there is a constant $N \in \mathbb{N}$ *such that for all* $\nu \in \mathbb{N}$*,* $\nu > 2N$*, there is a unique parameter value* λ_ν *for which a* 1*-homoclinic orbit to* p *exists that stays in* $\mathcal{U}_\Gamma$*. The value of* ν *determines the number of revolutions that the homoclinic orbit stays in a fixed neighbourhood of* Υ*. Moreover,* λ_ν *tends to* 0 *as* ν *tends to infinity.*

In other words, at discrete values of λ close to 0, homoclinic orbits to p accumulate with increasing revolution numbers around Υ. This result is in agreement with the results in [Rad05] and is also numerically verified in Section 3.5.2.
Now we consider homoclinic orbits to Υ that stay near the EtoP cycle:

Theorem 2.1.9 *Consider system* (1.2.1) *and let Conditions* (C1)–(C6)*, Hypothesis* (H 2.3) *and Hypothesis* (H 2.4) *hold. Additionally, assume that the eigenvalue situation Hypothesis* (H 2.1) *or Hypothesis* (H 2.2) *holds.*
Then there is a constant Ω *such that for all* $\omega > \Omega$ *there is a unique parameter value* $\lambda = \lambda(\omega)$ *for which a* 1*-homoclinic orbit to* Υ *exists that stays in* $\mathcal{U}_\Gamma$*. The function* $\lambda(\cdot)$ *is smooth and* λ *tends to* 0 *as* ω *tends to infinity.*

If the leading eigenvalues are real, we observe a so-called 'blue sky catastrophe' scenario, see Figures 2.11 and 2.14 below for a geometrical interpretation and Section 3.5.1 for numerical evidence of that scenario. In the case of complex leading eigenvalues, the function $\lambda(\cdot)$ has infinitely many roots, see Figures 2.12 and 2.15 for a geometrical interpretation.
The proof of Theorem 2.1.9 and a discussion of the bifurcation equation for homoclinic orbits to p if Condition (C6') applies can be found in Section 2.4.

2.2 Extension and adaptation of Lin's method

In the following sections we explain how to adapt and extend Lin's method to deal with the presented setting. The main difference to the classical setting for heteroclinic cycles connecting hyperbolic equilibria (as for example in [KLW07]) is that one hyperbolic equilibrium is replaced by a hyperbolic periodic orbit. The idea how to use Lin's method in this setting is to describe the dynamics near the periodic orbit by the associated discrete dynamical system defined by the Poincaré map with respect to a cross-section Σ_Υ of Υ. An advantage of this approach is that it provides a 'kit' which can be used to deal with almost any kind of setting involving periodic orbits and equilibria, while it utilises the well-established theory for continuous and discrete systems. So the approach boils down to a coupling of a continuous and a discrete dynamical system using certain projection boundary conditions. The actual procedure is as follows: First, we prove the unique existence of solutions inside $W^u_\lambda(p)$ and $W^s_\lambda(\Upsilon)$ that stay near Γ_1 and have a jump inside Σ_1 in the subspace Z_1. Similarly, we prove the unique existence of solutions inside $W^s_\lambda(p)$ and $W^u_\lambda(\Upsilon)$ that stay near Γ_2 and have a jump inside Σ_2 in the subspace Z_2. Then we prescribe two projection boundary conditions inside Σ_Υ and prove that there is exactly one 'partial Lin orbit' inside $\mathcal{U}_\Gamma$ that connects Σ_Υ to itself and satisfies these conditions (and the jump conditions) and takes a prescribed transition time ω from Σ_2 to Σ_1. Similarly, for the discrete dynamical system inside Σ_Υ we prove that for given projection boundary conditions (similar to the conditions known from the theory of Shilnikov variables) there is exactly one solution that takes ν steps from boundary to boundary. In the last step, we couple both of these solutions inside Σ_Υ to construct a Lin orbit that stays inside $\mathcal{U}_\Gamma$ and has jumps only inside Σ_1 and Σ_2 parallel to the subspaces Z_1 and Z_2.
To perform Lin's method, we introduce certain directions that are important for the coupling and jump conditions. We define W_1^+ and W_1^- as the complements of the vector field direction within the tangent spaces of $W^s(\Upsilon)$ and $W^u(p)$, respectively, at $\gamma_1(0)$:

$$\big(T_{\gamma_1(0)}W^s(\Upsilon) \cap T_{\gamma_1(0)}W^u(p)\big) \oplus W_1^+ = T_{\gamma_1(0)}W^s(\Upsilon),$$
$$\big(T_{\gamma_1(0)}W^s(\Upsilon) \cap T_{\gamma_1(0)}W^u(p)\big) \oplus W_1^- = T_{\gamma_1(0)}W^u(p).$$

In this setting, we still have some freedom in choosing the cross-section Σ_1 and in particular the subspace W_1^+. It is crucial for the discussed method that W_1^+ is chosen such that it is the image of a certain projection. We return to the exact setting in Section 2.2.2.
Finally, we choose an additional subspace Z_1 such that $\mathbb{R}^n = \operatorname{span}\{f(\gamma_1(0),0)\} \oplus W_1^+ \oplus W_1^- \oplus Z_1$ and thus define $Y_1 := W_1^+ \oplus W_1^- \oplus Z_1$ and the cross-section Σ_1 of the heteroclinic orbit Γ_1 as follows:

$$\Sigma_1 := \gamma_1(0) + (W_1^+ \oplus W_1^- \oplus Z_1). \tag{2.2.1}$$

Note that since we exclude all degeneracities other than the dimensions of the stable and unstable manifolds, $\dim Z_1 = d$.
For Σ_2 we introduce similar subspaces as follows:

$$\big(T_{\gamma_2(0)}W^u(\Upsilon) \cap T_{\gamma_2(0)}W^s(p)\big) \oplus W_2^+ = T_{\gamma_2(0)}W^s(p),$$
$$\big(T_{\gamma_2(0)}W^u(\Upsilon) \cap T_{\gamma_2(0)}W^s(p)\big) \oplus W_2^- = T_{\gamma_2(0)}W^u(\Upsilon).$$

We define additional subspaces Z_2 and U such that

$$\operatorname{span}\{f(\gamma_2(0),0)\} \oplus U = T_{\gamma_2(0)}W^u(\Upsilon) \cap T_{\gamma_2(0)}W^s(p)$$

and

$$\mathbb{R}^n = \operatorname{span}\{f(\gamma_2(0),0)\} \oplus U \oplus W_2^+ \oplus W_2^- \oplus Z_2.$$

Note that if we assume Condition (C6), the subspace U is $d-1$-dimensional and $\dim Z_2 = 0$; if we assume Condition (C6'), the subspace U is d-dimensional and $\dim Z_2 = 1$.
Then we can define $Y_2 := U \oplus W_2^+ \oplus W_2^- \oplus Z_2$ and thus

$$\Sigma_2 := \gamma_2(0) + (U \oplus W_2^+ \oplus W_2^- \oplus Z_2). \tag{2.2.2}$$

Special cases
We briefly discuss the dimensions of the introduced subspaces for two important cases that are also numerically considered in Chapter 3. The examples in Section 3.5.1 and Section 3.5.2 are in $\mathbb{R}^3$, the codimension of the respective EtoP connection is $d = 1$. Since $n = 3$ we have that $k = \dim W^u(p) = 1$ and $l = \dim W^s(\Upsilon) = 2$. Then $\dim W_1^- = 0$, $\dim W_1^+ = 1$ and $\dim Z_1 = 1$. For Condition (C6) the situation in Σ_2 is straightforward, $\dim Z_2 = 0$, $\dim W_2^+ = \dim W_2^- = 1$ and $\dim U = 0$. On the other hand, if we consider Condition (C6'), $\dim Z_2 = 1$, $\dim W_2^+ = \dim W_2^- = 0$ and $\dim U = 1$.
The second important case is the codimension-two case in $\mathbb{R}^4$ as considered in Section 3.5.3. Here we find that $k = \dim W^u(p) = 1$, $l = \dim W^s(\Upsilon) = 2$ and thus $\dim W_1^- = 0$, $\dim W_1^+ = 1$ and $\dim Z_1 = 2$. For Condition (C6), we find $\dim Z_2 = 0$, $\dim W_2^+ = \dim W_2^- = 1$ and thus $\dim U = 1$ in Σ_2.

2.2.1 Step one – Orbits in the stable and unstable manifolds

In general, the first step of Lin's method describes the splitting of the stable and unstable manifolds. In the described setting only the unstable manifold of p and the stable manifold of Υ actually split, whereas the heteroclinic connection from Υ to p does not break. The goal is to find solutions in the splitting manifolds that can be described as perturbations of the original heteroclinic solutions $\gamma_1(\cdot)$ and that satisfy certain jump conditions in the transversal section Σ_1.
Throughout the following sections we assume that the two technical hypotheses

(H 2.5) The hyperbolic equilibrium p does not change as long as the parameter λ is sufficiently close to λ^*, that is $p_\lambda \equiv p$.

(H 2.6) The hyperbolic periodic orbit Υ does not change as long as the parameter λ is sufficiently close to λ^*, that is $\Upsilon_\lambda \equiv \Upsilon$, and the vector field along Υ does not change: $f(\cdot,\lambda)|_\Upsilon = f(\cdot,\lambda^*)$.

hold. See Section A.3 for a justification of these hypotheses. Hypothesis (H 2.5) and Hypothesis (H 2.6) provide that the equilibrium and the periodic orbit (and the vector field along the periodic orbit) are kept fixed for λ close to λ^*; these technical assumptions allow us to handle certain estimates in the following considerations more easily.
The following theorem gives the first step of Lin's method and is a generalisation of Theorem 4.1.6 in [Rie03] to arbitrary dimension n.

Theorem 2.2.1 *Consider system* (1.2.1) *and assume Conditions* (C1)–(C5) *hold. Then there is a neighbourhood Λ of λ^* such that for each $\lambda \in \Lambda$ there is a unique pair of solutions $(\gamma_1^+(\lambda)(\cdot), \gamma_1^-(\lambda)(\cdot))$ that satisfy the following conditions:*

(i) $\gamma_1^+(\lambda)(0) \in W^s_\lambda(\Upsilon)$, $\gamma_1^-(\lambda)(0) \in W^u_\lambda(p)$,

(ii) $\gamma_1^+(\lambda)(0), \gamma_1^-(\lambda)(0) \in \Sigma_1$ *and*

(iii) $\gamma_1^+(\lambda)(0) - \gamma_1^-(\lambda)(0) \in Z_1$.

Outline of the proof. For $n = 3$ (and consequently $\dim Z_1 = 1$) this theorem is rigorously proved in [Rie03]; we give an outline of this proof and generalize it to $\mathbb{R}^n$, $n \geq 3$. We start with the heteroclinic solution $\gamma_1(\cdot)$ that exists for $\lambda = \lambda^*$ and look for orbits $\gamma_1^-(\lambda)(\cdot)$ in $W^u_\lambda(p)$ and $\gamma_1^+(\lambda)(\cdot)$ in $W^s_\lambda(\Upsilon)$ as perturbations of $\gamma_1(\cdot)$. Since the computations for the orbit in $W^u_\lambda(p)$ are completely analogous to the computations in the classical application of Lin's method for heteroclinic cycles between hyperbolic equilibria (see for example [Kno04]), we confine the following elaboration to the solution γ_1^+ in $W^s_\lambda(\Upsilon)$.
We define for $t \geq 0$ the solution $\gamma_1^+(t) := \gamma_1(t) + v_1^+(\lambda)(t)$ and deduce the nonlinear variational equation

$$\dot{v}_1^+(t) = D_1 f(\gamma_1(t), 0) v_1^+(t) + h_1^+(t, v_1^+(t), \lambda) \tag{2.2.3}$$

with $h_1^+(t, v, \lambda) := f(\gamma_1(t) + v, \lambda) - f(\gamma_1(t), 0) - D_1 f(\gamma_1(t), 0)v$. In a first approximation we replace the function $h(\cdot,\cdot,\cdot)$ by an arbitrary function $g(\cdot)$ that does not depend on v, thus (2.2.3) becomes

$$\dot{v}_1^+(t) = D_1 f(\gamma_1(t), 0) v_1^+(t) + g(t). \tag{2.2.4}$$

The only condition we impose on g is that it is exponentially bounded. More precisely, we assume that $g \in V^+_{\bar{\alpha}}$ for some $\bar{\alpha}$ where $V^+_{\bar{\alpha}}$ is the following Banach space

$$V^+_{\bar{\alpha}} := \left\{ v \in C^0\left([0,\infty), \mathbb{R}^n\right) : \sup_{t \geq 0} e^{\bar{\alpha} t} \left\| v(t) \right\|_{\mathbb{R}^n} =: \|v\|^+_{\bar{\alpha}} < \infty \right\}.$$

Note that the linear homogenuous equation associated with (2.2.4) has an exponential trichotomy on $\mathbb{R}^+$. Let $\bar{\delta}^c$ and $\bar{\delta}^s$ denote the exponents of the trichotomy, then $\bar{\alpha}$ has to be chosen such that $0 \leq \bar{\delta}^c < \bar{\alpha} < \bar{\delta}^s$ holds.

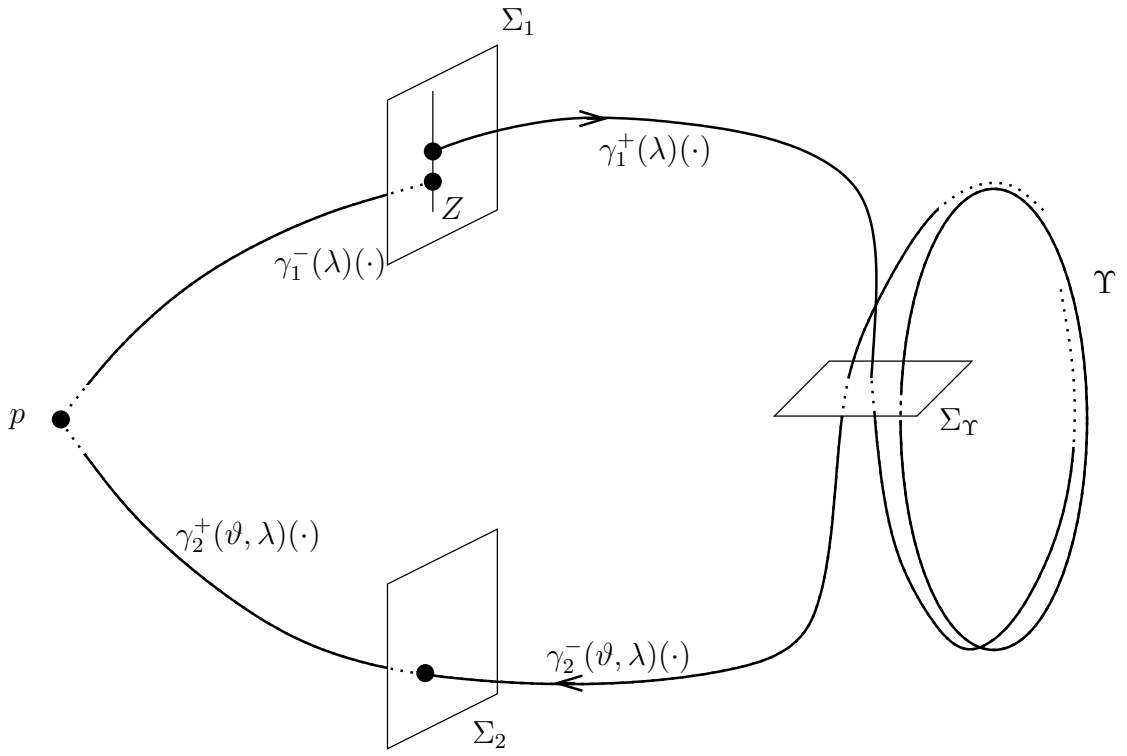

Figure 2.2: The splitting of the manifolds. Shown is the situation for Conditions (C1)–(C6) where the manifolds $W^u_\lambda(p)$ and $W^s_\lambda(\Upsilon)$ split up for $\lambda \neq \lambda^*$ while the connection Γ_2 is robust.

Exploiting the variation of constants formula and the estimates of the exponential trichotomy, we can now give a detailed equation for solutions of (2.2.4) that are exponentially bounded, namely: Exponentially bounded solutions of (2.2.4) on $\mathbb{R}^+$ take the form

$$v_1^+(t) = \Phi(t,0)w^+ + \int_0^t \Phi(t,\tau)Q_s^+(\tau)g(\tau)d\tau - \int_t^\infty \Phi(t,\tau)\left(\mathrm{id} - Q_s^+(\tau)\right)g(\tau)d\tau \qquad (2.2.5)$$

with $w^+ \in W_1^+$. Note that $Q_s^+(\cdot)$ denotes the projection associated with the exponential trichotomy.
After replacing the function $g(\cdot)$ by $h^+(\cdot, v_1^+(\cdot), \lambda)$, equation (2.2.5) can be read as a fixed point equation in $V_{\tilde{\alpha}}^+$. Near $\lambda = \lambda^*$ and for sufficiently small $w^+ \in W_1^+$ this equation can be solved for $v_1^+ = v_1^+(w^+, \lambda)$. Note that due to the exponential trichotomy it is important to solve the fixed point equation in the space of *exponentially* bounded functions.
For the solution v_1^- we use a similar approach, but here it is sufficient to use bounded solutions (instead of exponentially bounded solutions) and to exploit the exponential dichotomy on $\mathbb{R}^-$ with the associated projection $P^-(\cdot)$. Here we find that solutions have the form $v^- = v^-(w^-, \lambda)$ for sufficiently small $w^- \in W_1^-$ and λ close to λ^*.
Finally, using the decomposition (2.2.1) of Σ_1 we get the system

$$\begin{aligned} v^+(w^+,\lambda)(0) &= w^+ + \tilde{w}^-(w^+,\lambda) + z^+(w^+,\lambda), \\ v^-(w^-,\lambda)(0) &= \tilde{w}^+(w^-,\lambda) + w^- + z^-(w^-,\lambda) \end{aligned} \qquad (2.2.6)$$

with $w^-, \tilde{w}^- \in W_1^-$, $w^+, \tilde{w}^+ \in W_1^+$ and $z^-, z^+ \in Z_1$. Using that $\gamma_1^+(\lambda)(0) - \gamma_1^-(\lambda)(0) \in Z_1$ results in

$$\begin{aligned} w^+ &= \tilde{w}^+(w^-,\lambda), \\ w^- &= \tilde{w}^-(w^+,\lambda), \end{aligned}$$

which then can be solved for $(w^+, w^-) = (\hat{w}^+(\lambda), \hat{w}^-(\lambda))$ around $\lambda = \lambda^*$ (exploiting that $\tilde{w}^{+/-}(0,\lambda^*) = 0$ and $D_1\tilde{w}^{+/-}(0,\lambda^*) = 0$).
Now we can plug this into (2.2.3) which gives

$$\begin{aligned} \gamma_1^+(\lambda)(\cdot) &:= \gamma_1(\cdot) + v_1^+(\hat{w}^+(\lambda),\lambda)(\cdot), \\ \gamma_1^-(\lambda)(\cdot) &:= \gamma_1(\cdot) + v_1^-(\hat{w}^-(\lambda),\lambda)(\cdot). \end{aligned}$$

Since the $v_1^{+/-}$ are (exponentially) bounded, the solutions $\gamma_1^{+/-}$ stay close to γ_1 for all $t \to \infty$ ($t \to -\infty$, respectively). Since p and Υ are hyperbolic, it immediatly follows that $\{\gamma_1^+(\lambda)(t); t \in \mathbb{R}^+\} \subset W_\lambda^s(\Upsilon)$ and $\{\gamma_1^-(\lambda)(t); t \in \mathbb{R}^-\} \subset W_\lambda^u(p)$. This proves the theorem. □

In other words, Theorem 2.2.1 allows us to define a jump function $\xi^\infty : \mathbb{R}^m \to Z_1$, $\xi^\infty(\lambda) := \gamma_1^+(\lambda)(0) - \gamma_1^-(\lambda)(0)$ which measures how the manifolds $W_\lambda^u(p)$ and $W_\lambda^s(\Upsilon)$ split for $\lambda \neq \lambda^*$. Note that if we assume Condition (C6), $Z_1 \cong \mathbb{R}^m$. Condition (C5) then is equivalent to the non-singularity of $D_1\xi^\infty(0)$ and thus we can transform $\xi^\infty(\lambda)$ such that

(H 2.7) $\xi^\infty(\lambda) = \lambda - \lambda^*$

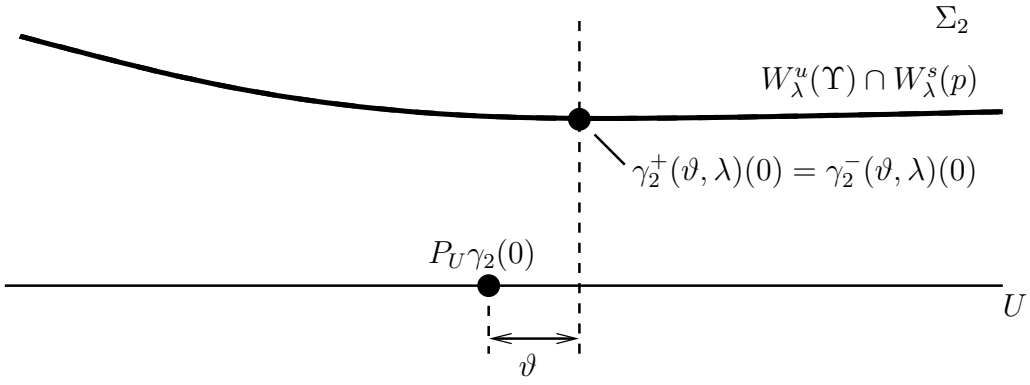

Figure 2.3: Inside Σ_2 – generic case (Condition (C6)). Sketch of the situation inside Σ_2 for $\mathbb{R}^3$. Shown are the traces of intersection curve $W^u(\Upsilon) \cap W^s(p)$ and the subspace U in Σ_2. The projection of $\gamma_2^\pm(\vartheta,\lambda)(0)$ onto U is determined by ϑ.

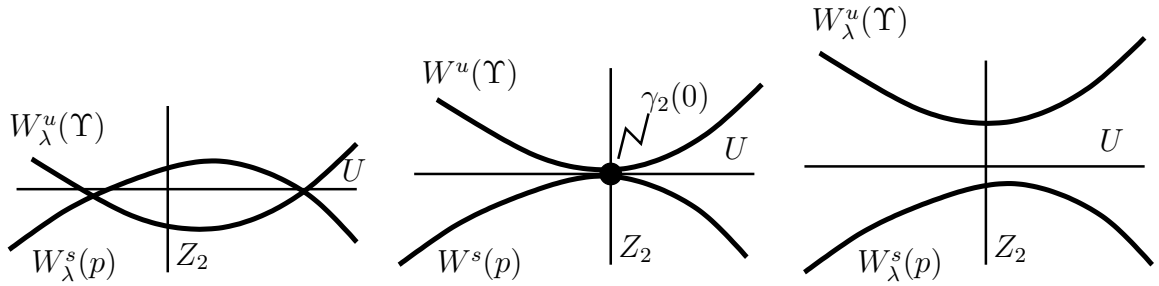

(a) $\lambda > 0$ (b) $\lambda = 0$ (c) $\lambda < 0$

Figure 2.4: Sketch of the situation inside Σ_2 (for $\mathbb{R}^3$) – Condition (C6'), quadratic tangency case. Shown are the traces of the intersection curves $W^u_\lambda(\Upsilon) \cap \Sigma_2$ and $W^s(p) \cap \Sigma_2$ in Σ_2 as well as the subspaces Z_2 and U.

holds. We use Theorem 2.2.1 in Chapter 3 extensively to introduce a novel numerical method for finding and continuing EtoP connections. Note that the notation in Chapter 3 changes, there the unique solutions in the stable and unstable manifolds are denoted by $q^\pm$ (instead of $\gamma_1^\pm$) and the periodic orbit is denoted by Γ (instead of Υ).
Before formulating a similar theorem for the EtoP connection Γ_2, we define a projection $P_U : Y_2 \to U$ that projects onto U along $W_2^+ \oplus W_2^- \oplus Z_2$ in accordance with the decomposition (2.2.2).

Theorem 2.2.2 *Consider system* (1.2.1) *and assume Conditions* (C1)–(C3) *hold. Additionally, either Condition* (C6) *or Condition* (C6') *holds. Then there is a neighbourhood* Λ *of* λ^* *such that for each* $\lambda \in \Lambda$ *and each* $\vartheta \in U$ *sufficiently close to* 0 *there is a unique pair of solutions* $(\gamma_2^+(\vartheta,\lambda)(\cdot), \gamma_2^-(\vartheta,\lambda)(\cdot))$ *that satisfy the following conditions:*

(i) $\gamma_2^+(\vartheta,\lambda)(0) \in W^s_\lambda(p)$, $\gamma_2^-(\vartheta,\lambda)(0) \in W^u_\lambda(\Upsilon)$,

(ii) $\gamma_2^+(\vartheta,\lambda)(0), \gamma_2^-(\vartheta,\lambda)(0) \in \Sigma_2$,

(iii) $P_U\left(\gamma_2^\pm(\vartheta,\lambda) - \gamma_2(0)\right) = \vartheta$ *and*

(iv) $\gamma_2^+(\vartheta,\lambda)(0) - \gamma_2^-(\vartheta,\lambda)(0) \in Z_2$.

Outline of the proof. The proof runs completely parallel to the proof of Theorem 2.2.1, the additional direction U can be worked in in a straightforward way. Finally, in place of Equation (2.2.6) we get

$$\begin{aligned} v^+(w^+,\vartheta^+,\lambda)(0) &= w^+ + \tilde{w}^-(w^+,\vartheta^+,\lambda) + z^+(w^+,\vartheta^+,\lambda) + \vartheta^+, \\ v^-(w^-,\vartheta^-,\lambda)(0) &= \tilde{w}^+(w^-,\vartheta^-,\lambda) + w^- + z^-(w^-,\vartheta^-,\lambda) + \vartheta^- \end{aligned} \tag{2.2.7}$$

and by claiming $\gamma_2^+(\vartheta,\lambda)(0) - \gamma_2^-(\vartheta,\lambda)(0) \in Z_2$ it follows that $\vartheta^+ = \vartheta^- =: \vartheta$ and

$$\begin{aligned} w^+ &= \tilde{w}^+(\vartheta, w^-, \lambda), \\ w^- &= \tilde{w}^-(\vartheta, w^+, \lambda) \end{aligned}$$

can be solved for $(w^+, w^-) = (\hat{w}^+(\vartheta,\lambda), \hat{w}^-(\vartheta,\lambda))$ and thus we finally can define

$$\begin{aligned} \gamma_2^+(\vartheta,\lambda)(\cdot) &:= \gamma_2(\cdot) + v^+(\vartheta + \hat{w}^+(\vartheta,\lambda),\lambda)(\cdot), \\ \gamma_2^-(\vartheta,\lambda)(\cdot) &:= \gamma_2(\cdot) + v^-(\vartheta + \hat{w}^-(\vartheta,\lambda),\lambda)(\cdot). \end{aligned}$$

The same argument as in the proof of Theorem 2.2.1 concludes the proof of this theorem. □

Remark 2.2.3 *In case of Condition* (C6)*, due to the transversal intersection of* $W^u(\Upsilon)$ *and* $W^s(p)$*, the heteroclinic orbit* Γ_2 *persists and thus the solutions* $\gamma_2^+(\vartheta,\lambda)$ *and* $\gamma_2^-(\vartheta,\lambda)$ *coincide. Then the parameter* ϑ *is only used to select one of the infinitely many orbits in case* $\dim\left(W^u(\Upsilon) \cap W^s(p)\right) \geq 2$.

In essence, the previous theorems provide us with solutions within the involved stable and unstable manifolds that can then be further perturbed to finally obtain Lin orbits as defined in Definition 2.1.2. This is also known as the first step of Lin's method which is dedicated to the 'infinite' time solutions. The transition to finite time intervals is done in steps two to four of the presented method (in the classical application of Lin's method this is also known as the 'second step').

2.2.2 Step two – The continuous system

In this section we perform the coupling near the equilibrium p, i.e. we look for piecewise continuous solutions of the system that start and end in Σ_Υ and satisfy certain linear boundary conditions in Σ_Υ and jump conditions in Σ_1 and Σ_2. As it turns out, for given transition times and given projection conditions in Σ_Υ we get a unique solution that starts in Σ_Υ, follows γ_2, has a jump in Σ_2 in Z_2 direction, then follows γ_1, has a jump in Σ_1 in Z_1 direction and ends in Σ_Υ again. For convenience and without loss of generality, from now on we assume $\lambda^* = 0$.

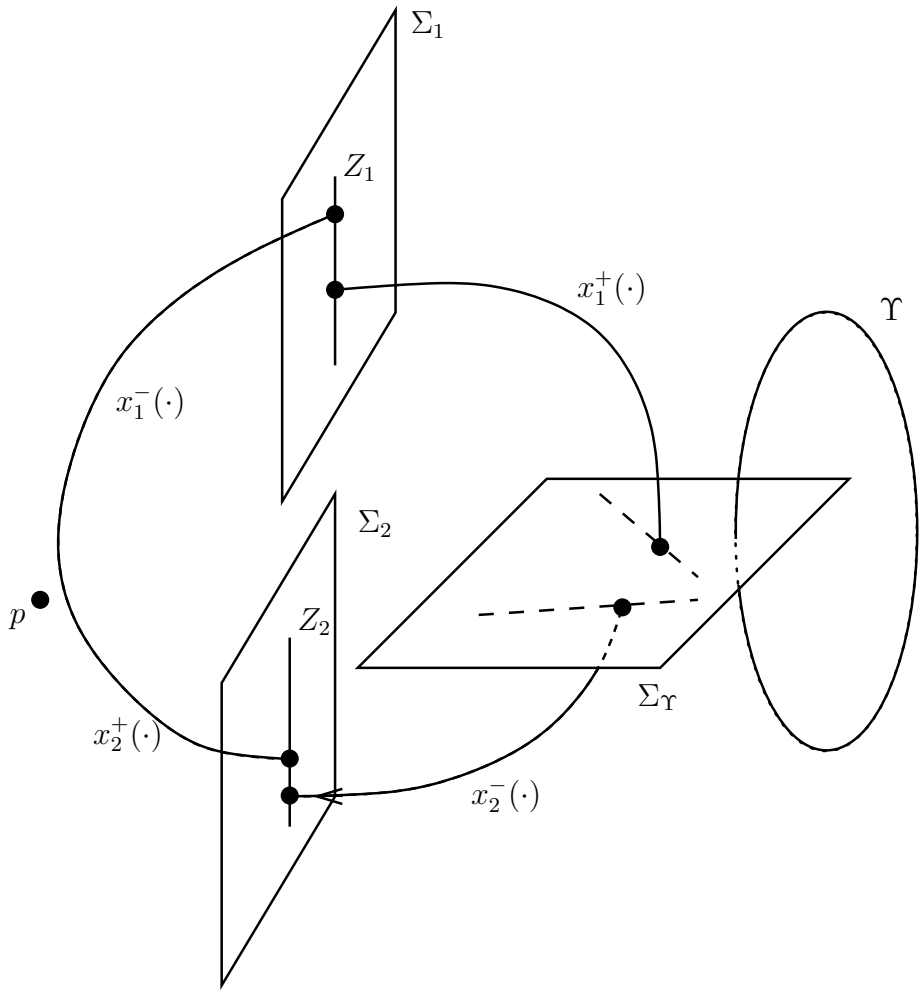

Figure 2.5: Draft of the continuous system. Shown are the solutions $x_1^\pm(\cdot)$ that have a jump in Σ_1 in Z_1 direction and the solutions $x_2^\pm$ that have a jump in Σ_2 in Z_2 direction and that satisfy the projection boundary conditions (2.2.18) in Σ_Υ. Moreover, x_1^- and x_2^+ are coupled near the equilibrium p.

We express the corresponding solutions as perturbations of the solutions $\gamma_{1,2}^{\pm}$ in the stable and unstable manifolds of p and Υ and denote them by $x_{1,2}^{\pm}$, see Figure 2.5.

$$\begin{aligned} x_1^-(t,\lambda) &= \gamma_1^-(\lambda)(t) + v_1^-(t,\lambda), \\ x_1^+(t,\lambda) &= \gamma_1^+(\lambda)(t) + v_1^+(t,\lambda), \\ x_2^-(t,\vartheta,\lambda) &= \gamma_2^-(\vartheta,\lambda)(t) + v_2^-(t,\vartheta,\lambda), \\ x_2^+(t,\vartheta,\lambda) &= \gamma_2^+(\vartheta,\lambda)(t) + v_2^+(t,\vartheta,\lambda). \end{aligned} \tag{2.2.8}$$

Plugging (2.2.8) into the original system (1.2.1) we get the nonlinear equations

$$\begin{aligned} \dot{v}_1^- &= A_1^-(t,\lambda)v_1^- + h_1^-(t,v_1^-,\lambda), \\ \dot{v}_1^+ &= A_1^+(t,\lambda)v_1^+ + h_1^+(t,v_1^+,\lambda), \\ \dot{v}_2^- &= A_2^-(t,\vartheta,\lambda)v_2^- + h_2^-(t,v_2^-,\vartheta,\lambda), \\ \dot{v}_2^+ &= A_2^+(t,\vartheta,\lambda)v_2^+ + h_2^+(t,v_2^+,\vartheta,\lambda) \end{aligned} \tag{2.2.9}$$

where

$$\begin{aligned} A_1^{\pm}(t,\lambda) &:= D_1 f(\gamma_1^{\pm}(\lambda)(t),\lambda), \\ A_2^{\pm}(t,\vartheta,\lambda) &:= D_1 f(\gamma_2^{\pm}(\vartheta,\lambda)(t),\lambda) \end{aligned}$$

and

$$\begin{aligned} h_1^{\pm}(t,v,\lambda) &:= f(\gamma_1^{\pm}(\lambda)(t)+v,\lambda) - f(\gamma_1^{\pm}(\lambda)(t),\lambda) - A_1^{\pm}(t,\lambda)v, \\ h_2^{\pm}(t,v,\vartheta,\lambda) &:= f(\gamma_2^{\pm}(\vartheta,\lambda)(t)+v,\lambda) - f(\gamma_2^{\pm}(\vartheta,\lambda)(t),\lambda) - A_2^{\pm}(t,\vartheta,\lambda)v. \end{aligned}$$

In order to find solutions that meet our premises, we state the following general boundary conditions for the solutions $v_j^{\pm}$ of (2.2.9):

$$v_1^{\pm}(0) \in Y_1, \quad v_2^{\pm}(0) \in W_2^- \oplus W_2^+ \oplus Z_2, \quad v_1^+(0) - v_1^-(0) \in Z_1, \quad v_2^+(0) - v_2^-(0) \in Z_2. \tag{2.2.10}$$

Note that the $v_2^{\pm}(0)$ are not in the subspace U. The U component of $x_2^{\pm}(0)$ is contributed only by $\gamma_2^{\pm}(0)$.
In a first step towards solutions of (2.2.9) we replace the function h by an arbitrary but small function g that only depends on t. Thus we get the following 'linearised equations':

$$\dot{v}_1^- = A_1^-(t,\lambda)v_1^- + g_1^-(t), \tag{2.2.11a}$$
$$\dot{v}_1^+ = A_1^+(t,\lambda)v_1^+ + g_1^+(t), \tag{2.2.11b}$$
$$\dot{v}_2^- = A_2^-(t,\vartheta,\lambda)v_2^- + g_2^-(t), \tag{2.2.11c}$$
$$\dot{v}_2^+ = A_2^+(t,\vartheta,\lambda)v_2^+ + g_2^+(t). \tag{2.2.11d}$$

The theory of exponential trichotomies (see Section A.1) tells us that due to the hyperbolicity of the equilibrium the homogenuous linear equation that corresponds to Equation (2.2.11a) has an exponential dichotomy on $\mathbb{R}^-$. Similarly, the homogenuous linear equation corresponding to Equation (2.2.11d) has an exponential dichotomy on $\mathbb{R}^+$. We denote the corresponding projections by P^+,$(\mathrm{id} - P^+)$ and P^-,$(\mathrm{id} - P^-)$.

Moreover, the homogenuous linear equation that corresponds to Equation (2.2.11b) has an exponential trichotomy on $\mathbb{R}^+$ due to the hyperbolicity of the periodic orbit. Similarly, the homogenuous linear equation corresponding to Equation (2.2.11c) has an exponential trichotomy on $\mathbb{R}^-$. We denote the corresponding projections by $Q_s^+, Q_c^+, Q_{sc}^+ = Q_s^+ + Q_c^+, Q_u^+$ and $Q_u^-, Q_c^-, Q_{cu}^- = Q_u^- + Q_c^-, Q_s^-$.
The exponential dichotomies and trichotomies fix the images of the projections $P^+(\cdot)$ and $P^-(\cdot)$, $Q_{sc}^+(\cdot)$ and $Q_{cu}^-(\cdot)$ such that

$$\begin{aligned} \mathrm{im}P^+(t,\vartheta,\lambda) &= T_{\gamma_2^+(\vartheta,\lambda)(t)} W_\lambda^s(p), \quad \mathrm{im}P^-(t,\lambda) = T_{\gamma_1^-(\lambda)(t)} W_\lambda^u(p), \\ \mathrm{im}Q_{sc}^+(t,\lambda) &= T_{\gamma_1^+(\lambda)(t)} W_\lambda^s(\Upsilon), \quad \mathrm{im}Q_{cu}^-(t,\vartheta,\lambda) = T_{\gamma_2^-(\vartheta,\lambda)(t)} W_\lambda^u(\Upsilon). \end{aligned}$$

Now we return to our remark from the beginning of Section 2.2 that we have some restrictions on choosing the linear subspace $W_1^+ \subset Y_1$. Here we choose W_1^+ such that $\mathrm{im}Q_s^+(0) = W_1^+$, this is always possible because $\mathrm{im}Q_s^+(0) \subset T_{\gamma_1(0)} W^s(\Upsilon)$ and the dimensions match. This setting implies that $\mathrm{im}Q_s^+(0) \subset Y_1$, this is important for the following considerations.
The exponential dichotomy/trichotomy fixes the images of the projections, however, we have some freedom in choosing the kernels (note that the image of the kernel of a projection P is equal to the image of $(\mathrm{id} - P)$). Here we stick to

$$\mathrm{im}\left(\mathrm{id} - P^+(0,\vartheta,\lambda)\right) = W_2^- \oplus Z_2, \quad \mathrm{im}\left(\mathrm{id} - P^-(0,\lambda)\right) = W_1^+ \oplus Z_1 \text{ and} \tag{2.2.12a}$$

$$\mathrm{im}\left(\mathrm{id} - Q_{sc}^+(0,\lambda)\right) = W_1^- \oplus Z_1, \quad \mathrm{im}\left(\mathrm{id} - Q_{cu}^-(0,\vartheta,\lambda)\right) = W_2^+ \oplus Z_2. \tag{2.2.12b}$$

The following lemma gives an important property of the projections $P^\pm$:

Lemma 2.2.4 *There are constants $c, \Omega > 0$ such that for all $\|\lambda\|, \|\vartheta\| < c$ and for all $\omega^\pm > \Omega$ the following holds:*

$$\mathrm{im}\left(\mathrm{id} - P^+(\omega^+,\vartheta,\lambda)\right) \oplus \mathrm{im}\left(\mathrm{id} - P^-(-\omega^-,\lambda)\right) = \mathbb{R}^n.$$

Moreover, this decomposition defines a projection $\tilde{P}(\omega^+,\omega^-,\vartheta,\lambda)$.
We set $\mathrm{im}\,\tilde{P}(\omega^+,\omega^-,\vartheta,\lambda) = \mathrm{im}\left(\mathrm{id} - P^+(\omega^+,\vartheta,\lambda)\right)$. The projection $\tilde{P}$ is uniformly bounded, i.e. there is a constant $M > 0$ such that $\left\|\tilde{P}(\omega^+,\omega^-,\vartheta,\lambda)\right\| \leq M$.

The proof of Lemma 2.2.4 can be found in [VF92].
Similarly, the following lemma holds for the projections of the exponential trichotomy.

Lemma 2.2.5 *There are constants $c, \Omega > 0$ such that for all $\|\lambda\|, \|\vartheta\| < c$ and for all $\omega^\pm > \Omega$ the following holds:*

$$\mathrm{im}\left(\mathrm{id} - Q_s^+(\omega^+,\lambda)\right) \oplus \mathrm{im}\left(\mathrm{id} - Q_{cu}^-(-\omega^-,\vartheta,\lambda)\right) = \mathbb{R}^n.$$

A proof can be found in [Rad04].
To simplify the following considerations and proofs we use a rescaling of the original ODE that allows us to handle the coupling conditions easily. The hypothesis below pays tribute to that rescaling, we postpone a justification to Section A.3.

(H 2.8) All solutions starting in a sufficiently small neighbourhood of $\gamma_1^+(0)$ ($\gamma_2^-(0)$, resp.) in Σ_1 (Σ_2, resp.) need the same time ϖ^+ (ϖ^-, resp.) to hit the Poincaré section $\Sigma_\Upsilon = \Upsilon_0 + Y_\Upsilon$ ($\Upsilon_0 \in \Upsilon$, Y_Υ is a $(n-1)$-dimensional linear subspace).

Now we state some important consequences of Hypothesis (H 2.8).

Lemma 2.2.6 *Let Φ_1^+ and Φ_2^- be the transition matrices of the homogenuous linear systems associated with* (2.2.11b) *and* (2.2.11c)*. Assume that Hypothesis* (H 2.8) *holds.*
Then the following holds:

$$\Phi_1^+(\varpi^+, 0, \lambda)(Y_1) = Y_\Upsilon \text{ and } \Phi_2^-(-\varpi^-, 0, \vartheta, \lambda)(Y_2) = Y_\Upsilon.$$

Proof. Let φ^t be the flow of system (1.2.1). Then Hypothesis (H 2.8) provides

$$\varphi^{\varpi^+}(\Sigma_1) = \Sigma_\Upsilon.$$

From $\Phi_1^+(\varpi^+, 0, \lambda) = D\varphi^{\varpi^+}(\gamma_1^+(\lambda)(0))$ and $T_{\gamma_1^+(\lambda)(0)}\Sigma_1 = Y_1$ follows the result for Φ_1^+. A similar computation gives the result for Φ_2^-. □

Lemma 2.2.7 *Using the notation introduced above, the following holds:*

$$\operatorname{im}\left(\mathrm{id} - Q_{sc}^+(\varpi^+, \lambda)\right) \subset Y_\Upsilon \text{ and } \operatorname{im}\left(\mathrm{id} - Q_{cu}^-(-\varpi^-, \vartheta, \lambda)\right) \subset Y_\Upsilon.$$

Proof. Let Φ_1^+ denote the transition matrix of the linear homogenuous system associated with (2.2.11b). First we show that $(\mathrm{id} - Q_{sc}^+(\varpi^+, \lambda))(\Phi_1^+(\varpi^+, 0, \lambda)\operatorname{im}(\mathrm{id} - Q_{sc}^+(0, \lambda))) \subset Y_\Upsilon$. Let $y \in \operatorname{im}(\mathrm{id} - Q_{sc}^+(0, \lambda)) \subset Y_1$. Then $y = (\mathrm{id} - Q_{sc}^+(0, \lambda))\, y$ holds since $(\mathrm{id} - Q_{sc}^+(0, \lambda))$ is a projection. Using the exponential trichotomy (A.1.4) and Lemma 2.2.6 we get

$$\begin{aligned}\left(\mathrm{id} - Q_{sc}^+(\varpi^+, \lambda)\right)(\Phi_1^+(\varpi^+, 0, \lambda)y) &= \Phi_1^+(\varpi^+, 0, \lambda)\left(\mathrm{id} - Q_{sc}^+(0, \lambda)\right) y \\ &= \Phi(\varpi^+, 0, \lambda)y \in Y_\Upsilon.\end{aligned}$$

Hence

$$(\mathrm{id} - Q_{sc}^+(\varpi^+, \lambda))\left(\Phi_1^+(\varpi^+, 0, \lambda)\operatorname{im}\left(\mathrm{id} - Q_{sc}^+(0, \lambda)\right)\right) \subset Y_\Upsilon. \tag{2.2.13}$$

Next we show that

$$\dim\left(\mathrm{id} - Q_{sc}^+(\varpi^+, \lambda)\right)(\Phi_1^+(\varpi^+, 0, \lambda)\operatorname{im}\left(\mathrm{id} - Q_{sc}^+(0, \lambda)\right)) = \dim\left(\mathrm{id} - Q_{sc}^+(\varpi^+, \lambda)\right).$$

Let $y \neq 0, y \in \operatorname{im}(\mathrm{id} - Q_{sc}^+(0, \lambda))$. Then $\Phi_1^+(\varpi^+, 0, \lambda)y \neq 0$. On the other hand,

$$\left(\mathrm{id} - Q_{sc}^+(\varpi^+, \lambda)\right)(\Phi_1^+(\varpi^+, 0, \lambda)y = \Phi_1^+(\varpi^+, 0, \lambda)\left(\mathrm{id} - Q_{sc}^+(0, \lambda)\right) y$$

holds.
Using that $\Phi_1^+(\varpi^+, 0, \lambda)$ is a diffeomorphism and $(\mathrm{id} - Q_{sc}^+(0, \lambda))\, y = y \neq 0$ it follows that

$$\dim\left(\Phi_1^+(\varpi^+, 0, \lambda)\operatorname{im}\left(\mathrm{id} - Q_{sc}^+(0, \lambda)\right)\right) = \dim\operatorname{im}\left(\mathrm{id} - Q_{sc}^+(0, \lambda)\right)$$

and hence

$$\begin{aligned}\dim\left(\left(\mathrm{id}-Q_{sc}^{+}(\varpi^{+},\lambda)\right)\left(\Phi_1^{+}(\varpi^{+},0,\lambda)\mathrm{im}\left(\mathrm{id}-Q_{sc}^{+}(0,\lambda)\right)\right)\right) &= \dim\mathrm{im}\left(\mathrm{id}-Q_{sc}^{+}(0,\lambda)\right)\\ &= \dim\mathrm{im}\left(\mathrm{id}-Q_{sc}^{+}(\varpi^{+},\lambda)\right),\end{aligned}$$

thus

$$\dim\left(\mathrm{id}-Q_{sc}^{+}(\varpi^{+},\lambda)\right)\left(\Phi_1^{+}(\varpi^{+},0,\lambda)\mathrm{im}\left(\mathrm{id}-Q_{sc}^{+}(0,\lambda)\right)\right)=\dim\left(\mathrm{id}-Q_{sc}^{+}(\varpi^{+},\lambda)\right). \quad (2.2.14)$$

From (2.2.13) and (2.2.14) follows $\mathrm{im}\,(\mathrm{id}-Q_{sc}^{+}(\varpi^{+},\lambda))\subset Y_\Upsilon$. Analogous considerations using Q_{cu}^{-} and Φ_2^{-} conclude the proof of the lemma.

□

Lemma 2.2.8 *Using the notation introduced above,*

$$Y_\Upsilon=\mathrm{im}\left(\mathrm{id}-Q_{sc}^{+}(\varpi^{+},\lambda)\right)\oplus\mathrm{im}\left(\mathrm{id}-Q_{cu}^{-}(-\varpi^{-},\vartheta,\lambda)\right)$$

holds.

Proof. For ϖ^{+},ϖ^{-} sufficiently large,

$$\mathrm{im}\left(\mathrm{id}-Q_{sc}^{+}(\varpi^{+},\lambda)\right)\cap\mathrm{im}\left(\mathrm{id}-Q_{cu}^{-}(-\varpi^{-},\vartheta,\lambda)\right)=\{0\}$$

holds, see Lemma 2.2.5.
The result follows immediately from Lemma 2.2.7 and

$$\begin{aligned}\dim\mathrm{im}\left(\mathrm{id}-Q_{sc}^{+}(\varpi^{+},\lambda)\right)+\dim\mathrm{im}\left(\mathrm{id}-Q_{cu}^{-}(-\varpi^{-},\vartheta,\lambda)\right) &= n-1\\ &= \dim Y_\Upsilon.\end{aligned}$$

□

Hence, due to the rescaling, it is possible to represent the Poincaré section Σ_Υ through the point $\Upsilon_0\in\Upsilon$ by

$$\Sigma_\Upsilon=\Upsilon_0+\underbrace{\left(\mathrm{im}\left(\mathrm{id}-Q_{sc}^{+}(\varpi^{+},\lambda)\right)\oplus\mathrm{im}\left(\mathrm{id}-Q_{cu}^{-}(-\varpi^{-},\vartheta,\lambda)\right)\right)}_{=:\,Y_\Upsilon}.$$

Remark 2.2.9 *In the following considerations, we always assume ϖ^{+} and ϖ^{-} to be sufficiently large and we usually omit the dependence on ϖ^{+} and ϖ^{-} in the notation.*

Function spaces

In this section we search for solutions of system (2.2.9) that satisfy certain (linear) boundary and certain jump conditions. Later we use the Banach Fixed Point Theorem and therefore we need to define appropriate function spaces.

Definition 2.2.10 *Let $\varpi^{+},\varpi^{-},\omega\in\mathbb{R}^{+}$. The space $\mathcal{V}_\omega$ denotes the space of quadruples of functions $v=(v_1^{-},v_1^{+},v_2^{-},v_2^{+})\in C([-\omega,0],\mathbb{R}^n)\times C([0,\varpi^{+}],\mathbb{R}^n)\times C([-\varpi^{-},0],\mathbb{R}^n)\times C([0,\omega],\mathbb{R}^n)$.*

We equip the function space $\mathcal{V}_\omega$ with a maximum norm as follows (we use the supremum norm for the C spaces):

$$\|v\|_{\mathcal{V}_\omega} := \max\left\{\left\|v_1^-\right\|, \left\|v_1^+\right\|, \left\|v_2^-\right\|, \left\|v_2^+\right\|\right\}.$$

Remark 2.2.11 *In the formulation of the boundary conditions in the following lemmas we use the notation* $\alpha = (\alpha^-, \alpha^+) \in (\mathrm{id} - Q_{cu}^-(-\varpi^-, \vartheta, \lambda)) \times (\mathrm{id} - Q_{sc}^+(\varpi^+, \lambda))$.

Here is the main theorem of this section:

Theorem 2.2.12 *There are constants* $\bar{c}, \tilde{c}, \Omega > 0$ *such that for all* $\omega > \Omega$ *and given* $\lambda \in \mathbb{R}^m$, $\alpha = (\alpha^-, \alpha^+)$, $\vartheta \in U$ *with* $\|\lambda\|, \|\vartheta\| < \bar{c}$ *and* $\|\alpha\| < \tilde{c}$, *there is a unique solution* $v \in \mathcal{V}_\omega$ *of* (2.2.9) *such that*

(i) $v_1^-(0), v_1^+(0) \in W_1^- \oplus W_1^+ \oplus Z_1$ *and* $v_2^-(0), v_2^+(0) \in W_2^- \oplus W_2^+ \oplus Z_2$,

(ii) $v_1^-(0) - v_1^+(0) \in Z_1$ *and* $v_2^-(0) - v_2^+(0) \in Z_2$,

(iii) $v_1^-(-\omega) - v_2^+(\omega) = \gamma_2^+(\omega) - \gamma_1^-(-\omega)$ *and*

(iv) $(\mathrm{id} - Q_{sc}^+(\varpi^+, \lambda))\, v_1^+(\varpi^+) = \alpha^+$ *and* $(\mathrm{id} - Q_{cu}^-(-\varpi^-, \vartheta, \lambda))\, v_2^-(-\varpi^-) = \alpha^-$.

Moreover, for the functions

$$\begin{aligned}\tilde{\alpha}_\perp^+(\alpha, \vartheta, \lambda) &:= Q_s^+(\varpi^+, \lambda) v_1^+(\alpha, \vartheta, \lambda)(\varpi^+),\\ \tilde{\alpha}_\perp^-(\alpha, \vartheta, \lambda) &:= Q_u^-(-\varpi^-, \vartheta, \lambda) v_2^-(\alpha, \vartheta, \lambda)(-\varpi^-)\end{aligned}$$

there are constants $\hat{C}, \bar{\delta}^s, \bar{\delta}^u > 0$ *such that the estimates*

$$\begin{aligned}\left\|\tilde{\alpha}_\perp^+(\alpha, \vartheta, \lambda)\right\| &\le 2\hat{C}\tilde{c}e^{-\bar{\delta}^s\varpi^+} + \frac{2\tilde{c}}{3},\\ \left\|\tilde{\alpha}_\perp^-(\alpha, \vartheta, \lambda)\right\| &\le 2\hat{C}\tilde{c}e^{-\bar{\delta}^u\varpi^-} + \frac{2\tilde{c}}{3}\end{aligned} \tag{2.2.15}$$

hold.
For the derivatives the estimates

$$\begin{aligned}\left\|D_1\alpha_\perp^+(\alpha, \vartheta, \lambda)\right\| &\le \frac{1}{6}\left(e^{-\bar{\delta}^s\varpi^+} + 1\right) + \hat{C}e^{-\bar{\delta}^s\varpi^+},\\ \left\|D_1\alpha_\perp^-(\alpha, \vartheta, \lambda)\right\| &\le \frac{1}{6}\left(e^{-\bar{\delta}^u\varpi^-} + 1\right) + \hat{C}e^{-\bar{\delta}^u\varpi^-}\end{aligned} \tag{2.2.16}$$

hold.

We prove this theorem in several steps. First, we show that a boundary value problem with purely linear boundary conditions near the equilibrium and near the periodic orbit has a unique solution. Then we adjust the boundary condition near the equilibrium in terms of a difference condition. Finally, we formulate and solve a fixed point equation which has the sought-after solution as a unique solution.

Fully linearised problem

Now we are prepared for the first result which states that there is a unique solution of system (2.2.11) satisfying fully linear boundary conditions.
To formulate these boundary conditions we use $a \in \mathbb{R}^n$ and $\alpha = (\alpha^-, \alpha^+)$ as described in Remark 2.2.11.
More precisely, we approximate the coupling of x_2^+ and x_1^- near the equilibrium by

$$\begin{aligned} \left(\mathrm{id} - P^+(\omega, \vartheta, \lambda)\right) v_2^+(\omega) = a^+(\omega) := \left(\mathrm{id} - P^+(\omega, \vartheta, \lambda)\right) a, \\ \left(\mathrm{id} - P^-(-\omega, \lambda)\right) v_1^-(-\omega) = a^-(\omega) := \left(\mathrm{id} - P^-(-\omega, \lambda)\right) a, \end{aligned} \tag{2.2.17}$$

and we use

$$\begin{aligned} \left(\mathrm{id} - Q_{sc}^+(\varpi^+, \lambda)\right) v_1^+(\varpi^+) = \alpha^+, \\ \left(\mathrm{id} - Q_{cu}^-(-\varpi^-, \vartheta, \lambda)\right) v_2^-(-\varpi^-) = \alpha^- \end{aligned} \tag{2.2.18}$$

as boundary conditions near the periodic orbit.
Then there is one unique solution that satisfies these linear boundary conditions.

Lemma 2.2.13 *There are constants $c, \Omega > 0$ such that for all $\omega > \Omega$ and $\vartheta \in U$, $\lambda \in \mathbb{R}^m$ with $\|\vartheta\|, \|\lambda\| < c$ and for given $g \in \mathcal{V}_\omega$ and given $a \in \mathbb{R}^n$ and $\alpha = (\alpha^-, \alpha^+)$, the boundary value problem* (2.2.11),((2.2.10),(2.2.17),(2.2.18)) *has a unique solution*

$$\bar{v}(g, a, \alpha, \vartheta, \lambda) = \left(\bar{v}_1^-, \bar{v}_1^+, \bar{v}_2^-, \bar{v}_2^+\right)(g, a, \alpha, \vartheta, \lambda) \in \mathcal{V}_\omega.$$

Proof. Let $\Phi_i^\pm(\cdot, \cdot)$ denote the transition matrix of the homogenuous linear equations corresponding to (2.2.11). In this proof we keep λ fixed for the moment and do not write down the dependencies of Q_{sc}^+, Q_{cu}^-, P^+, P^- and $\Phi_j^\pm$ on λ and ϑ.
Using the variation of constant formula for (2.2.11) gives

$$\begin{aligned} v_j^+(t) = \Phi_j^+(t, 0) v_j^+(0) + \int_0^t \Phi_j^+(t, \tau) g_j^+(\tau) d\tau, \\ v_j^-(t) = \Phi_j^-(t, 0) v_j^-(0) + \int_0^t \Phi_j^-(t, \tau) g_j^-(\tau) d\tau \end{aligned} \tag{2.2.19}$$

$(j = 1, 2)$ as solutions.
Setting $t = \omega$ ($t = -\omega, t = \varpi^+, t = -\varpi^-$ resp.) yields

$$\begin{aligned} v_1^-(-\omega) &= \Phi_1^-(-\omega, 0) v_1^-(0) + \int_0^{-\omega} \Phi_1^-(-\omega, \tau) g_1^-(\tau) d\tau, \\ v_1^+(\varpi^+) &= \Phi_1^+(\varpi^+, 0) v_1^+(0) + \int_0^{\varpi^+} \Phi_1^+(\varpi^+, \tau) g_1^+(\tau) d\tau, \\ v_2^-(-\varpi^-) &= \Phi_2^-(-\varpi^-, 0) v_2^-(0) + \int_0^{-\varpi^-} \Phi_2^-(-\varpi^-, \tau) g_2^-(\tau) d\tau, \\ v_2^+(\omega) &= \Phi_2^+(\omega, 0) v_2^+(0) + \int_0^{\omega} \Phi_2^+(\omega, \tau) g_2^+(\tau) d\tau. \end{aligned}$$

The above system of equations can be rewritten as

$$\begin{aligned}
\Phi_1^-(0,-\omega)\,v_1^-(-\omega) &= v_1^-(0) - \int_{-\omega}^{0} \Phi_1^-(0,\tau) g_1^-(\tau) d\tau,\\
\Phi_1^+(0,\varpi^+) v_1^+(\varpi^+) &= v_1^+(0) + \int_0^{\varpi^+} \Phi_1^+(0,\tau) g_1^+(\tau) d\tau,\\
\Phi_2^-(0,-\varpi^-) v_2^-(-\varpi^-) &= v_2^-(0) - \int_{-\varpi^-}^{0} \Phi_2^-(0,\tau) g_2^-(\tau) d\tau,\\
\Phi_2^+(0,\omega)\,v_2^+(\omega) &= v_2^+(0) + \int_0^{\omega} \Phi_2^+(0,\tau) g_2^+(\tau) d\tau.
\end{aligned}$$

Finally, we apply $(\mathrm{id} - Q_{sc}^+(0))$, $(\mathrm{id} - Q_{cu}^-(0))$, $(\mathrm{id} - P^+(0))$ and $(\mathrm{id} - P^-(0))$ and use properties (A.1.2) and (A.1.4) of the exponential dichotomy/trichotomy:

$$\begin{aligned}
(\mathrm{id} - P^-(0)) v_1^-(0) &= \Phi_1^-(0,-\omega)\left(\mathrm{id} - P^-(-\omega)\right) v_1^-(-\omega)\\
&\quad + \int_{-\omega}^{0} \Phi_1^-(0,\tau)(\mathrm{id} - P^-(\tau)) g_1^-(\tau) d\tau,\\
(\mathrm{id} - Q_{sc}^+(0)) v_1^+(0) &= \Phi_1^+(0,\varpi^+)(\mathrm{id} - Q_{sc}^+(\varpi^+)) v_1^+(\varpi^+)\\
&\quad - \int_0^{\varpi^+} \Phi_1^+(0,\tau)(\mathrm{id} - Q_{sc}^+(\tau)) g_1^+(\tau) d\tau,\\
(\mathrm{id} - Q_{cu}^-(0)) v_2^-(0) &= \Phi_2^-(0,-\varpi^-)(\mathrm{id} - Q_{cu}^-(-\varpi^-)) v_2^-(-\varpi^-)\\
&\quad + \int_{-\varpi^-}^{0} \Phi_2^-(0,\tau)(\mathrm{id} - Q_{cu}^-(\tau)) g_2^-(\tau) d\tau,\\
(\mathrm{id} - P^+(0)) v_2^+(0) &= \Phi_2^+(0,\omega)\left(\mathrm{id} - P^+(\omega)\right) v_2^+(\omega)\\
&\quad - \int_0^{\omega} \Phi_2^+(0,\tau)(\mathrm{id} - P^+(\tau)) g_2^+(\tau) d\tau
\end{aligned}$$

and thus

$$\begin{aligned}
(\mathrm{id} - P^-(0)) v_1^-(0) &= \Phi_1^-(0,-\omega)\, a^- + \int_{-\omega}^{0} \Phi_1^-(0,\tau)(\mathrm{id} - P^-(\tau)) g_1^-(\tau) d\tau,\\
(\mathrm{id} - Q_{sc}^+(0)) v_1^+(0) &= \Phi_1^+(0,\varpi^+)\alpha^+ - \int_0^{\varpi^+} \Phi_1^+(0,\tau)(\mathrm{id} - Q_{sc}^+(\tau)) g_1^+(\tau) d\tau,
\end{aligned} \tag{2.2.20a}$$

$$\begin{aligned}
(\mathrm{id} - Q_{cu}^-(0)) v_2^-(0) &= \Phi_2^-(0,-\varpi^-)\alpha^- + \int_{-\varpi^-}^{0} \Phi_2^-(0,\tau)(\mathrm{id} - Q_{cu}^-(\tau)) g_2^-(\tau) d\tau,\\
(\mathrm{id} - P^+(0)) v_2^+(0) &= \Phi_2^+(0,\omega)\, a^+ - \int_0^{\omega} \Phi_2^+(0,\tau)(\mathrm{id} - P^+(\tau)) g_2^+(\tau) d\tau.
\end{aligned} \tag{2.2.20b}$$

We look for solutions that satisfy (2.2.10), thus we can decompose $v_{1,2}^{\pm}(0)$ as follows

$$\begin{aligned} v_1^+(0) &= w_1^+ + w_1^- + z_1^+, \\ v_1^-(0) &= w_1^+ + w_1^- + z_1^-, \\ v_2^+(0) &= w_2^+ + w_2^- + z_2^+, \\ v_2^-(0) &= w_2^+ + w_2^- + z_2^- \end{aligned} \tag{2.2.21}$$

where $w_1^+ \in W_1^+$, $w_1^- \in W_1^-$, $z_1^\pm \in Z_1$, $z_2^\pm \in Z_2$ and $w_2^\pm \in W_2^\pm$.
So, the left-hand side of (2.2.20a) can be considered as a linear mapping

$$L_1 : W_1^+ \times W_1^- \times Z_1 \times Z_1 \to (W_1^+ \oplus Z_1) \times (W_1^- \oplus Z_1).$$

Similarly, the left-hand side of (2.2.20b) can be considered as a linear mapping

$$L_2 : W_2^+ \times W_2^- \times Z_2 \times Z_2 \to (W_2^+ \oplus Z_2) \times (W_2^- \oplus Z_2).$$

These mappings L_1, L_2 are invertible and so we can solve (2.2.20) for

$$(w_1^+, w_1^-, z_1^+, z_1^-, w_2^+, w_2^-, z_2^+, z_2^-) = (w_1^+, w_1^-, z_1^+, z_1^-, w_2^+, w_2^-, z_2^+, z_2^-)(g, a, \alpha, \vartheta, \lambda).$$

This together with (2.2.21) and (2.2.19) completes the proof. □

In the following lemma we give norm estimates for the solutions $\bar{v}$ and the quantities $\bar{\alpha}_\perp^\pm$ which are complementary to $\alpha^\pm$.

Lemma 2.2.14 *Let Lemma 2.2.13 hold. Then there is a constant $C > 0$ such that the following estimate holds:*

$$\|\bar{v}(g, a, \alpha, \vartheta, \lambda)\| \le C \left(\|a\| + \|\alpha\| + \|g\| \right). \tag{2.2.22}$$

Moreover, there is a constant $\delta > 0$ such that

$$\begin{aligned} &\left\| P^+(\omega) \bar{v}_2^+(g, a, \alpha, \vartheta, \lambda)(\omega) \right\| + \left\| P^-(-\omega) \bar{v}_1^-(g, a, \alpha, \vartheta, \lambda)(-\omega) \right\| \\ &\quad \le C e^{-\delta\omega} (\|\alpha\| + \|a\|) + C \|g\| \end{aligned} \tag{2.2.23}$$

holds.
For the functions

$$\begin{aligned} \bar{\alpha}_\perp^+(g, a, \alpha, \vartheta, \lambda) &:= Q_s^+(\varpi^+, \lambda) \bar{v}_1^+(g, a, \alpha, \vartheta, \lambda)(\varpi^+), \\ \bar{\alpha}_\perp^-(g, a, \alpha, \vartheta, \lambda) &:= Q_u^-(-\varpi^-, \vartheta, \lambda) \bar{v}_2^-(g, a, \alpha, \vartheta, \lambda)(-\varpi^-) \end{aligned} \tag{2.2.24}$$

there are constants $\bar{\delta}^s, \bar{\delta}^u > 0$ such that the estimates

$$\begin{aligned} \left\| \bar{\alpha}_\perp^+(g, a, \alpha, \vartheta, \lambda) \right\| &\le C \left(\left\| a^- \right\| + \left\| \alpha^+ \right\| + \|g\| \right) e^{-\bar{\delta}^s \varpi^+} + C \|g\|, \\ \left\| \bar{\alpha}_\perp^-(g, a, \alpha, \vartheta, \lambda) \right\| &\le C \left(\left\| a^+ \right\| + \left\| \alpha^- \right\| + \|g\| \right) e^{-\bar{\delta}^u \varpi^-} + C \|g\| \end{aligned} \tag{2.2.25}$$

hold.

For the derivatives of $\bar{\alpha}_\perp^+$ and $\bar{\alpha}_\perp^-$ the estimates

$$\begin{aligned}\left\|D_3\bar{\alpha}_\perp^+(g,a,\alpha,\vartheta,\lambda)\right\| &\leq Ce^{-\bar{\delta}^s\varpi^+},\\ \left\|D_3\bar{\alpha}_\perp^-(g,a,\alpha,\vartheta,\lambda)\right\| &\leq Ce^{-\bar{\delta}^u\varpi^-}\end{aligned} \tag{2.2.26}$$

and

$$\begin{aligned}\left\|D_2\bar{\alpha}_\perp^+(g,a,\alpha,\vartheta,\lambda)\right\| &\leq Ce^{-\bar{\delta}^s\varpi^+},\\ \left\|D_2\bar{\alpha}_\perp^-(g,a,\alpha,\vartheta,\lambda)\right\| &\leq Ce^{-\bar{\delta}^u\varpi^-}\end{aligned} \tag{2.2.27}$$

and

$$\begin{aligned}\left\|D_1\bar{\alpha}_\perp^+(g,a,\alpha,\vartheta,\lambda)\right\| &\leq C\left(e^{-\bar{\delta}^s\varpi^+}+1\right),\\ \left\|D_1\bar{\alpha}_\perp^-(g,a,\alpha,\vartheta,\lambda)\right\| &\leq C\left(e^{-\bar{\delta}^u\varpi^-}+1\right)\end{aligned} \tag{2.2.28}$$

hold.

Proof. To prove estimate (2.2.22) we decompose v_1^+ by means of the projection Q_{sc}^+:

$$v_1^+(...)(t) = (\mathrm{id} - Q_{sc}^+(t))v_1^+(...)(t) + Q_{sc}^+(t)v_1^+(...)(t).$$

Thus we have

$$\left\|v_1^+(...)(t)\right\| \leq \left\|(\mathrm{id} - Q_{sc}^+(t))v_1^+(...)(t)\right\| + \left\|Q_{sc}^+(t)v_1^+(...)(t)\right\|. \tag{2.2.29}$$

We use the variation of constants formula and the estimates of the exponential trichotomy to derive an estimate for the second term of (2.2.29):

$$\begin{aligned}\left\|Q_{sc}^+(t)v_1^+(...)(t)\right\| &= \left\|Q_{sc}^+(t)\left(\Phi_1^+(t,0)v_1^+(0)+\int_0^t\Phi_1^+(t,\tau)g_1^+(\tau)d\tau\right)\right\|\\ &\leq \left\|Q_{sc}^+(t)\Phi_1^+(t,0)v_1^+(0)\right\| + \left\|Q_{sc}^+(t)\int_0^t\Phi_1^+(t,\tau)g_1^+(\tau)d\tau\right\|\\ &\leq K(e^{-\bar{\delta}^s t}+e^{\bar{\delta}^c t})\left\|v_1^+(0)\right\| + M\left\|g_1^+\right\|\\ &\leq K(e^{-\bar{\delta}^s t}+1)\left\|v_1^+(0)\right\| + M\left\|g_1^+\right\|.\end{aligned}$$

The constants $\bar{\delta}^s$, $\bar{\delta}^c$ and K are the corresponding constants of the exponential trichotomy ($\bar{\delta}^s > \bar{\delta}^c = 0$, see Section A.1.1).
We estimate $\left\|v_1^+(0)\right\|$ by applying L_1^{-1} to (2.2.20a) and exploiting the exponential trichotomy once again:

$$\left\|v_1^+(0)\right\| \leq \left\|L_1^{-1}\right\|\tilde{K}\left(\left\|\alpha^+\right\|+\left\|a^-\right\|\right) + M\left\|(g_1^+,g_1^-)\right\|. \tag{2.2.30}$$

Thus we have

$$\left\|Q_{sc}^+(t)v_1^+(...)(t)\right\| \leq C_1(\|\alpha\|+\|a\|+\|g\|).$$

For the first term of the right hand side of (2.2.29) we use

$$\begin{aligned}(\mathrm{id}-Q^+_{sc}(t))v^+_1(...)(t) =&\Phi^+_1(t,\varpi^+)(\mathrm{id}-Q^+_{sc}(\varpi^+))\alpha^+\\ &-\int_t^{\varpi^+}\Phi^+_1(t,\tau)(\mathrm{id}-Q^+_{sc}(\tau))g^+_1(\tau)d\tau\end{aligned}$$

and thus we finally get

$$\left\|(\mathrm{id}-Q^+_{sc}(t))v^+_1(...)(t)\right\|\leq C_2(\left\|\alpha^+\right\|+\|g\|).$$

Proceeding with v^-_1, v^+_2 and v^-_2 in a similar way we finally end up with estimate (2.2.22). Now we consider estimate (2.2.23).

$$\begin{aligned}&\left\|P^+(\omega)\bar v^+_2(g,a,\alpha,\vartheta,\lambda)(\omega)\right\|+\left\|P^-(-\omega)\bar v^-_1(g,a,\alpha,\vartheta,\lambda)(-\omega)\right\|\\ &=\left\|P^+(\omega)\left(\Phi^+_2(\omega,0)v^+_2(0)+\int_0^{\omega}\Phi^+_2(\omega,\tau)g^+_2(\tau)d\tau\right)\right\|\\ &\quad+\left\|P^-(-\omega)\left(\Phi^-_1(-\omega,0)v^-_1(0)-\int_{-\omega}^{0}\Phi^-_1(-\omega,\tau)g^-_1(\tau)d\tau\right)\right\|\\ &\leq e^{-\delta\omega}(\left\|v^+_2(0)\right\|+\left\|v^-_1(0)\right\|)+M\left\|g\right\|.\end{aligned}$$

Note that $\delta:=\min\{\delta^u,\delta^s\}$ where δ^s and δ^u are the exponents of the exponential dichotomies (δ^s is from the dichotomy on $\mathbb{R}^+$ while δ^u is from the dichotomy on $\mathbb{R}^-$. This notation is unambiguous since we do not use the remaining exponents). Together with (2.2.30) this gives the desired estimate.
For estimate (2.2.25) we exploit the exponential trichotomy again (note that $\bar\alpha^\pm_\perp$ is defined in (2.2.24)):

$$\begin{aligned}\left\|\bar\alpha^+_\perp(g,a,\alpha,\lambda)\right\|&=\left\|Q^+_s(\varpi^+)\left(\Phi^+_1(\varpi^+,0)v^+_1(0)+\int_0^{\varpi^+}\Phi^+_1(\varpi^+,\tau)g^+_1(\tau)d\tau\right)\right\|\\ &\leq\left\|Q^+_s(\varpi^+)\Phi^+_1(\varpi^+,0)v^+_1(0)\right\|+\left\|Q^+_s(\varpi^+)\int_0^{\varpi^+}\Phi^+_1(\varpi^+,\tau)g^+_1(\tau)d\tau\right\|\\ &\leq Ke^{-\bar\delta^s\varpi^+}\left\|v^+_1(0)\right\|+M\left\|g^+_1\right\|\\ &\leq C(\left\|a^-\right\|+\left\|\alpha^+\right\|+\|g\|)e^{-\bar\delta^s\varpi^+}+C\|g\|.\end{aligned}$$

For the derivative we note that the dependencies of $v^\pm_{1/2}$ on (g,a,α) are linear (this can be seen by applying $L^{-1}_{1/2}$ to (2.2.20)). This means that we can write (exemplarily for v^+_1) $v^+_1(g,a,\alpha,\vartheta,\lambda)=L(\vartheta,\lambda)(g,a,\alpha)=L(\vartheta,\lambda)(g,0,0)+L(\vartheta,\lambda)(0,a,0)+L(\vartheta,\lambda)(0,0,\alpha)$ for some linear operator L depending on ϑ and λ and hence (due to the definition) $\alpha_\perp$ also depends linearly on (g,a,α). Thus we can establish the estimates

$$\left\|D_3\bar\alpha^+_\perp(g,a,\alpha,\vartheta,\lambda)\right\|\leq Ce^{-\bar\delta^s\varpi^+}$$

and

$$\left\|D_2\bar\alpha^+_\perp(g,a,\alpha,\vartheta,\lambda)\right\|\leq Ce^{-\bar\delta^s\varpi^+}$$

and

$$\left\|D_1\bar{\alpha}_\perp^+(g,a,\alpha,\vartheta,\lambda)\right\| \leq C\left(e^{-\bar{\delta}^s\varpi^+}+1\right).$$

For $\bar{\alpha}_\perp^-$ similar estimates can be drawn. This completes the proof of the lemma.

□

The next step towards the coupling of the solutions near the equilibrium is given by the following lemma. Instead of the boundary condition (2.2.17) we now use

$$v_2^+(\omega) - v_1^-(-\omega) = d \tag{2.2.31}$$

for given $d \in \mathbb{R}^n$.
Then we can state:

Lemma 2.2.15 *There are constants $c, \Omega > 0$ such that for all $\omega > \Omega$ and $\vartheta \in U$, $\lambda \in \mathbb{R}^m$ with $\|\vartheta\|, \|\lambda\| < c$ and for given $g \in \mathcal{V}_\omega$ and given $d \in \mathbb{R}^n$ and $\alpha = (\alpha^-, \alpha^+)$, the boundary value problem* (2.2.11),((2.2.10),(2.2.31),(2.2.18)) *has a unique solution*

$$\hat{v}(g,d,\alpha,\vartheta,\lambda) = \left(\hat{v}_1^-, \hat{v}_1^+, \hat{v}_2^-, \hat{v}_2^+\right)(g,d,\alpha,\vartheta,\lambda) \in \mathcal{V}_\omega.$$

Proof. The idea of the proof is to find an $a = a^+ + a^-$ such that the conditions for Lemma 2.2.13 are satisfied.
We consider

$$\bar{v}_2^+(g,a,\alpha,\vartheta,\lambda)(\omega) - \bar{v}_1^-(g,a,\alpha,\vartheta,\lambda)(-\omega) = d$$

with boundary conditions

$$\begin{aligned}
(\mathrm{id} - Q_{cu}^-(-\varpi^-,\vartheta,\lambda))\bar{v}_2^-(-\varpi^-) &= \alpha^-,\\
(\mathrm{id} - Q_{sc}^+(\varpi^+,\lambda))\bar{v}_1^+(\varpi^+) &= \alpha^+,\\
\left(\mathrm{id} - P^+(\omega,\vartheta,\lambda)\right)\bar{v}_2^+(\omega) &= a^+,\\
\left(\mathrm{id} - P^-(-\omega,\lambda)\right)\bar{v}_1^-(-\omega) &= a^-
\end{aligned}$$

and solve this system for a.
We have

$$a^+ - a^- = d - P^+(\omega,\vartheta,\lambda)\,\bar{v}_2^+(\omega) + P^-(-\omega,\lambda)\,\bar{v}_1^-(-\omega).$$

Now we can use the projection $\tilde{P} := \tilde{P}(\omega,\vartheta,\lambda)$ introduced in Lemma 2.2.4 (such that $\tilde{P}a = a^+$ and $(\mathrm{id} - \tilde{P})a = a^-$). With $a = a^+ + a^-$ we write

$$a = \left(-\mathrm{id} + 2\tilde{P}(\omega,\vartheta,\lambda)\right)\left(d - P^+(\omega,\vartheta,\lambda)\,\bar{v}_2^+(\omega) + P^-(-\omega,\lambda)\,\bar{v}_1^-(-\omega)\right).$$

Since the dependence of $\bar{v}_{1,2}^\pm$ on (g,a,α) is linear, the right-hand side of the above equation also depends linearly on (g,a,α) and thus the equation can be written as

$$a = L_1(\vartheta,\lambda)a + L_2(\vartheta,\lambda)g + L_3(\vartheta,\lambda)d + L_4(\vartheta,\lambda)\alpha, \tag{2.2.32}$$

where $L_i(\vartheta,\lambda)(\cdot)$, $i = 1,2,3,4$, are linear operators depending on ϑ and λ.
The operator $(\mathrm{id} - L_1)$ is invertible (see (2.2.23)) for sufficiently large ω, hence we can solve the equation for $a = a(g,d,\alpha,\vartheta,\lambda)$ and thus we have finally $\hat{v} = \bar{v}(g,a(g,d,\alpha,\vartheta,\lambda),\alpha,\vartheta,\lambda)$.

□

Lemma 2.2.16 *Let Lemma 2.2.15 hold. Then there is a constant $\hat{C} > 0$ such that*

$$\|\hat{v}(g,d,\alpha,\vartheta,\lambda)\| \leq \hat{C}\left(\|g\| + \|d\| + \|\alpha\|\right). \tag{2.2.33}$$

For the functions

$$\begin{aligned}\hat{\alpha}_\perp^+(g,d,\alpha,\vartheta,\lambda) &:= Q_s^+(\varpi^+,\lambda)\hat{v}_1^+(g,d,\alpha,\vartheta,\lambda)(\varpi^+),\\ \hat{\alpha}_\perp^-(g,d,\alpha,\vartheta,\lambda) &:= Q_u^-(-\varpi^-,\vartheta,\lambda)\hat{v}_2^-(g,d,\alpha,\vartheta,\lambda)(-\varpi^-)\end{aligned}$$

there are constants $\bar{\delta}^s, \bar{\delta}^u > 0$ such that the estimates:

$$\begin{aligned}\left\|\hat{\alpha}_\perp^+(g,d,\alpha,\vartheta,\lambda)\right\| &\leq \hat{C}\left(\|g\| + \|d\| + \|\alpha\|\right)e^{-\bar{\delta}^s\varpi^+} + \hat{C}\|g\|,\\ \left\|\hat{\alpha}_\perp^-(g,d,\alpha,\vartheta,\lambda)\right\| &\leq \hat{C}\left(\|g\| + \|d\| + \|\alpha\|\right)e^{-\bar{\delta}^u\varpi^-} + \hat{C}\|g\|\end{aligned} \tag{2.2.34}$$

hold.
For the derivatives

$$\begin{aligned}\left\|D_3\hat{\alpha}_\perp^+(g,d,\alpha,\vartheta,\lambda)\right\| &\leq \hat{C}e^{-\bar{\delta}^s\varpi^+},\\ \left\|D_3\hat{\alpha}_\perp^-(g,d,\alpha,\vartheta,\lambda)\right\| &\leq \hat{C}e^{-\bar{\delta}^u\varpi^-}\end{aligned} \tag{2.2.35}$$

and

$$\begin{aligned}\left\|D_1\hat{\alpha}_\perp^+(g,d,\alpha,\vartheta,\lambda)\right\| &\leq \hat{C}(e^{-\bar{\delta}^s\varpi^+} + 1),\\ \left\|D_1\hat{\alpha}_\perp^-(g,d,\alpha,\vartheta,\lambda)\right\| &\leq \hat{C}(e^{-\bar{\delta}^u\varpi^-} + 1)\end{aligned} \tag{2.2.36}$$

hold.

Proof. Recall from the proof of Lemma 2.2.15 that $\hat{v}(g,d,\alpha,\vartheta,\lambda) = \bar{v}(g,a(g,d,\alpha,\vartheta,\lambda),\alpha,\vartheta,\lambda)$. From (2.2.32) and (2.2.23) we get $\|a\| \leq \hat{C}_2(\|g\| + \|d\| + \|\alpha\|)$. The estimate (2.2.33) then follows immediately from (2.2.22); the remaining estimates follow from (2.2.26), (2.2.27) and (2.2.28).

□

Coupling near the equilibrium

The next step is the coupling of the solutions x_2^+ and x_1^- near the equilibrium. We use

$$x_2^+(\omega) = \gamma_2^+(\omega) + v_2^+(\omega) = \gamma_1^-(-\omega) + v_1^-(-\omega) = x_1^-(-\omega) \tag{2.2.37}$$

as the corresponding boundary condition.
Based on Lemma 2.2.15, we can formulate a fixed point problem in the function space $\mathcal{V}_\omega$ (as stated in Definition 2.2.10) such that a solution of this fixed point equation corresponds to a solution of the nonlinear boundary value problem (2.2.9),((2.2.10),(2.2.37),(2.2.18)).
To formulate the fixed point equation we need a so-called Nemyzki operator to deal with the nonlinearity h. First we introduce four operators as follows:

$$\begin{aligned}H_1^- : C([-\omega,0],\mathbb{R}^n) \times \mathbb{R}^m &\to C([-\omega,0],\mathbb{R}^n)\\ (v,\lambda) &\mapsto H_1^-(v,\lambda) := h_1^-(\cdot,v(\cdot),\lambda);\end{aligned}$$

$$
\begin{aligned}
H_1^+ : C([0,\varpi^+],\mathbb{R}^n)\times\mathbb{R}^m &\to C([0,\varpi^+],\mathbb{R}^n)\\
(v,\lambda) &\mapsto H_1^+(v,\lambda) := h_1^+(\cdot,v(\cdot),\lambda);\\
H_2^- : C([-\varpi^-,0],\mathbb{R}^n)\times U\times\mathbb{R}^m &\to C([-\varpi^-,0],\mathbb{R}^n)\\
(v,\vartheta,\lambda) &\mapsto H_2^-(v,\vartheta,\lambda) := h_2^-(\cdot,v(\cdot),\vartheta,\lambda);\\
H_2^+ : C([0,\omega],\mathbb{R}^n)\times U\times\mathbb{R}^m &\to C([0,\omega],\mathbb{R}^n)\\
(v,\vartheta,\lambda) &\mapsto H_2^+(v,\vartheta,\lambda) := h_2^+(\cdot,v(\cdot),\vartheta,\lambda).
\end{aligned}
$$

Lemma 2.2.17 *The operators $H_{1,2}^{\pm}$ are smooth mappings and the following holds:*

$$
\begin{aligned}
\left(D_1H_1^{\pm}(v,\lambda)w\right)(t) &= D_2h_1^{\pm}(t,v(t),\lambda)w(t),\\
\left(D_1H_2^{\pm}(v,\vartheta,\lambda)w\right)(t) &= D_2h_2^{\pm}(t,v(t),\vartheta,\lambda)w(t).
\end{aligned}
$$

Proof. The proof is carried out exemplarily for H_1^+.
Using the mean value theorem leads to

$$
\begin{aligned}
&\left\|H_1^+(v+w,\lambda)-H_1^+(v,\lambda)-D_2h_1^+(\cdot,v(\cdot),\lambda)w(\cdot)\right\|\frac{1}{\|w\|}\\
&=\sup_{t\in[0,\varpi^+]}\left\|h_1^+(t,(v+w)(t),\lambda)-h_1^+(t,v(t),\lambda)-D_2h_1^+(t,v(t),\lambda)w(t)\right\|\frac{1}{\|w\|}\\
&\le\sup_{t\in[0,\varpi^+]}\int_0^1\left\|D_2h_1^+(t,v(t)+\tau w(t),\lambda)-D_2h_1^+(t,v(t),\lambda)\right\|d\tau.
\end{aligned}
$$

The last term tends to zero as $\|w\|\to 0$, thus H_1^+ is differentiable with respect to v.
The differentiability with respect to λ follows from the differentiability of h_1^+ with respect to λ. □

Then we define the operator $\mathcal{H}$ as

$$
\mathcal{H} := \left(H_1^-,H_1^+,H_2^-,H_2^+\right).
$$

More precisely,

$$
\begin{aligned}
\mathcal{H}:\mathcal{V}_\omega\times U\times\mathbb{R}^m &\to \mathcal{V}_\omega\\
(v,\vartheta,\lambda) &\mapsto (H_1^-(v_1^-,\lambda),H_1^+(v_1^+,\lambda),H_2^-(v_2^-,\vartheta,\lambda),H_2^+(v_2^+,\vartheta,\lambda)).
\end{aligned}
$$

Now we can formulate the fixed point equation in $\mathcal{V}_\omega$ that corresponds to the boundary value problem:

$$
\begin{aligned}
v &= \hat{v}_\omega(\mathcal{H}(v,\vartheta,\lambda),d_\omega(\vartheta,\lambda),\alpha,\vartheta,\lambda)\\
&= \mathcal{F}_\omega(v,\alpha,\vartheta,\lambda).
\end{aligned}
\tag{2.2.38}
$$

We define $d_\omega(\vartheta,\lambda) := \gamma_1^-(\lambda)(-\omega)-\gamma_2^+(\vartheta,\lambda)(\omega)$ such that the coupling condition (2.2.37) is satisfied.
Then the following lemma concludes the coupling near the equilibrium:

Lemma 2.2.18 *There are constants $\bar{c}, \tilde{c}, \Omega > 0$ such that for all $\omega > \Omega$, $\vartheta \in U$, $\lambda \in \mathbb{R}^m$ with $\|\lambda\|, \|\vartheta\| < \bar{c}$ and given $\alpha = (\alpha^-, \alpha^+)$ with $\|\alpha\| < \tilde{c}$, the fixed point equation (2.2.38) has (in a sufficiently small neighbourhood of $0 \in \mathcal{V}_\omega$) a unique solution*

$$v(\alpha, \vartheta, \lambda) = \left(v_1^-, v_1^+, v_2^-, v_2^+\right)(\alpha, \vartheta, \lambda) \in \mathcal{V}_\omega.$$

Proof. We use the Banach Fixed Point Theorem to prove the existence and uniqueness of a solution to the fixed point problem (2.2.38). First we show that there is a ball that is invariant under $\mathcal{F}_\omega$ and then that $\mathcal{F}_\omega$ is a contraction with respect to v.
We start with the $\mathcal{F}_\omega$-invariant closed ball $B(0, \bar{\varepsilon}) \subset \mathcal{V}_\omega$.
Using (2.2.33) we get

$$\|\mathcal{F}_\omega(v, \alpha, \vartheta, \lambda)\| \leq \hat{C}\left(\|d\| + \|\mathcal{H}\| + \|\alpha\|\right).$$

We show that for all $\varepsilon > 0$ there is an $\bar{\varepsilon} < \varepsilon$ such that

$$\|\mathcal{F}_\omega(v, \alpha, \vartheta, \lambda)\| \leq \frac{6}{7}\bar{\varepsilon}$$

for $\|v\| < \bar{\varepsilon}$ and sufficiently small $\|\lambda\|$, $\|\vartheta\|$ and $\|\alpha\|$.
We start with an estimate for $\|\mathcal{H}\|$. From the definition of $h_{1,2}^{\pm}(...)$ we see that $\mathcal{H}(0,0,0) = 0$ and thus we can use the mean value theorem to get an estimate for $\|\mathcal{H}\|$:

$$\begin{aligned}\|\mathcal{H}(v, \vartheta, \lambda)\| &= \left\| \left(\int_0^1 D\mathcal{H}(s(v, \vartheta, \lambda)) ds \right)(v, \vartheta, \lambda) \right\| \\ &\leq \int_0^1 \|D_1\mathcal{H}(s(v, \vartheta, \lambda))\| \, ds \, \|v\| + \int_0^1 \|D_2\mathcal{H}(s(v, \vartheta, \lambda))\| \, ds \, \|\vartheta\| \\ &\qquad + \int_0^1 \|D_3\mathcal{H}(s(v, \vartheta, \lambda))\| \, ds \, \|\lambda\|.\end{aligned}$$

Let $\|\lambda\|, \|v\|, \|\vartheta\| < \varepsilon$. Then there is a constant $C_2 > 0$ such that

$$\int_0^1 \|D_2\mathcal{H}(s(v, \vartheta, \lambda))\| \, ds < C_2 \text{ and } \int_0^1 \|D_3\mathcal{H}(s(v, \vartheta, \lambda))\| \, ds < C_2.$$

Moreover, since $D_2 h_{1,2}^{\pm}(t, 0, \vartheta, \lambda) \equiv 0$, $D_1\mathcal{H}(0,0,0) = 0$ holds. Hence there is an $\bar{\varepsilon} \leq \varepsilon$ such that for $\|v\|, \|\lambda\|, \|\vartheta\| < \bar{\varepsilon}$

$$\|D_1\mathcal{H}(s(v, \vartheta, \lambda))\| \leq \frac{1}{7\hat{C}^2} \tag{2.2.39}$$

holds and thus

$$\int_0^1 \|D_1\mathcal{H}(s(v, \vartheta, \lambda))\| \, ds \leq \frac{1}{7\hat{C}^2}.$$

So there is a constant $c_2 > 0$ such that for $\|\lambda\|, \|\vartheta\| < c_2 < \frac{\bar{\varepsilon}}{2 \cdot 7\hat{C}^2 C_2}$ the following holds:

$$\int_0^1 \|D_3\mathcal{H}(s(v, \vartheta, \lambda))\| \, ds \, \|\lambda\| + \int_0^1 \|D_2\mathcal{H}(s(v, \vartheta, \lambda))\| \, ds \, \|\vartheta\| \leq \frac{\bar{\varepsilon}}{7\hat{C}^2}.$$

So for $\|v\| < \bar{\varepsilon}$ and assuming $\hat{C} \geq 1$ we have

$$\|\mathcal{H}\| \leq \frac{2\bar{\varepsilon}}{7\hat{C}^2} \leq \frac{2\bar{\varepsilon}}{7\hat{C}}.$$

Now we estimate $\|d\|$. From the definition of d we get

$$\begin{aligned}\|d\| &= \left\|\gamma_1^-(\lambda)(-\omega) - \gamma_2^+(\lambda)(\omega)\right\| \\ &\leq \left\|\gamma_1^-(\lambda)(-\omega) - \gamma_1(-\omega)\right\| + \|\gamma_1(-\omega) - \gamma_2(\omega)\| + \left\|\gamma_2^+(\lambda)(\omega) - \gamma_2(\omega)\right\|.\end{aligned}$$

Now let Ω be according to Lemma 2.2.15. Then there is an $\tilde{\Omega} > \Omega$ such that for all $\tilde{\omega}_1, \tilde{\omega}_2 > \tilde{\Omega}$, $\|\gamma_1(-\tilde{\omega}_1) - \gamma_2(\tilde{\omega}_2)\| < \bar{\varepsilon}/(21\hat{C})$ holds. Moreover, there is a constant $\bar{c} > 0$ with $\bar{c} \leq c_2$ such that for all $\|\vartheta\|, \|\lambda\| < \bar{c}$ holds

$$\left\|\gamma_1^-(\lambda)(-\tilde{\omega}_1) - \gamma_1(-\tilde{\omega}_1)\right\| < \frac{\bar{\varepsilon}}{21\hat{C}} \text{ and } \left\|\gamma_2^+(\vartheta,\lambda)(\tilde{\omega}_2) - \gamma_2(\tilde{\omega}_2)\right\| < \frac{\bar{\varepsilon}}{21\hat{C}}.$$

Hence the norm of d can be estimated by $\|d_\omega\| < \frac{\bar{\varepsilon}}{7\hat{C}}$.
Using the estimate for $\|d\|$ and $\|\mathcal{H}\|$ and choosing α such that $\|\alpha\| \leq \frac{3\bar{\varepsilon}}{7\hat{C}} =: \tilde{c}$ we find that the mapping $\mathcal{F}_\omega$ leaves the ball $B(0,\bar{\varepsilon}) \subset \mathcal{V}_\omega$ invariant for $\|\lambda\| < \bar{c}$.
Moreover, using these values for the estimates, we have

$$\|D_1\mathcal{F}(v,\lambda)\| \leq \|D_1\hat{v}(\mathcal{H},d,\alpha,\lambda)\| \cdot \|D_1\mathcal{H}(v,\vartheta,\lambda)\| = \hat{C}\frac{1}{7\hat{C}} = \frac{1}{7}$$

and thus $\mathcal{F}_\omega$ is a contraction on $B(0,\bar{\varepsilon})$. The existence and uniqueness follows immediatly from the Banach fixed point theorem. □

Lemma 2.2.19 *Let Lemma 2.2.18 hold. Then for the functions*

$$\begin{aligned}\alpha_\perp^+(\alpha,\vartheta,\lambda) &:= Q_s^+(\varpi^+,\lambda)v_1^+(\alpha,\vartheta,\lambda)(\varpi^+), \\ \alpha_\perp^-(\alpha,\vartheta,\lambda) &:= Q_u^-(-\varpi^-,\vartheta,\lambda)v_2^-(\alpha,\vartheta,\lambda)(-\varpi^-)\end{aligned}$$

there are constants $\hat{C}, \bar{\delta}^s, \bar{\delta}^u > 0$ such that the estimates

$$\begin{aligned}\left\|\alpha_\perp^+(\alpha,\vartheta,\lambda)\right\| &\leq 2\hat{C}\tilde{c}e^{-\bar{\delta}^s\varpi^+} + \frac{2\tilde{c}}{3}, \\ \left\|\alpha_\perp^-(\alpha,\vartheta,\lambda)\right\| &\leq 2\hat{C}\tilde{c}e^{-\bar{\delta}^u\varpi^-} + \frac{2\tilde{c}}{3}\end{aligned} \tag{2.2.40}$$

hold ($\tilde{c}$ as above).
For the derivatives the estimates

$$\begin{aligned}\left\|D_1\alpha_\perp^+(\alpha,\vartheta,\lambda)\right\| &\leq \frac{1}{6}\left(e^{-\bar{\delta}^s\varpi^+} + 1\right) + \hat{C}e^{-\bar{\delta}^s\varpi^+}, \\ \left\|D_1\alpha_\perp^-(\alpha,\vartheta,\lambda)\right\| &\leq \frac{1}{6}\left(e^{-\bar{\delta}^u\varpi^-} + 1\right) + \hat{C}e^{-\bar{\delta}^u\varpi^-}\end{aligned} \tag{2.2.41}$$

hold.

Proof. We consider the estimates (2.2.34) and (2.2.35). With $\|d\| < \frac{\bar{\varepsilon}}{7\hat{C}}$, $\|\alpha\| < \frac{3\bar{\varepsilon}}{7\hat{C}} =: \tilde{c}$ and $\|\mathcal{H}\| \leq \frac{2\bar{\varepsilon}}{7\hat{C}^2}$ it follows from (2.2.34)

$$\begin{aligned}\left\|\alpha_\perp^+(\alpha,\vartheta,\lambda)\right\| &\leq \hat{C}\left(\frac{\bar{\varepsilon}}{7\hat{C}} + \|\alpha\| + \frac{2\bar{\varepsilon}}{7\hat{C}}\right)e^{-\bar{\delta}^s\varpi^+} + \hat{C}\frac{2\bar{\varepsilon}}{7\hat{C}^2}\\ &\leq \frac{6\bar{\varepsilon}}{7}e^{-\bar{\delta}^s\varpi^+} + \frac{2\bar{\varepsilon}}{7\hat{C}}\\ &\leq 2\hat{C}\tilde{c}e^{-\bar{\delta}^s\varpi^+} + \frac{2\tilde{c}}{3}.\end{aligned}$$

For the derivative with respect to α

$$\begin{aligned}\left\|D_1\alpha_\perp^+(\alpha,\vartheta,\lambda)\right\| \leq \left\|D_1\hat{\alpha}_\perp^+(\mathcal{H},d,\alpha,\vartheta,\lambda)\right\| \cdot \|D_1\mathcal{H}(v,\vartheta,\lambda)\| \cdot \|D_1v(\alpha,\vartheta,\lambda)\|\\ + \left\|D_3\hat{\alpha}_\perp^+(\mathcal{H}(v,\vartheta,\lambda),d,\alpha,\vartheta,\lambda)\right\|\end{aligned} \tag{2.2.42}$$

holds.
First we consider $\|D_1v(\alpha,\vartheta,\lambda)\|$. We use $v(\alpha,\vartheta,\lambda) = \hat{v}(\mathcal{H}(v,\vartheta,\lambda),d,\alpha,\vartheta,\lambda)$ to see that

$$\begin{aligned}\|D_1v(\alpha,\vartheta,\lambda)\| \leq \|D_1\hat{v}(\mathcal{H},d,\alpha,\vartheta,\lambda)\| \cdot \|D_1\mathcal{H}(v,\vartheta,\lambda)\| \cdot \|D_1v(\alpha,\vartheta,\lambda)\|\\ + \left\|D_3\hat{v}_1^+(\mathcal{H},d,\alpha,\vartheta,\lambda)\right\|\end{aligned}$$

and thus

$$\|D_1v(\alpha,\vartheta,\lambda)\| \leq \frac{\|D_3\hat{v}(\mathcal{H},d,\alpha,\vartheta,\lambda)\|}{1 - \|D_1\hat{v}(\mathcal{H},d,\alpha,\vartheta,\lambda)\| \cdot \|D_1\mathcal{H}(v,\vartheta,\lambda)\|}.$$

We use $\|D_3\hat{v}(\mathcal{H},d,\alpha,\vartheta,\lambda)\| \leq \hat{C}$, $\|D_1\hat{v}(\mathcal{H},d,\alpha,\vartheta,\lambda)\| \leq \hat{C}$ (which follows from the linear dependence of $\hat{v}$ on (g,d,α) and Equation (2.2.33)) and $\|D_1\mathcal{H}(v,\vartheta,\lambda)\| < \frac{1}{7\hat{C}^2}$ (from (2.2.39)). Then it is obvious that

$$\|D_1v(\alpha,\vartheta,\lambda)\| \leq \frac{7}{6}\hat{C}.$$

Inserting this and estimates (2.2.39),(2.2.35) and (2.2.36) into (2.2.42) we finally get

$$\left\|D_1\alpha_\perp^+(\alpha,\vartheta,\lambda)\right\| \leq \hat{C}(e^{-\bar{\delta}^s\varpi^+}+1)\cdot\frac{1}{7\hat{C}^2}\cdot\frac{7}{6}\hat{C} + \hat{C}e^{-\bar{\delta}^s\varpi^+} = \frac{1}{6}\left(e^{-\bar{\delta}^s\varpi^+}+1\right) + \hat{C}e^{-\bar{\delta}^s\varpi^+}.$$

For $\left\|\tilde{\alpha}_\perp^-(\alpha,\vartheta,\lambda)\right\|$ and $\left\|D_1\tilde{\alpha}_\perp^-(\alpha,\vartheta,\lambda)\right\|$ similar estimates can be drawn.

□

This concludes the coupling near the equilibrium and thus Theorem 2.2.12 is proved. We continue with the coupling near the periodic orbit which is done using the discrete dynamical system defined by the Poincaré map.

2.2.3 Step three – The discrete system

In this section we use the discrete system that is defined by the Poincaré map

$$\Pi : \Sigma_\Upsilon \times \mathbb{R}^m \to \Sigma_\Upsilon$$

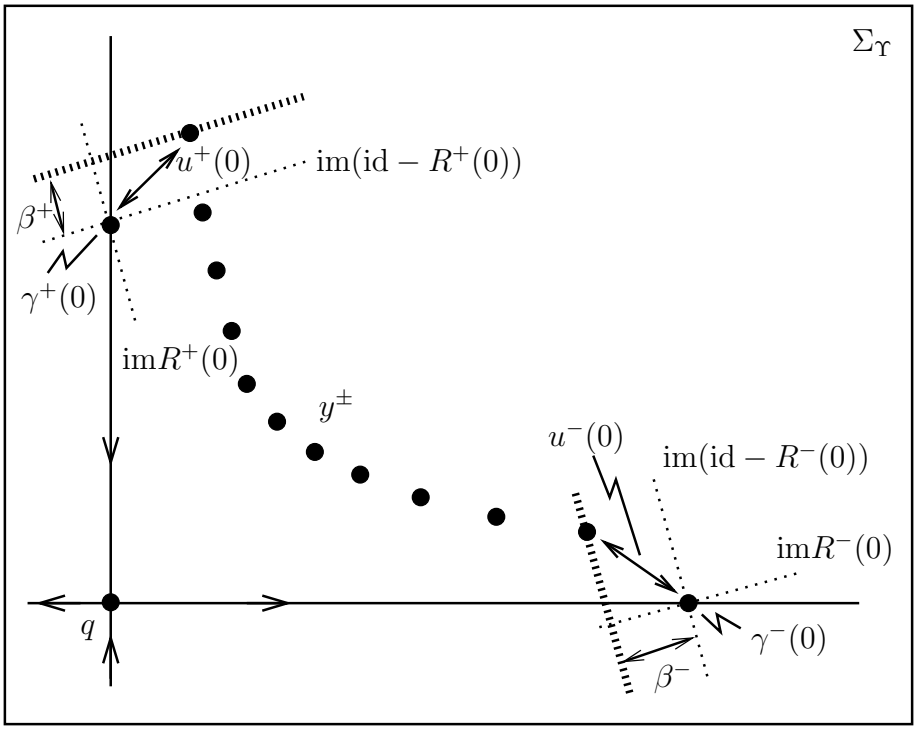

Figure 2.6: The coupling near the periodic orbit. Shown are the 'local coordinate systems' at $\gamma^+(0)$ and $\gamma^-(0)$ as well as the projection boundary conditions for $u^+(0)$ and $u^-(0)$ as defined by $\beta = (\beta^-, \beta^+)$. The solutions $y^+(n) = \gamma^+(n) + u^+(n)$ and $y^-(n) = \gamma^-(n) + u^-(n)$ are coupled near $q = \Upsilon \cap \Sigma_\Upsilon$, which is an equilibrium of the discrete dynamical system (2.2.43).

to find a (discrete) partial orbit inside the Poincaré section Σ_Υ that satisfies certain projection boundary conditions. Recall from Section 2.2.2 that $\Sigma_\Upsilon = \Upsilon_0 + Y_\Upsilon$ with $\Upsilon_0 \in \Upsilon$ and

$$Y_\Upsilon = \operatorname{im}\left(\mathrm{id} - Q^+_{sc}(\varpi^+, \lambda)\right) \oplus \operatorname{im}\left(\mathrm{id} - Q^-_{cu}(-\varpi^-, \vartheta, \lambda)\right).$$

The discrete dynamical system defined on Σ_Υ then reads

$$y(n+1) = \Pi(y(n), \lambda). \tag{2.2.43}$$

We denote the equilibrium $\Upsilon \cap \Sigma_\Upsilon$ by q (note that q does not depend on λ, see Hypothesis (H 2.6)). The solution of (2.2.43) that arises as intersection points of $\gamma_1^+(\lambda)(\cdot)$ with Σ_Υ, is denoted by $\gamma^+(\lambda)(\cdot)$, starting with $\gamma^+(\lambda)(0) = \gamma_1^+(\lambda)(\varpi^+) \in \Sigma_\Upsilon$. Similarly, the solution (2.2.43) arising from the intersection points of $\gamma_2^-(\vartheta, \lambda)(\cdot)$ with Σ_Υ is denoted by $\gamma^-(\vartheta, \lambda)(\cdot)$, starting with $\gamma^-(\vartheta, \lambda)(0) = \gamma_2^-(\vartheta, \lambda)(-\varpi^-) \in \Sigma_\Upsilon$.
Similar to the considerations in Section 2.2.2, we consider the sought solutions $y^\pm(n)$ of (2.2.43) as perturbations of the solutions $\gamma^-(\vartheta, \lambda)(\cdot)$ and $\gamma^+(\lambda)(\cdot)$, thus we write

$$y^\pm(n) = \gamma^\pm(n) + u^\pm(n) \quad , n \in \mathbb{N}_0 \quad (-n \in \mathbb{N}_0 \text{ , respectively}).$$

This gives the following difference equation for $u^\pm(\cdot)$:

$$\begin{aligned} u^-(n+1) &= A^-(n, \vartheta, \lambda)u^-(n) + h^-(n, u^-, \vartheta, \lambda), \\ u^+(n+1) &= A^+(n, \lambda)u^+(n) + h^+(n, u^+, \lambda) \end{aligned} \tag{2.2.44}$$

where $A^+(n, \lambda) := D_1\Pi(\gamma^+(\lambda)(n), \lambda)$ and $A^-(n, \vartheta, \lambda) := D_1\Pi(\gamma^-(\vartheta, \lambda)(n), \lambda)$ and

$$\begin{aligned} h^+(n, u, \lambda) &:= \Pi(\gamma^+(\lambda)(n) + u, \lambda) - \Pi(\gamma^+(\lambda)(n), \lambda) - A^+(n, \lambda)u, \\ h^-(n, u, \vartheta, \lambda) &:= \Pi(\gamma^-(\vartheta, \lambda)(n) + u, \lambda) - \Pi(\gamma^-(\vartheta, \lambda)(n), \lambda) - A^-(n, \vartheta, \lambda)u. \end{aligned}$$

First we look at the 'linearised' equation (as we did before, see Section 2.2.2, Equation (2.2.11)) where we replace the function h by a function g that only depends on n:

$$u^+(n+1) = A^+(n, \lambda)u^+(n) + g^+(n), \tag{2.2.45a}$$
$$u^-(n+1) = A^-(n, \vartheta, \lambda)u^-(n) + g^-(n). \tag{2.2.45b}$$

Analogous to Equation (2.2.11) in Section 2.2.2, the linear homogenuous equation associated with (2.2.45a) has an exponential dichotomy on $\mathbb{R}^+$ with projection R^+ and exponent $\hat{\delta}^s$. Similarly, the linear homogenuous equation associated with (2.2.45b) has an exponential dichotomy on $\mathbb{R}^-$ with projection R^- and exponent $\hat{\delta}^u$.

Geometry

Before we continue with our considerations of the discrete system, we discuss the geometry of the setting. Due to Lemma 2.2.6, for the solutions v_1^+ and v_2^- according to Theorem 2.2.12 $v_1^+(\vartheta, \lambda)(\varpi^+) \in Y_\Upsilon$ and $v_2^-(\vartheta, \lambda)(-\varpi^-) \in Y_\Upsilon$ holds.
Then we can show:

Lemma 2.2.20 *For the projections R^+ and R^- of the exponential dichotomy of the homogenuous linear equation associated with* (2.2.45) *the following holds:*

$$\mathrm{im}R^+(0) = \mathrm{im}Q_s^+(\varpi^+) \text{ and } \mathrm{im}R^-(0) = \mathrm{im}Q_u^-(-\varpi^-).$$

Proof. First we show that $Q_s^+(\varpi^+)v_1^+(\vartheta,\lambda)(\varpi^+) \in Y_\Upsilon$. Consider

$$\begin{aligned} Q_s^+(\varpi^+)v_1^+(\vartheta,\lambda)(\varpi^+) &= Q_s^+(\varpi^+)\Phi_1^+(\varpi^+,0)v_1^+(\vartheta,\lambda)(0) \\ &= \Phi_1^+(\varpi^+,0)Q_s^+(0)v_1^+(\vartheta,\lambda)(0). \end{aligned}$$

Using $Q_s^+(0)v_1^+(\vartheta,\lambda)(0) \in Y_1$ and Lemma 2.2.6 we find that $\Phi_1^+(\varpi^+,0)Q_s^+(0)v_1^+(\vartheta,\lambda)(0) \in Y_\Upsilon$ and thus

$$Q_s^+(\varpi^+)v_1^+(\vartheta,\lambda)(\varpi^+) \in Y_\Upsilon. \tag{2.2.46}$$

Further, we know that $\mathrm{im}Q_{sc}^+(\varpi^+) = \mathrm{im}(Q_s^+(\varpi^+) + Q_c^+(\varpi^+)) = T_{\gamma_1^+(\varpi^+)}W^s(\Upsilon)$ and thus

$$\mathrm{im}Q_s^+(\varpi^+) \subset T_{\gamma_1^+(\varpi^+)}W^s(\Upsilon). \tag{2.2.47}$$

From (2.2.46) and (2.2.47) follows that

$$Q_s^+(\varpi^+)v_1^+(\varpi^+) \in \left(T_{\gamma_1^+(\varpi^+)}W^s(\Upsilon)\right) \cap Y_\Upsilon.$$

On the other hand, $\left(T_{\gamma_1^+(\varpi^+)}W^s(\Upsilon)\right) \cap Y_\Upsilon = \mathrm{im}R^+(0)$ because

$$\begin{aligned} \mathrm{im}R^+(0) &= T_{\gamma^+(0)}W^s(q) \\ &= \left(T_{\gamma^+(0)}W^s(\Upsilon)\right) \cap Y_\Upsilon \\ &= \left(T_{\gamma_1^+(\varpi^+)}W^s(\Upsilon)\right) \cap Y_\Upsilon. \end{aligned} \tag{2.2.48}$$

Using that $\dim R^+(0) = \dim Q_s^+(\varpi^+) = l-1$ (and similar computations for R^-) gives the result of the lemma.

□

The images of R^+ and R^- are given by Lemma 2.2.20, however, we have some freedom in choosing the kernels. Using that $\mathrm{im}R^+(0) \subset \mathrm{im}Q_{sc}^+(\varpi^+)$ (from (2.2.48) and $\mathrm{im}Q_{sc}^+(t) = T_{\gamma_1^+(t)}W^s(\Upsilon)$), it is clear that $\mathrm{im}(\mathrm{id} - Q_{sc}^+(\varpi^+)) \cap \mathrm{im}R^+(0) = \{0\}$.
Using this argument and similar considerations for R^-, we can choose the kernels of R^+ and R^- as follows:

$$\begin{aligned} \ker R^+(0,\lambda) &= \mathrm{im}\left(\mathrm{id} - R^+(0,\lambda)\right) = \mathrm{im}\left(\mathrm{id} - Q_{sc}^+(\varpi^+,\lambda)\right), \\ \ker R^-(0,\vartheta,\lambda) &= \mathrm{im}\left(\mathrm{id} - R^-(0,\vartheta,\lambda)\right) = \mathrm{im}\left(\mathrm{id} - Q_{cu}^-(-\varpi^-,\vartheta,\lambda)\right). \end{aligned} \tag{2.2.49}$$

Similar to Lemma 2.2.4 and Lemma 2.2.5 we can formulate the following lemma:

Lemma 2.2.21 *There are constants $c > 0$ and $N \in \mathbb{N}$ such that*

$$\dim\left(\operatorname{im}\left(\mathrm{id} - R^+\left(n^+, \lambda\right)\right) \oplus \operatorname{im}\left(\mathrm{id} - R^-\left(-n^-, \vartheta, \lambda\right)\right)\right) = n - 1$$

holds for all $\|\lambda\|, \|\vartheta\| < c$ and for all $n^\pm > N$. Moreover, this decomposition defines a projection $\tilde{R}(n^+, n^-, \vartheta, \lambda)$ with $\operatorname{im}\tilde{R}(n^+, -n^-, \vartheta, \lambda) = \operatorname{im}(\mathrm{id} - R^+(n^+, \lambda))$. The projection $\tilde{R}$ is uniformly bounded: there is a constant $M \in \mathbb{R}^+$ such that $\left\|\tilde{R}(n^+, -n^-, \vartheta, \lambda)\right\| \leq M$.

The function space

Now we introduce the function space that we need to find the solutions.

Definition 2.2.22 *Let $\nu \in \mathbb{N}$. We use the notations $\nu^- := \left\lfloor \frac{\nu}{2} \right\rfloor$ (the integer part of $\frac{\nu}{2}$) and $\nu^+ := \nu - \nu^-$.*
By S_ν ($S_{-\nu}$) we denote a function space that maps the set $\{0, 1, ..., \nu\}$ ($\{-\nu, ..., 2, 1, 0\}$, respectively) to Y_Υ, equipped with the maximum norm.
By $\mathcal{U}_\nu$ we denote a space that consists of pairs of functions (u^-, u^+) such that $u^- \in S_{-\nu^-}$ and $u^+ \in S_{\nu^+}$.

We equip the function space $\mathcal{U}_\nu$ with the following maximum norm:

$$\|u\|_{\mathcal{U}_\nu} := \max\left\{\left\|u^-\right\|, \left\|u^+\right\|\right\}.$$

Remark 2.2.23 *We use the notation $\beta = (\beta^-, \beta^+) \in \operatorname{im}R^-(0, \lambda) \times \operatorname{im}R^+(0, \vartheta, \lambda)$ throughout this section.*

Here is the main theorem of this section:

Theorem 2.2.24 *There are constants $\bar{c}, \tilde{c}, N > 0$ such that for all $\nu > 2N$ and given $\lambda \in \mathbb{R}^m$, $\beta = (\beta^-, \beta^+)$, $\vartheta \in U$ with $\|\vartheta\|, \|\lambda\| < \bar{c}$ and $\|\beta\| < \tilde{c}$ there is a unique solution $u \in \mathcal{U}_\nu$ of (2.2.44) such that*

(i) $u^-(-\nu^-) - u^+(\nu^+) = \gamma^+(\nu^+) - \gamma^-(-\nu^-)$ and

(ii) $R^+(0, \lambda)u^+(0) = \beta^+$ and $R^-(0, \vartheta, \lambda)u^-(0) = \beta^-$.

Moreover, for the functions

$$\begin{aligned}\tilde{\beta}^+_\perp(\beta, \vartheta, \lambda) &:= \left(\mathrm{id} - R^+(0, \lambda)\right) u^+(\beta, \vartheta, \lambda)(0),\\ \tilde{\beta}^-_\perp(\beta, \vartheta, \lambda) &:= \left(\mathrm{id} - R^-(0, \vartheta, \lambda)\right) u^-(\beta, \vartheta, \lambda)(0)\end{aligned}$$

there are constants $\hat{C}, \hat{\delta}^s, \hat{\delta}^u > 0$ such that the estimates

$$\begin{aligned}\left\|\tilde{\beta}^+_\perp(\beta, \vartheta, \lambda)\right\| &\leq 2\hat{C}\tilde{c}e^{-\hat{\delta}^s N} + \frac{2\tilde{c}}{3},\\ \left\|\tilde{\beta}^-_\perp(\beta, \vartheta, \lambda)\right\| &\leq 2\hat{C}\tilde{c}e^{-\hat{\delta}^u N} + \frac{2\tilde{c}}{3}\end{aligned} \tag{2.2.50}$$

hold.

For the derivatives the estimates

$$\begin{aligned}\left\|D_1\tilde{\beta}_\perp^+(\beta,\lambda)\right\| &\leq \frac{1}{6}\left(e^{-\hat{\delta}^s N}+1\right)+\hat{C}e^{-\hat{\delta}^s N},\\ \left\|D_1\tilde{\beta}_\perp^-(\beta,\lambda)\right\| &\leq \frac{1}{6}\left(e^{-\hat{\delta}^u N}+1\right)+\hat{C}e^{-\hat{\delta}^u N}\end{aligned} \tag{2.2.51}$$

hold.

We prove this theorem in several steps. First, we show that a boundary value problem with purely linear boundary conditions near the equilibrium and near the periodic orbit has a unique solution. Then we adjust the boundary condition near the equilibrium in terms of a difference condition. Finally, we formulate and solve a fixed point equation such that the sought solution is the unique solution of the fixed point problem.

Fully linearised problem

In principle, we proceed as we did in Section 2.2.2, but we choose a slightly different approach for the linearised boundary conditions. In view of the general theory of Lin's method, our approach can be seen as a replacement of the jump condition by the following linear projection conditions.

$$\begin{aligned}R^+(0,\lambda)u^+(0) &= \beta^+,\\ R^-(0,\vartheta,\lambda)u^-(0) &= \beta^-\end{aligned} \tag{2.2.52}$$

The projection boundary conditions near the fixed point p on the other hand have the same meaning as the conditions (2.2.17):

$$\begin{aligned}(\mathrm{id}-R^+(\nu^+,\lambda))u^+(\nu^+) &= b^+(\nu^+) := (\mathrm{id}-R^+(\nu^+,\lambda))b,\\ (\mathrm{id}-R^-(-\nu^-,\vartheta,\lambda))u^-(-\nu^-) &= b^-(\nu^-) := (\mathrm{id}-R^-(-\nu^-,\vartheta,\lambda))b.\end{aligned} \tag{2.2.53}$$

Note that $b\in\mathbb{R}^{n-1}$ and β as in Remark 2.2.23 are given and that $b=b^+(\nu^+)+b^-(\nu^-)$ for sufficiently large ν.
Then there is a unique solution that satisfies these linear boundary conditions.

Lemma 2.2.25 *There are constants $c>0$, $N\in\mathbb{N}$ such that for all $\nu>2N$ and $\vartheta\in U$, $\lambda\in\mathbb{R}^m$ with $\|\vartheta\|,\|\lambda\|<c$ and for given $g\in\mathcal{U}_\nu$, $b\in Y_\Upsilon$ and $\beta=(\beta^-,\beta^+)$, the boundary value problem* (2.2.45),((2.2.52),(2.2.53)) *has a unique solution*

$$\bar{u}(g,b,\beta,\vartheta,\lambda)=\left(\bar{u}^-,\bar{u}^+\right)(g,b,\beta,\vartheta,\lambda)\in\mathcal{U}_\nu.$$

Proof. In this proof we do not indicate the dependence on λ and ϑ. Let $\Phi^\pm$ denote the transition matrices of the homogenuous linear equations associated with (2.2.45).
Using the variation of constants formula for (2.2.45) we start with

$$\begin{aligned}u^+(n) &= \Phi(n,0)u^+(0)+\sum_{m=1}^{n}\Phi(n,m)g^+(m-1),\\ u^-(n) &= \Phi(n,0)u^-(0)-\sum_{m=0}^{n+1}\Phi(n,m)g^-(m-1).\end{aligned} \tag{2.2.54}$$

Proceeding in a similar way as in the proof of Lemma 2.2.13, we use the dichotomy and finally arrive at

$$\begin{aligned}(\mathrm{id}-R^+(0))u^+(0) &= \Phi(0,\nu^+)b^+ - \sum_{m=1}^{\nu^+}\Phi(0,m)(\mathrm{id}-R^+(m))g^+(m-1),\\ (\mathrm{id}-R^-(0))u^-(0) &= \Phi(0,-\nu^-)b^- + \sum_{m=-\nu^-+1}^{0}\Phi(0,m)(\mathrm{id}-R^-(m))g^-(m-1).\end{aligned} \tag{2.2.55}$$

Now we take (2.2.52) and (2.2.49) into consideration. Decomposition of $u^{\pm}(0)$ by means of $R^+(0)$ and $R^-(0)$, respectively, yields

$$\begin{aligned}u^+(0) &= \beta^+ + \Phi(0,\nu^+)b^+ - \sum_{m=1}^{\nu^+}\Phi(0,m)(\mathrm{id}-R^+(m))g^+(m-1),\\ u^-(0) &= \beta^- + \Phi(0,-\nu^-)b^- + \sum_{m=-\nu^-+1}^{0}\Phi(0,m)(\mathrm{id}-R^-(m))g^-(m-1).\end{aligned} \tag{2.2.56}$$

Thus the $u^+(0)$ and $u^-(0)$ are completely determinded by b and β, and using the variation of constants formula (2.2.54), the solutions $u^{\pm}$ can be expressed as $(\bar{u}^-,\bar{u}^+)(g,b,\beta,\vartheta,\lambda)$.

□

Lemma 2.2.26 *Assume Lemma 2.2.25 holds. Then there is a constant $C>0$ such that*

$$\|\bar{u}(g,b,\beta,\vartheta,\lambda)\| \le C\left(\|b\|+\|\beta\|+\|g\|\right). \tag{2.2.57}$$

There is a constant $\hat{\delta}>0$ such that

$$\begin{aligned}&\left\|R^+(\nu^+)\bar{u}^+(g,b,\beta,\vartheta,\lambda)(\nu^+)\right\| + \left\|R^-(-\nu^-)\bar{u}^-(g,b,\beta,\vartheta,\lambda)(-\nu^-)\right\|\\ &\quad\le Ce^{-\hat{\delta}N}\|\beta\| + C\|g\|.\end{aligned} \tag{2.2.58}$$

For the functions

$$\begin{aligned}\bar{\beta}^+_\perp(g,b,\beta,\vartheta,\lambda) &:= \left(\mathrm{id}-R^+(0,\lambda)\right)\bar{u}^+(g,b,\beta,\vartheta,\lambda)(0),\\ \bar{\beta}^-_\perp(g,b,\beta,\vartheta,\lambda) &:= \left(\mathrm{id}-R^-(0,\vartheta,\lambda)\right)\bar{u}^-(g,b,\beta,\vartheta,\lambda)(0)\end{aligned}$$

the following estimates hold:

$$\begin{aligned}\left\|\bar{\beta}^+_\perp(g,b,\beta,\vartheta,\lambda)\right\| &\le C\left(\|b\|+\|g\|\right)e^{-\hat{\delta}N} + C\|g\|,\\ \left\|\bar{\beta}^-_\perp(g,b,\beta,\vartheta,\lambda)\right\| &\le C\left(\|b\|+\|g\|\right)e^{-\hat{\delta}N} + C\|g\|.\end{aligned} \tag{2.2.59}$$

For the derivatives of $\bar{\beta}^{+(-)}_\perp$ the following estimates hold:

$$\begin{aligned}\left\|D_2\bar{\beta}^+_\perp(g,b,\beta,\vartheta,\lambda)\right\| &\le Ce^{-\hat{\delta}N},\\ \left\|D_2\bar{\beta}^-_\perp(g,b,\beta,\vartheta,\lambda)\right\| &\le Ce^{-\hat{\delta}N}\end{aligned} \tag{2.2.60}$$

and

$$\begin{aligned}\left\|D_1\bar{\beta}_\perp^+(g,b,\beta,\vartheta,\lambda)\right\| &\leq C(e^{-\hat{\delta}N}+1),\\ \left\|D_1\bar{\beta}_\perp^-(g,b,\beta,\vartheta,\lambda)\right\| &\leq C(e^{-\hat{\delta}N}+1).\end{aligned} \tag{2.2.61}$$

Proof. For the norm estimate we decompose u^+ using the projection R^+:

$$u^+(...)(n) = (\mathrm{id} - R^+(n,\lambda))u^+(...)(n) + R^+(n,\lambda)u^+(...)(n).$$

Thus

$$\left\|u^+(...)(n)\right\| \leq \left\|(\mathrm{id} - R^+(n,\lambda))u^+(...)(n)\right\| + \left\|R^+(n,\lambda)u^+(...)(n)\right\| \tag{2.2.62}$$

holds.
Using the variation of constants formula and the exponential dichotomy we get

$$\begin{aligned}\left\|R^+(n,\lambda)u^+(n)\right\| &= \left\|R^+(n,\lambda)\left(\Phi^+(n,0)u^+(0) + \sum_{j=0}^{n}\Phi^+(n,j)g^+(j)\right)\right\|\\ &\leq \left\|R^+(n,\lambda)\Phi^+(n,0)u^+(0)\right\| + \left\|R^+(n,\lambda)\sum_{j=1}^{n}\Phi^+(n,j)g^+(j-1)\right\|\\ &\leq \left\|\Phi^+(n,0)R^+(0,\lambda)R^+(0,\lambda)u^+(0)\right\| + \left\|\sum_{j=1}^{n}\Phi^+(n,j)R^+(j,\lambda)g^+(j-1)\right\|\\ &\leq Ke^{-\hat{\delta}^s n}\left\|\beta^+\right\| + M\left\|g^+\right\|.\end{aligned}$$

For the first term of the right-hand side in (2.2.62) we use the variation of constants formula again

$$\begin{aligned}&\left\|(\mathrm{id} - R^+(n,\lambda))u^+(n)\right\|\\ &= \left\|(\mathrm{id} - R^+(n,\lambda))\Phi(n,\nu^+)u^+(\nu^+) + (\mathrm{id} - R^+(n,\lambda))\sum_{m=1}^{n}\Phi(n,m)g^+(m-1)\right\|\\ &\leq \left\|\Phi(n,\nu^+)(\mathrm{id} - R^+(\nu^+,\lambda))u^+(\nu^+)\right\|\\ &\quad + \left\|\sum_{m=1}^{n}\Phi(n,m)(\mathrm{id} - R^+(m,\lambda))g^+(m-1)\right\|\\ &\leq Ke^{-\hat{\delta}^s(\nu^+-n)}\left\|b^+\right\| + M\left\|g^+\right\|.\end{aligned}$$

Using the same approach for $\|u^-(n)\|$ and putting everything together we finally get estimate (2.2.57).
The estimate (2.2.58) can be derived in the following way: First, we use the variation of constants formula and the properties of the dichotomy on $R^+(\nu^+)u^+(\nu^+)$ and $R^-(-\nu^-)u^-(-\nu^-)$.

That leads to

$$\begin{aligned}
&\left\|R^+(\nu^+)u^+(...)(\nu^+)\right\| + \left\|R^-(-\nu^-)u^-(...)(-\nu^-)\right\| \\
&= \left\| R^+(\nu^+)\left(\Phi^+(\nu^+,0)u^+(0) + \sum_{j=1}^{\nu^+}\Phi^+(\nu^+,j)g^+(j-1)\right)\right\| \\
&\quad + \left\| R^-(-\nu^-)\left(\Phi^-(-\nu^-,0)u^-(0) - \sum_{j=-\nu^-+1}^{0}\Phi^-(-\nu^-,j)g^-(j-1)\right)\right\| \\
&\leq \left\|\Phi^+(\nu^+,0)R^+(0)R^+(0)u^+(0)\right\| + M_1\left\|g^+\right\| \\
&\quad + \left\|\Phi^-(-\nu^-,0)R^-(0)R^-(0)u^-(0)\right\| + M_2\left\|g^-\right\| \\
&\leq Ke^{-\hat{\delta}^s\nu^+}\left\|\beta^+\right\| + Ke^{-\hat{\delta}^u\nu^-}\left\|\beta^-\right\| + M\left\|(g^-,g^+)\right\| \\
&\leq Ke^{-\hat{\delta}N}\left\|\beta\right\| + M\left\|g\right\|.
\end{aligned}$$

Here, $\hat{\delta} := \min\{\hat{\delta}^s, \hat{\delta}^u\}$ and $\hat{\delta}^s$ and $\hat{\delta}^u$ are the exponents of the exponential dichotomy on $\mathbb{R}^+$ and $\mathbb{R}^-$.
Now we consider estimate (2.2.59). Using (2.2.55) we get

$$\begin{aligned}
\left\|\bar{\beta}_\perp^-(g,b,\beta,\vartheta,\lambda)\right\| &= \left\|\Phi(0,-\nu^-)b^- + \sum_{m=-\nu^-+1}^{0}\Phi(0,m)(\mathrm{id}-R^-(m,\vartheta,\lambda))g^-(m-1)\right\| \\
&\leq \left\|\Phi(0,-\nu^-)(\mathrm{id}-R^-(-\nu^-,\vartheta,\lambda))b^-\right\| + C\left\|g^-\right\| \\
&\leq Ke^{-\hat{\delta}^u\nu^-}\left\|b^-\right\| + C\left\|g\right\|.
\end{aligned}$$

Since the dependency of $\beta_\perp^\pm$ on b and on g is linear the derivatives with respect to b and g can be estimated as follows:

$$\begin{aligned}
\left\|D_2\bar{\beta}_\perp^-(g,b,\beta,\vartheta,\lambda)\right\| &\leq Ce^{-\hat{\delta}^u\nu^-}, \\
\left\|D_1\bar{\beta}_\perp^-(g,b,\beta,\vartheta,\lambda)\right\| &\leq C(e^{-\hat{\delta}^u\nu^-}+1).
\end{aligned}$$

This completes the proof of the lemma.

□

The next step towards the coupling of the solutions near the periodic orbit is given by the following lemma. We replace the boundary condition (2.2.53) by

$$u^+(\nu^+) - u^-(-\nu^-) = d. \tag{2.2.63}$$

Then we can state:

Lemma 2.2.27 *There are constants $c > 0$, $N \in \mathbb{N}$ such that for all $\nu > 2N$ and $\vartheta \in U$, $\lambda \in \mathbb{R}^m$ with $\|\vartheta\|, \|\lambda\| < c$ and for given $g \in \mathcal{U}_\nu$, $d \in Y_\Upsilon$ and $\beta = (\beta^-, \beta^+)$, the boundary value problem* (2.2.45),((2.2.52),(2.2.63)) *has a unique solution*

$$\hat{u}(g,d,\beta,\vartheta,\lambda) = \left(\hat{u}^-,\hat{u}^+\right)(g,d,\beta,\vartheta,\lambda) \in \mathcal{U}_\nu.$$

Proof. Let $\beta = (\beta^-, \beta^+)$ be fixed. We use that for any given d there is a unique $b = (b^+, b^-)$ such that the corresponding solutions of the boundary value problem in Lemma 2.2.25 solve the boundary value problem stated above.
We consider the system

$$u^+(g, b, \beta, \vartheta, \lambda)(\nu^+) - u^-(g, b, \beta, \vartheta, \lambda)(-\nu^-) = d$$

with boundary conditions

$$\begin{aligned}(\mathrm{id} - R^+(\nu^+, \lambda))u^+(\nu^+) &= b^+,\\ (\mathrm{id} - R^-(-\nu^-, \vartheta, \lambda))u^-(-\nu^-) &= b^-\end{aligned}$$

and solve this system for b.
Then we have

$$b^+ - b^- = d - R^+(\nu^+, \lambda)u^+(g, b, \beta, \vartheta, \lambda)(\nu^+) + R^-(-\nu^-, \vartheta, \lambda)u^-(g, b, \beta, \vartheta, \lambda)(-\nu^-). \quad (2.2.64)$$

Now we use the projection $\tilde{R} := \tilde{R}(\nu^+, \nu^-, \vartheta, \lambda)$ as defined in Lemma 2.2.21. With $b = b^+ + b^-$ we can write

$$\begin{aligned}b = (-\mathrm{id} + 2\tilde{R}(\nu^+, \nu^-, \vartheta, \lambda)) \big(&d - R^+(\nu^+, \lambda)u^+(g, b, \beta, \vartheta, \lambda)(\nu^+)\\ &+R^-(-\nu^-, \vartheta, \lambda)u^-(g, b, \beta, \vartheta, \lambda)(-\nu^-)\big).\end{aligned}$$

Since the dependencies of $u^+(g, b, \beta, \vartheta, \lambda)(\nu^+)$ and $u^-(g, b, \beta, \vartheta, \lambda)(-\nu^-)$ on (g, b, β) are linear, the equation can be written as

$$b = L_1(\vartheta, \lambda)b + L_2(\vartheta, \lambda)g + L_3(\vartheta, \lambda)d + L_4(\vartheta, \lambda)\beta, \quad (2.2.65)$$

where $L_{1/2/3/4}(\vartheta, \lambda)(\cdot)$ are linear operators depending on λ and ϑ.
The operator $(\mathrm{id} - L_1)$ is invertible, hence we can solve the equation for $b = b(g, d, \beta, \vartheta, \lambda)$ and thus we finally have $\hat{u} = \bar{u}(g, b_\nu(g, d, \beta, \vartheta, \lambda), \beta, \vartheta, \lambda)$.

□

Lemma 2.2.28 *Assume the conditions of Lemma 2.2.27 hold. Then there is a constant $\hat{C} > 0$ such that*

$$\|\hat{u}(g, d, \beta, \vartheta, \lambda)\| \le \hat{C}\left(\|d\| + \|\beta\| + \|g\|\right). \quad (2.2.66)$$

For the functions

$$\begin{aligned}\hat{\beta}^+_\perp(g, d, \beta, \vartheta, \lambda) &:= \left(\mathrm{id} - R^+(0, \lambda)\right)\hat{u}^+_\nu(g, d, \beta, \vartheta, \lambda)(0)\\ \hat{\beta}^-_\perp(g, d, \beta, \vartheta, \lambda) &:= \left(\mathrm{id} - R^-(0, \vartheta, \lambda)\right)\hat{u}^-_\nu(g, d, \beta, \vartheta, \lambda)(0)\end{aligned}$$

there are constants $\hat{\delta}^s, \hat{\delta}^u > 0$ such that the estimates

$$\begin{aligned}\left\|\hat{\beta}^+_\perp(g, d, \beta, \vartheta, \lambda)\right\| &\le C\left(\|d\| + \|\beta\| + \|g\|\right)e^{-\hat{\delta}^s N} + C\|g\|,\\ \left\|\hat{\beta}^-_\perp(g, d, \beta, \vartheta, \lambda)\right\| &\le C\left(\|d\| + \|\beta\| + \|g\|\right)e^{-\hat{\delta}^u N} + C\|g\|\end{aligned} \quad (2.2.67)$$

hold.
For the partial derivatives the following estimates hold:

$$\begin{aligned}\left\|D_3\hat{\beta}_\perp^+(g,d,\beta,\vartheta,\lambda)\right\| &\leq Ce^{-\hat{\delta}^s N},\\ \left\|D_3\hat{\beta}_\perp^-(g,d,\beta,\vartheta,\lambda)\right\| &\leq Ce^{-\hat{\delta}^u N}\end{aligned} \tag{2.2.68}$$

and

$$\begin{aligned}\left\|D_1\hat{\beta}_\perp^+(g,d,\beta,\vartheta,\lambda)\right\| &\leq C(e^{-\hat{\delta}^s N}+1),\\ \left\|D_1\hat{\beta}_\perp^-(g,d,\beta,\vartheta,\lambda)\right\| &\leq C(e^{-\hat{\delta}^u N}+1).\end{aligned} \tag{2.2.69}$$

Proof. The estimate (2.2.66) follows directly from (2.2.57) together with

$$\|b\| \leq \hat{C}_1(\|\beta\|+\|d\|+\|g\|), \tag{2.2.70}$$

which is a consequence of (2.2.65) and (2.2.58).
From (2.2.70) together with (2.2.59), (2.2.60) and (2.2.61) follow the estimates of the lemma. □

Coupling near the periodic orbit
The next step is the coupling of the solutions y^+ and y^- near the periodic orbit. We use

$$y^+(\nu^+) = \gamma^+(\nu^+) + u^+(\nu^+) = u^-(-\nu^-) + \gamma^-(-\nu^-) = y^-(-\nu^-) \tag{2.2.71}$$

as the corresponding boundary condition.
Based on Lemma 2.2.27, we can formulate a fixed point problem in the function space $\mathcal{U}_\nu$ as stated in Definition 2.2.22 such that a solution of this fixed point equation corresponds to a solution of the nonlinear boundary value problem (2.2.44),((2.2.52),(2.2.71)).
To formulate the fixed point problem, we introduce the following Nemyzki operators:

$$\begin{aligned}H^- : S_{-\nu^-}\times U\times\mathbb{R}^m &\to S_{-\nu^-}\\ (u,\vartheta,\lambda) &\mapsto H^-(u,\vartheta,\lambda) := h^-(n,u(n),\vartheta,\lambda)\end{aligned}$$

and

$$\begin{aligned}H^+ : S_{\nu^+}\times\mathbb{R}^m &\to S_{\nu^+}\\ (u,\lambda) &\mapsto H^+(u,\lambda) := h^+(n,u(n),\lambda).\end{aligned}$$

We use the operator $\mathcal{H} := (H^-, H^+)$ defined by

$$\begin{aligned}\mathcal{H} : \mathcal{U}_\nu\times U\times\mathbb{R}^m &\to \mathcal{U}_\nu\\ (u,\vartheta,\lambda) &\mapsto (H^-(u^-,\vartheta,\lambda), H^+(u^+,\lambda)).\end{aligned}$$

The fixed point equation in $\mathcal{U}_\nu$ reads

$$\begin{aligned}u &= \hat{u}(\mathcal{H}(u,\vartheta,\lambda), d_\nu(\vartheta,\lambda),\beta,\vartheta,\lambda)\\ &= \mathcal{F}_\nu(u,\beta,\vartheta,\lambda).\end{aligned} \tag{2.2.72}$$

We choose $d_\nu(\vartheta,\lambda)$ such that

$$d_\nu(\vartheta,\lambda) := \gamma^-(-\nu^-,\vartheta,\lambda) - \gamma^+(\nu^+,\lambda). \tag{2.2.73}$$

Here is the main lemma of this section:

Lemma 2.2.29 *There are constants $N \in \mathbb{N}$, $\bar{c},\tilde{c} > 0$ such that for all $\nu > 2N$, $\vartheta \in U$ and $\lambda \in \mathbb{R}^m$ with $\|\vartheta\|, \|\lambda\| < \bar{c}$ and given $\beta = (\beta^-,\beta^+)$ with $\|\beta\| < \tilde{c}$, the fixed point problem (2.2.72) has (in a sufficiently small neighbourhood of $0 \in \mathcal{U}_\nu$) a unique solution*

$$u(\beta,\vartheta,\lambda) = \left(u^-,u^+\right)(\beta,\vartheta,\lambda) \in \mathcal{U}_\nu.$$

Proof. The proof runs completely analogous to the proof of Lemma 2.2.18, again we use the Banach Fixed Point Theorem to prove the existence and uniqueness of the solution in $\mathcal{U}_\nu$. □

Lemma 2.2.30 *Assume that Lemma 2.2.29 holds. Then for the functions*

$$\tilde{\beta}^+_\perp(\beta,\lambda) := \left(\mathrm{id} - R^+(0,\lambda)\right) u^+(\beta,\lambda)(0),$$
$$\tilde{\beta}^-_\perp(\beta,\lambda) := \left(\mathrm{id} - R^-(0,\lambda)\right) u^-(\beta,\lambda)(0)$$

there is a constant $\hat{C} > 0$ such that the following estimates hold:

$$\left\|\tilde{\beta}^+_\perp(\beta,\lambda)\right\| \le 2\hat{C}\tilde{c}e^{-kN} + \frac{2\tilde{c}}{3},$$
$$\left\|\tilde{\beta}^-_\perp(\beta,\lambda)\right\| \le 2\hat{C}\tilde{c}e^{-kN} + \frac{2\tilde{c}}{3}$$

and for the derivatives

$$\left\|D_1\tilde{\beta}^+_\perp(\beta,\lambda)\right\| \le \frac{1}{6}\left(e^{-\hat{\delta}^s\nu^+} + 1\right) + \hat{C}e^{-\hat{\delta}^s\nu^+},$$
$$\left\|D_1\tilde{\beta}^-_\perp(\beta,\lambda)\right\| \le \frac{1}{6}\left(e^{-\hat{\delta}^u\nu^-} + 1\right) + \hat{C}e^{-\hat{\delta}^u\nu^-}.$$

Proof. The proof runs completely parallel to the proof of Lemma 2.2.19. □

2.2.4 Step four – Construction of the Lin orbit

In this section we couple the solutions $x^\pm_{1/2}(\cdot) = \gamma^\pm_{1/2}(\cdot) + v^\pm_{1/2}(\cdot)$ from Section 2.2.2 and $y^\pm(\cdot) = \gamma^\pm(\cdot) + u^\pm(\cdot)$ from Section 2.2.3 to construct a Lin orbit as stated in Definition 2.1.2. In particular, our goal is to find sequences $\boldsymbol{\alpha}$ and $\boldsymbol{\beta}$ such that the corresponding solutions of (1.2.1) and (2.2.43)

$$x^\pm_{1,i}(\alpha_i,\vartheta_i,\lambda)(t) := \gamma^\pm_1(\lambda)(t) + v^\pm_1(\alpha_i,\vartheta_i,\lambda)(t),$$
$$x^\pm_{2,i}(\alpha_i,\vartheta_i,\lambda)(t) := \gamma^\pm_2(\vartheta_i,\lambda)(t) + v^\pm_2(\alpha_i,\vartheta_i,\lambda)(t),$$
$$y^+_i(\beta_i,\vartheta_i,\lambda)(n) := \gamma^\pm(\lambda)(n) + u^+(\beta,\vartheta_i,\lambda)(n),$$
$$y^-_i(\beta_i,\vartheta_i,\lambda)(n) := \gamma^\pm(\vartheta_i,\lambda)(n) + u^-(\beta,\vartheta_i,\lambda)(n)$$

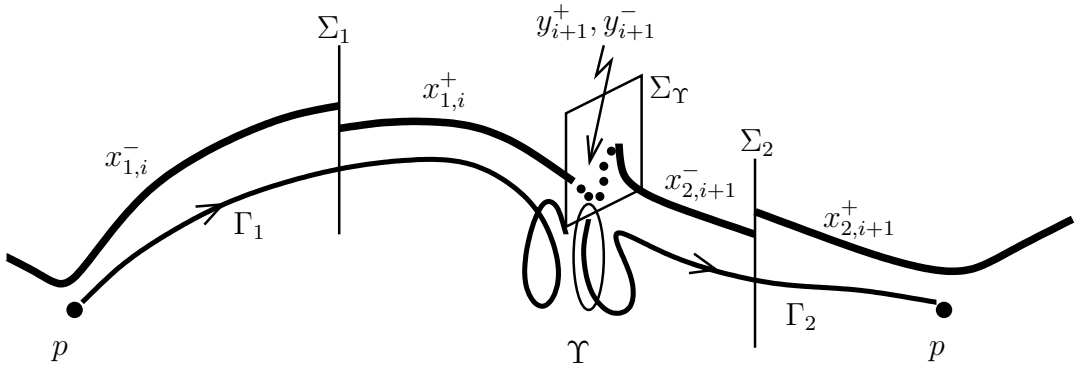

Figure 2.7: Heteroclinic chain. Shown are the solutions $x^\pm_{1/2} := \gamma^\pm_{1/2} + v^\pm_{1/2}$ given by Theorem 2.2.12 and $y^\pm := \gamma^\pm + u^\pm$ given by Theorem 2.2.24.

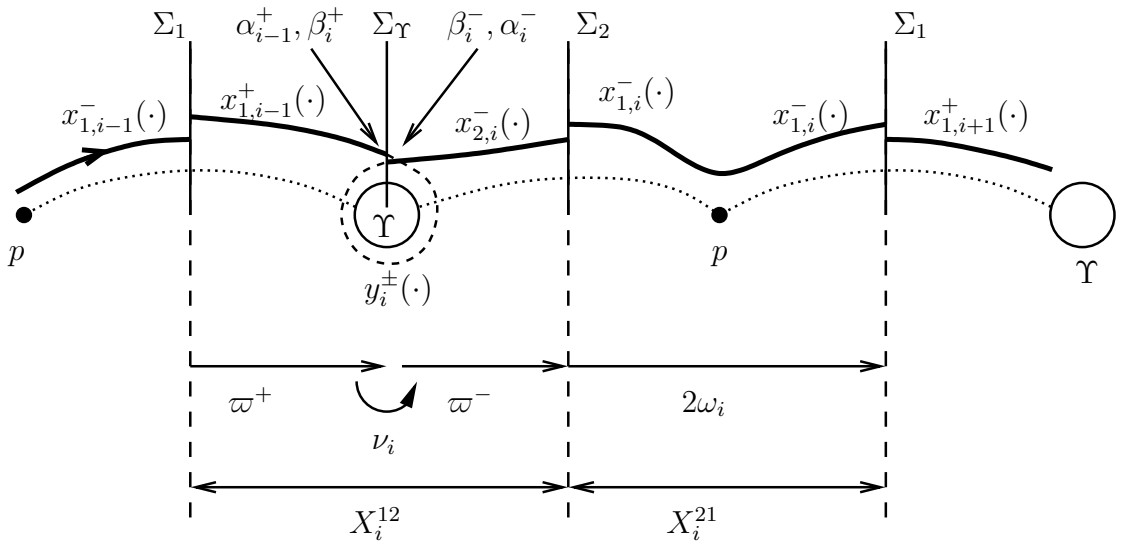

Figure 2.8: Heteroclinic chain. The relation of the solutions $x^\pm_{1/2}$, $y^\pm$ and the Lin orbit $\boldsymbol{X} = (X^{12}_i, X^{21}_i)_{i\in\mathbb{Z}}$. Also shown are the transition times and the place where the boundary conditions ($\alpha^\pm_i$ and $\beta^\pm_i$) apply.

are coupled inside Σ_Υ, that means $x_1^+(\alpha_{i-1},\vartheta_{i-1},\lambda)(\varpi^+) = y^+(\beta_i,\vartheta_i,\lambda)(0)$ and $y^-(\beta_i,\vartheta_i,\lambda)(0) = x_2^-(\alpha_i,\vartheta_i,\lambda)(-\varpi^+)$. Because (by definition) $\gamma^+(\lambda)(0) = \gamma_1^+(\lambda)(\varpi^+)$ and $\gamma^-(\vartheta,\lambda)(-\varpi^-) = u^-(\vartheta,\lambda)(0)$, it is sufficient to couple the perturbance terms, hence we look for

$$\begin{aligned} v_1^+(\alpha_{i-1},\vartheta_{i-1},\lambda)(\varpi^+) &= u^+(\beta_i,\vartheta_i,\lambda)(0) \text{ and} \\ u^-(\beta_i,\vartheta_i,\lambda)(0) &= v_2^-(\alpha_i,\vartheta_i,\lambda)(-\varpi^+). \end{aligned}$$

For an illustration of how the orbits X_i^{12} and X_i^{21} are constructed using the solutions $x_{1,2}^\pm$ and $y^\pm$ from Section 2.2.2 and Section 2.2.3, see Figure 2.8.
To make clear that the coupling inside Σ_Υ indeed makes sense, recall that, according to Hypothesis (H 2.8), $v_1^+(\varpi^+) \in Y_\Upsilon$ and $v_2^-(-\varpi^-) \in Y_\Upsilon$. Moreover, the following two lemmas justify that the boundary conditions that are imposed on v_1^+ and v_2^- and the boundary conditions that are imposed on u^- and u^+ are reasonable to allow to couple these solutions inside Y_Υ.

Lemma 2.2.31 *For the projections Q_c^+ and Q_c^- of the exponential trichotomy of the linear homogenuous equation associated with* (2.2.11) *the following holds:*

$$Q_c^+(\varpi^+,\lambda)(Y_\Upsilon) = \{0\} \text{ and } Q_c^-(-\varpi^-,\vartheta,\lambda)(Y_\Upsilon) = \{0\}.$$

Proof. Similar to the proof of Lemma 2.2.20 we can show that $\mathrm{im}Q_u^+(\varpi^+,\lambda) \subset Y_\Upsilon$. By counting the dimensions, it is obvious that even

$$Y_\Upsilon = \mathrm{im}Q_s^+(\varpi^+,\lambda) \oplus \mathrm{im}Q_u^+(\varpi^+,\lambda).$$

Thus $Q_c^+(\varpi^+,\lambda)(Y_\Upsilon) = \{0\}$; for $Q_c^-(\varpi^-,\vartheta,\lambda)$ a similar conclusion can be drawn. □

Lemma 2.2.32 *Let v_1^+ and v_2^- be solutions according to Theorem* 2.2.12. *For the projections Q_s^+ and Q_{sc}^+ (Q_u^- and Q_{cu}^-, respectively) of the exponential trichotomy of the linear homogenuous equation associated with* (2.2.11) *the following holds:*

$$(\mathrm{id} - Q_{sc}^+(\varpi^+,\lambda))v_1^+(\varpi^+) = (\mathrm{id} - Q_s^+(\varpi^+,\lambda))v_1^+(\varpi^+)$$

and

$$(\mathrm{id} - Q_{cu}^-(-\varpi^-,\vartheta,\lambda))v_2^-(-\varpi^-) = (\mathrm{id} - Q_u^-(-\varpi^-,\vartheta,\lambda))v_2^-(-\varpi^-).$$

Proof. The result follows from Lemma 2.2.31 using that $v_1^+(\varpi^+), v_2^-(-\varpi^-) \in Y_\Upsilon$, $Q_{sc}^+ = Q_s^+ + Q_c^+$ and $Q_{cu}^- = Q_u^- + Q_c^-$. □

In Section 2.2.2 we showed that for a given projection boundary condition (2.2.18) (with $\alpha = (\alpha^-,\alpha^+)$) in Σ_Υ and for a given transition time ω from Σ_2 to Σ_1 there is a unique solution $v(\alpha,\vartheta,\lambda)(\cdot) \in \mathcal{V}_\omega$ of system (2.2.9) that only has jumps inside Σ_1 in Z_1 and inside Σ_2 in Z_2. Additionally, in Section 2.2.3 we showed that for given 'complementary' projection boundary conditions (2.2.52) (with $\beta = (\beta^-,\beta^+)$) and a given step number ν there is a unique solution $u(\beta,\vartheta,\lambda)(\cdot) \in \mathcal{U}_\nu$ of system (2.2.44).

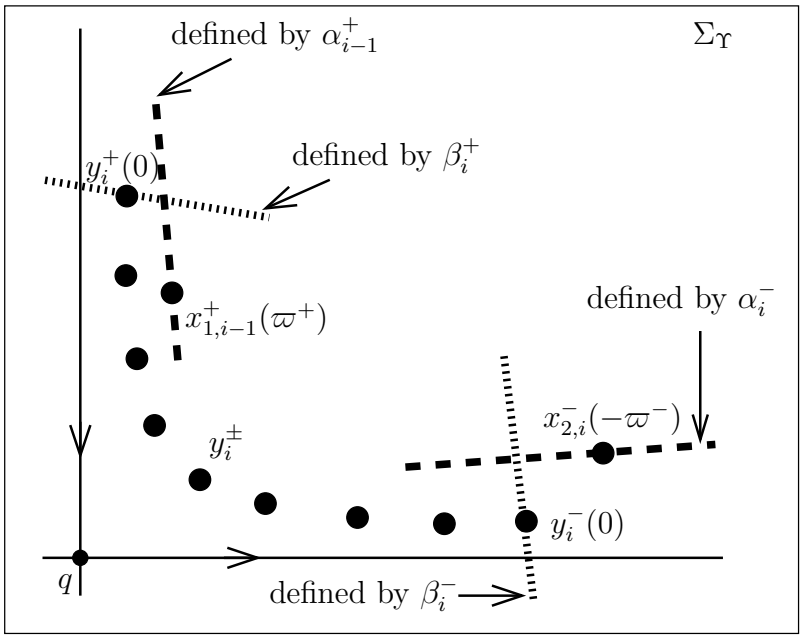

Figure 2.9: The 'global coupling' inside Σ_Υ. Shown are the points $x_{1,i-1}^+(\varpi^+)$ and $x_{2,i}^-(-\varpi^-)$ along with the points $y_i^+(0)$ and $y_i^-(0)$. All of them are restricted to lie in certain linear subspaces that are defined by α_{i-1}^+, α_i^-, β_i^+ and β_i^-.

In this section we consider sequences of parameters $\boldsymbol{\vartheta} = (\vartheta_i)_{i\in\mathbb{Z}}$, $\vartheta_i \in U$, transition times $\boldsymbol{\omega} = (\omega_i)_{i\in\mathbb{Z}}$ and $\boldsymbol{\nu} = (\nu_i)_{i\in\mathbb{Z}}$ and sequences $\boldsymbol{\alpha} = (\alpha_i)_{i\in\mathbb{Z}}$ and $\boldsymbol{\beta} = (\beta_i)_{i\in\mathbb{Z}}$. With these quantities the associated sequences of solutions $\boldsymbol{v} = (v_i)_{i\in\mathbb{Z}}$ and $\boldsymbol{u} = (u_i)_{i\in\mathbb{Z}}$ are determined by Theorem 2.2.12 and Theorem 2.2.24. The objective here is to adjust α_i and β_i in such a way that the solutions $x_{1,i-1}^+(\alpha_{i-1}, \vartheta_{i-1}, \lambda)$ and $y_i^+(\beta_i, \vartheta_i, \lambda)$ and the solutions $y_i^-(\beta_i, \vartheta_i, \lambda)$ and $x_{2,i}^-(\alpha_i, \vartheta_i, \lambda)$ are coupled inside Σ_Υ. With this coupling we finally construct a Lin orbit as stated in Definition 2.1.2.
Figure 2.7 shows a visualisation of such a sequence of partial orbits; for a clearer visualisation the EtoP heteroclinic cycle is shown as a heteroclinic chain. In more detail, Figure 2.8 shows how the partial orbits X_i^{12} and X_i^{21} of the sought Lin orbit relate to the solutions $x_{1/2}^\pm$ and $y^\pm$.
We start with the definition of a space of sequences which we use to couple the solutions.

Definition 2.2.33 *We define the space* Δ *as*

$$\Delta := \{(\boldsymbol{\alpha}, \boldsymbol{\beta}) = (\alpha_i, \beta_i)_{i\in\mathbb{Z}} : \alpha_i \in \operatorname{im}\left(\mathrm{id} - Q_{cu}^-(-\varpi^-, \vartheta_i, \lambda)\right) \times \operatorname{im}\left(\mathrm{id} - Q_{sc}^+(\varpi^+, \lambda)\right), \\ \beta_i \in \operatorname{im} R^-(0, \vartheta_i, \lambda) \times \operatorname{im} R^+(0, \lambda)\}.$$

We use the norm $\|(\boldsymbol{\alpha}, \boldsymbol{\beta})\|_\Delta := \max\{\|\boldsymbol{\alpha}\|, \|\boldsymbol{\beta}\|\}$ *in* Δ.

We now give the main theorem that provides the coupling in the Poincaré section Σ_Υ, see Figure 2.9 for a visualisation of this procedure.

Theorem 2.2.34 *Consider system* (1.2.1) *and assume that Conditions* (C1)–(C5) *and either Condition* (C6) *or* (C6') *hold.*
There are constants $c, \Omega > 0$, $N \in \mathbb{N}$ *such that for* $\boldsymbol{\omega} > \Omega$, $\boldsymbol{\nu} > N$, $\lambda \in \mathbb{R}^m$ *and* $\boldsymbol{\vartheta}$, $\vartheta_i \in U$, *with* $\|\boldsymbol{\vartheta}\|, \|\lambda\| < c$ *the following holds:*
There is a sequence $(\boldsymbol{\alpha}, \boldsymbol{\beta}) \in \Delta$ *such that for the corresponding solutions* $v_i(\alpha_i, \vartheta_i, \lambda)(\cdot) \in \mathcal{V}_{\omega_i}$ *and* $u_i(\beta_i, \vartheta_i, \lambda)(\cdot) \in \mathcal{U}_{\nu_i}$ *the following holds:*

$$\begin{aligned} v^+_{1,i-1}(\alpha_{i-1}, \vartheta_{i-1}, \lambda)(\varpi^+) - u^+_i(\beta_i, \vartheta_i, \lambda)(0) = 0 \text{ and} \\ v^-_{2,i}(\alpha_i, \vartheta_i, \lambda)(-\varpi^-) - u^-_i(\beta_i, \vartheta_i, \lambda)(0) = 0. \end{aligned} \tag{2.2.74}$$

To prove this theorem we formulate an equivalent fixed point problem and solve it using the Banach Fixed Point Theorem.
Consider the first coupling condition in (2.2.74). The decomposition of the corresponding terms by means of the projection $R^+(0)$ gives

$$\begin{aligned} R^+(0)v^+_{1,i-1}(\alpha_{i-1}, \vartheta_{i-1}, \lambda)(\varpi^+) = R^+(0)u^+_i(\beta_i, \vartheta_i, \lambda)(0), \\ (\mathrm{id} - R^+(0))v^+_{1,i-1}(\alpha_{i-1}, \vartheta_{i-1}, \lambda)(\varpi^+) = (\mathrm{id} - R^+(0))u^+_i(\beta_i, \vartheta_i, \lambda)(0). \end{aligned} \tag{2.2.75}$$

Using that $\mathrm{im}R^+(0) = \mathrm{im}Q^+_s(\varpi^+)$ and Lemma 2.2.32 we find that

$$\mathrm{im}(\mathrm{id} - R^+(0)) = \mathrm{im}(\mathrm{id} - Q^+_{sc}(\varpi^+)) = \mathrm{im}(\mathrm{id} - Q^+_s(\varpi^+).$$

Therefore (2.2.75) can be rewritten as

$$\begin{aligned} Q^+_s(0)v^+_{1,i-1}(\alpha_{i-1}, \vartheta_{i-1}, \lambda)(\varpi^+) = R^+(0)u^+_i(\beta_i, \vartheta_i, \lambda)(0), \\ (\mathrm{id} - Q^+_s(0))v^+_{1,i-1}(\alpha_{i-1}, \vartheta_{i-1}, \lambda)(\varpi^+) = (\mathrm{id} - R^+(0))u^+_i(\beta_i, \vartheta_i, \lambda)(0). \end{aligned} \tag{2.2.76}$$

Taking the boundary conditions (2.2.18) and (2.2.52) into consideration gives

$$\begin{aligned} (\mathrm{id} - R^+(0))u^+_i(\beta_i, \vartheta_i, \lambda)(0) = \alpha^+_{i-1}, \\ Q^+_s(\varpi^+)v^+_{1,i-1}(\alpha_{i-1}, \vartheta_{i-1}, \lambda)(\varpi^+) = \beta^+_i. \end{aligned}$$

Similar computations regarding the second coupling condition in (2.2.74) lead to

$$\begin{aligned} (\mathrm{id} - R^-(0))u^-_i(\beta_i, \vartheta_i, \lambda)(0) = \alpha^-_i, \\ Q^+_u(-\varpi^-)v^-_{2,i}(\alpha_i, \vartheta_i, \lambda)(-\varpi^-) = \beta^-_i. \end{aligned}$$

Definition 2.2.35 *The function* $\mathcal{G} = (\mathcal{G}_i)_{i\in\mathbb{Z}}$ *is defined as*

$$\begin{array}{rccc} \mathcal{G}: & \Delta \times U^{\mathbb{Z}} \times \mathbb{R}^m & \to & \Delta \\ & ((\boldsymbol{\alpha}, \boldsymbol{\beta}), \boldsymbol{\vartheta}, \lambda) & \mapsto & \mathcal{G}((\boldsymbol{\alpha}, \boldsymbol{\beta}), \boldsymbol{\vartheta}, \lambda) = (\mathcal{G}_i((\boldsymbol{\alpha}, \boldsymbol{\beta}), \boldsymbol{\vartheta}, \lambda))_{i\in\mathbb{Z}} \end{array} \tag{2.2.77}$$

with

$$\begin{aligned} &\mathcal{G}_i\left((\boldsymbol{\alpha}, \boldsymbol{\beta}), \boldsymbol{\vartheta}, \lambda\right) := \\ &\begin{pmatrix} \left((\mathrm{id} - R^-(0, \vartheta_i, \lambda))\, u^-_i(\beta_i, \vartheta_i, \lambda)(0), (\mathrm{id} - R^+(0, \lambda))\, u^+_{i+1}(\beta_{i+1}, \vartheta_{i+1}, \lambda)(0)\right) \\ \left(Q^-_u(-\varpi^-, \vartheta_i, \lambda)v^-_{2,i}(\alpha_i, \vartheta_i, \lambda)(-\varpi^-), Q^+_s(\varpi^+, \lambda)v^+_{1,i-1}(\alpha_{i-1}, \vartheta_{i-1}, \lambda)(\varpi^+)\right) \end{pmatrix}. \end{aligned} \tag{2.2.78}$$

Note that due to (2.2.49), Lemma 2.2.32 and Lemma 2.2.20, the function $\mathcal{G}(\cdot, \boldsymbol{\vartheta}, \lambda)$ indeed maps to Δ.
Hence the fixed point problem (for fixed λ and $\boldsymbol{\vartheta}$) in Δ reads

$$\mathcal{G}((\boldsymbol{\alpha}, \boldsymbol{\beta}), \boldsymbol{\vartheta}, \lambda) = (\boldsymbol{\alpha}, \boldsymbol{\beta}). \tag{2.2.79}$$

First we show that the function $\mathcal{G}$ is indeed differentiable with respect to $(\boldsymbol{\alpha}, \boldsymbol{\beta})$.

Lemma 2.2.36 *The function $\mathcal{G}$ as defined in* (2.2.77), (2.2.78) *is differentiable with respect to $(\boldsymbol{\alpha}, \boldsymbol{\beta})$.*
For the derivative of $\mathcal{G}$ at $(\boldsymbol{\alpha}_0, \boldsymbol{\beta}_0)$ the following holds:

$$D_1\mathcal{G}((\boldsymbol{\alpha}_0, \boldsymbol{\beta}_0), \boldsymbol{\vartheta}, \lambda) = \left(D_1\mathcal{G}_i((\boldsymbol{\alpha}_0, \boldsymbol{\beta}_0), \boldsymbol{\vartheta}, \lambda)\right)_{i\in\mathbb{Z}}.$$

Proof. We show that the function $\mathcal{G} : \Delta \times U^{\mathbb{Z}} \times \mathbb{R}^m \to \Delta$ is differentiable with respect to $(\boldsymbol{\alpha}, \boldsymbol{\beta})$.
For the proof we use the notation $\mathcal{G} = (\mathcal{G}_i)_{i\in\mathbb{Z}}$. We exploit that $\mathcal{G}_i$ is differentiable at $(\boldsymbol{\alpha}_0, \boldsymbol{\beta}_0)$ and that there is a constant $K > 0$ such that $\forall i \in \mathbb{Z} : \|D_1\mathcal{G}_i((\boldsymbol{\alpha}_0, \boldsymbol{\beta}_0), \boldsymbol{\vartheta}, \lambda)\| < K$. Moreover, we use that $D_1\mathcal{G}_i(\cdot, \boldsymbol{\vartheta}, \lambda)$ is continuous, uniformly in i.
Let $\boldsymbol{h} \in \Delta$. We write $\mathcal{G}((\boldsymbol{\alpha}_0, \boldsymbol{\beta}_0) + \boldsymbol{h}, \boldsymbol{\vartheta}, \lambda) = \mathcal{G}((\boldsymbol{\alpha}_0, \boldsymbol{\beta}_0), \boldsymbol{\vartheta}, \lambda) + (D_1\mathcal{G}_i((\boldsymbol{\alpha}_0, \boldsymbol{\beta}_0), \boldsymbol{\vartheta}, \lambda)\boldsymbol{h})_{i\in\mathbb{Z}} + \mathcal{R}(\boldsymbol{h})$. The existence of the constant K ensures that $\boldsymbol{h} \mapsto (D_1\mathcal{G}_i((\boldsymbol{\alpha}_0, \boldsymbol{\beta}_0), \boldsymbol{\vartheta}, \lambda)\boldsymbol{h})_{i\in\mathbb{Z}}$ is a bounded linear mapping from Δ into Δ. It remains to prove that $\mathcal{R}(\boldsymbol{h}) = o(\|\boldsymbol{h}\|)$. Let $\mathcal{R}^i(\boldsymbol{h}) := P^i\mathcal{R}(\boldsymbol{h})$ where P^i projects to the i-th component. Then we can show that $\sup_{i\in\mathbb{Z}} \mathcal{R}^i(\boldsymbol{h}) = o(\|\boldsymbol{h}\|)$ as follows. We apply the mean value theorem, this leads to

$$\exists \eta \in (0,1), \text{ such that } \mathcal{G}_i((\boldsymbol{\alpha}_0, \boldsymbol{\beta}_0) + \boldsymbol{h}, \boldsymbol{\vartheta}, \lambda) = D_1\mathcal{G}_i((\boldsymbol{\alpha}_0, \boldsymbol{\beta}_0) + \eta\boldsymbol{h}, \boldsymbol{\vartheta}, \lambda)\boldsymbol{h}$$

and thus

$$\begin{aligned}
\mathcal{R}^i(\boldsymbol{h}) &= P^i\mathcal{G}((\boldsymbol{\alpha}_0, \boldsymbol{\beta}_0) + \boldsymbol{h}, \boldsymbol{\vartheta}, \lambda) - P^i\mathcal{G}((\boldsymbol{\alpha}_0, \boldsymbol{\beta}_0), \boldsymbol{\vartheta}, \lambda) - P^i(D_1\mathcal{G}((\boldsymbol{\alpha}_0, \boldsymbol{\beta}_0), \boldsymbol{\vartheta}, \lambda)\boldsymbol{h})_{i\in\mathbb{Z}} \\
&= D_1\mathcal{G}_i((\boldsymbol{\alpha}_0, \boldsymbol{\beta}_0) + \eta\boldsymbol{h}, \boldsymbol{\vartheta}, \lambda)\boldsymbol{h} - D_1\mathcal{G}_i((\boldsymbol{\alpha}_0, \boldsymbol{\beta}_0), \boldsymbol{\vartheta}, \lambda)\boldsymbol{h} \\
&= (D_1\mathcal{G}_i((\boldsymbol{\alpha}_0, \boldsymbol{\beta}_0) + \eta\boldsymbol{h}, \boldsymbol{\vartheta}, \lambda) - D_1\mathcal{G}_i((\boldsymbol{\alpha}_0, \boldsymbol{\beta}_0), \boldsymbol{\vartheta}, \lambda))\boldsymbol{h}.
\end{aligned}$$

Since $D_1\mathcal{G}_i(\cdot, \boldsymbol{\vartheta}, \lambda)$ is continuous, uniformly in i, $\mathcal{R} = o(\|\boldsymbol{h}\|)$ follows.
Now, if $\mathcal{G}(\cdot, \boldsymbol{\vartheta}, \lambda)$ is differentiable at $(\boldsymbol{\alpha}_0, \boldsymbol{\beta}_0)$, the derivative is composed of the derivatives of the $\mathcal{G}_i$: $D_1\mathcal{G}((\boldsymbol{\alpha}_0, \boldsymbol{\beta}_0), \boldsymbol{\vartheta}, \lambda) = (D_1\mathcal{G}_i((\boldsymbol{\alpha}_0, \boldsymbol{\beta}_0), \boldsymbol{\vartheta}, \lambda))_{i\in\mathbb{Z}}$. □

Now we can utilise the Banach Fixed Point Theorem to prove the existence and uniqueness of a solution to the fixed point equation (2.2.79).

Lemma 2.2.37 *There are constants $c, \Omega > 0$, $N \in \mathbb{N}$ such that for given sequences $\boldsymbol{\omega} > \Omega$, $\boldsymbol{\nu} > N$ and for $\boldsymbol{\vartheta}$, $\vartheta_i \in U$, $\lambda \in \mathbb{R}^m$ with $\|\boldsymbol{\vartheta}\|, \|\lambda\| < c$ (in a sufficiently small neighbourhood of $0 \in \Delta$), there is a unique solution to the fixed point problem* (2.2.79).

Proof. First we show that there is a ball $B \subset \Delta$ such that $\mathcal{G}$ leaves B invariant. Then we show that there is a $K > 0$ such that $\|D_1\mathcal{G}\| \leq K < 1$ and thus the Banach Fixed Point Theorem tells us that there is one unique solution to the fixed point problem.

Let $\|(\boldsymbol{\alpha},\boldsymbol{\beta})\| < \tilde{c}$, according to Lemma 2.2.18. Then there is a constant $\hat{C} \geq 1$ such that

$$\left\|Q_s^+(\varpi^+,\lambda)v_{1,i}^+(\alpha_i,\vartheta,\lambda)(\varpi^+)\right\| \leq 2\hat{C}\tilde{c}e^{-l\varpi^+} + \frac{2\tilde{c}}{3},$$

and thus if ϖ^+ is large enough

$$\left\|Q_s^+(\varpi^+,\lambda)v_{1,i}^+(\alpha_i,\vartheta,\lambda)(\varpi^+)\right\| \leq \frac{5}{6}\tilde{c}$$

holds.
Proceeding in the same manner with the remaining components of $\mathcal{G}$ we find that $\mathcal{G}(\cdot,\vartheta,\lambda)$ leaves the ball $B(0,\tilde{c}) \subset \Delta$ invariant.
Next we consider the derivative of $\mathcal{G}(\cdot,\vartheta,\lambda)$ and show that its norm is smaller than one.

$$\begin{aligned}\|D_1\mathcal{G}((\boldsymbol{\alpha},\boldsymbol{\beta}),\boldsymbol{\vartheta},\lambda)\| = \sup_{i\in\mathbb{Z}}\Big\{\max\Big\{&\left\|D_\alpha Q_s^+(0,\lambda)v_{1,i-1}^+(\alpha_{i-1},\vartheta_{i-1},\lambda)(\varpi^+)\right\|,\\ &\left\|D_\beta(\mathrm{id}-R^+(0,\lambda))u_{i+1}^+(\beta_{i+1},\vartheta_{i+1},\lambda)(0)\right\|,\\ &\left\|D_\alpha Q_u^-(0,\vartheta_i,\lambda)v_{2,i}^-(\alpha_i,\vartheta_i,\lambda)(-\varpi^-)\right\|,\\ &\left\|D_\beta(\mathrm{id}-R^-(0,\vartheta_i,\lambda))u_i^-(\beta_i,\vartheta_i,\lambda)(0)\right\|\Big\}\Big\}.\end{aligned}$$

Using (2.2.16) and (2.2.51) on the terms in the above equations, it follows that there is a constant $\hat{K}$ such that for ϖ^+, ϖ^- and N large enough

$$\|D_1\mathcal{G}((\boldsymbol{\alpha},\boldsymbol{\beta}),\boldsymbol{\vartheta},\lambda)\| \leq \hat{K} < 1.$$

From the Banach Fixed Point Theorem immediately follows the existence of a unique solution to the fixed point problem (2.2.79).

□

Now we can give an explicite expression for the Lin orbit as stated in Definition 2.1.2.
To finally construct the Lin orbit, we need to incorporate the solutions of the discrete dynamical system into the (global) continuous system. This can be done as follows: Let $\varphi^t(\cdot)$ be the flow of (1.2.1) and let $y^\pm$ and $x^\pm$ denote the coupled solutions of (1.2.1) and (2.2.43), respectively. Then there are numbers T_ν^+ and T_ν^- such that $\varphi^{T_\nu^+}(y^+(0)) = y^+(\nu^+)$ and $\varphi^{-T_\nu^-}(y^-(0)) = y^-(-\nu^-)$. We define

$$\begin{aligned}X_i^{12} &:= \{x_{1,i-1}^+(t), t\in[0,\varpi^+]\} \cup \{\varphi^t(y_i^+(0)), t\in[0,T_\nu^+]\},\\ X_i^{21} &:= \{\varphi^t(y_i^-(0)), t\in[-T_\nu^-,0]\} \cup \{x_{2,i}^-(t), t\in[-\varpi^-,0]\}.\end{aligned}$$

This concludes our consideration of the coupling and proves Theorem 2.1.4. Note that in general the constructed Lin orbit is uniquely determined by selecting a sequence of transition times $\boldsymbol{\omega}$, a sequence of revolutions $\boldsymbol{\nu}$, a sequence of parameters $\boldsymbol{\vartheta}$ and a parameter value λ. However, in the case of Condition (C6), the dependence on the sequence $\boldsymbol{\vartheta}$ does not contribute to the dynamics and is therefore usually neglected, see also the discussion in Section 2.3.

2.3 Estimates of the jump

For the bifurcation analysis of a system with a heteroclinic cycle, it is important to know more about the jumps that occur in the constructed Lin orbit. In this section we derive estimates for the leading terms of the jump function that allow us to state (and solve) bifurcation equations for different types of orbits in Section 2.4.
The following explanations only cover the jump estimates mentioned in Theorem 2.1.5, but in principle they also apply to the complex leading eigenvalue situation in Theorem 2.1.6. The proof of the differentiability of the jump function is not carried out, we refer to the work of Sandstede [San93] and Knobloch [Kno04] for the corresponding results. Note that the jump estimates stated in Theorem 2.1.5 and Theorem 2.1.6 only refer to the situation described in Condition (C1)–(C6) and therefore only the jump in Z_1 is considered. Moreover, although the Lin orbit and the corresponding solutions that are used here are dependent on a sequence $\boldsymbol{\vartheta}$, $\vartheta_i \in U$, this dependence is neglected (also in the theorems and lemmas) as it does not contribute to the dynamical features (in essence, this dependence only selects which of the infinitely many possible orbits in $W^u(\Upsilon) \cap W^s(p)$ the Lin orbit follows, but this does not have immediate influence on the jump in Z_1). The situation in case of Condition (C6') is different, here we consider a tangency of $W^u(\Upsilon)$ and $W^s(p)$ and therefore there is a jump in Z_2 to be considered. Then the dependence on $\boldsymbol{\vartheta}$ is indeed crucial for the jumps. In Section 2.4.1 we give some results for this case (but for reasons of simplicity we restrict these considerations to $\mathbb{R}^3$).

2.3.1 Leading terms

According to the first step of Lin's method, the parameter λ itself can be used to measure the splitting of the stable and unstable manifolds. Therefore, the i-th jump of the jump function $\boldsymbol{\Xi} = (\Xi_i)_{i\in\mathbb{Z}}$ can be split into two parts:

$$\Xi_i(\boldsymbol{\omega}, \boldsymbol{\nu}, \lambda) := \xi^\infty(\lambda) + \xi_i(\boldsymbol{\omega}, \boldsymbol{\nu}, \lambda).$$

According to the result in Section 2.2.1 and in [Rie03] with Hypothesis (H 2.7), we can set $\xi^\infty(\lambda) = \lambda$, so it remains to examine the ξ_i. Due to this setting, the ξ_i are given by

$$\xi_i(\boldsymbol{\omega}, \boldsymbol{\nu}, \lambda) := v^+_{1,i}(0) - v^-_{1,i}(0).$$

The structure of the terms of Ξ_i under Hypothesis (H 2.1) is stated in Theorem 2.1.5, therefore proving the following lemma about the structure of ξ_i also proves Theorem 2.1.5. Note that we assume that Hypothesis (H 2.3) and Hypothesis (H 2.4) hold.

Lemma 2.3.1 *Assume that the leading eigenvalues are as stated in Hypothesis* (H 2.1)*. Let* $\Omega, N, \boldsymbol{\omega}, \boldsymbol{\nu}$ *be as in Theorem* 2.1.4*.*
Then the structure of the function ξ_i *is as follows:*

$$\xi_i(\boldsymbol{\omega}, \boldsymbol{\nu}, \lambda) = c_1(\lambda) e^{2\mu^s(\lambda)\omega_i} + c_2(\lambda) \left(\mu^u_\Upsilon(\lambda)\right)^{-\nu_{i+1}} + o\left(e^{2\mu^s(\lambda)\Omega}\right) + o\left(\left(\mu^u_\Upsilon(\lambda)\right)^{-N}\right) + \mathcal{R}(\Omega, N)$$

with $\mathcal{R}(\Omega, N) = O\left(\left(\mu_\Upsilon^u(\lambda)\right)^{-N} e^{2\mu^s(\lambda)\Omega}\right)$.
The functions $c_{1,2} : \mathbb{R}^m \to \mathbb{R}^{\dim Z_1}$ *are continuous and* $c_{1,2}(0) \neq 0$ *holds. The o-terms and the O-term are valid for* Ω *and* N *tending to infinity.*

We prove Lemma 2.3.1 in several steps. Note that in this section we denote solutions and auxiliary variables that correspond to the discrete system with a subscript 'Π' where the notation may be ambiguous.
First, we consider the basis of Z_1 denoted by $\{z^j, 1 \leq j \leq \dim Z_1\}$. Now let $\langle \cdot, \cdot \rangle$ be a scalar product in Y_1. Then we can write

$$\xi_i(\boldsymbol{\omega}, \boldsymbol{\nu}, \lambda) = \sum_{j=1}^{\dim Z_1} \left\langle z^j, \xi_i(\boldsymbol{\omega}, \boldsymbol{\nu}, \lambda) \right\rangle z^j.$$

Assuming that $\langle \cdot, \cdot \rangle$ is such that the direct sum decomposition (2.2.1) is orthogonal gives

$$\begin{aligned} \left\langle z^j, \xi_i(\boldsymbol{\omega}, \boldsymbol{\nu}, \lambda) \right\rangle = &\left\langle z^j, \left(\mathrm{id} - Q_{sc}^+(0, \lambda)\right) v_{1,i}^+(\boldsymbol{\omega}, \boldsymbol{\nu}, \lambda)(0) \right\rangle \\ &- \left\langle z^j, \left(\mathrm{id} - P^-(0, \lambda)\right) v_{1,i}^-(\boldsymbol{\omega}, \boldsymbol{\nu}, \lambda)(0) \right\rangle. \end{aligned} \tag{2.3.1}$$

The term $\left\langle z^j, \left(\mathrm{id} - P^-(0, \lambda)\right) v_{1,i}^-(\boldsymbol{\omega}, \boldsymbol{\nu}, \lambda)(0) \right\rangle$ in (2.3.1) can be treated exactly as in [Kno04], Section 3.6.3. This results in

$$\begin{aligned} \left\langle z^j, \left(\mathrm{id} - P^-(0, \lambda)\right) v_{1,i}^-(\boldsymbol{\omega}, \boldsymbol{\nu}, \lambda)(0) \right\rangle = &\Bigg\langle \Phi_1^- \left(0, -\omega_i\right)^T \left(\mathrm{id} - P^-(0)\right)^T z^j, \\ &\left(\mathrm{id} - \tilde{P}(\omega_i, \lambda)\right) \Big\{ \gamma_1^- \left(-\omega_i, \lambda\right) - \gamma_2^+ \left(\omega_i, \lambda\right) \\ &- P^+ \left(\omega_i, \lambda\right) v_{2,i}^+ \left(\omega_i\right) + P^- \left(-\omega_i, \lambda\right) v_{1,i}^- \left(-\omega_i\right) \Big\} \Bigg\rangle \\ &+ \left\langle z^j, \int_{-\omega_i}^0 \Phi_1^-(0, \tau)(\mathrm{id} - P^-(\tau)) h_1^-(\tau, v_{1,i}^-(\tau), \lambda) d\tau \right\rangle. \end{aligned} \tag{2.3.2}$$

In the same spirit we can treat the scalar product $\left\langle z^j, (\mathrm{id} - Q_{sc}^+(0, \lambda)) v_{1,i}^+(\boldsymbol{\omega}, \boldsymbol{\nu}, \lambda)(0) \right\rangle$. However, the details differ slightly in comparison with the situation in [Kno04]. For that reason we discuss our procedure in more detail.
First recall from Section 2.2.2 that

$$\begin{aligned} \left(\mathrm{id} - Q_{sc}^+(0)\right) v_{1,i}^+(\boldsymbol{\omega}, \boldsymbol{\nu}, \lambda)(0) = &\Phi_1^+(0, \varpi^+)\alpha_i^+ \\ &- \int_0^{\varpi^+} \Phi_1^+(0, \tau)(\mathrm{id} - Q_{sc}^+(\tau)) h_1^+(\tau, v_{1,i}^+(\tau), \lambda) d\tau. \end{aligned} \tag{2.3.3}$$

Using the boundary condition (2.2.18) for $v_{1,i}^+$ and the global coupling (2.2.74) gives

$$\begin{aligned} \alpha_i^+ &= \left(\mathrm{id} - Q_{sc}^+(\varpi^+, \lambda)\right) v_{1,i}^+(\varpi^+) = \left(\mathrm{id} - R^+(0, \lambda)\right) u_{i+1}^+(0) \\ &= \Phi_\Pi^+(0, \nu) b_{i+1}^+ - \sum_{m=1}^{\nu} \Phi_\Pi^+(0, m)(\mathrm{id} - R^+(0, \lambda)) h_\Pi^+(m-1, u_{i+1}^+(m-1), \lambda). \end{aligned} \tag{2.3.4}$$

And for b^+_{i+1} we use the equation (see (2.2.64))

$$b^+_{i+1} - b^-_{i+1} = \gamma^-_\Pi(-\nu^-_{i+1}, \lambda) - \gamma^+_\Pi(\nu^+_{i+1}, \lambda) - R^+(\nu^+_{i+1}, \lambda)u^+_{i+1}(\nu^+_{i+1}) + R^-(-\nu^-_{i+1}, \lambda)u^-_{i+1}(-\nu^-_{i+1}).$$

Applying $\tilde{R}$ as defined in Lemma 2.2.21 yields an expression for b^+ that can be plugged into (2.3.4) and thus we can finally establish the equation

$$\begin{aligned}\left(\mathrm{id} - Q^+_{sc}(0)\right) v^+_{1,i}(\boldsymbol{\omega}, \boldsymbol{\nu}, \lambda)(0) =& \Phi^+_1(0, \varpi^+)\circ \\ &\Bigg[\Phi^+_\Pi(0, \nu^+_{i+1})\left(\mathrm{id} - R^+(\nu^+_{i+1})\right)\tilde{R}(\nu^+_{i+1}, \nu^-_{i+1}, \lambda)\circ \\ &\Big\{\gamma^-_\Pi(-\nu^-_{i+1}, \lambda) - \gamma^+_\Pi(\nu^+_{i+1}, \lambda) \\ &- R^+(\nu^+_{i+1}, \lambda)u^+_{i+1}(\nu^+_{i+1}) + R^-(-\nu^-_{i+1}, \lambda)u^-_{i+1}(-\nu^-_{i+1})\Big\} \\ &- \sum_{m=1}^{\nu^+_{i+1}} \Phi^+_\Pi(0, m)(\mathrm{id} - R^+(0, \lambda))h^+_\Pi(m-1, u^+_{i+1}(m-1), \lambda)\Bigg] \\ &- \int_0^{\varpi^+} \Phi^+_1(0, \tau)(\mathrm{id} - Q^+_{sc}(\tau))h^+_1(\tau, v^+_{1,i}(\tau), \lambda)d\tau.\end{aligned} \tag{2.3.5}$$

Plugging (2.3.5) and (2.3.2) into (2.3.1) we end up with the following equation:

$$
\begin{aligned}
\left\langle z^j, \xi_i(\boldsymbol{\omega}, \boldsymbol{\nu}, \lambda) \right\rangle = \\
&\Bigg\langle \Phi_\Pi^+(0,\nu_{i+1}^+)^T \left(\mathrm{id} - R^+(0,\lambda)\right)^T \Phi_1^+(0,\varpi^+)^T z^j, \\
&\quad \tilde{R}(\nu_{i+1}^+, \nu_{i+1}^-, \lambda) \Big\{ \gamma_\Pi^-(-\nu_{i+1}^-,\lambda) - \gamma_\Pi^+(\nu_{i+1}^+,\lambda) \\
&\qquad - R^+(\nu_{i+1}^+,\lambda) u_{i+1}^+(\nu_{i+1}^+) + R^-(-\nu_{i+1}^-,\lambda) u_{i+1}^-(-\nu_{i+1}^-) \Big\} \Bigg\rangle \\
&- \left\langle \Phi_1^+(0,\varpi^+)^T z^j, \sum_{m=1}^{\nu_{i+1}^+} \Phi_\Pi^+(0,m)(\mathrm{id} - R^+(0,\lambda)) h_\Pi^+(m-1, u_{i+1}^+(m-1),\lambda) \right\rangle \\
&- \left\langle z^j, \int_0^{\varpi^+} \Phi_1^+(0,\tau)(\mathrm{id} - Q_{sc}^+(\tau)) h_1^+(\tau, v_{1,i}^+(\tau),\lambda) d\tau \right\rangle \\
&- \Bigg\langle \Phi_1^-(0,-\omega_i)^T \left(\mathrm{id} - P^-(0)\right)^T z^j, \\
&\quad \left(\mathrm{id} - \tilde{P}(\omega_i,\lambda)\right) \Big\{ \gamma_1^-(-\omega_i,\lambda) - \gamma_2^+(\omega_i,\lambda) \\
&\qquad - P^+(\omega_i,\lambda) v_{2,i}^+(\omega_i) + P^-(-\omega_i,\lambda) v_{1,i}^-(-\omega_i) \Big\} \Bigg\rangle \\
&- \left\langle z^j, \int_{-\omega_i}^0 \Phi_1^-(0,\tau)(\mathrm{id} - P^-(\tau)) h_1^-(\tau, v_{1,i}^-(\tau),\lambda) d\tau \right\rangle .
\end{aligned}
\tag{2.3.6}
$$

Next we estimate the individual terms in (2.3.6) to finally find the leading terms of the jump function. Note that most of the following estimates are similar to the estimates in [Kno04], however, the terms $\tilde{R}(-R^+u_{i+1}^+ + R^-u_{i+1}^-)$ and $\int_0^{\varpi^+} \Phi_1^+(\mathrm{id} - Q_{sc}^+)h_1^+$ are different from the 'classical' case and therefore we look at these terms in greater detail. Also note that the following estimates basically also hold true for complex leading eigenvalues.

Estimates of $(\Phi_\Pi^+)^T(\mathrm{id} - R^+)^T(\Phi_1^+)^T z^j$
We define $\tilde{z}^j := \Phi_1^+(0,\varpi^+)^T z^j$ and therefore look for an estimate of $(\Phi_\Pi^+)^T(\mathrm{id} - R^+)^T \tilde{z}^j$.
In accordance with the consideration in [Kno04], Section 3.6.3, we find

$$
\begin{aligned}
&\Phi_\Pi^+(0,\nu_{i+1}^+,\lambda)^T(\mathrm{id} - R^+(0,\lambda))^T \tilde{z}^j \\
&\quad = (\mu_\Upsilon^u(\lambda))^{-\nu_{i+1}^+} \eta^+(\tilde{z}^j,\lambda) + O\left(\left(\max\{(\bar{\mu}_\Upsilon^u)^{-2}, (\bar{\mu}_\Upsilon^{uu})^{-1}\} \right)^{\nu_{i+1}^+} \right).
\end{aligned}
$$

Here, η^+ is a nonzero eigenvector of $\left((D_1\Pi(q,\lambda))^{-1}\right)^T$ belonging to the eigenvalue $(\mu_\Upsilon^u(\lambda))^{-1}$. For more details, see again [Kno04].

Estimates of $\tilde{R}(\gamma_\Pi^- + \gamma_\Pi^+)$
Also the estimates of $\tilde{R}(\nu_{i+1}^+, \nu_{i+1}^-, \lambda)\gamma_\Pi^-(-\nu_{i+1}, \lambda)$ and $\tilde{R}(\nu_{i+1}^+, \nu_{i+1}^-, \lambda)\gamma_\Pi^+(\nu_{i+1}, \lambda)$ run completely parallel to the computations in [Kno04], Section 3.6.3. Following the procedure presented there, we find

$$\begin{aligned}\tilde{R}(\nu_{i+1}^+, \nu_{i+1}^-, \lambda)\gamma_\Pi^-(-\nu_{i+1}^-, \lambda) = &(\mu_\Upsilon^u(\lambda))^{-\nu_{i+1}^-}\eta^u(\lambda)\\ &+ O\left(\left(\max\{\bar{\mu}_\Upsilon^s, (\bar{\mu}_\Upsilon^u)^{-1}\}(\mu_\Upsilon^u(\lambda))^{-1}\right)^{\nu_{i+1}^-}\right)\\ &+ O\left(\left(\max\{(\bar{\mu}_\Upsilon^u)^{-2}, (\bar{\mu}_\Upsilon^{uu})^{-1}\}\right)^{\nu_{i+1}^-}\right)\end{aligned} \tag{2.3.7}$$

and

$$\begin{aligned}\tilde{R}(\nu_{i+1}^+, \nu_{i+1}^-, \lambda)\gamma_\Pi^+(\nu_{i+1}^+, \lambda) =&O\left(\left(\max\{\bar{\mu}_\Upsilon^s, (\bar{\mu}_\Upsilon^u)^{-1}\}\mu_\Upsilon^s(\lambda)\right)^{\nu_{i+1}^+}\right)\\ &+ O\left(\left(\max\{\bar{\mu}_\Upsilon^s, (\bar{\mu}_\Upsilon^u)^{-1}\}\max\{(\bar{\mu}_\Upsilon^s)^2, \bar{\mu}_\Upsilon^{ss}\}\right)^{\nu_{i+1}^+}\right).\end{aligned} \tag{2.3.8}$$

Here, $\eta^u(\lambda)$ is a nonzero eigenvector of $D_1\Pi(q, \lambda)$ belonging to the eigenvalue μ_Υ^u.

First summary
Our above considerations so far yield

$$\left\langle \Phi_\Pi^T(\mathrm{id} - R^+)\tilde{z}^j, \tilde{R}(\gamma_\Pi^- + \gamma_\Pi^+)\right\rangle = \left\langle \eta^+(\tilde{z}^j, \lambda), \eta^u(\lambda)\right\rangle (\mu_\Upsilon^u)^{-\nu_{i+1}} + o\left((\mu_\Upsilon^u)^{-\nu_{i+1}}\right).$$

Furthermore, linear algebra tells that

$$c_2^j(\lambda) := \left\langle \eta^+(\tilde{z}^j, \lambda), \eta^u(\lambda)\right\rangle \neq 0. \tag{2.3.9}$$

In what follows we show that $c_2^j(\lambda)(\mu_\Upsilon^u)^{\nu_{i+1}}$ is one of the leading terms of the expression in (2.3.6).

Estimates of $\tilde{R}(R^- u_{i+1}^- - R^+ u_{i+1}^+)$
We consider $\left\|R^-(-\nu_{i+1}^-, \lambda)u_{i+1}^-(-\nu_{i+1}^-) - R^+(\nu_{i+1}^+, \lambda)u_{i+1}^+(\nu_{i+1}^+)\right\|$ and follow the lines of the proof in [Kno04].
Let $\mathcal{H}_\Pi = (H_\Pi^-, H_\Pi^+)$ be the Nemyzki operator as introduced in Section 2.2.3. Then we have (looking carefully at the proof of Lemma 2.2.26)

$$\begin{aligned}&\left\|R^-(-\nu_{i+1}^-, \lambda)u_{i+1}^-(-\nu_{i+1}^-) - R^+(\nu_{i+1}^+, \lambda)u_{i+1}^+(\nu_{i+1}^+)\right\|\\ &\quad\leq \tilde{C}_1 e^{2\max\{\ln\bar{\mu}_\Upsilon^s, -\ln\bar{\mu}_\Upsilon^u\}\nu_{i+1}^+}\|\beta_{i+1}\| + C_2(\left\|H_\Pi^+(u_{i+1}^+, \lambda)\right\| + \left\|H_\Pi^-(u_{i+1}^-, \lambda)\right\|)\\ &\quad\leq C_1 e^{2\max\{\ln\bar{\mu}_\Upsilon^s, -\ln\bar{\mu}_\Upsilon^u\}\nu_{i+1}^+} + C_2(\left\|H_\Pi^+(u_{i+1}^+, \lambda)\right\| + \left\|H_\Pi^-(u_{i+1}^-, \lambda)\right\|).\end{aligned} \tag{2.3.10}$$

Due to the definition of $H_\Pi^{+/-}$, we have $H_\Pi^{+/-}(0, \lambda) = 0$ and $D_1 H_\Pi^{+/-}(0, \lambda) = 0$ and hence

$$H_\Pi^{+/-}(u^{+/-}, \lambda) = O\left(\left\|u^{+/-}\right\|^2\right). \tag{2.3.11}$$

Now $u^{+/-}$ can be estimated (according to (2.2.66))

$$\left\|(u^-_{i+1}, u^+_{i+1})\right\| \leq C(\left\|(H^-_\Pi(u^-_{i+1}, \lambda), H^+_\Pi(u^+_{i+1}, \lambda))\right\| + \|\beta_{i+1}\| + \|d_{\Pi,i+1}(\nu_{i+1}, \lambda)\|).$$

Due to (2.3.11), there is $\varepsilon > 0$ such that for $\|u_{i+1}\| < \varepsilon$ the following holds:

$$C\left\|(H^-_\Pi(u^-_{i+1}, \lambda), H^+_\Pi(u^+_{i+1}, \lambda))\right\| < \frac{1}{2}\left\|(u^-_{i+1}, u^+_{i+1})\right\|$$

and thus there is a constant C such that

$$\left\|(u^-_{i+1}, u^+_{i+1})\right\| \leq C(\|\beta_{i+1}\| + \|d_{\Pi,i+1}\|). \tag{2.3.12}$$

The term $\|d_{\Pi,i+1}\|$ can be estimated by using the definition of $d = d_\Pi$ (see (2.2.73)) and a representation of $\gamma^\pm_\Pi$ (similar to the one used in (2.3.7) and (2.3.8)), thus

$$\begin{aligned}\|d_{\Pi,i+1}\| &= \left\|\gamma^-_\Pi(\lambda)(-\nu^-_{i+1}) - \gamma^+_\Pi(\lambda)(\nu^+_{i+1})\right\| \\ &\leq \left\|(\mu^u_\Upsilon(\lambda))^{-\nu^-_{i+1}}\eta^u(\lambda)\right\| + O\left((\max\{(\bar\mu^u_\Upsilon)^{-2}, (\bar\mu^{uu}_\Upsilon)^{-1}\})^{\nu^-_{i+1}}\right) \\ &\quad + \left\|(\mu^s_\Upsilon(\lambda))^{\nu^+_{i+1}}\eta^s(\lambda)\right\| + O\left((\max\{(\bar\mu^s_\Upsilon)^{2}, \bar\mu^{ss}_\Upsilon\})^{\nu^+_{i+1}}\right)\end{aligned}$$

holds. So we have $d_{\Pi,i+1} = O((\max\{\bar\mu^s_\Upsilon, (\bar\mu^u_\Upsilon)^{-1}\})^{\nu^+_{i+1}})$.
It remains to estimate $\|\beta_{i+1}\|$ in (2.3.12). The global coupling from Section 2.2.4 yields

$$\left\|\beta^+_{i+1}\right\| = \left\|\alpha^+_{\perp,i}\right\| \text{ and } \left\|\beta^-_{i+1}\right\| = \left\|\alpha^-_{\perp,i+1}\right\|.$$

Using estimate (2.2.15) we get

$$\begin{aligned}\left\|\alpha^+_{\perp,i}\right\| &\leq C\left(\left\|H^+_1(v^+_{1,i})\right\| + \|d_i\| + \|\alpha_i\|\right)e^{\ln\bar\mu^s_\Upsilon\varpi^+} + C\left\|H^+_1(v^+_{1,i})\right\|, \\ \left\|\alpha^-_{\perp,i+1}\right\| &\leq C\left(\left\|H^-_2(v^-_{2,i+1})\right\| + \|d_{i+1}\| + \|\alpha_{i+1}\|\right)e^{\ln\bar\mu^s_\Upsilon\varpi^+} + C\left\|H^-_2(v^-_{2,i+1})\right\|.\end{aligned} \tag{2.3.13}$$

Next we consider the individual terms in the right-hand side of (2.3.13). Due to the coupling, we get

$$\|\alpha_i\| = \left\|(\alpha^-_i, \alpha^+_i)\right\| = \left\|(\beta^-_{\perp,i}, \beta^+_{\perp,i+1})\right\|.$$

To estimate the term $\left\|(\beta^-_{\perp,i}, \beta^+_{\perp,i+1})\right\|$ we use results from the considerations in [Den89]. There, solutions that pass by a hyperbolic equilibrium are considered. These solutions satisfy certain linear boundary conditions as known from the theory of Shilnikov variables, cf. Figure 2.6 for a visualisation of such boundary conditions. The main result is that for given projection boundary conditions the complementary projections of the start and the end point of the solutions decay exponentially fast for increasing transition time. Using the same argument for discrete dynamical systems (as briefly introduced in the remarks of [Den89]) the exponential decay of $\left\|\beta^-_{\perp,i}\right\|$ and $\left\|\beta^+_{\perp,i+1}\right\|$ for increasing transition steps follows immediately. The rate of the exponential decay is determined by the leading eigenvalues of the linearisation at the equilibrium. Thus we have

$$\left\|(\beta^-_{\perp,i}, \beta^+_{\perp,i+1})\right\| \leq C\left(\max(\bar\mu^s_\Upsilon, (\bar\mu^u_\Upsilon)^{-1})\right)^{\nu_i} + C\left(\max(\bar\mu^s_\Upsilon, (\bar\mu^u_\Upsilon)^{-1})\right)^{\nu_{i+1}},$$

and hence

$$\|\alpha_i\| = O(\big(\max(\bar{\mu}^s_\Upsilon, (\bar{\mu}^u_\Upsilon)^{-1})\big)^{\nu_i}) + O(\big(\max(\bar{\mu}^s_\Upsilon, (\bar{\mu}^u_\Upsilon)^{-1})\big)^{\nu_{i+1}}). \tag{2.3.14}$$

The term $\|d_i\|$ (note that this d_i is from the continuous system, Section 2.2.2) can be estimated similar to the discrete $\|d_\Pi\|$ as done before. This yields $d_i = O(e^{\max\{\bar{\mu}^s, -\bar{\mu}^u\}\omega_i})$.
Finally, we estimate H_1^+ by using that $H_1^+(v_1^+) = O\left(\left\|v_1^+\right\|^2\right)$ and (from (2.2.33))

$$\left\|v_{1,i}^+\right\| \leq C\left(\left\|H_1^+(v_{1,i}^+)\right\| + \|d_i\| + \|\alpha_i\|\right).$$

Then there is an $\varepsilon > 0$ such that for $\left\|v_{1,i}^+\right\| < \varepsilon$

$$C\left\|H_1^+(v_{1,i}^+)\right\| < \frac{1}{2}\left\|v_{1,i}^+\right\|$$

holds and hence

$$\left\|v_{1,i}^+\right\| \leq C(\|d_i\| + \|\alpha_i\|).$$

Using the above estimates for $\|\alpha_i\|$ and $\|d_i\|$ yields

$$\left\|v_{1,i}^+\right\| = O((e^{\max\{\bar{\mu}^s, -\bar{\mu}^u\}\omega_i}) + O(\big(\max(\bar{\mu}^s_\Upsilon, (\bar{\mu}^u_\Upsilon)^{-1})\big)^{\nu_i}) + O(\big(\max(\bar{\mu}^s_\Upsilon, (\bar{\mu}^u_\Upsilon)^{-1})\big)^{\nu_{i+1}}). \tag{2.3.15}$$

Furthermore, using $H_1^+(v_1^+) = O\left(\left\|v_1^+\right\|^2\right)$ and plugging this (and a similar estimate for H_2^-) in (2.3.13), then from (2.3.12) follows

$$\begin{aligned}\left\|(u_{i+1}^-, u_{i+1}^+)\right\| =& O((e^{\max\{\bar{\mu}^s, -\bar{\mu}^u\}\omega_i}) + O((e^{\max\{\bar{\mu}^s, -\bar{\mu}^u\}\omega_{i+1}}) \\ &+ O(\big(\max(\bar{\mu}^s_\Upsilon, (\bar{\mu}^u_\Upsilon)^{-1})\big)^{\nu_i}) + O(\big(\max(\bar{\mu}^s_\Upsilon, (\bar{\mu}^u_\Upsilon)^{-1})\big)^{\nu_{i+1}}) \\ &+ O(\big(\max(\bar{\mu}^s_\Upsilon, (\bar{\mu}^u_\Upsilon)^{-1})\big)^{\nu_{i+2}}).\end{aligned}$$

Hence, by (2.3.11), we find that

$$\begin{aligned}(H_\Pi^-, H_\Pi^+) =& O((e^{2\max\{\bar{\mu}^s, -\bar{\mu}^u\}\omega_i}) + O((e^{2\max\{\bar{\mu}^s, -\bar{\mu}^u\}\omega_{i+1}}) \\ &+ O(\big(\max(\bar{\mu}^s_\Upsilon, (\bar{\mu}^u_\Upsilon)^{-1})\big)^{\nu_i}) + O(\big(\max(\bar{\mu}^s_\Upsilon, (\bar{\mu}^u_\Upsilon)^{-1})\big)^{\nu_{i+1}}) \\ &+ O(\big(\max(\bar{\mu}^s_\Upsilon, (\bar{\mu}^u_\Upsilon)^{-1})\big)^{\nu_{i+2}}).\end{aligned}$$

Plugging this estimate for $H_\Pi^\pm$ into (2.3.10) and using the boundedness of $\tilde{R}$ finally yields

$$\begin{aligned}&\tilde{R}(\nu_{i+1}^+, \nu_{i+1}^-, \lambda)\left[R^-(-\nu_{i+1}^-, \lambda)u_{i+1}^-(-\nu_{i+1}^-) - R^+(\nu_{i+1}^+, \lambda)u_{i+1}^+(\nu_{i+1}^+)\right] \\ &\quad = O((e^{2\max\{\bar{\mu}^s, -\bar{\mu}^u\}\omega_i}) + O((e^{2\max\{\bar{\mu}^s, -\bar{\mu}^u\}\omega_{i+1}}) \\ &\qquad + O(\big(\max(\bar{\mu}^s_\Upsilon, (\bar{\mu}^u_\Upsilon)^{-1})\big)^{\nu_i}) + O(\big(\max(\bar{\mu}^s_\Upsilon, (\bar{\mu}^u_\Upsilon)^{-1})\big)^{\nu_{i+1}}) \\ &\qquad + O(\big(\max(\bar{\mu}^s_\Upsilon, (\bar{\mu}^u_\Upsilon)^{-1})\big)^{\nu_{i+2}}).\end{aligned}$$

Estimates of $\sum \Phi_\Pi^+(\mathrm{id} - R^+)h_\Pi^+$
The estimates of $\sum \Phi_\Pi^+(\mathrm{id} - R^+)h_\Pi^+$ run completely parallel to the computation in [Kno04], Section 3.6.3. From there we get

$$\sum_{m=1}^{\nu_{i+1}^+} \Phi_\Pi^+(0,m)(\mathrm{id} - R^+(0,\lambda))h_\Pi^+(m-1, u_{i+1}^+(m-1),\lambda) = o\left((\mu_\Upsilon^u)^{-\nu_{i+1}}\right).$$

Estimates of $\int \Phi_1^+(\mathrm{id} - Q_{sc}^+)h_1^+$
Now we consider $\int_0^{\varpi^+} \Phi_1^+(0,\tau)(\mathrm{id} - Q_{sc}^+(\tau))h_1^+(\tau, v_{1,i}^+(\tau),\lambda)d\tau$.
For $\left\|(\mathrm{id} - Q_{sc}^+(t))h_1^+(t, v_{1,i}^+(\tau),\lambda)\right\|$, we use the definition of h_1^+ and we split $v_{1,i}^+$ into a stable and an unstable part. The stable part is defined as $v^s(t) := Q_{sc}^+(t)v_{1,i}^+(t)$, the unstable part is defined as $v^u(t) := (\mathrm{id} - Q_{sc}^+(t))v_{1,i}^+(t)$, and thus $v_{1,i}^+(t) = v^u(t) + v^s(t)$.
By using the same procedure as in [Kno04], we can establish

$$\left\|(\mathrm{id} - Q_{sc}^+(t))h_1^+(t, v_{1,i}^+(t),\lambda)\right\| \le C\left\|v^u(t)\right\|\left(\left\|v^s(t)\right\| + \left\|v^u(t)\right\|\right).$$

Now we exploit $(\mathrm{id} - Q_{sc}^+(t)) = (\mathrm{id} - Q_{sc}^+(t))^2$ and the exponential trichotomy of Φ_1^+ to get

$$\begin{aligned}&\left\|\int_0^{\varpi^+} \Phi_1^+(0,\tau)(\mathrm{id} - Q_{sc}^+(\tau))^2 h_1^+(\tau, v_{1,i}^+(\tau),\lambda)d\tau\right\| \\ &\quad\le e^{-\ln\bar\mu_\Upsilon^u \varpi^+}\varpi^+ \left(\sup_{t\in[0,\varpi^+]} K e^{-\ln\bar\mu_\Upsilon^u(t-\varpi^+)}\left\|(\mathrm{id} - Q_{sc}^+(t))h_1^+(t, v_{1,i}^+(t),\lambda)\right\|\right).\end{aligned}$$

Next we choose $\delta > 0$ such that $0 < \delta < \ln\bar\mu_\Upsilon^u$ and we assume ϖ^+ to be large enough such that $e^{-\delta\varpi^+}\varpi^+ < 1$ (this results in $\varpi^+ < e^{\delta\varpi^+}$). Then

$$\begin{aligned}&\left\|\int_0^{\varpi^+} \Phi_1^+(0,\tau)(\mathrm{id} - Q_{sc}^+(\tau))^2 h_1^+(\tau, v_{1,i}^+(\tau),\lambda)d\tau\right\| \\ &\quad\le e^{(-\ln\bar\mu_\Upsilon^u + \delta)\varpi^+} K\left\|v_{1,i}^+\right\|\left(\sup_{t\in[0,\varpi^+]} e^{-\ln\bar\mu_\Upsilon^u(t-\varpi^+)}\left\|v^u(t)\right\|\right).\end{aligned}$$

We use that $\left\|v_{1,i}^+\right\| = O(\bar\mu_\Upsilon^{\nu_i}) + O(\bar\mu_\Upsilon^{\nu_{i+1}}) + O(e^{\bar\mu\omega_i})$, where $\bar\mu_\Upsilon = \max\{\bar\mu_\Upsilon^s, (\bar\mu_\Upsilon^u)^{-1}\}$ and $\bar\mu = \max\{\bar\mu^s, -\bar\mu^u\}$, (see (2.3.15)) to get

$$\begin{aligned}&\left\|\int_0^{\varpi^+} \Phi_1^+(0,\tau)(\mathrm{id} - Q_{sc}^+(\tau))^2 h_1^+(\tau, v_{1,i}^+(\tau),\lambda)d\tau\right\| \\ &\quad\le e^{(-\ln\bar\mu_\Upsilon^u + \delta)\varpi^+} K\left(O(\bar\mu_\Upsilon^{\nu_i}) + O(\bar\mu_\Upsilon^{\nu_{i+1}}) + O(e^{\bar\mu\omega_i})\right)\left(\sup_{t\in[0,\varpi^+]} e^{-\ln\bar\mu_\Upsilon^u(t-\varpi^+)}\left\|v^u(t)\right\|\right)\end{aligned}$$

and we show that the term $\sup_{t\in[0,\varpi^+]} e^{-\ln\bar\mu_\Upsilon^u(t-\varpi^+)}\left\|v^u(t)\right\|$ can also be estimated by the terms $O(\bar\mu_\Upsilon^{\nu_i}) + O(\bar\mu_\Upsilon^{\nu_{i+1}}) + O(e^{\bar\mu\omega_i})$.

From the definition of v^u we get

$$\|v^u(t)\| = \left\|\left(\mathrm{id} - Q^+_{sc}(t)\right) v^+_{1,i}(t)\right\| \leq \left\|\Phi^+_1(t,\varpi^+)\left(\mathrm{id} - Q^+_{sc}(t)\right)\right\| \cdot \left\|\alpha^+_i\right\| + \left\|\int_t^{\varpi^+} \Phi^+_1(t,\tau)(\mathrm{id} - Q^+_{sc}(\tau))h^+_1(\tau, v^+_{1,i}(\tau),\lambda)d\tau\right\|.$$

Using the trichotomy of Φ^+_1 and the quadratic influence of v in h again we get

$$e^{-ln\bar{\mu}^u_\Upsilon(t-\varpi^+)}\|v^u(t)\| \leq e^{-ln\bar{\mu}^u_\Upsilon(t-\varpi^+)}e^{ln\bar{\mu}^u_\Upsilon(t-\varpi^+)}\left\|\alpha^+\right\| + Ce^{-ln\bar{\mu}^u_\Upsilon(t-\varpi^+)}\int_t^{\varpi^+} e^{-\ln\bar{\mu}^u_\Upsilon(t-\tau)}\|v^u(\tau)\|\left(\|v^s(\tau)\| + \|v^u(\tau)\|\right)d\tau$$

and thus

$$\sup_{t\in[0,\varpi^+]} e^{-ln\bar{\mu}^u_\Upsilon(t-\varpi^+)}\|v^u(t)\| \leq \left\|\alpha^+\right\| + C\sup_{t\in[0,\varpi^+]} e^{-ln\bar{\mu}^u_\Upsilon(t-\varpi^+)}\|v^u(t)\| \cdot \sup_{t\in[0,\varpi^+]}\left(\|v^s(t)\| + \|v^u(t)\|\right)\varpi^+.$$

Using that $\sup_{t\in[0,\varpi^+]}(\|v^s(t)\| + \|v^u(t)\|) \leq \left\|v^+_{1,i}\right\|$ and (2.3.15) for ν_i, ν_{i+1} and ω_i sufficiently large, $\left\|v^+_{1,i}\right\|\varpi^+ < \frac{1}{2C}$ holds and thus there is another constant C such that

$$\sup_{t\in[0,\varpi^+]} e^{-ln\bar{\mu}^u_\Upsilon(t-\varpi^+)}\|v^u(t)\| \leq C\left\|\alpha^+\right\|.$$

Finally, we use (2.3.14) and hence

$$\sup_{t\in[0,\varpi^+]} e^{-ln\bar{\mu}^u_\Upsilon(t-\varpi^+)}\|v^u(t)\| = O(\left(\max(\bar{\mu}^s_\Upsilon, (\bar{\mu}^u_\Upsilon)^{-1})\right)^{\nu_i}) + O(\left(\max(\bar{\mu}^s_\Upsilon, (\bar{\mu}^u_\Upsilon)^{-1})\right)^{\nu_{i+1}}).$$

Putting all this together we finally end up with the desired estimate

$$\int_0^{\varpi^+} \Phi^+_1(0,\tau)(\mathrm{id} - Q^+_{sc}(\tau))h^+_1(\tau, v^+_{1,i}(\tau),\lambda)d\tau = O((e^{\max\{\bar{\mu}^s,-\bar{\mu}^u\}\omega_i}) + O(\left(\max(\bar{\mu}^s_\Upsilon, (\bar{\mu}^u_\Upsilon)^{-1})\right)^{\nu_i}) + O(\left(\max(\bar{\mu}^s_\Upsilon, (\bar{\mu}^u_\Upsilon)^{-1})\right)^{\nu_{i+1}}).$$

The remaining term in (2.3.6)

The considerations in [Kno04] yield

$$\begin{aligned}&\left\langle \Phi^-_1(0,-\omega_i)^T\left(\mathrm{id} - P^-(0)\right)^T z^j, \left(\mathrm{id} - \tilde{P}(\omega_i,\lambda)\right)\left\{\gamma^-_1(-\omega_i,\lambda) - \gamma^+_2(\omega_i,\lambda)\right.\right. \\ &\qquad\left.\left. - P^+(\omega_i,\lambda)v^+_{2,i}(\omega_i) + P^-(-\omega_i,\lambda)v^-_{1,i}(-\omega_i)\right\}\right\rangle \\ &+ \left\langle z^j, \int_{-\omega_i}^0 \Phi^-_1(0,\tau)(\mathrm{id} - P^-(\tau))h^-_1(\tau, v^-_{1,i}(\tau),\lambda)d\tau\right\rangle \\ &= c_1(\lambda)e^{2\mu^s(\lambda)\omega_i} + o\left(e^{2\mu^s(\lambda)\Omega}\right).\end{aligned} \tag{2.3.16}$$

Combining (2.3.16) and the other terms of (2.3.6) as estimated above yields the result of Lemma 2.3.1.

2.4 Applications

In this section we discuss some of the bifurcation equations that arise if one looks for specific types of solutions near the heteroclinic cycle. Such specific solutions include homoclinic orbits to the equilibrium and homoclinic orbits to the periodic orbit. We assume different leading eigenvalue situations (as stated in Hypothesis (H 2.1) and Hypothesis (H 2.2)) and derive and discuss the arising bifurcation equations.
Recall that the general jump functions that are used to derive the bifurcation equations are given in Theorem 2.1.5 and Theorem 2.1.6, depending on the eigenvalue situation. The bifurcation equations then follow from 'closing the gaps' of the Lin orbit and thus constructing a real orbit that stays close to the EtoP cycle.
We focus our considerations on the discussion of bifurcation equations for orbits that are closely related to the numerical examples discussed in Chapter 3. In particular, we consider homoclinic orbits to p and homoclinic orbits to Υ.
When searching for a single 1-homoclinic orbit, the infinitely dimensional equation (2.1.1) for the jump function comes down to a single equation

$$\Xi(\omega,\nu,\lambda) = \lambda + c_1(\lambda)e^{2\mu^s(\lambda)\omega} + c_2(\lambda)\left(\mu^u_\Upsilon(\lambda)\right)^{-\nu} + o\left(e^{2\mu^s(\lambda)\omega}\right) + o\left(\left(\mu^u_\Upsilon(\lambda)\right)^{-\nu}\right) + \mathcal{R}(\omega,\nu). \quad (2.4.1)$$

2.4.1 Homoclinic orbits to the equilibrium

Here we look for solutions in the intersection of the stable and unstable manifolds of p, so we have to consider the limit $\omega \to \infty$ of the jump estimate (2.4.1) (cf. Remark 2.1.7).
Then the bifurcation equation reads

$$\Xi(\nu,\lambda) = \lambda + \xi(\nu,\lambda) = 0$$

with

$$\xi(\nu,\lambda) = c_2(\lambda)\left(\mu^u_\Upsilon(\lambda)\right)^{-\nu} + o\left(\left(\mu^u_\Upsilon(\lambda)\right)^{-\nu}\right).$$

Formulating this as a fixed point equation yields

$$\lambda = -c_2(\lambda)\left(\mu^u_\Upsilon(\lambda)\right)^{-\nu} + o\left(\left(\mu^u_\Upsilon(\lambda)\right)^{-\nu}\right). \quad (2.4.2)$$

Now we consider the fact that $\xi(\nu,\cdot)$ is smooth and $D_\lambda\xi(\nu,\lambda) = D_\lambda\left(c_2(\lambda)\left(\mu^u_\Upsilon(\lambda)\right)^{-\nu}\right) + o\left(\left(\mu^u_\Upsilon(\lambda)\right)^{-\nu}\right)$ (see [San93, Kno04]). Thus there is an $N \in \mathbb{N}$ and a constant $K < 1$ such that for all $\nu > 2N$ and sufficiently small $\|\lambda\|$, $\|D_1\xi(\lambda)\| \le K < 1$ holds. Then it is straightforward to use the Banach Fixed Point Theorem to show that for each ν sufficiently large there is a unique solution λ_ν of (2.4.2). Moreover, we observe that the λ_ν accumulate at $\lambda^* = 0$ for $\nu \to \infty$.
We manifest this result in the following lemma:

Lemma 2.4.1 *Assume that Condition* (C6) *and eigenvalue situation Hypothesis* (H 2.1) *or* (H 2.2) *hold.*
Then there is a constant $N \in \mathbb{N}$ such that for all $\nu \in \mathbb{N}$ with $\nu > 2N$ the fixed point equation (2.4.2) *has a unique solution $\lambda = \lambda_\nu$. Moreover, $\lambda_\nu \to \lambda^* = 0$ as $\nu \to \infty$.*

Remark 2.4.2 *Note that this lemma is true for the codimension-d case, that means we have* $\lambda = (\lambda^1, \ldots, \lambda^d)^T \in \mathbb{R}^d$. *Depending on the sign of* μ^u_Υ, *for each* $j \in \{1, \ldots, d\}$ *the sequence* $(\lambda^j_\nu)_{\nu>2N}$ *is either strictly monotonic or alternating. Moreover, the sequence* (λ^j_ν) *decays exponentially as* $\nu \to \infty$, *the rate is determined by the leading unstable Floquet multiplier.*

In Section 3.5.2 we find numerical evidence for Lemma 2.4.1 (in $\mathbb{R}^3$): A (codimension-one) Shilnikov-type homoclinic orbit to an equilibrium is numerically continued (in two parameters) and a 'snaking' behaviour in the parameter plane is observed, see Figure 3.9 below. In the figure, the bifurcation curve h^b_1 of the homoclinic orbit accumulates to a curve segment on the curve c_b (where the codimension-one EtoP connection exists), namely to the segment where the complete EtoP cycle exists. If we now choose parameter values $\nu_1 = \nu_1^*$ and $\nu_2 = \nu_2^*$ such that (ν_1^*, ν_2^*) is on c_b, in between the tangency lines t_b, then the EtoP cycle exists for (ν_1^*, ν_2^*). Keeping ν_2 fix at ν_2^* and only varying ν_1 (to the left) while monitoring the intersection points with h^b_1 yields an accumulation of these intersection points as predicted by Lemma 2.4.1.
Taking a closer look at this accumulation process, we observe that (in phase space) the homoclinic orbit itself accumulates to a heteroclinic EtoP cycle as the bifurcation curve h^b_1 approaches c_b. Taking a closer look at the phase portrait we observe that the homoclinic orbit takes one more loop around the periodic orbit for each turning point of the snaking curve h^b_1. The numerics strongly suggest that the snaking is closely related to the tangency of $W^u(\Upsilon)$ and $W^s(p)$ (the turning points are close to the tangency curves t_b), thus we now consider Condition (C6') to find a (partial) explanation for the snaking behaviour.

Tangencies of homoclinic orbits to p

In this section, we consider the situation that the intersection $W^u(\Upsilon) \cap W^s(p)$ becomes tangent, that is, we consider Condition (C6'). For reasons of simplicity and to keep the result closely related to the numerical observations, we restrict the following to $\mathbb{R}^3$. Then we have the case that $d = 1$ and thus $\dim Z_1 = 1$. Moreover, in Σ_2 we find that $\dim Z_2 = 1$ and $\dim U = 1$. To unfold the bifurcation of the EtoP cycle in this situation, the dimension of the parameter space has to be increased and thus we now consider a two-dimensional parameter $\lambda = (\lambda_1, \lambda_2)^T$.
Note that all our considerations in Section 2.2.1 to 2.2.4 hold true, but we have not given jump estimates for the jump in Z_2. This can be done in a similar way as in Section 2.3, but omitting the details we only use the result.
At this stage, we assume a 'quadratic tangency' of $W^u(\Upsilon)$ and $W^s(p)$, that means that the situation inside Σ_2 is as shown in Figure 2.4. Then the function $\xi^\infty : \mathbb{R} \times \mathbb{R}^2 \to \mathbb{R}^2$ that describes the splitting of the manifolds inside Σ_1 in the first component and the splitting of the manifolds in Σ_2 in the second component, takes the following form:

$$\xi^\infty(\vartheta, \lambda) = \begin{pmatrix} \lambda_1 \\ \lambda_2 - \vartheta^2 \end{pmatrix}. \tag{2.4.3}$$

For the jump function for homoclinic orbits to p (that again describes the jump in Z_1 in the first component and the jump in Z_2 in the second component) we get

$$\Xi(\nu, \vartheta, \lambda) = \xi^\infty(\vartheta, \lambda) + \xi(\nu, \vartheta, \lambda) \tag{2.4.4}$$

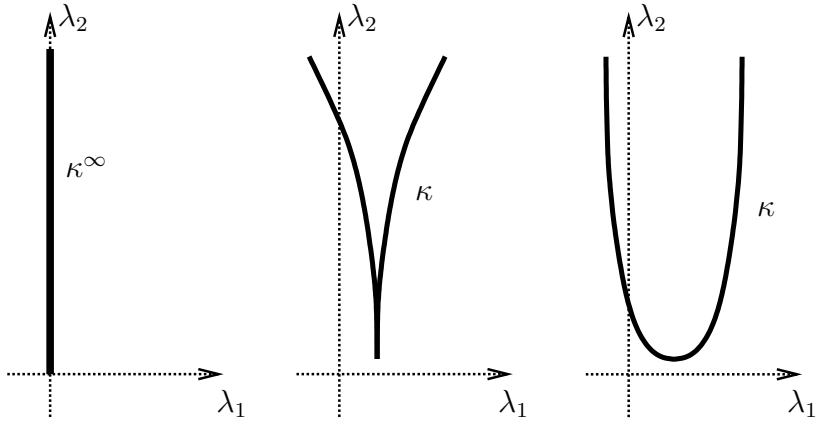

(a) $\xi^\infty(\vartheta, \lambda) = 0$ (b) $\Xi(\nu^*, \vartheta, \lambda) = 0$, nonsmooth (c) $\Xi(\nu^*, \vartheta, \lambda) = 0$, smooth

Figure 2.10: The solution curve κ^∞ (a) and the possible perturbances (b) and (c). If the solution curve κ is not smooth (b) at the minimum, it is possible to reparametrise such that the curve becomes smooth and looks like (c).

with

$$\xi(\nu, \vartheta, \lambda) = \begin{pmatrix} c_2^1(\vartheta, \lambda)(\mu_\Upsilon^u(\lambda))^{-\nu} + o((\mu_\Upsilon^u(\lambda))^{-\nu}) \\ c_2^2(\vartheta, \lambda)(\mu_\Upsilon^s(\lambda))^{\nu} + o((\mu_\Upsilon^s(\lambda))^{\nu}) \end{pmatrix}. \tag{2.4.5}$$

Note that in this case the factors c_2^1 and c_2^2 indeed depend on ϑ; this follows from the considerations in Section 2.3. (Working in the dependence on ϑ, we find that $c_2^j(\vartheta, \lambda) := \left\langle \eta^+(\tilde{z}^j, \vartheta, \lambda), \eta^u(\vartheta, \lambda) \right\rangle$, see (2.3.9).)

To investigate the structure of the solutions of $\Xi(\nu, \vartheta, \lambda) = 0$, we first look at the solutions of $\xi^\infty(\vartheta, \lambda) = 0$. It is obvious that the graph of the solution in the (λ_2, ϑ)-plane is a simple parabola, while the solution curve in the (λ_1, λ_2)-plane $\kappa^\infty := \{(\lambda_1(\vartheta), \lambda_2(\vartheta)) = (0, \vartheta^2)\}$ is a line from the origin upwards (which is covered twice as ϑ varies), see Figure 2.10(a).

Now we use that the solution curve κ of $\Xi(\nu, \vartheta, \lambda) = 0$ for fixed $\nu = \nu^*$ is a perturbation of the solution curve κ^∞; this can be seen by considerations similar to [Kno04], Section 4.3.1. We first note that the perturbed solution curve in the (λ_2, ϑ)-plane is also a parabola, therefore the solution curve κ in (λ_1, λ_2) has a local minimum. Due to the fact that in this situation ($\dim W^u(p) = 1$) we have a one-to-one correspondence of the existence of a homoclinic orbit to p and the value of λ_1, the solution curve κ must qualitatively look like depicted in Figure 2.10 (b) or (c) (as perturbances of (a)). Note that if the curve κ is not smooth at the minimum, then it is possible to reparametrise such that the reparametrised curve is smooth and looks like Figure 2.10(c). This explains the shape of the snaking curve locally around the turning points, see again Figure 3.9.

However, the analysis so far does not grasp the full snaking behaviour. For further analysis of the snaking behaviour, considerations analogous to [BKL$^+$08] are necessary. This is beyond the scope of this thesis and remains a challenge for future research.

2.4.2 Homoclinic orbits to the periodic orbit

For homoclinic orbits to Υ we consider the limit $\nu \to \infty$ of the jump function (2.4.1) (cf. Remark 2.1.7).
The bifurcation equation for 1-homoclinic orbits to Υ reads

$$\Xi(\omega, \lambda) = \lambda + \xi(\omega, \lambda).$$

Homoclinic orbits to Υ – real eigenvalues
For the eigenvalue assumption Hypothesis (H 2.1) we get

$$\xi(\omega, \lambda) = c_1(\lambda) e^{2\mu^s(\lambda)\omega} + o\left(e^{2\mu^s(\lambda)\omega}\right).$$

Then we have to solve $\Xi(\omega, \lambda) = 0$. Formulating this as a fixed point equation yields

$$\lambda = -c_1(\lambda) e^{2\mu^s(\lambda)\omega} + o\left(e^{2\mu^s(\lambda)\omega}\right). \tag{2.4.6}$$

It is straightforward to use the Banach Fixed Point Theorem to solve this equation for sufficiently large ω, hence there is a constant $\Omega > 0$ such that for all $\omega > \Omega$ there is a unique solution $\lambda = \lambda(\omega)$ of (2.4.6). Moreover, assuming that $c_1(0) < 0$, for all $\omega > \Omega$, $\lambda(\omega) > 0$ holds; there is no solution $\lambda \leq 0$, cf. Figure 2.11.

Lemma 2.4.3 *Let* (C6) *be satisfied. Assume that the leading eigenvalues are as given in Hypothesis* (H 2.1).
Then there is a constant $\Omega > 0$ such that the fixed point equation (2.4.6) *has a unique solution $\lambda = \lambda(\omega)$. Moreover, $\lambda(\omega) \to 0$ as $\omega \to \infty$.*

Note that $\lambda(\omega)$ decays exponentially as $\omega \to \infty$, see Figure 2.11 for a draft. The rate of the decay is given by the leading stable eigenvalue.

Homoclinic orbits to Υ – complex eigenvalues
For the eigenvalue situation Hypothesis (H 2.2) we have

$$\xi(\omega, \lambda) = c_1(\lambda) \sin(\mathrm{Im}\mu^s \omega + \phi) e^{2\mathrm{Re}\mu^s(\lambda)\omega} + o\left(e^{2\mathrm{Re}\mu^s(\lambda)\omega}\right).$$

Then we have to solve $\Xi(\omega, \lambda) = 0$, formulating this as a fixed point equation yields

$$\lambda = -c_1(\lambda) \sin(\mathrm{Im}\mu^s \omega + \phi) e^{2\mathrm{Re}\mu^s(\lambda)\omega} + o\left(e^{2\mathrm{Re}\mu^s(\lambda)\omega}\right). \tag{2.4.7}$$

Lemma 2.4.4 *Let* (C6) *be satisfied. Assume that the leading eigenvalues are as given in Hypothesis* (H 2.2).
Then there is a constant $\Omega > 0$ such that for all $\omega > \Omega$ the fixed point equation (2.4.7) *has a unique solution $\lambda(\omega)$. Moreover, $\lambda(\omega) \to 0$ as $\omega \to \infty$ and the function $\lambda(\cdot)$ has infinitely many roots.*

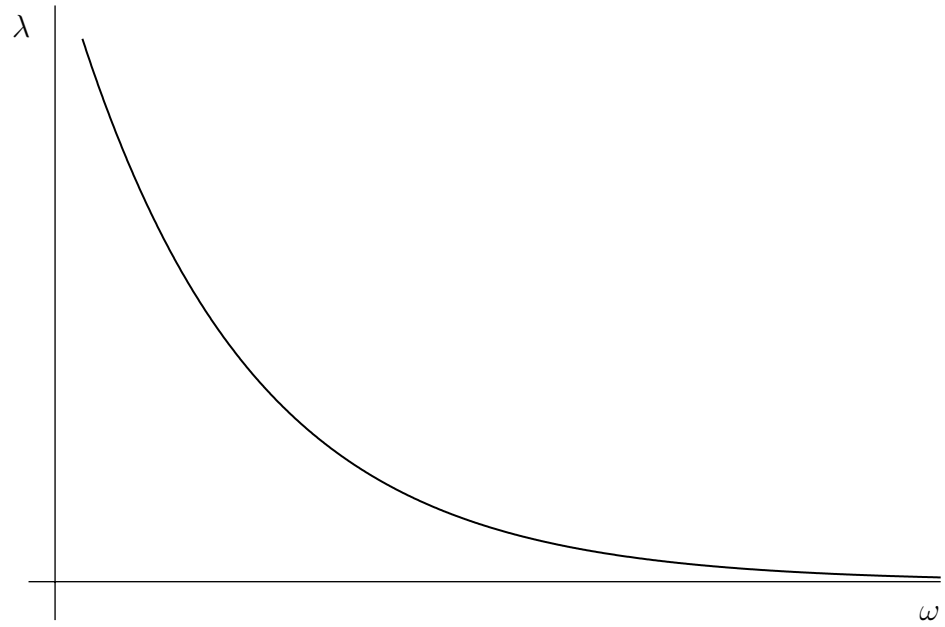

Figure 2.11: Homoclinic 'blue sky catastrophe'. Draft of the solutions of (2.4.6) that indicate the existence of homoclinic orbits to Υ.

Note that $\sup_{\omega>\Omega} |\lambda(\omega)|$ decays exponentially as $\Omega \to \infty$, see Figure 2.12.

Geometry

The statements of Lemma 2.4.3 and Lemma 2.4.4 are in perfect agreement with the geometrical implications. First we consider the eigenvalue situation (H 2.1). We expect a point in $W^u(\Upsilon) \cap \Sigma_2$ to be transported with the flow towards p, then $W^u(\Upsilon)$ is 'split in two', where only one part is transported along Γ_1, see Figure 2.13. Thus we expect to see Figure 2.14 in Σ_1, that is, we expect the curve $W^u(\Upsilon) \cap \Sigma_1$ to intersect $W^s(\Upsilon) \cap \Sigma_1$ either in exactly one point (for $\lambda > 0$) or not at all (for $\lambda \leq 0$). This is in agreement with Equation (2.4.6) and explains the 'blue sky catastrophe' of the homoclinic orbit to Υ. The numerical example in Section 3.5.1 shows how a homoclinic orbit to a periodic orbit is continued in this eigenvalue situation. We use the numerical data of the complete EtoP cycle as starting data for the continuation and set the correct projection boundary conditions to approximate the homoclinic orbit. The situation is as depicted in Figure 2.14, where the parameter λ is ϱ and the critical parameter value is ϱ_{het}. Then we continue the homoclinic orbit, but due to the blue sky situation this is only possible in one direction, see Figure 3.5.

On the other hand, if we consider the eigenvalue situation (H 2.2), Equation (2.4.7) is as sketched in Figure 2.12 (there are infinitely many solutions for $\lambda = 0$ and finitely many for $\lambda \neq 0$).

In Σ_1 we expect to see the spiralling curve of $W^u(\Upsilon) \cap \Sigma_1$ intersecting the curve $W^s(\Upsilon)$ as shown in Figure 2.15, that is, with infinitely many intersection points for $\lambda = 0$ and finitely many intersection points for $\lambda \neq 0$.

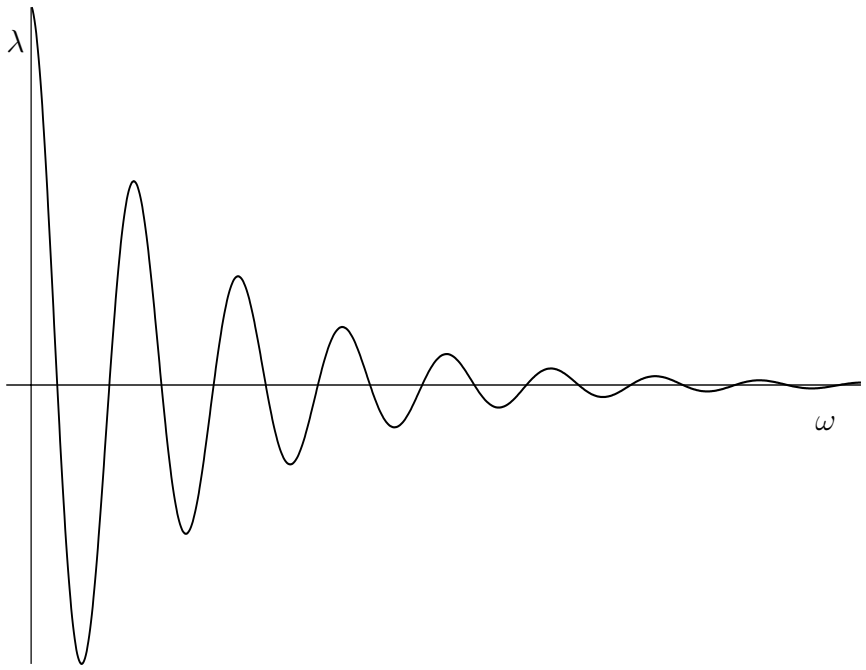

Figure 2.12: The graph shows the existence of homoclinic orbits to Υ and how it depends on the values of λ and ω. For $\lambda = 0$ there are (countably) infinitely many homoclinic orbits to Υ. For $\lambda \neq 0$ there are only finitely many, but the number tends to infinity as $\lambda \to 0$.

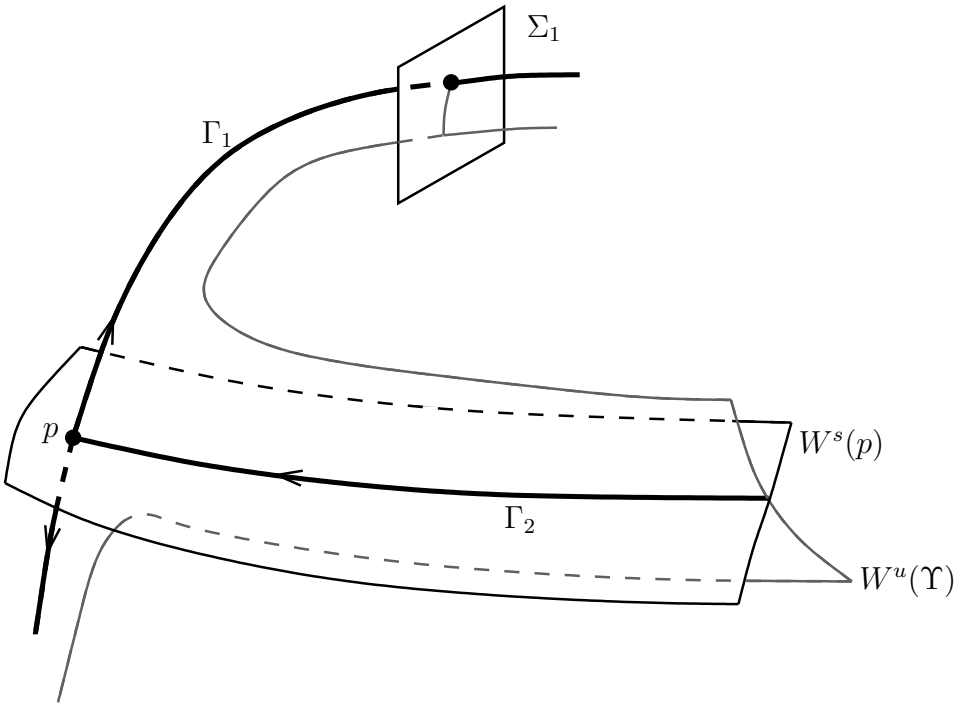

Figure 2.13: Homoclinic 'blue sky catastrophe'. Draft of the behaviour of the manifolds in the real eigenvalue case. See also Figure 2.14 for the situation in Σ_1 for varying λ.

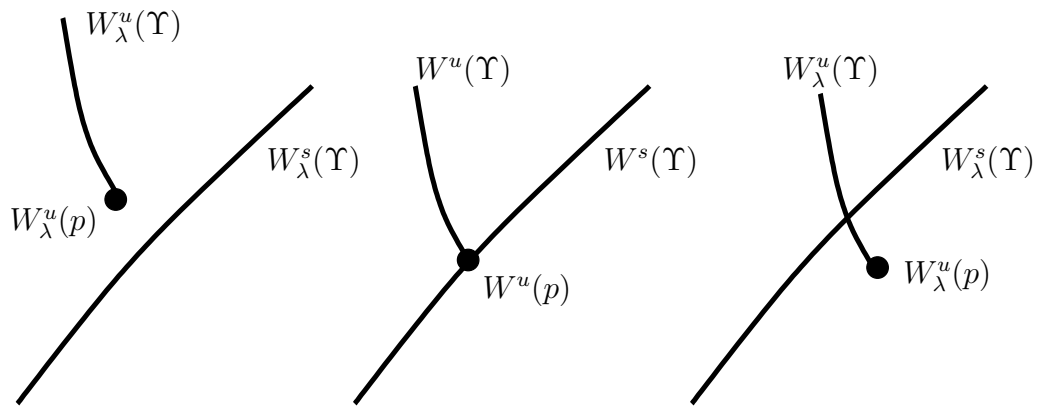

(a) $\lambda < 0$ (b) $\lambda = 0$ (c) $\lambda > 0$

Figure 2.14: Homoclinic 'blue sky catastrophe'. Shown are the traces of the respective manifolds inside Σ_1 in the $\mathbb{R}^3$ case. For $\lambda < 0$ there are no homoclinic orbits to Υ (a), for $\lambda = 0$ the EtoP cycle exists (there are also no homoclinic orbit to Υ) (b) and for $\lambda > 0$ there is exactly one homoclinic orbit to Υ (c).

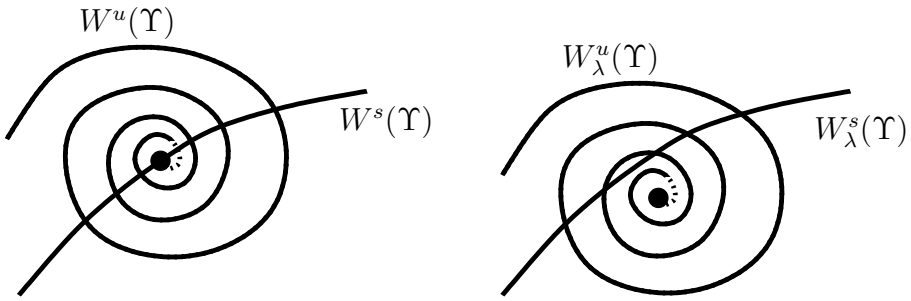

(a) $\lambda = 0$ (b) $\lambda \neq 0$

Figure 2.15: Spiral inside Σ_1. The trace of the manifold $W^u(\Upsilon)$ spirals around the trace of $W^u(p)$, thus there are infinitely many intersection points of $W^u(\Upsilon)$ and $W^s(\Upsilon)$ (resulting in infinitely many homoclinic orbits to Υ) for $\lambda = 0$ (a) and only finitely many intersection points for $\lambda \neq 0$ (b).

This concludes our considerations of bifurcation equations. In Chapter 4 we give some ideas for further applications and future research.

CHAPTER 3

Finding and continuing EtoP and PtoP connections

In this chapter we introduce a numerical method to perform the bifurcation analysis of a setting as described in Section 1.2. We restrict most of the following considerations to conditions (C1)–(C5) only, so in the general context no codimension-zero connection has to be present. In some of the examples however we show how such a 'returning' codimension-zero connection influences the dynamics and how the heteroclinic cycle interacts with other (connecting) solutions nearby.
This chapter is a version of [KR08] and uses a slightly different notation than in Chapter 2. The periodic orbit is denoted by Γ (instead of Υ) and the orbits in the stable and unstable manifolds are denoted by Q^+ and Q^-, respectively (instead of Γ_1^+ and Γ_1^-). Moreover, as we generally consider only one EtoP connection Q ($= \Gamma_1$), we omit the subscript '1' in the notation of the cross-section Σ ($= \Sigma_1$) and subspaces Y ($= Y_1$) and Z ($= Z_1$).

3.1 Motivation

The development of numerical methods for the continuation of homoclinic and heteroclinic orbits has been an active field of research [Bey94, Bey90, CKS96, Doe07, DF89, FD93, KOGV07, LK80]. Today, homoclinic and heteroclinic orbits to equilibria can readily be continued, for example, with the HomCont [CKS96] part of the well-known continuation package Auto [DPC+00]. The underlying idea is to represent the connecting orbit as the solution of a boundary value problem over a finite time interval by imposing projection boundary conditions, which ensure that the two endpoints lie in the stable and unstable eigenspaces of the respective equilibria; see, for example, [Bey90, DF89]. This makes it possible to explore and understand complicated bifurcation diagrams involving homoclinic and heteroclinic orbits to equilibria; recent examples include the study of global bifurcations in a semiconductor laser system [WK05] and in models of calcium dynamics in cells [CKK+07].

This chapter is concerned with the next logical step: the continuation of connecting orbits involving saddle periodic orbits. One distinguishes two types of such orbits: connections from a saddle equilibrium to a saddle periodic orbit, which we refer to as *EtoP connections*, and heteroclinic connections between the same or two different periodic orbits, or *PtoP connections* for short. Codimension-one EtoP connections are of particular relevance, because their existence can be inferred from the occurence of certain codimension-two bifurcations of connections to equilibria. An example is a Shilnikov-Hopf bifurcation where the saddle focus involved in a codimension-one homoclinic orbit undergoes a Hopf bifurcation; see [CKK+07, HK93, WK05]. Another example is the possibility that homoclinic bifurcations of a saddle equilibrium may accumulate on a heteroclinic EtoP cycle of an equilibrium and a saddle periodic orbit. This phenomenon was studied theoretically in [Rad05] and in Section 2.4 and was numerically found near a saddle-node Hopf bifurcation with a global reinjection mechanism [KO06].
We present here a Lin's method approach to finding and continuing heteroclinic connecting orbits involving periodic orbits. We concentrate on the case of codimension-d EtoP connections, but our approach can also be applied to PtoP connections. Lin's method [Lin90] is an analytical theory that can be used to analyse the recurrent dynamics near, for example, homoclinic orbits or heteroclinic cycles; see also [Kno04, Rad05, Rie03, San93, Yew01]. The main result in the present context is that for any value of the system parameter there are two well-defined orbit segments from the equilibrium to a suitable section Σ and from Σ to the periodic orbit, whose difference lies in a d-dimensional subspace; see Section 3.3 for details. This gives rise to d well-defined test functions, which are also called the *Lin gaps*. The sought-after codimension-d EtoP connection can then be found by closing each of the Lin gaps one by one via suitable continuation runs. The two orbit segments are represented as solutions of a boundary value problem subject to projection boundary conditions. Near the equilibrium we use a well-established condition [Bey90] as implemented in HomCont [CKS96], while the projection boundary condition near the periodic orbit is adapted from the method in [EKO05]. All boundary value problems are solved with the continuation package Auto in the flavours Auto2000 [DPC+00] and Auto07p [DPC+06]. Once a codimension-d EtoP connection has been detected as a common zero of the d test functions, it can readily be continued in additional system parameters. Furthermore, by considering the corresponding EtoP heteroclinic cycle, other global orbits that bifurcate from it, for example, a codimension-zero homoclinic orbit of the periodic orbit, can be found and continued as well.
A number of other methods for the continuation of EtoP and PtoP connections have been proposed recently [Bey94, DR04b, DKKvVa, Pam01]. They have in common that the connecting orbit is represented as *a single orbit segment* over a finite time interval by imposing suitable boundary conditions at the periodic orbit. A common difficulty is that of finding an initial approximate connecting orbit that satisfies the boundary value problem. The seminal work by Beyn [Bey94] introduces a general setup in terms of suitable projection boundary conditions and establishes corresponding error bounds. Pampel [Pam01] further analyses and implements the EtoP connection scheme and uses it to compute the codimension-one EtoP connection in the Lorenz system; here an initial connecting orbit is obtained by continuation (in a system parameter) of intersection curves of the stable and unstable manifold in a suitably chosen plane. Dieci and Rebaza [DR04b, DR04a] follow the general approach of [Bey94] and combine it with the method of continuing invariant subspaces from [DDF00] to

formulate the boundary conditions at the equilibrium and the periodic orbit. They compute and continue in parameters the codimension-one EtoP connection in the Lorenz system and a codimension-zero PtoP connection in a coupled oscillator system; in both cases, a simple shooting method is used to find an initial connecting orbit. Finally, Doedel *et al.* [DKKvVa] present an implementation for EtoP connections, where the adjoint variational equation along the periodic orbit is used to formulate projection boundary conditions. As examples they continue codimension-one EtoP connections in the Lorenz system, in a three-dimensional model of an electronic circuit, and in a three-dimensional food-chain model. Doedel *et al.* use a homotopy-type method to find an initial connecting orbit. They start by continuing an orbit from near the equilibrium in the unstable eigenspace to find an intersection point with the stable eigenspace of the periodic orbit. The distance of this intersection point to the periodic orbit is then reduced in additional continuation steps. This homotopy approach has been extended in [DKKvVb] to the case of PtoP orbits of three-dimensional vector fields (which are of codimension zero). Finding an initial connecting orbit by homotopy works well when the (un)stable manifold of the equilibrium is of dimension one and the dimension n of the phase space is not too large ($n = 3$ is considered in [DKKvVa, DKKvVb]). However, it requires that one starts quite close to the EtoP or PtoP connection, and it is less systematic when higher-dimensional manifolds are involved.

3.2 Idea and main result

The main property of our method is that it uses *two separate orbits segments* up to a suitably chosen section as a means of setting up a systematic way of finding codimension-d EtoP connections for any $d \geq 1$ and for arbitrary dimensions of the stable and unstable manifolds of the equilibrium and periodic orbit involved. Namely, one chooses the section Σ to divide the phase space into two regions, one of which contains the equilibrium and the other the periodic orbit (for parameters chosen from a region of interest). Then any EtoP connection will intersect Σ and, generically, this intersection is transverse. Therefore, it is possible to set up the boundary value problem for the two orbit segments that define the Lin gaps. While this requires some extra work because we consider two orbit segments (rather than a single orbit segment), the advantage is that the resulting boundary value problem is well defined and has a unique solution for any value of the system parameters, and not just in some neighbourhood of the EtoP connection itself. This means that specific knowledge of the location of EtoP orbits in phase and/or parameter space is not required for our setup. The Lin gaps are well-defined test functions throughout and the task of finding an EtoP connection reduces to finding their zeros. As for any test function, zeros of the Lin gaps can be found by performing suitable continuation runs that involve system parameters. Any common zero of the Lin gaps corresponds to an EtoP connection. It is possible that several common zeros are found, which then correspond to different EtoP connections. Hence, different EtoP connections can be found with the same boundary value problem setup. Conversely, if no common zero of the Lin gaps can be found in a parameter region of interest (and this requires some careful checking) then this constitutes numerical evidence that the sought-after EtoP connection does not exist in the considered parameter region. Note that our approach is similar in spirit to

the implementation of Lin's method in [OCK03], where regular test functions are set up that allow one to switch branches from a known homoclinic orbit (to an equilibrium) to nearby n-homoclinic orbits that pass close to the equilibrium $(n-1)$ times before returning back to it.
The performance of our method, and its use as a stepping stone for the study of complicated bifurcation diagrams with EtoP connections, is discussed in detail with three examples in Section 3.5. In Section 3.5.1 we find the codimension-one EtoP heteroclinic cycle of the origin in the Lorenz system, which consists of a codimension-one EtoP connection and a codimension-zero EtoP connection from the periodic orbit back to the origin. The entire EtoP heteroclinic cycle is then continued in two parameters. We also demonstrate how the continuation of a codimension-zero homoclinic orbit to the periodic orbit can be started from the data for the EtoP cycle. Section 3.5.2 is a thorough investigation of EtoP connections and associated global bifurcations in the three-dimensional model vector field from [KO06] for the dynamics near a saddle-node Hopf bifurcation with a global reinjection mechanism. This reveals the bifurcation phenomena behind the accumulation of a curve of homoclinic orbits (to an equilibrium) on a curve of codimension-one EtoP connections. Successive maxima and minima of this accumulation process appear close to curves of tangencies that bound a region where the codimension-zero connection of the overall EtoP cycle exists. This completes the study in [KO06] in agreement with the theoretical results in [Rad05] and Section 2.4. What is more, we detect and continue a second EtoP connection, which reveals a new accumulation phenomenon: the EtoP connection itself accumulates on a segment of a curve of the first EtoP connection. In the process, a codimension-zero homoclinic orbit to the periodic orbit 'splits off'. Our results suggest that the accumulation of a connecting orbit onto a curve segment is quite a general mechanism. In Section 3.5.3 is an example that shows that our method also works for EtoP connections of a higher codimension. Namely, we find and continue a codimension-two EtoP connection in a four-dimensional Duffing-type system, which involves closing two Lin gaps in succession.
Finally we generalise our method to PtoP connections in Section 3.6 and compute a codimension-zero PtoP connection in a four-dimensional vector field; while the Lin direction is trivial in this case, we can nevertheless use continuation runs (which now do not involve system parameters) to bring the endpoints of the two orbit segments together.

3.3 Lin's method for an EtoP connection

In this section we briefly repeat some of the relevant definitions, assumptions and results from Chapter 2.
We consider a sufficiently smooth vector field (1.2.1) in the phase space $\mathbb{R}^n$ and the parameter $\lambda \in \mathbb{R}^m$. The flow is denoted by ϕ^t. All the relevant objects in this section (equilibrium, periodic orbit, their respective invariant manifolds) depend on λ, but we generally do not indicate this explicitely in the notation.
Our main object of study is one single EtoP connection, that is, a heteroclinic connecting orbit Q of (1.2.1) between a hyperbolic equilibrium p and a hyperbolic periodic orbit Γ at some parameter value λ^*. For definiteness we assume in the formulation below that the flow

along the connection is from p to Γ. (This can always be achieved by a reversal of time in (1.2.1) if the flow is in the opposite direction.) We consider a generic EtoP connection, more precisely, we assume that the Conditions (C1)–(C5) are satisfied.
Our goal is to find the EtoP connection Q for λ^* in a systematic way by starting nearby, that is, in the neighbourhood Λ of λ^*. To formulate our method we use the cross-section $\Sigma = \Sigma_1$ as introduced in Section 2.2. We denote a specific point on Σ by p_Σ and the normal vector by n_Σ, thus we can express $Y = Y_1$ by $Y := \{x : \langle x, n_\Sigma\rangle = 0\}$ and Σ by

$$\Sigma = p_\Sigma + Y. \tag{3.3.1}$$

Note that, even when Q is yet unknown, transversality of its intersection with Σ can be achieved by making sure that the flow ϕ^t is transverse to the relevant part of Σ throughout Λ. While the choice of section Σ is effectively arbitrary, it is in the spirit of the method to choose Σ far from p and far from Γ.
Due to transversality of Q and Σ, for all $\lambda \in \Lambda$ we can find (λ-dependent) orbit segments

$$Q^- = \{q^-(t) \mid t \le 0\} \subset W^u(p) \tag{3.3.2}$$

from p to Σ, and

$$Q^+ = \{q^+(t) \mid t \ge 0\} \subset W^s(\Gamma) \tag{3.3.3}$$

from Σ to Γ. In other words, $q^-(\cdot)$ and $q^+(\cdot)$ satisfy (1.2.1) and the boundary conditions

$$\lim_{t\to-\infty} q^-(t) = p, \tag{3.3.4}$$

$$q^-(0) \in \Sigma, \tag{3.3.5}$$

and

$$\lim_{t\to\infty} \operatorname{dist}(q^+(t), \Gamma) = 0, \tag{3.3.6}$$

$$q^+(0) \in \Sigma, \tag{3.3.7}$$

respectively.
By construction, the EtoP connection Q for $\lambda = \lambda^*$ is given as $Q = Q^- \cup Q^+$, which means that Q is characterized by

$$q^-(0) = q^+(0). \tag{3.3.8}$$

Since $\dim(W^u(p) \cap \Sigma) = k-1$ and $\dim(W^s(\Gamma) \cap \Sigma) = l-1$, equation (3.3.8) consists formally of $n-(k-1)-(l-1) = d+1$ conditions. However, the existence of the EtoP connection Q is only of codimension d, so the task is now to find d well-defined test functions that are zero exactly when (3.3.8) is satisfied.
The key idea due to Lin is that the orbit segments Q^- and Q^+ can be chosen in such a way that the difference of $q^-(0)$ and $q^+(0)$ lies in a d-dimensional linear subspace $Z \subset Y$. This d-dimensional linear subspace Z (*Lin space* for short) is defined in (2.2.1).

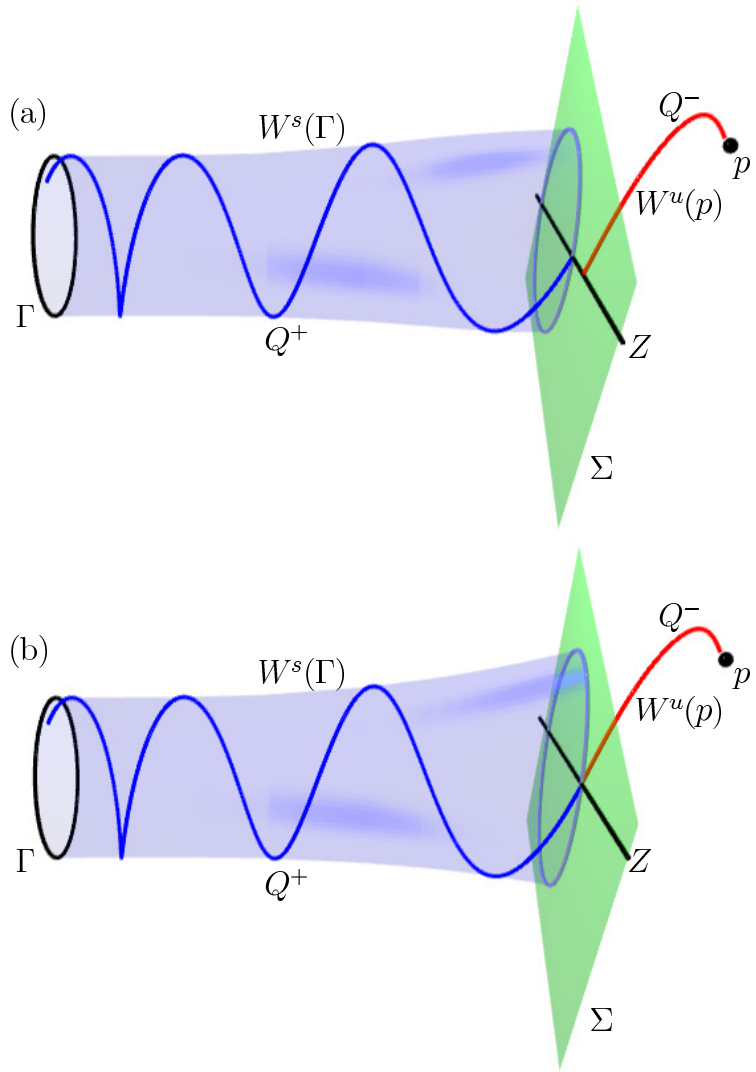

Figure 3.1: Sketch of the statement of Theorem 2.2.1 in $\mathbb{R}^3$, showing the two-dimensional section Σ and the one-dimensional Lin space Z together with the orbit segments $Q^- \subset W^u(p)$ and $Q^+ \subset W^s(\Gamma)$. Panel (a) shows the situation for λ near λ^*, and panel (b) that for $\lambda = \lambda^*$ where the EtoP connection $Q = Q^- \cup Q^+$ exists.

Due to the genericity conditions (C4) and (C3) the subspace Z is of dimension d, and we choose basis vectors $z_1, \cdots, z_d$ of Z. Note that there is still an element of choice for Z, which corresponds to the choice of the scalar product for which (2.2.1) is satisfied. One well-known possibility is that Z is expressed as a linear combination of initial values for bounded (on $\mathbb{R}$) solutions of the adjoint variational equation along Q [San93, Kno04, OCK03].
Then the statement of Theorem 2.2.1 is that there is a neighbourhood Λ of λ^* such that for each $\lambda \in \Lambda$ there is a unique pair of orbits Q^+ and Q^- as defined above and the difference of their end points $\xi^\infty(\lambda)$ in Σ lies exclusively in Z: $\xi^\infty(\lambda) := q^+(0) - q^-(0) \in Z$.
As a result of theorem 2.2.1, for a choice of basis vectors $z_1, \cdots, z_d$ of the Lin space Z there are smooth functions $\eta_i : \mathbb{R}^m \to \mathbb{R}$, $i = 1, \ldots, d$, such that

$$\xi^\infty(\lambda) = \sum_{i=1}^{d} \eta_i(\lambda) z_i$$

on the neighbourhood Λ and

$$\eta_i(\lambda^*) = 0 \ \text{ for all } \ i = 1, \ldots, d.$$

Due to Condition (C5) the matrix $D\xi^\infty$ is non-singular. This means that the d smooth functions $\eta_i(\lambda)$ are well-defined test-functions, which we refer to as the *Lin gaps*.
In light of Theorem 2.2.1, a generic codimension-d EtoP connection Q can be found as follows. After choosing a suitable d-dimensional Lin space Z we can find for a fixed λ near λ^* the unique orbit segments $Q^- \subset W^u(p)$ and $Q^+ \subset W^s(\Gamma)$, such that their difference $\xi(\lambda) = q^+(0) - q^-(0) \in Y$ lies exclusively in the Lin space $Z \subset Y$; recall that $\Sigma = p_\Sigma + Y$ and see Figure 3.1(a) for a sketch of this situation for $n = 3$. The main idea is now to continue the λ-dependent orbit segments Q^- and Q^+ in a suitable combination of system and internal parameters in such a way that the Lin gaps $\eta_i(\lambda)$ become zero one by one. When this has been achieved, we have $\lambda = \lambda^*$ and the EtoP connection Q has been found; see Figure 3.1(b). How this general scheme can be implemented in practice is discussed next.

3.4 Implementation of the method

For the implementation of the method we formulate the orbit segments Q^- and Q^+ in the form of well-posed boundary value problems, which are then continued with the software package AUTO [DPC+00, DPC+06] in suitable parameters to close the Lin gaps. In particular, Q^- and Q^+ need to be truncated to finite time intervals. This can be achieved by using projection boundary conditions [Bey94, CKS96], where the end points near the equilibrium p and the periodic orbit Γ, respectively, are forced to lie in the local linear eigenspaces. During the continuation both p and Γ need to be continued as discretised objects together with their relevant linearisations. The orbit segments Q^- and Q^+ themselves are represented within the collocation setup of AUTO by Gauss-Legendre polynomials on a variable mesh. As is common, we consider the vector field (1.2.1) in the time-rescaled form

$$\dot{u} = T\, f(u, \lambda), \tag{3.4.1}$$

where any orbit segment is parameterised over the unit interval $[0, 1]$ and the associated integration time T appears as a separate parameter [Doe07]. In practice, all objects that need to be continued are condensed into one large boundary value problem. We proceed by defining this large system piece by piece. Note that all involved objects depend on the family parameter λ, but for convenience we do not represent this explicitly in the notation.

3.4.1 Equilibrium and periodic orbit

The equilibrium p simply satisfies the equation

$$f(p, \lambda) = 0 \tag{3.4.2}$$

and can be continued in λ as such. We also need to continue the unstable linear eigenspace $E^u(p)$ (which is assumed to be of fixed dimension throughout Λ). In the case that $E^u(p)$ is the span of a single unstable eigenvector, it is often possible to find an explicit formula for it as a function of λ. This has been used in the examples in Section 3.5. More generally, the linearisation at p can be continued in λ by extending the system with the eigenvalue problem of the Jacobian (together with a normalisation equation for the eigenvector). The eigenspace $E^u(p)$ can then be found for each value of λ. This approach is quite standard and implemented, for example, in the HomCont part of Auto; see [CKS96] for more details.
The periodic solution $\Gamma = \{\gamma(t) \mid 0 \le t \le T_\gamma\}$ is represented as an orbit segment u_γ that satisfies (3.4.1) for the (minimal) period $T = T_\gamma$ of Γ, subject to the boundary conditions

$$u_\gamma(0) = u_\gamma(1), \tag{3.4.3}$$

$$\int_0^1 \left\langle \dot{\tilde{u}}_\gamma(\tau), u_\gamma(\tau) \right\rangle d\tau = 0. \tag{3.4.4}$$

Here (3.4.4) is a standard integral phase condition with respect to a reference solution $\tilde{u}_\gamma$ (usually that of the previous continuation step) to ensure that the solution $u_\gamma(\cdot)$ is isolated, so that the boundary value problem for u_γ is well-posed [Doe07]. In practice, the numerical representation u_γ of the saddle periodic orbit Γ can be found by continuation, for example, from a known stable periodic orbit or from a Hopf bifurcation of an equilibrium.
Our method requires knowledge of the stable eigendirections of the monodromy matrix of Γ that are associated with the $(l-1)$ stable Floquet multipliers $\mu_1, \ldots, \mu_{l-1}$ of Γ. Each eigendirection corresponds to a solution $\mathrm{v}_i \not\equiv 0$ of the variational equation along Γ that satisfies $\mathrm{v}_i(T_\gamma) = \mu_i \mathrm{v}_i(0)$. Note that the vectors $\mathrm{v}_i(t)$ form a linear bundle along Γ, which is also known as a Floquet bundle.
A numerical representation u_i of the ith stable eigendirection v_i can be obtained as the solution of the boundary value problem

$$\dot{u}_i(t) = T_\gamma D_u f(u_\gamma(t), \lambda) u_i(t), \tag{3.4.5}$$

$$u_i(1) = \mu\, u_i(0), \tag{3.4.6}$$

$$\langle u_i(0), u_i(0) \rangle = h, \tag{3.4.7}$$

where u_γ represents the periodic orbit Γ of period T_γ as above; see [EKO05, Der07]. The idea is to start from the trivial solution $u_i \equiv 0$ for $\mu = 0$ and $h = 0$. Continuation in μ results in a branch point at each Floquet multiplier $\mu = \mu_i$. Now one can switch the branch by continuing in the internal parameter h while fixing $\mu = \mu_i$. Note that (3.4.7) is a normalisation that uniquely determines u_i, and we stop the continuation when $h = 1$ is reached. Each stable eigendirection u_i $(i = 1, \dots, l-1)$ can now be continued in the system parameter λ as a solution of (3.4.5)–(3.4.7) for fixed $\mu = \mu_i$ and $h = 1$. Exactly the same procedure can also be applied to get a numerical representation of the unstable eigenfunctions $\mathrm{v}_l, \dots, \mathrm{v}_{n-1}$ and the associated unstable Floquet multipliers $\mu_l, \dots, \mu_{n-1}$.
We remark that it may be advantageous to improve the numerical stability of the computation by continuing u_i as the solution of the equivalent boundary value problem

$$\dot{u}_i(t) = T_\gamma D_u f(u_\gamma(t), \lambda) u_i(t) + \ln|\mu_i|\, u_i(t), \tag{3.4.8}$$
$$u_i(1) = \mathrm{sign}(\mu_i) u_i(0), \tag{3.4.9}$$
$$\langle u_i(0), u_i(0) \rangle = 1; \tag{3.4.10}$$

see [DKKvVa] for details (in short, the equations $\lambda_{old} = \pm e^\lambda$ and $u(t) = e^{\lambda t} u_{old}(t)$ are used to transform the system (3.4.5)–(3.4.7) to (3.4.8)–(3.4.10)). Equations (3.4.8)–(3.4.10) were in fact used for the computations in Section 3.5.3.

3.4.2 Step one – Finding orbit segments up to Σ

As was mentioned before, the $(n-1)$-dimensional section Σ should be chosen such that it intersects the sought-after EtoP connection Q transversely. This can be achieved by choosing Σ such that the equilibrium p is on one side and the periodic orbit Γ on the other side of Σ for all $\lambda \in \Lambda$. What is more, then any connecting orbit from p to Γ (that may exist for one or more $\lambda \in \Lambda$) intersects Σ, and the intersection is generically transverse. Indeed, the exact choice of Σ depends on the system under consideration; see the examples in Section 3.5.
The first step of the method is now to find discretisations u^- and u^+ of the orbit segments Q^- and Q^+ from p to Σ and Γ to Σ, respectively. To this end, we fix the parameter λ at some value near λ^*. From Section 3.4.1 we know (numerical representations of) the equilibrium p with its unstable eigendirections e_i^u, $i = 1, \dots, k$, as well as the periodic orbit u_γ with the stable eigenfunctions u_i, $i = 1, \dots, l-1$.
For u^- we consider the boundary value problem

$$\dot{u}^-(t) = T^- f(u^-(t), \lambda), \tag{3.4.11}$$
$$\left\langle u^-(1) - p_\Sigma, n_\Sigma \right\rangle = \sigma^-, \tag{3.4.12}$$
$$u^-(0) = p + \sum_{i=1}^{k} \varepsilon_i e_i^u. \tag{3.4.13}$$

Here (3.4.13) imposes a projection boundary condition on $u(0)$ at the equilibrium p. Namely, the parameters ε_i are the distances of $u^-(0)$ from p along the unstable eigendirections. Furthermore, the parameter σ^- measures the distance of the other endpoint $u^-(1)$ from Σ. For a

fixed choice of small ε_i and starting from the trivial solution $u^- \equiv p + \sum_{i=1}^{k} \varepsilon_i e_i^u$ we continue (3.4.11)–(3.4.13) in the integration time $T^- > 0$ and in σ^-. The continuation is stopped when a zero of σ^- is detected, which means that we have found an initial orbit segment u^- starting near p in the unstable eigenspace and ending in Σ. We remark that it is convenient after the initial continuation up to Σ to implement the projection boundary condition in the form of a projection operation $L_u(p, \lambda)$ (represented by an $(n-k) \times n$ matrix) in combination with a phase condition; compare with [CKS96, Doe07]. This means that we replace (3.4.13) with

$$L_u(p, \lambda) u^-(0) = 0, \tag{3.4.14}$$

$$\int_0^1 \langle \dot{\tilde{u}}^-(\tau), u^-(\tau) - \tilde{u}^-(\tau) \rangle d\tau = 0. \tag{3.4.15}$$

The orbit segment u^+ is found similarly by considering the boundary value problem

$$\dot{u}^+(t) = T^+ f(u^+(t), \lambda), \tag{3.4.16}$$

$$\left\langle u^+(0) - p_\Sigma, n_\Sigma \right\rangle = \sigma^+, \tag{3.4.17}$$

$$u^+(1) = u_\gamma(0) + \sum_{i=1}^{l-1} \delta_i u_i(0). \tag{3.4.18}$$

Here (3.4.18) imposes a projection boundary condition on $u^+(1)$ at the point $u_\gamma(0)$ on the periodic orbit Γ. Namely, the parameters δ_i are the distances of $u^+(1)$ from $u_\gamma(0)$ along the stable Floquet directions $u_i(0)$, while σ^+ measures the distance of the other endpoint $u^+(0)$ from Σ. (It may be advantageous in some situations to work with a basis of the stable Floquet space instead to avoid that the u_i become (numerically) linearly dependent; however, this is not an issue in our examples.) We again start with a fixed choice of small δ_i and the trivial solution $u^+ \equiv u_\gamma(0) + \sum_{i=1}^{l-1} \delta_i u_i(0)$ and continue (3.4.16)–(3.4.18) in the integration time $T^+ > 0$ and in σ^+. When $\sigma^+ = 0$ is detected we will have found an initial orbit segment u^+ that starts in Σ and ends near Γ in the stable eigenspace. We remark that after the initial continuation in T it would also be possible to replace (3.4.18) by a projection operator and an additional phase condition [Bey94]. However, we find it more convenient to stick with the formulation (3.4.18) in terms of the internal parameters δ_i, which indeed implements a projection boundary condition at Γ since the δ_i are free to vary during the continuation.

3.4.3 Step two – Setting up the Lin space

The Lin space Z is a d-dimensional subspace of the space Y (from the definition (3.3.1) of Σ) that satisfies (2.2.1). Once Z has been chosen we need to ensure that $u^+(0) - u^-(1) \in Z$. While there is not a single 'optimal' way of choosing Z, we discuss here a few convenient choices as used in Section 3.5.

We first consider the case that $\dim Z = 1$ when we also talk of Z as the Lin direction. Then a straightforward option is to define $Z = \text{span}\{u^+(0) - u^-(1)\}$, which generically satisfies (2.2.1). (Note that here $\lambda \neq \lambda^*$.) Another option is to consider the curves that are traced out by $u^-(1)$ and $u^+(0)$ (still for fixed λ) when one continues the orbit segments u^- and u^+ in (a

suitable combination of) (ε_i, T^-) and (δ_i, T^+), respectively. The Lin direction Z can then be chosen as that through the two points of these families that are closest to each other. In this way, the initial Lin gap along Z is as small as possible; see Section 3.5.1 and Section 3.5.2. More generally, one can choose Z as any d-dimensional subspace. A convenient choice used in Section 3.5.3 is that of a d-dimensional hyperplane parallel to some of the coordinate axes. A continuation of (3.4.16)–(3.4.18) for fixed $\sigma^+ = 0$ in T^+ and (a suitable combination of) δ_i can then be used to ensure that $u^+(0) - u^-(1) \in Z$.
Finally, we select an orthonormal basis z_i, $i = 1, \ldots, d$ of Z. This allows us to initialize the (signed) Lin gaps η_i, $i = 1, \ldots, d$, such that

$$u^+(0) - u^-(1) = \sum_{i=1}^{d} \eta_i z_i \,, \tag{3.4.19}$$

in accordance with Theorem 2.2.1.

3.4.4 Step three – Closing the Lin gaps

The orbit segments u^- and u^+ that we have obtained after steps 1 and 2 above represent a solution of a large λ-dependent boundary value problem, as formulated step-by-step in the above sections, that also involves the equilibrium, the periodic orbit and their linear eigendirections. It can be formulated as

$$\begin{aligned}
f(p,\lambda) &= 0, && (3.4.20)\\
\dot{u}_\gamma(t) &= T_\gamma f(u_\gamma(t),\lambda), && (3.4.21)\\
u_\gamma(0) &= u_\gamma(1), && (3.4.22)\\
\int_0^1 \left\langle \dot{\tilde{u}}_\gamma(\tau), u_\gamma(\tau)\right\rangle d\tau &= 0, && (3.4.23)\\
\dot{u}_i(t) &= T_\gamma D_u f(u_\gamma(t),\lambda) u_i(t), && (3.4.24)\\
u_i(1) &= \mu_i u_i(0), && (3.4.25)\\
\langle u_i(0), u_i(0)\rangle &= 1, \qquad (i = 1, \ldots, l-1) && (3.4.26)\\
\dot{u}^-(t) &= T^- f(u^-(t),\lambda), && (3.4.27)\\
\left\langle u^-(1) - p_\Sigma, n_\Sigma\right\rangle &= 0, && (3.4.28)\\
L_u(p,\lambda) u^-(0) &= 0, && (3.4.29)\\
\int_0^1 \langle \dot{\tilde{u}}^-(\tau), u^-(\tau) - \tilde{u}^-(\tau)\rangle d\tau &= 0, && (3.4.30)\\
\dot{u}^+(t) &= T^+ f(u^+(t),\lambda), && (3.4.31)\\
u^+(1) &= u_\gamma(0) + \sum_{i=1}^{l-1} \delta_i u_i(0), && (3.4.32)
\end{aligned}$$

$$(u^+(0) - u^-(1)) \;=\; \sum_{i=1}^{d} \eta_i z_i. \tag{3.4.33}$$

Equations (3.4.21), (3.4.24), (3.4.27) and (3.4.31) form a system of $N = (3n+(l-1)n)$ equations. (Note that equation (3.4.20) for the equilibrium is well-posed in itself and, hence, is not included in this count.) Similarly, we can combine the boundary conditions and integral constraints (3.4.22), (3.4.23), (3.4.25), (3.4.26), (3.4.28), (3.4.29), (3.4.30), (3.4.32) and (3.4.33) into a system of $B = (4n+(l-1)n+l-k+2)$ constraints. Thus for every value of the system parameter $\lambda \in \Lambda$ the $B - N = n + l - k + 2$ internal parameters T_γ, T^+, T^-, $\delta_1, \ldots, \delta_{l-1}$, $\mu_1, \ldots, \mu_{l-1}$, $\eta_1, \ldots, \eta_d$ are uniquely determined, meaning that system (3.4.20)–(3.4.33) is well-posed [Doe07].

The strategy is now to free the system parameter $\lambda = (\lambda_1, \ldots, \lambda_m)$ in a systematic way to close the Lin gaps $\eta_1, \ldots, \eta_d$ one by one by performing well-defined continuation runs; compare with [OCK03]. Assuming that at the start $\eta_i \neq 0$ for all $i = 1, \ldots, d$ to begin with, we continue (3.4.20)–(3.4.33) in the first run in λ_1, T_γ, T^+, T^-, $\delta_1, \ldots, \delta_{l-1}$, $\mu_1, \ldots, \mu_{l-1}$, $\eta_1, \ldots, \eta_d$ until η_1 is zero. We then fix $\eta_1 = 0$ and replace the parameter η_1 by a second family parameter λ_2. That is, in the second run we continue (3.4.20)–(3.4.33) in λ_1, λ_2, T_γ, T^+, T^-, $\delta_1, \ldots, \delta_{l-1}$, $\mu_1, \ldots, \mu_{l-1}$, $\eta_2, \ldots, \eta_d$ until, without loss of generality, $\eta_2 = 0$. Proceeding in this manner, in the j-th run the continuation parameters are $\lambda_1, \ldots, \lambda_j$, T_γ, T^+, T^-, $\delta_1, \ldots, \delta_{l-1}$, $\mu_1, \ldots, \mu_{l-1}$, $\eta_j, \ldots, \eta_d$, while $\eta_1 = \cdots = \eta_{j-1} = 0$.

After d consecutive continuation runs all Lin gaps η_i are zero and we have $\lambda = \lambda^*$. The concatenation of the orbit segments u^- and u^+, which satisfy $u^-(1) = u^+(0)$, is the sought discretisation of the connecting orbit Q of (1.2.1). It can be continued in further system parameters λ_i for $i > d$ while keeping $\eta_1 = \cdots = \eta_d = 0$.

We remark that it is possible that there exist several solutions where all Lin gaps are closed. Each such solution corresponds to a different EtoP connection at an isolated point in $(\lambda_1, \ldots, \lambda_d)$-space. On the other hand, if it is not possible to find a solution where all Lin gaps are closed, then the sought-after EtoP connection Q does not exist in the parameter region Λ.

3.4.5 Computation of related objects

A codimension-d EtoP connection Q typically implies the existence of other orbits involved in the bifurcation diagram that are related to Q. Therefore, the continuation of Q provides a starting point for unravelling a bifurcation diagram. We now discuss some related objects and how they can be found and continued.

First of all, with the codimension-d EtoP connection Q one often finds a second connection R from Γ back to p. This second EtoP connection is generically of codimension zero. It can be found by performing steps 1 and 2 above to find a (generic) intersection point of $W^u(\Gamma) \cap \Sigma$ and $W^s(p) \cap \Sigma$ for some initial λ; in this continuation $\dim Z = 0$, so that restricting the difference of $u^-(1)$ and $u^+(0)$ to Z means achieving $u^-(1) - u^+(0) = 0$. Note that in the setup in Section 3.4.2 and Section 3.4.3 time T is reversed in (3.4.1). The resulting connecting orbit can then be continued in λ. However, in low-dimensional examples it is

generally easier to obtain a codimension-zero EtoP connection R by a so-called homotopy method; see [DKKvVa, EKO05]. Namely one starts in the linear unstable eigenspace near the periodic orbit Γ and continues in the integration time T (effectively performing shooting) until the linear stable eigenspace of p is reached. The distance to the equilibrium p can then be reduced in a further continuation. The codimension-zero EtoP connection in Sections 3.5.1 and 3.5.2 were found in this way. Specifically, the connecting orbit R is represented by an orbit segment u_r and can then be continued, together with p, Γ and their linear eigenspaces, as the solution of the boundary value problem

$$\dot{u}_r(t) = Tf(u_r(t), \lambda), \tag{3.4.34}$$

$$u_r(0) = u_\gamma(0) + \sum_{i=l}^{n-1} \delta_i u_i(0), \tag{3.4.35}$$

$$L_s(p, \lambda)u_r(1) = 0, \tag{3.4.36}$$

$$\int_0^T \left\langle \dot{\tilde{u}}_r(\tau), u_r(\tau) - \tilde{u}_r(\tau) \right\rangle d\tau = 0. \tag{3.4.37}$$

Here we use the unstable Floquet directions u_i, $i = l, \ldots, n-1$ for the approximation of $W^u(\Gamma)$, while the projection boundary condition near p is given by the projection $L_s(p, \lambda)$ onto the linear stable eigenspace of p. The boundary value problem (3.4.34)–(3.4.37) is well-posed if $W^u(\Gamma)$ and $W^s(p)$ intersect transversely along an isolated orbit, which is R. Note that generically this is always the case when the original EtoP connection Q is of codimension one. In this situation u_r can be continued in the parameter λ as a solution of (3.4.34)–(3.4.37). We only remark that if $W^u(\Gamma)$ and $W^s(p)$ intersect along a manifold of dimension larger than one, additional conditions are needed to select a single connecting orbit R within the intersection.

Together the codimension-d EtoP connection Q and the codimension-zero EtoP connection R form an EtoP heteroclinic cycle between p and Γ, which can be continued in parameters. Theory predicts that other types of global orbits exists near such an EtoP heteroclinic cycle; see [CKK$^+$07, KO06, Rad05] and Section 2.4. Start data for these expected global objects can be obtained by concatenating the orbit segments representing Q and R in appropriate ways. For example, a codimension-d homoclinic orbit connecting p back to itself can be constructed in good approximation as the concatenation of u^-, u^+ and u_r, provided $u_r(0)$ and $u^+(1)$ are sufficiently close together. After an initial Newton step, the homoclinic orbit can readily be continued with the HomCont extension of Auto; see Section 3.5.2 where we investigate the interaction of this kind of homoclinic orbit with the EtoP heteroclinic cycle. Another type of orbit that must be expected near the EtoP heteroclinic cycle is a homoclinic orbit to Γ, which is generically of codimension zero. Again, we can concatenate orbit segments as start data for the discretised homoclinic orbit u_h, which (for each λ) satisfies the boundary value

problem

$$\dot{u}_h(t) = T_h f(u_h(t), \lambda), \tag{3.4.38}$$

$$u_h(0) = u_\gamma(0) + \sum_{i=l}^{n-1} \delta_i u_i(0), \tag{3.4.39}$$

$$u_h(1) = u_\gamma(0) + \sum_{i=1}^{l-1} \delta_i u_i(0). \tag{3.4.40}$$

Note that (3.4.38)–(3.4.40) is well-posed, as it consists of $2n$ boundary conditions that determine u_h and the n additional parameters T_h, $\delta_1, \ldots, \delta_{n-1}$.
More generally, the boundary value problems in Section 3.4 provide a 'toolkit' for the continuation of the connecting orbits that we are interested in. As is demonstrated in the next section, the construction of the initial codimension-d EtoP connection with Lin's method serves as a stepping stone for the continuation of many associated connecting orbits.

3.5 Demonstration of the method

We now demonstrate our method for finding and continuing EtoP connections and related EtoP heteroclinic cycles with three examples. Namely, we consider the well-known Lorenz system [Lor63], a three-dimensional vector field model of a saddle-node Hopf bifurcation with global reinjection [KO06], and a four-dimensional coupled Duffing system [LX03]. All computations are performed with the numerical continuation package AUTO2000/AUTO07P [DPC+00, DPC+06], which uses pseudo-arclength continuation and orthogonal collocation to solve the boundary value problems that arise; see [Doe07] for more details. The size of the overall boundary value problems is given by the number of objects that are continued simultaneously, which typically include the equilibrium p, the periodic orbit Γ together with its stable and its unstable eigenfunctions, and the two orbit segments Q^- and Q^+ up to the specified section Σ. Throughout we use polynomials of degree `NCOL` $= 4$ in each collocation interval and, depending on the complexity of the orbit, between `NTST` $= 200$ and `NTST` $= 1000$ collocation intervals. (Note that this means that Γ, Q^- and Q^+ are all represented over the same mesh as given by `NCOL` and `NTST`).

3.5.1 Codimension-one EtoP heteroclinic cycle in the Lorenz system

In the 1960's Lorenz derived the much simplified model of atmospheric convection [Lor63] given by the three-dimensional vector field

$$\begin{cases} \dot{x} = \sigma(y - x), \\ \dot{y} = \varrho x - y - xz, \\ \dot{z} = xy - \beta z. \end{cases} \tag{3.5.1}$$

For the classical choice of parameters given by $\beta = \frac{8}{3}$, $\sigma = 10.0$ and $\varrho = 28$ he found the now well-known butterfly or Lorenz attractor, which is one of the best known examples of chaotic dynamics (i.e. sensitive dependence on the initial condition).

When the parameter ϱ is allowed to vary, there is a transition from simple to chaotic dynamics. It involves a homoclinic bifurcation at $\varrho_{\text{hom}} \approx 13.9265$ where there is a pair of homoclinic orbits to the origin $\mathbf{0}$ that are each other's images under the symmetry transformation

$$(x, y, z) \mapsto (-x, -y, z)$$

of (3.5.1). For $\varrho_{\text{het}} \approx 24.0579$ there exists a symmetric pair of EtoP connections between $\mathbf{0}$ and periodic orbits Γ^+ and Γ^-; see [DKO06, Spa82] for more details. Here we find and follow in parameters (one of) these EtoP connections and the associated EtoP heteroclinic cycle. The origin $\mathbf{0}$ is a saddle-point for $\varrho > 1$ with a one-dimensional unstable manifold and a two-dimensional stable manifold, as determined by the eigenvalues

$$-\beta \quad \text{and} \quad -\frac{1}{2}(\sigma+1) \pm \frac{1}{2}\sqrt{(\sigma+1)^2 + 4\sigma(\varrho-1)}.$$

The periodic orbit Γ can been found by continuation from a Hopf bifurcation at $\varrho_H \approx 24.7368$ of the non-zero secondary equilibria

$$p^{\pm} = (\pm\sqrt{\beta(\varrho-1)}, \pm\sqrt{\beta(\varrho-1)}, \varrho-1).$$

Indeed Γ is of saddle type and its stable eigenspace can be computed as described in Section 3.4. Due to the symmetry it is sufficient to consider only the connection from $\mathbf{0}$ to $\Gamma = \Gamma^-$ which lies in the one-dimensional unstable manifold of $\mathbf{0}$ and the two-dimensional stable manifold of Γ.

Finding the codimension-one EtoP connection

We define the section Σ by specifying the point $p_\Sigma \in W^u(\mathbf{0})$ (for $\varrho = 24.0579 \approx \varrho_{\text{het}}$ and β, σ at their classical values) that satisfies

$$\text{dist}(p_\Sigma, \mathbf{0}) \approx \text{dist}(p_\Sigma, \Gamma)$$

which gives

$$p_\Sigma = \begin{pmatrix} 17.2877 \\ 21.4376 \\ 31.7958 \end{pmatrix}.$$

Further, the normal vector n_Σ of Σ is defined as the direction of the flow at p_Σ.
To start, we choose $\varrho = 24.5$ as an initial parameter value reasonably close to ϱ_{het}. The first step (cf. Section 3.4.2) consists of a computation of the one-dimensional manifold $W^u(\mathbf{0})$ by continuation in the direction of positive time T^- from $\mathbf{0}$, subject to boundary condition (3.4.13), until the section Σ is reached. Similarly, we choose a point $g \in \Gamma$, $g = (-10.0437, -9.95751, 25.7945)$, and consider the corresponding fixed stable Floquet vector v for the formulation of boundary condition (3.4.18). We then continue in the direction of time T^+ until Σ is reached. A further continuation in the distance δ along v yields the one-dimensional intersection curve $W^s(\Gamma) \cap \Sigma$.
Figure 3.2(a) shows the end points $u^+(1)$ of orbit segments on v near the chosen fixed base point $g \in \Gamma$. The orbit denoted by A intersects the Floquet vector v twice and thus bounds a

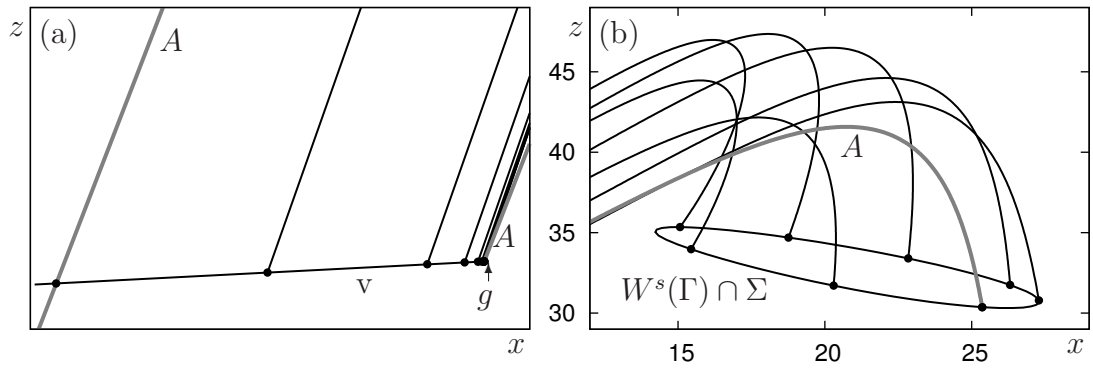

Figure 3.2: Orbit segments during the computation of $W^s(\Gamma)$ up to the section Σ in the Lorenz system (3.5.1) for $\sigma = 10.0$, $\varrho = 28.0$, and $\varrho = 24.5$. Panel (a) shows the end points of different orbit segments along the stable Floquet direction v; the orbit A bounds a fundamental domain. The length of the fundamental domain is 1.55752×10^{-5}. Panel (b) shows how the other end points trace out $W^s(\Gamma) \cap \Sigma$.

fundamental domain. While $u^+(1)$ on v covers the fundamental domain on v, the other end point $u^+(0)$ traces out the intersection curve $W^s(\Gamma) \cap \Sigma$. As Figure 3.2(b) shows, this curve is a smooth closed curve in Σ. Figure 3.3(a) shows the computed parts of $W^u(\mathbf{0})$ and $W^s(\Gamma)$ in (x, y, z)-space, where the section Σ is the grey plane. Notice that $W^s(\Gamma)$ is a topological cylinder that is represented well by the family of orbit segments parametrised by δ.
Next we need to make a suitable choice for the one-dimensional Lin direction Z; cf. Section 3.4.3. As was mentioned before, a good choice is to define Z as the direction given by $W^u(\mathbf{0}) \cap \Sigma$ and the point on $W^s(\Gamma) \cap \Sigma$ that lies closest to it. Then the initial Lin gap along Z is as small as possible. The respective orbit segments of $W^u(\mathbf{0})$ and $W^s(\Gamma)$ are shown in Figure 3.3(b); the initial gap size is $\eta = 1.39437$.
To close the Lin gap η and find the codimension-one EtoP connection we continue in the parameters T^-, T^+, η and ϱ; cf. Section 3.4.4 and (3.4.20)–(3.4.33). For $\varrho = 24.0579$ a zero of η is detected; Figure 3.3(c) depicts the EtoP connection from $\mathbf{0}$ to Γ. Note that this value agrees within the computational accuracy of ϱ_{het} found in [DKO06].
These computations show that our method is indeed able to find a first solution for the continuation of the codimension-one EtoP connection. Namely, the two orbit segments can now be continued in system parameters while keeping $\eta = 0$ fixed. As was explained in Section 3.4.5, we find the codimension-zero connection from Γ back to p as the solution of the boundary value problem defined by (3.4.34)–(3.4.37) by starting from a suitable initial orbit segment.

Continuation of the EtoP cycle

The entire codimension-one EtoP heteroclinic cycle can be continued in two system parameters. Figure 3.4(a) shows the resulting codimension-one bifurcation curve *het* and the bifurcation curve *hom* of the homoclinic explosion in the (ϱ, β)-plane; also shown is the Hopf

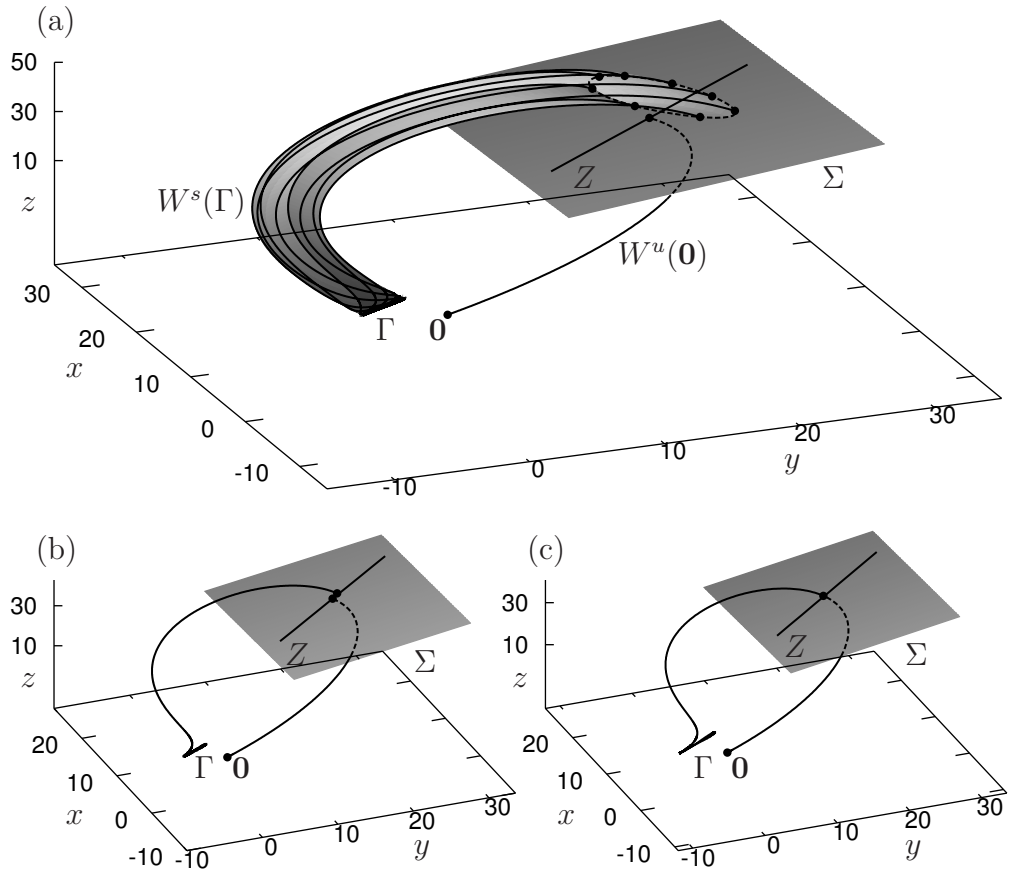

Figure 3.3: The manifolds $W^u(\mathbf{0})$ and $W^s(\Gamma)$ of (3.5.1) computed up to the section Σ for $\varrho = 24.5$ with a Lin gap along Z of $\eta = 1.39437$ (a); panel (b) only shows the two orbit segments up to Z. For $\varrho = 24.0579$, where $\eta = 0$ was detected, the two orbit segments connect in Σ (c). Throughout, $\beta = 8/3$ and $\sigma = 10.0$.

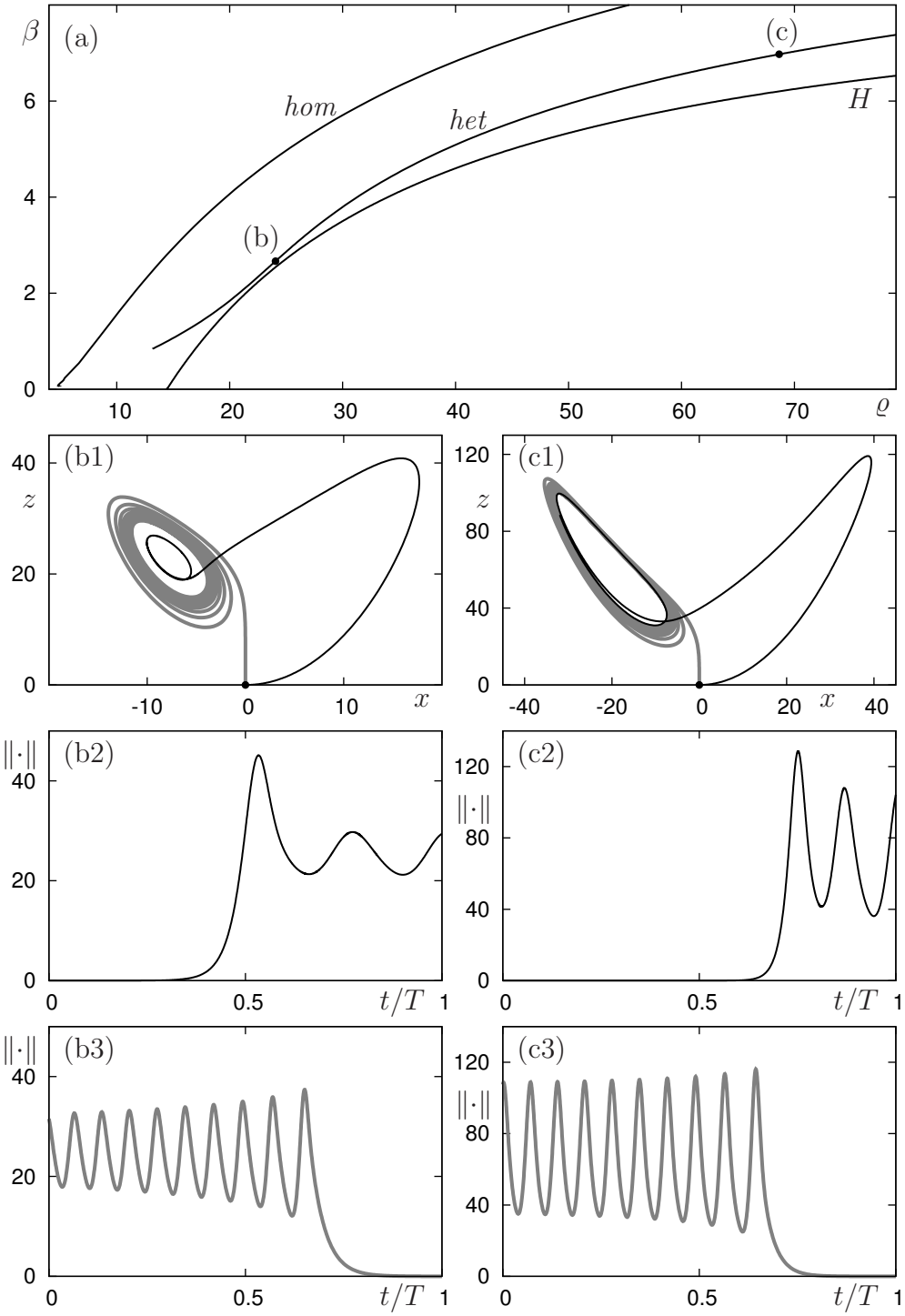

Figure 3.4: Panel (a) shows the curve *het* of EtoP connections from $\mathbf{0}$ to Γ, the curve *hom* of the homoclinic connection to $\mathbf{0}$ and the curve H of Hopf bifurcation in the (ϱ, β)-plane of (3.5.1). Panels (b) and (c) show the computed EtoP heteroclinic cycle for the two selected parameter values $(\varrho, \beta) = (24.0579, 2.66667)$ and $(\varrho, \beta) = (68.6494, 6.97370)$, respectively. Specifically, panels (b1) and (c1) show the projection onto the (x, z)-plane; panels (b2) and (c2) show the norm of the codimension-one connection from $\mathbf{0}$ to Γ; and panels (b3) and (c3) show the norm of the codimension-zero connection from Γ back to $\mathbf{0}$.

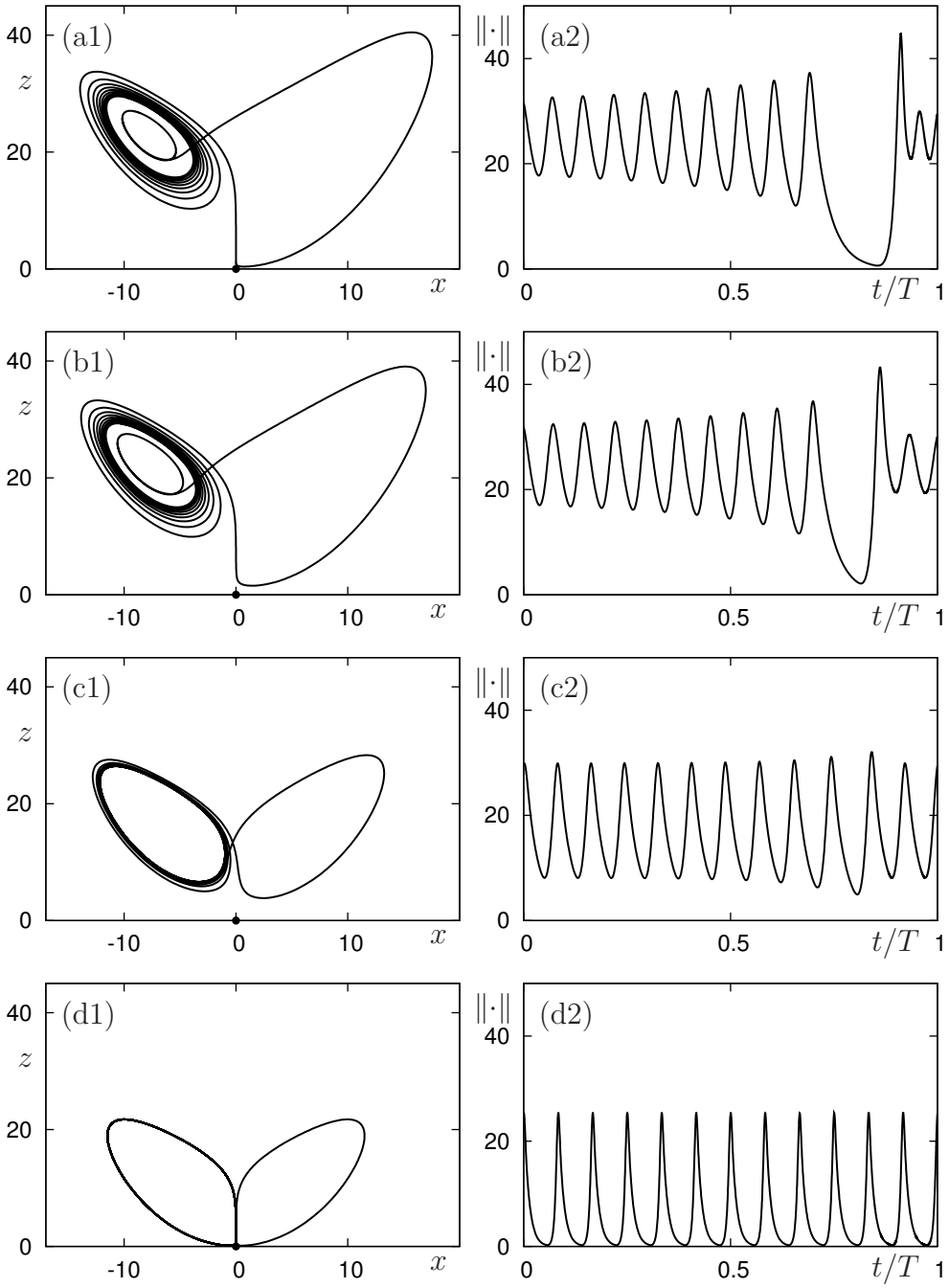

Figure 3.5: The codimension-zero homoclinic orbit to Γ of (3.5.1) for $\beta = 8/3$ and $\sigma = 10.0$ in dependence on ϱ. Shown are the projection onto the (x, z)-plane (left column) and the norm of the approximating orbit segment (right column) for $\varrho = 23.9666$ (a), $\varrho = 23.5575$ (b), $\varrho = 18.6310$ (c), and $\varrho = 13.9828$ (d).

bifurcation curve H. Panels (b1) and (c1) show two examples of the corresponding EtoP heteroclinic cycle in projection onto the (x, z)-plane, which consists of the codimension-one connection from $\mathbf{0}$ to Γ (black curve) and the codimension-zero connection from Γ back to $\mathbf{0}$ (grey curve). The two respective time traces of the norm $\|\cdot\|$ of the approximating orbit segments (subject to projection boundary conditions) are shown in Figure 3.4 (b2)/(c2) and (b3)/(c3), respectively.
When computing the codimension-one connection for decreasing ϱ towards the homoclinic bifurcation *hom* we encountered some difficulties with the calculation of the two Floquet multipliers of Γ, which could only be determined reliably for $\varrho > 13.1703$. This problem might be solved by employing a more accurate method for determining Floquet multipliers, such as that in [Lus01], but this is beyond the scope of this thesis. The codimension-zero connection from Γ back to $\mathbf{0}$, on the other hand, could be computed throughout, that is, the intersection of $W^u(\Gamma)$ and $W^s(\mathbf{0})$ remains transverse; an example where this intersection becomes tangential is presented in Section 3.5.2.
To demonstrate that the EtoP heteroclinic cycle can be used as a starting solution for the numerical continuation of other types of orbits, we compute the codimension-zero homoclinic orbit to Γ; for $\beta = 8/3$ and $\sigma = 10.0$ it exists for $\varrho \in (\varrho_{\text{hom}}, \varrho_{\text{het}}) \approx (13.9265, 24.0579)$. For an explanation for the disappearance of the homoclinic orbit in a 'blue sky catastrophe' as the parameter ϱ approaches ϱ_{het}, see Section 2.4.2 (real eigenvalue case) and Theorem 2.1.9. To obtain a first homoclinic orbit we concatenate the two separate heteroclinic connections near the fixed point p as a seed for a Newton solve of the boundary value problem defined by (3.4.38)–(3.4.40). The resulting approximation (subject to projection boundary conditions (3.4.39), (3.4.40) at both ends) of the homoclinic orbit to Γ can then be continued (together with Γ and its Floquet bundles) in a system parameter. Figure 3.5 shows the homoclinic orbits to Γ for different values of ϱ. Panel (a) is for ϱ close to ϱ_{het} and the homoclinic orbit passes very close to the origin $\mathbf{0}$ after a single excursion to the right, that is, into the region of positive x. As ϱ is decreased, the orbit deforms but maintains its overall structure with a single excursion to the right; see Figure 3.5(b) and (c). At the same time the periodic orbit $\Gamma = \Gamma^-$ (and its counterpart Γ^+) move toward $\mathbf{0}$ and the homoclinic orbit to Γ approaches the union of the two symmetrically related homoclinic orbits to $\mathbf{0}$ as the homoclinic explosion point at $\varrho_{\text{hom}} \approx 13.9265$ is approached; see Figure 3.5(d). This shows that the homoclinic orbit to Γ considered here is one of the infinitely many connecting orbits that are born in the homoclinic explosion; see also [DKO06].

3.5.2 Global reinjection orbits near a saddle-node Hopf bifurcation

In this section we compute connecting orbits in a three-dimensional model vector field that was introduced in [KO06] to describe the dynamics near a saddle-node Hopf bifurcation in the presence of a global reinjection mechanism. This type of dynamics with reinjection can be found, for example, in laser systems [KTL98, WKSL05, ZNS01], in dynamo theory [ARS04] and, more generally, near weak resonances [Vit03, chapter 4.3.2]. The vector field model can

be written in the form

$$\begin{cases} \dot{x} &= \nu_1 x - \omega y - (\alpha x - \beta y)\sin\varphi - (x^2+y^2)x \\ & \qquad\qquad +d(2\cos\varphi+\nu_2)^2, \\ \dot{y} &= \nu_1 y + \omega x - (\alpha y + \beta x)\sin\varphi - (x^2+y^2)y \\ & \qquad\qquad +f(2\cos\varphi+\nu_2)^2, \\ \dot{\varphi} &= \nu_2 + s(x^2+y^2) + 2\cos\varphi + c(x^2+y^2)^2, \end{cases} \tag{3.5.2}$$

where ν_1 and ν_2 are the unfolding parameters of the saddle-node Hopf bifurcation. The parameters ω, α, β, s, c, d and f determine the type of unfolding and we keep them fixed throughout at

$$\omega = 1.0,\ \alpha = -1.0,\ \beta = 0,\ s = -1.0,\ c = 0,\ d = 0.01,\ f = \pi d.$$

This choice corresponds to the unfolding of type A that was studied in [KO06], where more details can be found. The variable φ is 2π-periodic and global reinjection is realised by trajectories that connect a neighbourhood of a saddle-node Hopf point with one of its symmetric copies. When representing trajectories it is convenient to show them in (u,v,w)-space as given by the transformation

$$\begin{cases} u &= (R+x)\cos\varphi, \\ v &= (R+x)\sin\varphi, \\ w &= y, \end{cases} \tag{3.5.3}$$

where a global reinjection corresponds to a large excursion near the circle $\mathbb{S}^1 = \{x = y = 0\}$. Note that this circle is not invariant because $d \neq 0$ and $f \neq 0$ (where rational ratios are avoided). We fix the radius $R = 2$, which is large enough in light of the x-amplitudes of the observed solutions.
As was shown in [KO06], system (3.5.2) features a complicated structure of homoclinic orbits of equilibria that involve one or more global reinjections. Furthermore, some of the corresponding homoclinic bifurcation curves accumulate on curve segments, while the homoclinic orbit itself accumulates on a periodic orbit of saddle type. This global bifurcation phenomenon was studied theoretically in [Rad05] and Section 2.4 and (3.5.2) provides the first concrete example. Here we demonstrate how the bifurcation diagrams from [KO06] can be completed with our method.

Codimension-one EtoP heteroclinic cycle

Our starting point is the two-parameter bifurcation diagram of system (3.5.2) given in Figure 3.6, which only shows the bifurcation curves that were presented in [KO06]. Two saddle-node Hopf points $SNH^{\pm}$ on two lines S_0 of saddle-node bifurcations are connected by a Hopf bifurcation curve H. The curve S_l of saddle-node bifurcations of periodic orbits emerges from a degenerate Hopf point DH. The most interesting object is the curve h_b^1 of homoclinic orbits that connect the saddle-focus $b = (0, 0, \arccos(\nu_2/2))$ back to itself after a single global reinjection. As can be seen in the enlargement panels (b) and (c), h_b^1 emerges from a non-central saddle-node homoclinic point NS, crosses S_l and then accumulates on a curve segment in the

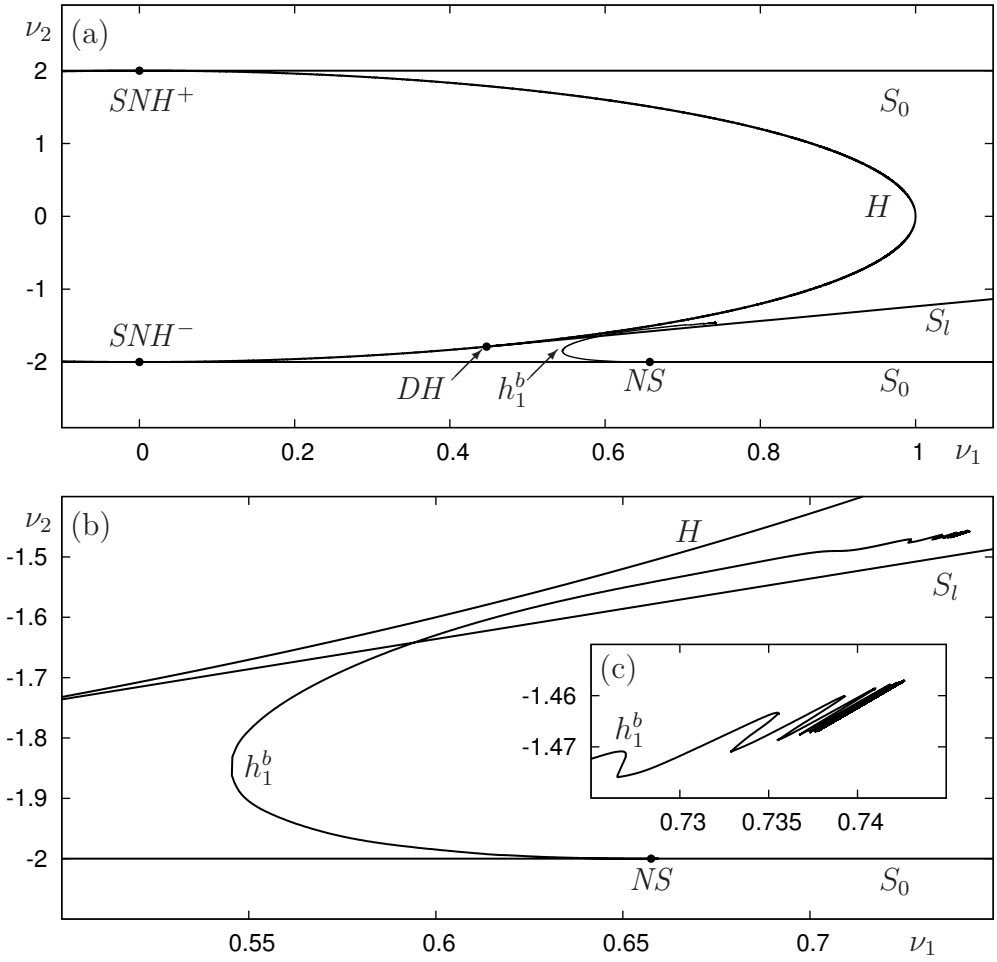

Figure 3.6: Bifurcation diagram in the (ν_1, ν_2)-plane of (3.5.2) consisting of two saddle-node bifurcation curves S_0 and a Hopf bifurcation curve H that meet at two saddle-node Hopf points $SNH^{\pm}$, a curve S_l of saddle-node bifurcations of periodic orbits, and a homoclinic bifurcation curve h_b^1. Panel (a) shows an overview, and panels (b) and (c) are successive enlargements of the curve h_b^1.

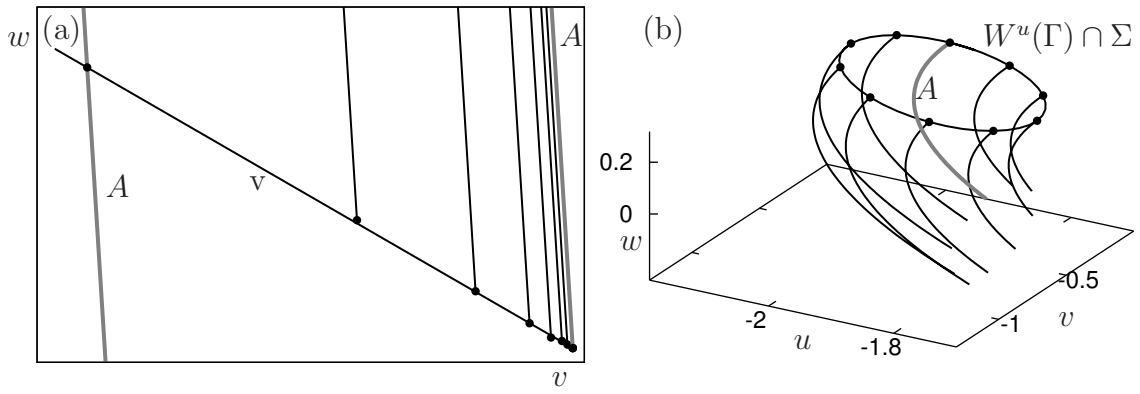

Figure 3.7: Orbit segments during the computation of $W^u(\Gamma)$ of (3.5.2) up to the section Σ. Panel (a) shows the end points of different orbit segments along the stable Floquet direction v; the orbit A bounds a fundamental domain; the length of the fundamental domain is $1.42163 \cdot 10^{-8}$. Panel (b) shows how the other end points trace out $W^u(\Gamma) \cap \Sigma$.

(ν_1, ν_2)-plane. As was mentioned, this accumulation process implies the existence of an EtoP heteroclinic cycle connecting the saddle point b with a periodic orbit Γ of saddle type. Note that we have $\dim W^u(\Gamma) = 2$ and $\dim W^s(b) = 1$, thus we reverse time in the formulation of the boundary value problems in Section 3.4.

To find the EtoP heteroclinic connection between the equilibrium b and the periodic orbit Γ, we choose the section $\Sigma = \{v = 0\}$ and start from a point in parameter space close to the segment of accumulation of h_1^b; compare with Figure 3.6(c). Specifically, we fix $\nu_2 = -1.46$ and start the computation from $\nu_1 = 0.706987$. First we compute $W^s(b)$ by continuation in T^+ until the section Σ is reached; cf. Section 3.4.2 and (3.4.11)–(3.4.13). We then fix a vector $\mathrm{v}(g)$ of the unstable bundle of Γ at a chosen point $g = (0.226499, -0.226726, 5.69218)$ to specify the boundary condition (3.4.18) and continue in the direction of time T^- until Σ is reached. Continuation in the distance δ along v over a fundamental domain is then used to compute the curve $W^u(\Gamma) \cap \Sigma$; Figure 3.7 shows that it is again a smooth closed curve in Σ. Figure 3.8(a) shows $W^s(b)$ and $W^u(\Gamma)$ in (u, v, w)-space as computed up to the section Σ (grey plane). $W^u(\Gamma)$ is a topological cylinder and well represented by a suitable selection of orbit segments as parametrised by δ.

As in Section 3.5.1, we choose the Lin direction Z as the line through $W^u(b) \cap \Sigma$ and the point on $W^s(\Gamma) \cap \Sigma$ closest to it; cf. Section 3.4.3. The respective orbit segments of $W^u(b)$ and $W^s(\Gamma)$ that end in Z are shown in Figure 3.8(b), where the gap size is $\eta = 0.1$. By continuation in T^-, T^+, η and ν_1 the Lin gap is closed; cf. Section 3.4.4 and (3.4.20)–(3.4.33). Namely, a zero of η is detected at $\nu_1 = 0.741189$; the corresponding connecting orbit is shown in Figure 3.8(c).

The codimension-one connecting orbit from Γ to b can now be continued in the parameters

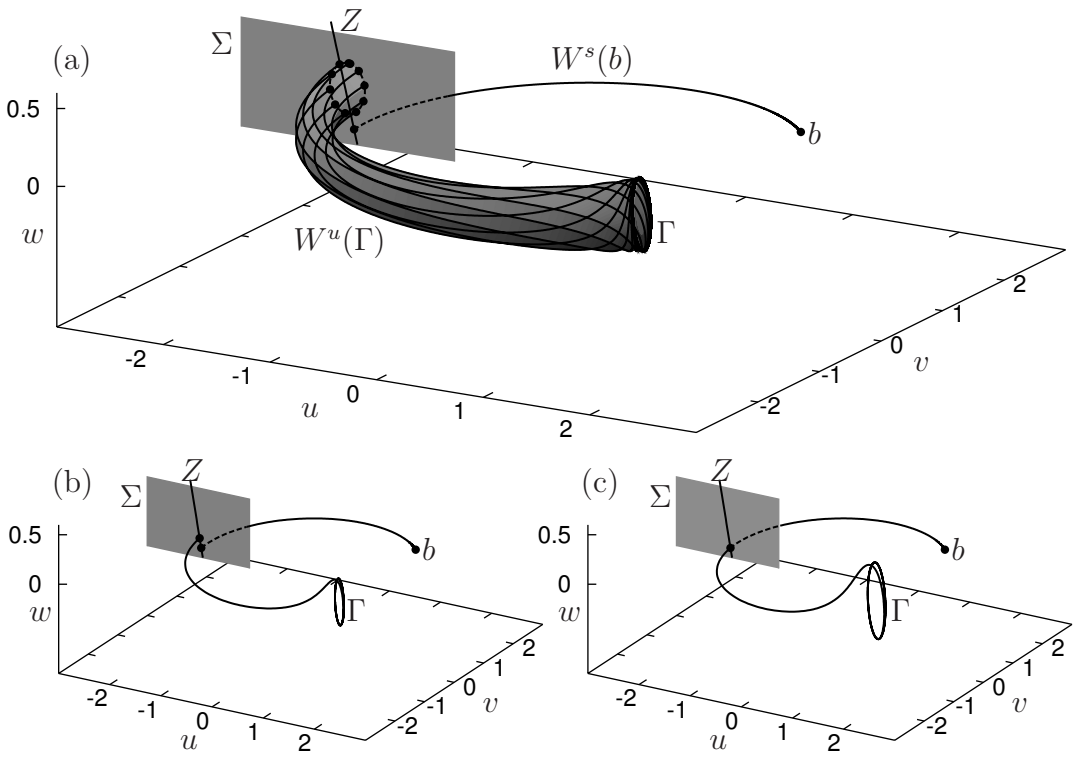

Figure 3.8: The manifolds $W^s(b)$ and $W^u(\Gamma)$ of (3.5.2) computed up to the section Σ for $\nu_1 = 0.706987$ with a Lin gap along Z of $\eta = 0.1$ (a); panel (b) only shows the two orbit segments up to Z. For $\nu_1 = 0.741189$, where $\eta = 0$ was detected, the two orbit segments connect in Σ (c). Throughout, $\nu_2 = -1.46$.

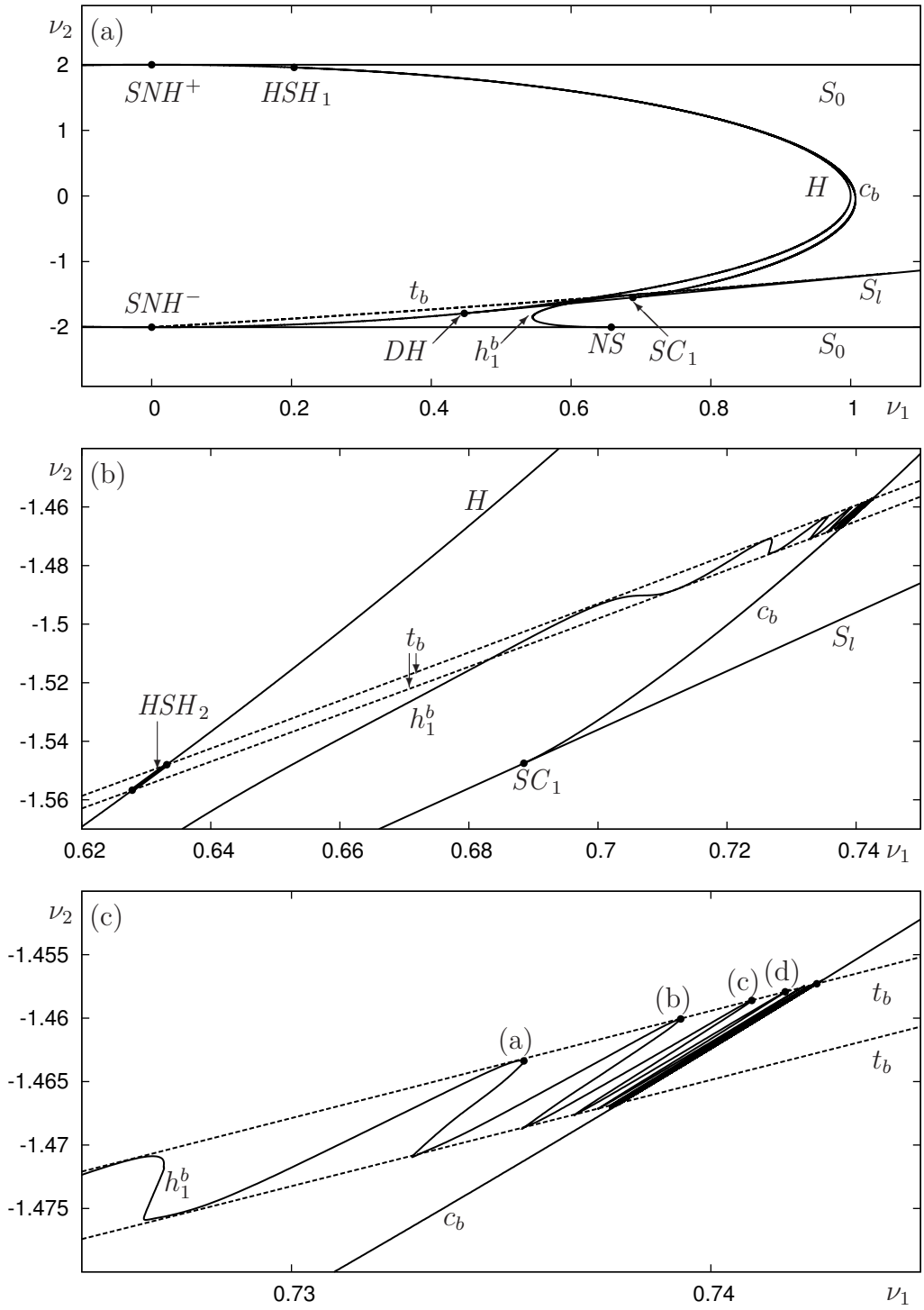

Figure 3.9: The bifurcation diagram of (3.5.2) from Figure 3.6 completed by the curve c_b of codimension-one EtoP connection from b to Γ, and the curves t_b of tangency bifurcation of the codimension-zero connection from Γ back to b. Panel (a) is an overview, and panels (b) and (c) show successive enlargements near the accumulation of h_b^1 onto c_b. Phase portraits and time plots of the orbits at labels (a)–(d) in panel (c) are shown in Figure 3.10, panels (a)–(d). The orbit at the indicated intersection point between c_b and t_b is shown in Figure 3.11.

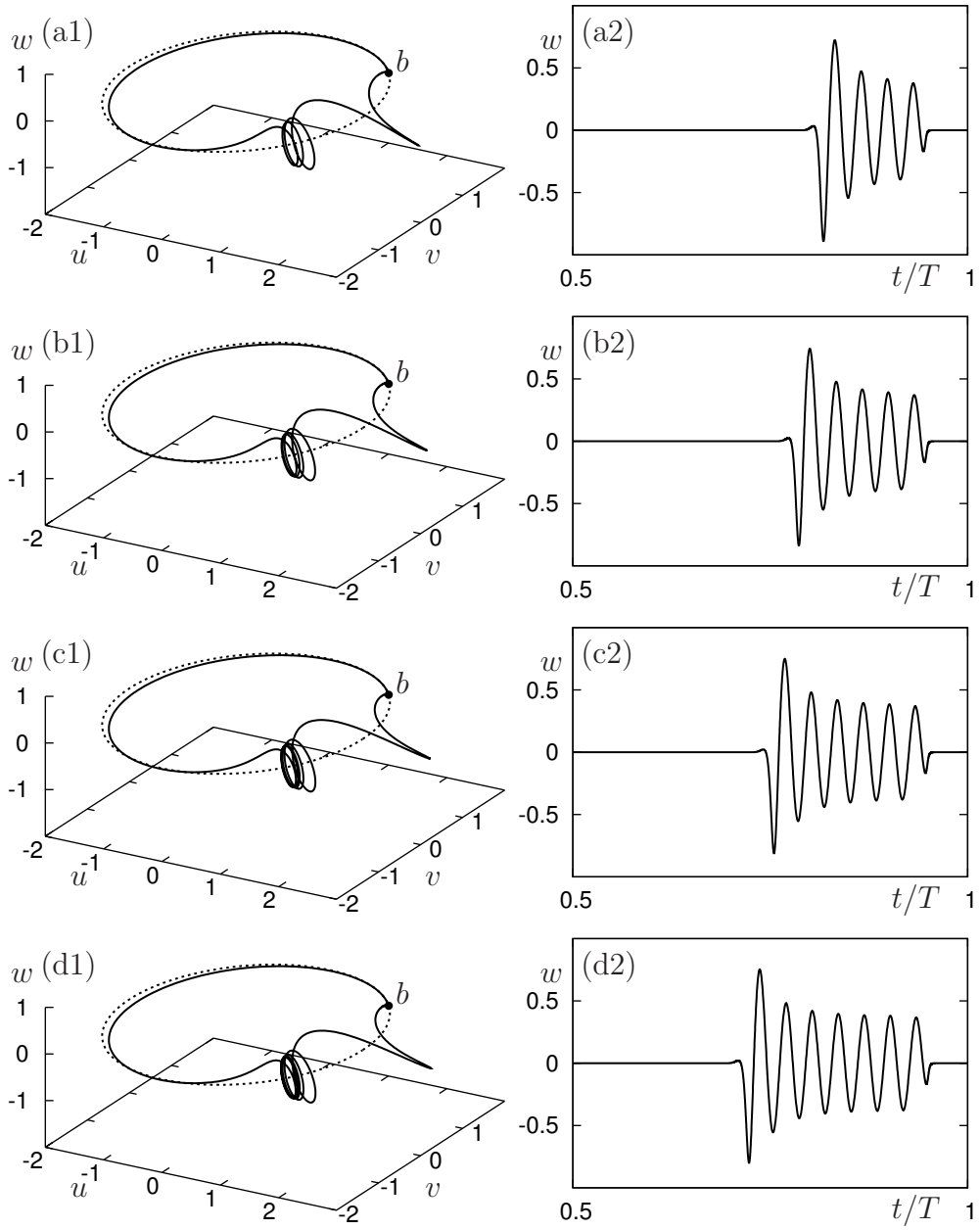

Figure 3.10: The homoclinic orbit to b of (3.5.2) for selected points along the curve h_1^b as indicated in Figure 3.9(c). Shown are the orbits in (u, v, w)-space (left column) and the w-value of the approximating orbit segment (right column) for $(\nu_1, \nu_2) = (0.735540, -1.46337)$ (a), $(\nu_1, \nu_2) = (0.739280, -1.46007)$ (b), $(\nu_1, \nu_2) = (0.740976, -1.45861)$ (c) and $(\nu_1, \nu_2) = (0.741773, -1.45793)$ (d).

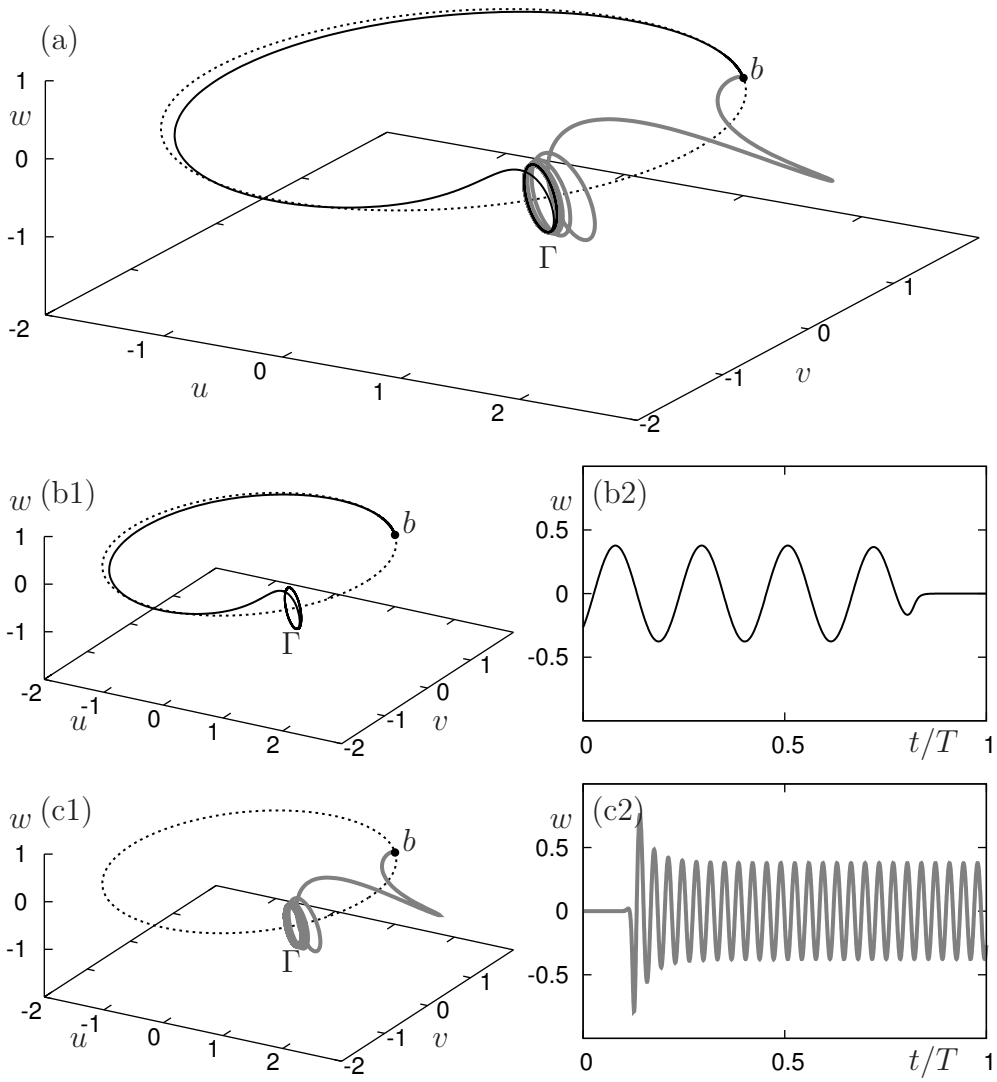

Figure 3.11: The EtoP heteroclinic cycle of (3.5.2) on c_b for $(\nu_1, \nu_2) = (0.742526, -1.45729)$ (a). Panels (b1) and (b2) show the codimension-one EtoP connection and its w-time plot, and panels (c1) and (c2) the codimension-zero EtoP connection and its w-time plot.

ν_1 and ν_2 while keeping the gap closed. This yields the curve c_b that is shown as part of the bifurcation diagram in Figure 3.9. One end point of c_b is the point SC_1 on the curve S_l of saddle-node bifurcations of the periodic orbit, where Γ disappears. The other end point of c_b is the point HSH_1 on the curve H of Hopf bifurcation where Γ shrinks down to the equilibrium a. At HSH_1 a codimension-two connection between b and a exists, that is, the branches of the one-dimensional manifolds $W^u(a)$ and $W^s(b)$ coincide. This codimension-two point is one of the possible 'heteroclinic equivalents' of a Shilnikov-Hopf bifurcation; see [HK93]. A segment of the curve c_b indeed appears to be the limit of the oscillating curve h_1^b; see Figure 3.9(c).

In system (3.5.2) the codimension-zero EtoP connection from b back to Γ exists only in a certain region of the (ν_1, ν_2)-plane, namely near the accumulation of the curve h_1^b on c_b. This structurally stable intersection of the two-dimensional manifolds $W^u(b)$ and $W^s(\Gamma)$ can be computed as was explained in Section 3.4.5 using the boundary value problem (3.4.34)–(3.4.37). The boundary of its region of existence is formed by curves t_b where $W^u(b)$ and $W^s(\Gamma)$ become tangent. The curves t_b can be continued as folds of the respective codimension-zero EtoP connection; they are shown in Figure 3.9(b) and (c) as part of the bifurcation diagram in the (ν_1, ν_2)-plane. For increasing ν_1, the curves t_b can be continued up a point (not shown) on S_l, where the periodic orbit Γ disappears in a saddle-node bifurcation. When ν_1 is decreased, the curves t_b cross the Hopf curve H where Γ disappears in the equilibrium a. As a consequence, the codimension-zero EtoP connection changes its nature along the curve segment HSH_2 on H; see Figure 3.9(b). Namely, beyond HSH_2 (for smaller ν_1) there is now a codimension-zero heteroclinic connection between the two-dimensional manifolds $W^u(b)$ and $W^s(a)$. Hence, beyond H the curves t_b correspond to tangencies of $W^u(b)$ and $W^s(a)$. Such tangencies, that is, the curves t_b, can be continued to the point SNH^-; see Figure 3.9(a). We remark that the heteroclinic bifurcation at HSH_2 can be described as another type of 'heteroclinic equivalent' of a Shilnikov-Hopf bifurcation; see [HK93].

We observe in Figure 3.9(b) and (c) that the curves t_b appear to bound the accumulation process of the curve h_1^b on c_b. After it enters the region in the (ν_1, ν_2)-plane that is bounded by t_b, the curve h_1^b oscillates between these bounds; see Figure 3.9(c). Figure 3.10 shows homoclinic orbits in parameter space and as w-time plots for the maxima (w.r.t. ν_1) that are indicated in Figure 3.9(c). From maximum to maximum of h_1^b the corresponding homoclinic orbit from b back to itself makes one more turn around the periodic orbit Γ; this is best seen in the time traces in the right column of Figure 3.10. In the limit one obtains the EtoP heteroclinic cycle shown in Figure 3.11 at the intersection point $(\nu_1, \nu_2) = (0.742526, -1.45729)$ of c_b and the upper curve t_b. Figure 3.11(a) shows the complete EtoP cycle from Γ to b (black) and back to Γ (grey) in (u, v, w)-space. The computed codimension-one and codimension-zero connections and their time traces are shown in rows (b) and (c), respectively.

Our calculations of the curves c_b and t_b allow us to bring out the missing ingredients of the two-dimensional nature of the accumulation process in the (ν_1, ν_2)-plane, which was already suggested by the oscillating nature of the curve h_1^b in [KO06]. Indeed, our numerical observations strongly suggest a close link between the details of the accumulation process of the homoclinic orbit and the tangency bifurcations. Note that existing analytical results only deal with the accumulation of points of a homoclinic connection on an EtoP heteroclinic cycle along a one-dimensional curve in parameter space (cf. [Rad05] and Theorem 2.1.8); in

Section 2.4.1 we discuss the shape of the snaking curve locally around the turning points. An explanation of the full snaking curve is beyond the scope of this thesis, advanced analytical considerations similar to [BKL+08] are necessary to do this.

Accumulation of an EtoP connection

By starting from $(\nu_1, \nu_2) = (0.66, -1.558)$ and following the steps shown in Section 3.4 it is possible to find a different EtoP connection between Γ and b than that discussed in Section 3.5.2. The continuation of this connection yields the codimension-one curve c_b^* in the bifurcation diagram in Figure 3.12. For decreasing ν_2 the curve c_b^* can be continued past a fold point until it ends at the point SC_2 on S_l. For increasing ν_2 the curve c_b^* appears to accumulate on a segment of c_b; see Figure 3.12(c). It turns out that this accumulation process is associated with a codimension-zero homoclinic orbit to Γ, that is, an intersection of the two-dimensional manifolds $W^u(\Gamma)$ and $W^s(\Gamma)$. The homoclinic orbit to Γ can be found numerically, using the numerical data of the homoclinic orbit to the equilibrium a and continuation through the Hopf bifurcation of a. It exists in a parameter region that is bounded by curves t_Γ where $W^s(\Gamma)$ and $W^u(\Gamma)$ are tangent. The curves t_Γ can also be calculated (using the boundary value problem (3.4.38)–(3.4.40)) and are shown in Figure 3.12 (grey curves) as part of the bifurcation diagram in the (ν_1, ν_2)-plane. For decreasing ν_1, the tangency curves t_Γ end at a Shilnikov-Hopf bifurcation point of equilibrium a; see [HK93]. For increasing ν_1, the curves t_Γ can be continued until they connect with S_l (not shown).
As Figure 3.12 shows, we have found an accumulation phenomenon of a curve of connecting orbits, but this time of a curve of EtoP connection. Note that the curve c_b^* also enters the region between the tangency curves t_Γ and then appears to oscillate in between these two curves. Figure 3.13 shows the respective EtoP connections of successive maxima (w.r.t. ν_1) along the curve c_b^* as indicated in Figure 3.12(c). The EtoP connection departs from Γ, makes one excursion along the homoclinic orbit to Γ, stays near Γ again before finally connecting to b. From maximum to maximum of c_b^*, the corresponding EtoP connection from the periodic orbit Γ to b makes one more turn around Γ after the excursion along the homoclinic orbit; this is best seen in the time traces in the right column of Figure 3.13. (Note that the number of turns near Γ before the excursions is due to the projection boundary condition; it is not related to the accumulation process.) The EtoP connection accumulates in the limit on the concatenation of the (different) EtoP connection along c_b and a homoclinic orbit of Γ. This limiting global object is shown in Figure 3.14; it corresponds to the intersection point $(\nu_1, \nu_2) = (0.726851, -1.48784)$ of c_b and the upper curve t_Γ. Figure 3.14(a) shows the complete object in (u, v, w)-space, which consists of the homoclinic part from Γ back to Γ (grey curve) and the EtoP connection from Γ to b (black curve) in (u, v, w)-space. The computed codimension-one and codimension-zero connections and their time traces are shown in rows (b) and (c), respectively.
Overall, Figure 3.12 to Figure 3.14 show a new example of the accumulation of a curve of global bifurcations in parameter space. We emphasize that no analytical results exist for this case. The main ingredient is again the fact that the connecting orbit increasingly 'loops around' a periodic orbit of saddle-type, which gives rise to a concatenation of a codimension-one connection with a codimension-zero connection in the limit. We conjecture that this

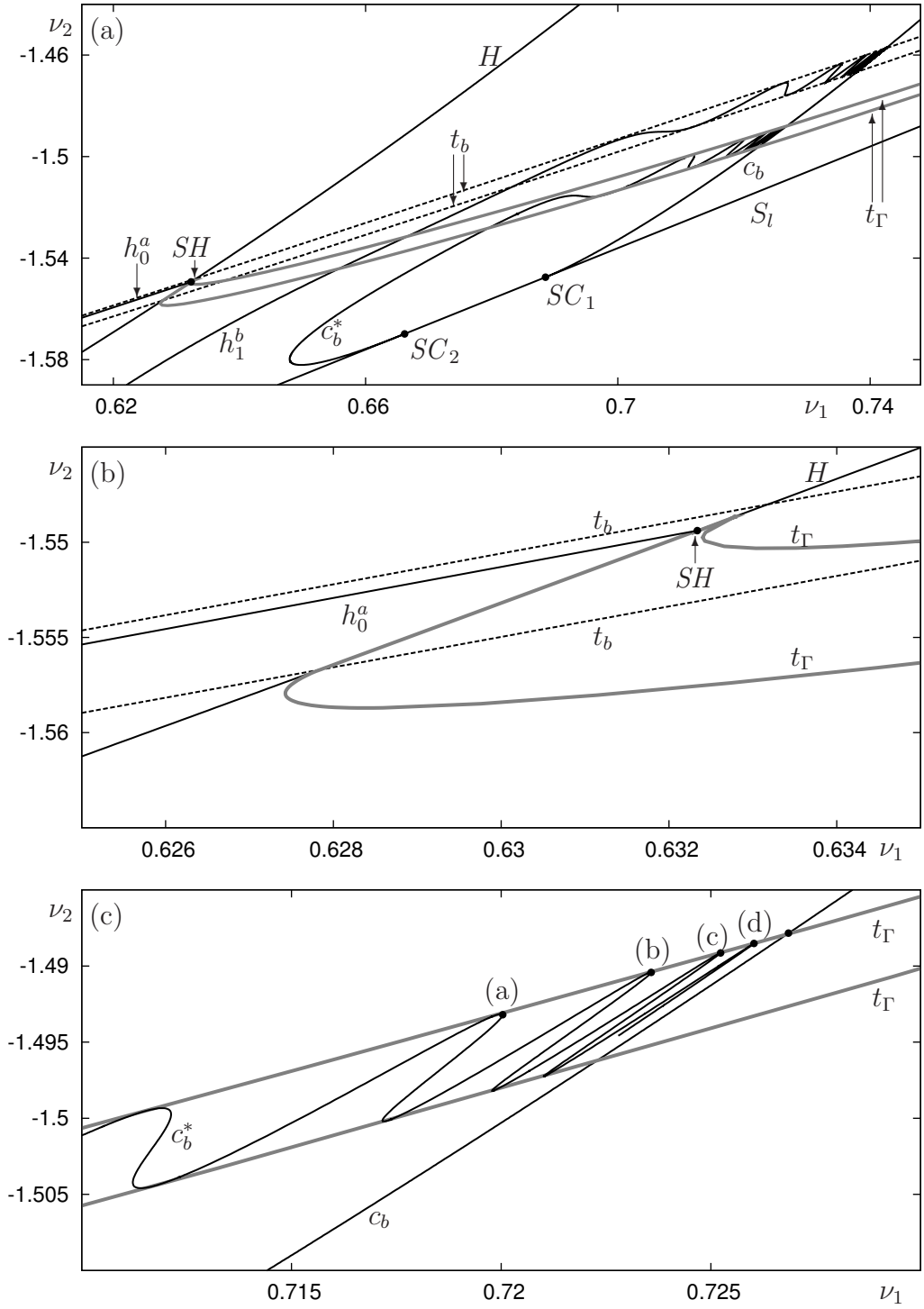

Figure 3.12: The bifurcation diagram of (3.5.2) from Figure 3.9 completed by the curves c_b^* of codimension-one EtoP connections from b to Γ, and the curves t_Γ of tangency bifurcations of the codimension-zero homoclinic connection to Γ. Panel (a) is an overview, panel (b) is an enlargement of the area around the point *SH* where the homoclinic connection to Γ is born, and panel (c) shows an enlargement near the accumulation of c_b^* onto c_b. The orbits at labels (a)–(d) in panel (c) are shown in Figure 3.13. The orbits at the indicated intersection point of c_b and t_Γ are shown in Figure 3.14.

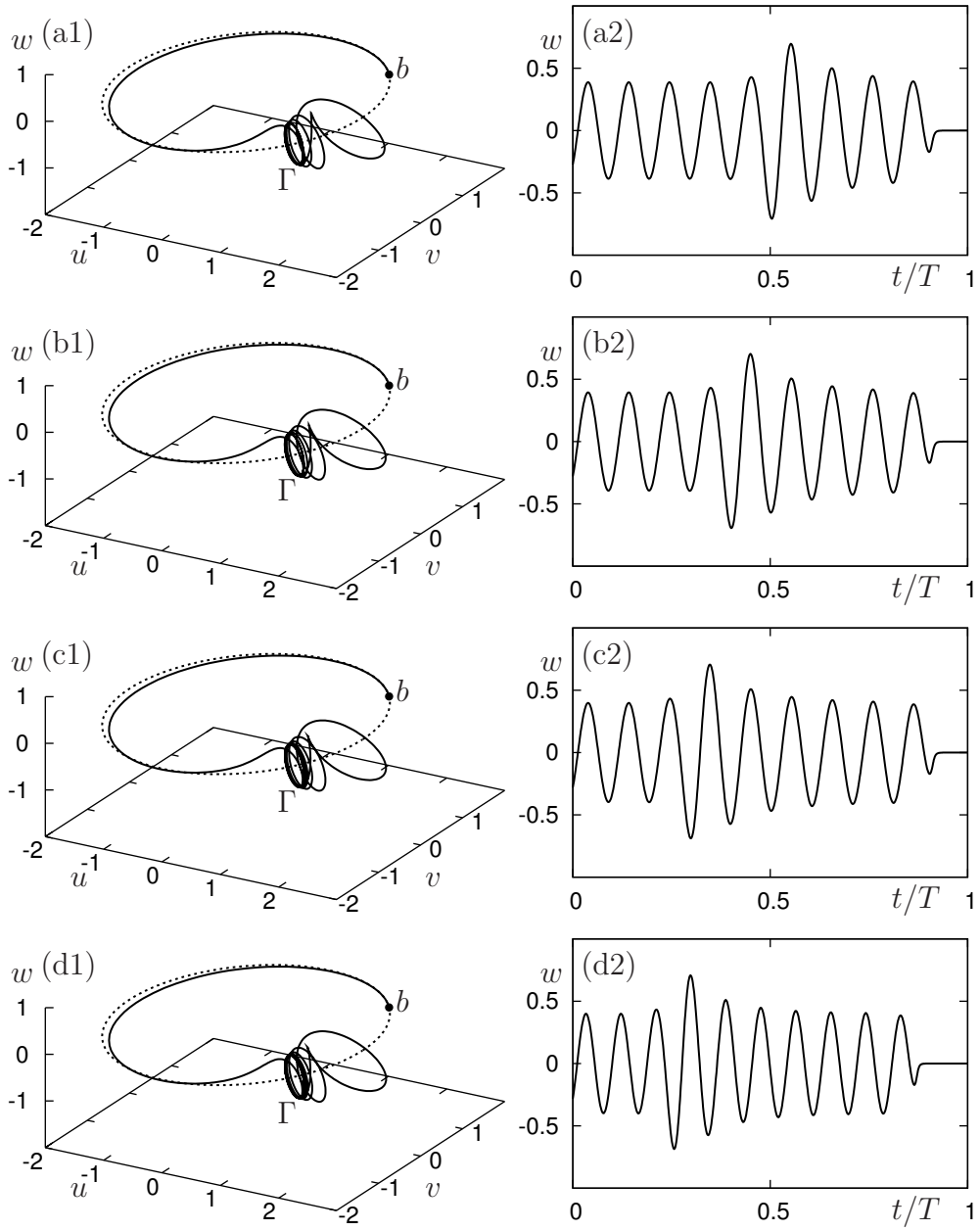

Figure 3.13: The EtoP connection from Γ to b of (3.5.2) for selected points along the curve c_b^* as indicated in Figure 3.12(c). Shown are the orbits in (u, v, w)-space (left column) and the time plot of the approximating orbit segment (right column) for $(\nu_1, \nu_2) = (0.720036, -1.49320)$ (a), $(\nu_1, \nu_2) = (0.723578, -1.49042)$ (b), $(\nu_1, \nu_2) = (0.725231, -1.48914)$ (c) and $(\nu_1, \nu_2) = (0.726028, -1.48852)$ (d). The orbits stay near Γ (the number of turns here is due to the projection boundary conditions and not related to the accumulation process) before taking one excursion along the homoclinic orbit to Γ, then stay near Γ again, where the number of turns increases by one for each consecutive oscillation of c_b^*, before finally connecting to b.

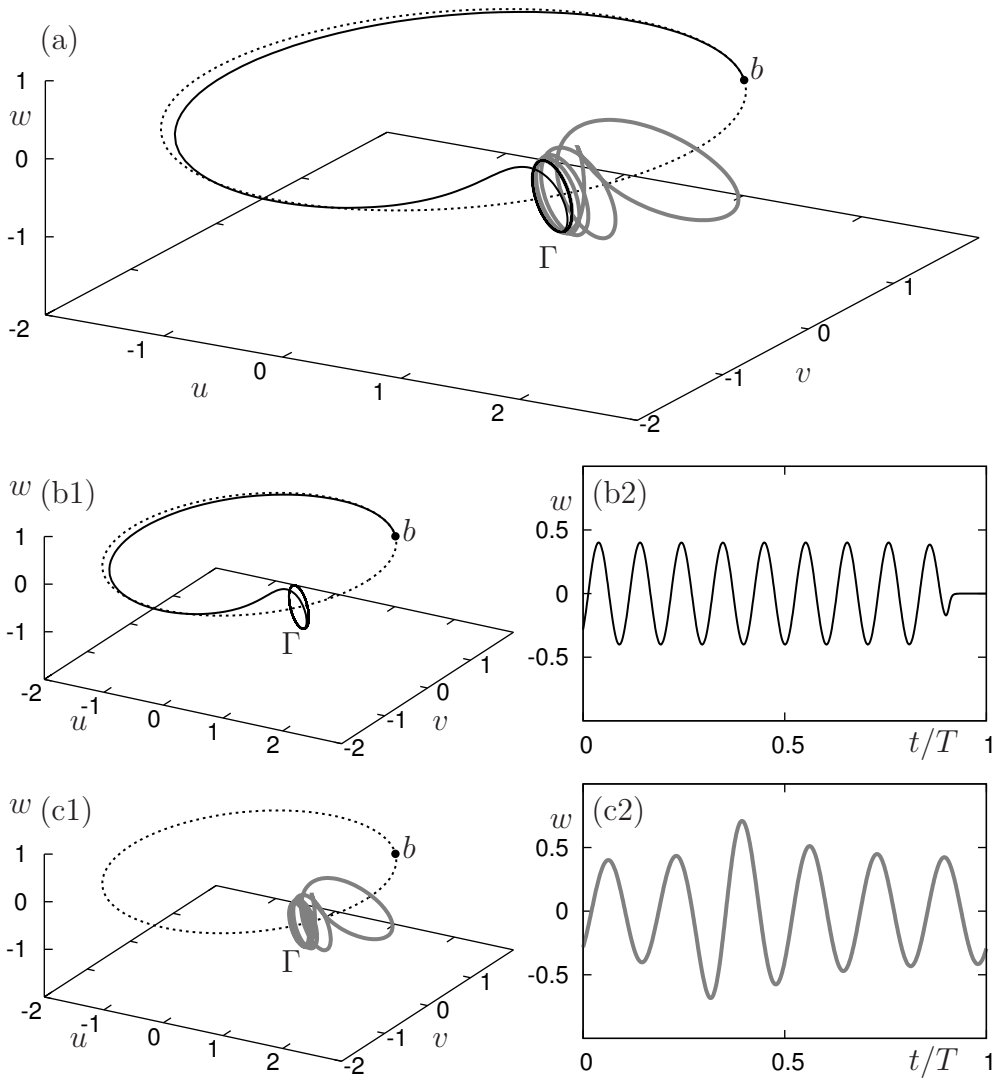

Figure 3.14: The EtoP connection and the homoclinic orbit to Γ (grey line) of (3.5.2) on c_b for $(\nu_1, \nu_2) = (0.726851, -1.48784)$ (a). Panels (b1) and (b2) show the codimension-one EtoP connection and its w-time plot, and panels (c1) and (c2) the codimension-zero homoclinic connection to Γ and its w-time plot.

general mechanism underlies the accumulation phenomenon of connecting orbits for vector fields in $\mathbb{R}^3$.

3.5.3 Codimension-two EtoP connection in a coupled Duffing system

Our method also works in the quite challenging situation when one wants to detect and subsequently continue an EtoP connection of higher codimension. This means that the Lin space is more than one-dimensional. As an example we consider here a codimension-two EtoP connection in a four-dimensional coupled Duffing system. This system was derived in [LX03] as a system with Shilnikov-type homoclinic orbits; it is given as the vector field

$$\begin{cases} \dot{x}_1 &= x_2, \\ \dot{x}_2 &= (a+y_2)x_1 - x_1^3 + \varepsilon(\alpha+\beta y_1)x_2, \\ \dot{y}_1 &= y_2 - \frac{x_1^2}{2}, \\ \dot{y}_2 &= \varepsilon(-y_1 + \gamma y_2 + \lambda y_1^2 y_2). \end{cases} \tag{3.5.4}$$

In [LX03] it was shown that (3.5.4) has Shilnikov-type homoclinic orbits to the origin $\mathbf{0}$ for $\lambda = -4\gamma$ and $2a\alpha + (2a\beta+3)(1-\sqrt{a}) = 0$, $0 < a < 1$, $\gamma > 0$. Therefore we also expect to find EtoP connections in this system. We fix $a = 0.0461071$, $\gamma = 2.63680$ and $\lambda = -27.6186$ and consider ε, α and β as continuation parameters. Specifically, we start the first step of our method from

$$\varepsilon = 0.0881558,\ \beta = 15.0,\ \alpha = -5.17613.$$

The eigenvalues of the Jacobian at $\mathbf{0}$ are given by

$$\frac{1}{2}\alpha\varepsilon \pm \sqrt{\frac{1}{4}\alpha^2\varepsilon^2 + a} \quad \text{and} \quad \frac{1}{2}\varepsilon\gamma \pm \sqrt{\frac{1}{4}\varepsilon^2\gamma^2 - \varepsilon}.$$

Throughout the parameter region we are considering, $\mathbf{0}$ has one negative eigenvalue and three eigenvalues with positive real part. Hence, $W^s(\mathbf{0})$ is of dimension one. Moreover, there is a saddle-type periodic orbit Γ, which can be found by continuation from a Hopf bifurcation of one of the secondary equilibria of (3.5.4). In the parameter region of interest Γ has two stable Floquet multipliers and one unstable Floquet multiplier. Hence, $W^u(\Gamma)$ is of dimension two. We are seeking here the codimension-two EtoP connection from Γ to $\mathbf{0}$ that exists when $W^s(\mathbf{0}) \subset W^u(\Gamma)$. Since the connection is from Γ to b, time needs to be reversed when formulating the respective boundary value problems from Section 3.4. We remark that the unstable Floquet multiplier of Γ is actually negative, which means that $W^u(\Gamma)$ is non-orientable.
One end point of the orbit segment u^+ starting from near $\mathbf{0}$ lies in $E^s(\mathbf{0})$. We choose a mesh point $g \in \Gamma$, namely the point

$$g = \begin{pmatrix} x_1 \\ x_2 \\ y_1 \\ y_2 \end{pmatrix} = \begin{pmatrix} 0.0969620 \\ -0.00183236 \\ -0.228516 \\ 0.0000130318 \end{pmatrix}.$$

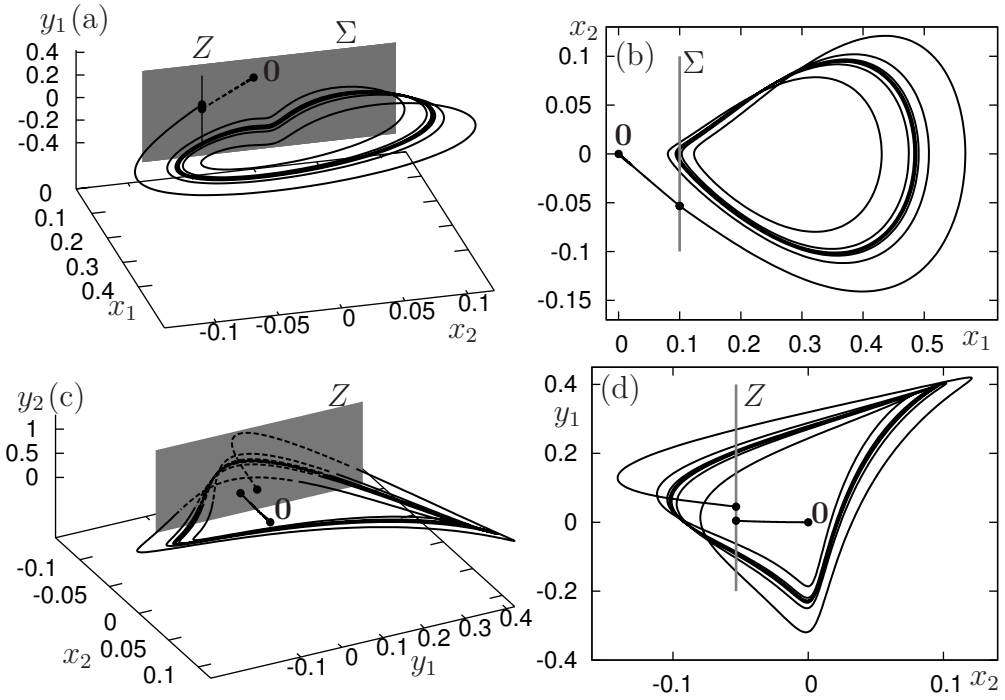

Figure 3.15: The orbit segments from Γ to Σ and from Σ to $\mathbf{0}$ of (3.5.4) for $\varepsilon = 0.0881558$, $\beta = 15.0$ and $\alpha = -5.17613$, shown in projection onto (x_1, x_2, y_1)-space (a) and onto the (x_1, x_2)-plane (b). The end points of both orbit segments in Σ actually lie in the two-dimensional Lin plane Z, as is shown in projection onto (x_1, x_2, y_2)-space (c) and onto the (x_2, x_1)-plane (d).

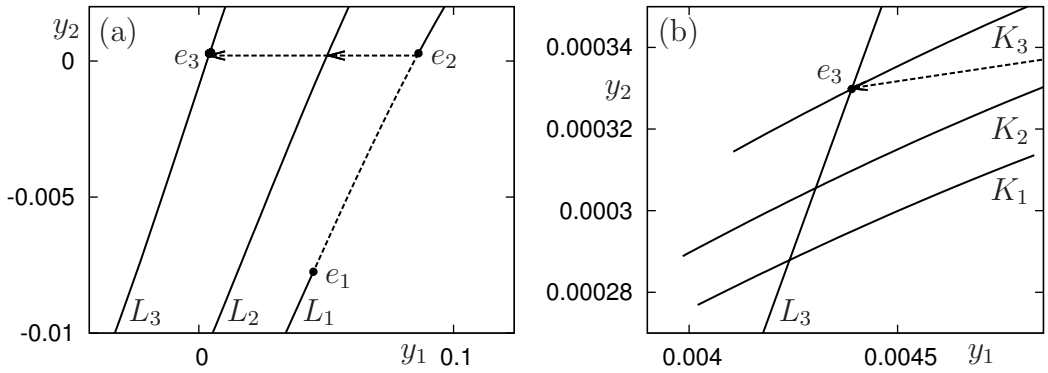

Figure 3.16: The curves L_i and K_i are traced out in the Lin plane Z by the end points of orbit segments during continuation in the gap sizes η_1, η_2 and the system parameter ε. Namely the L_i are traced out by the orbit segment u^- from Γ to Σ, and the K_i by the orbit segment u^+ from Σ to $\mathbf{0}$; here L_1 and K_1 are for $\alpha = \alpha_1 = -5.17613$, L_2 and K_2 are for $\alpha = \alpha_2 = -4.86955$, and L_3 and K_3 are for $\alpha = \alpha_3 = -4.5$. The enlargement in panel (b) indicates that the K_i change only very little with the system parameters. To close the gap we start from e_1 and follow L_1 until $\eta_1 = 0$ at e_2. Then we continue in η_2 and the system parameters ε and α until $\eta_2 = 0$, which happens at the point $L_3 \cap K_3 = e_3$.

One end point of the orbit segment u^- starting near Γ is then chosen to lie at distance δ from g on the corresponding Floquet vector v at g. Integration by continuation as described in Section 3.4.2 can be used to extend the orbit segments u^+ and u^- so that their other end points lie in the fixed section

$$\Sigma := \{x_1 = 0.1\}.$$

Figure 3.15 shows different projections of the orbit segments u^+ from Σ to $\mathbf{0}$ and u^- from Γ to Σ. Note that Σ is three-dimensional but, due to the chosen projections, it appears as a plane and as a line in Figure 3.15(a) and (b), respectively. For computational convenience and for the sake of clear illustrations we choose the two-dimensional Lin space Z parallel to the (y_1, y_2)-plane. Figure 3.15(c) and (d) are two different projections that show Z as a plane and as a line. Note that the distance δ along the Floquet vector v has been chosen such that the difference $u^+(0) - u^-(1)$ already lies in the Lin space Z; cf. Section 3.4.3.
Given the choice of Z it is natural to measure the Lin gaps η_1 and η_2 along the y_1 and y_2 coordinate directions, respectively. The initial gap sizes are $\eta_1 = -0.0405882$ and $\eta_2 = 0.00803835$. In order to close the two gaps, we first continue in η_1, η_2 and the system parameter ε; cf. Section 3.4.4, (3.4.20)–(3.4.33). The end points of the orbit segments inside Z that are computed during the continuation are depicted in Figure 3.16. Namely, the end points of the orbit segments u^- from Γ to Σ trace out the curve L_1 shown in Figure 3.16(a). At the same time, the end points of the orbit segment u^+ from Σ to $\mathbf{0}$ trace out a curve K_1. In fact, the point u^+ hardly changes and the curve K_1 is visible only in the enlarged

Figure 3.16(b). The curves L_1 and K_1 (which are parametrised by the system parameter ε) are for $\alpha = \alpha_1 = -5.17613$. Also shown in Figure 3.16 are the curves L_2, L_3, K_2 and K_3 for $\alpha = \alpha_2 = -4.86955$ and for $\alpha = \alpha_3 = -4.5$, respectively. The curves L_i and K_i, $i = 1, 2, 3$, show that the Lin plane Z is locally given by two one-parameter families of unique one-dimensional curves that intersect transversely. In other words, the gap can be closed in a systematic way. Namely, we first continue in η_1, η_2 and ε starting at the point e_1 along L_1 until a $\eta_2 = 0$ is detected; see the point e_2 in Figure 3.16(a). We then fix $\eta_2 = 0$ and change to a continuation in η_1, ε and α. The continuation traces out the (almost) horizontal dashed line in Figure 3.16(a) and stops when a zero of η_1 is detected, which happens for $\varepsilon = 0.1$ and $\alpha = -4.5$. In the enlargement Figure 3.16(b) this occurs at the intersection of L_3 and K_3, denoted by e_3.
Once both Lin gaps have been closed, that is, $\eta_1 = \eta_2 = 0$, we have found a codimension-two EtoP connection from Γ to $\mathbf{0}$. The connecting orbits can now be continued in the three system parameters ε, β and α. Figure 3.17(a) and (b) shows the resulting curve h of connecting orbits in $(\varepsilon, \alpha, \beta)$-space and in projection onto the (ε, β)-plane, respectively. We remark that the curve h does not self-intersect, even though one may get this impression due to the projection. Five points along h are labelled and the respective connecting orbits are shown in Figure 3.17(c)–(g) in (x_1, x_2, y_1)-space and as a time series of the norm. Notice how the connecting orbit changes along the curve h. In Figure 3.17(c) the connection follows Γ closely and then quickly connects to $\mathbf{0}$. This gradually changes and the connecting orbit makes a closer and closer pass near $\mathbf{0}$ and then makes another large excursion before it connects to $\mathbf{0}$; see Figure 3.17(f) and (g). We remark that the curve h could not be computed beyond what is shown in Figure 3.17(a) and (b). It appears that this is due to the connecting orbit passing very close to $\mathbf{0}$ at an intermediate point. In the limit, it seems that the connection becomes a concatenation of a new codimension-two connection from Γ to $\mathbf{0}$ and a codimension-one homoclinic orbit from $\mathbf{0}$ back to itself. A more detailed study of the global bifurcations of (3.5.4) is beyond the scope of this thesis, but we remark that a similar phenomenon has been found for codimension-zero EtoP connections in the Lorenz system [DKO06].

3.6 Finding PtoP connections

It is quite straightforward to generalise our approach for finding EtoP connections to the case of codimension-d PtoP connections from one periodic orbit Γ_1 to another periodic orbit Γ_2. Suppose that $\dim(W^u(\Gamma_1)) = k \geq 2$, $\dim(W^s(\Gamma_2)) = l \geq 2$, and that these manifolds intersect in an isolated orbit that is generic (in the sense of (C4) from Section 3.3). We consider two orbit segments u^- from Γ_1 to a suitable section Σ, and u^- from Σ to Γ_2 subject

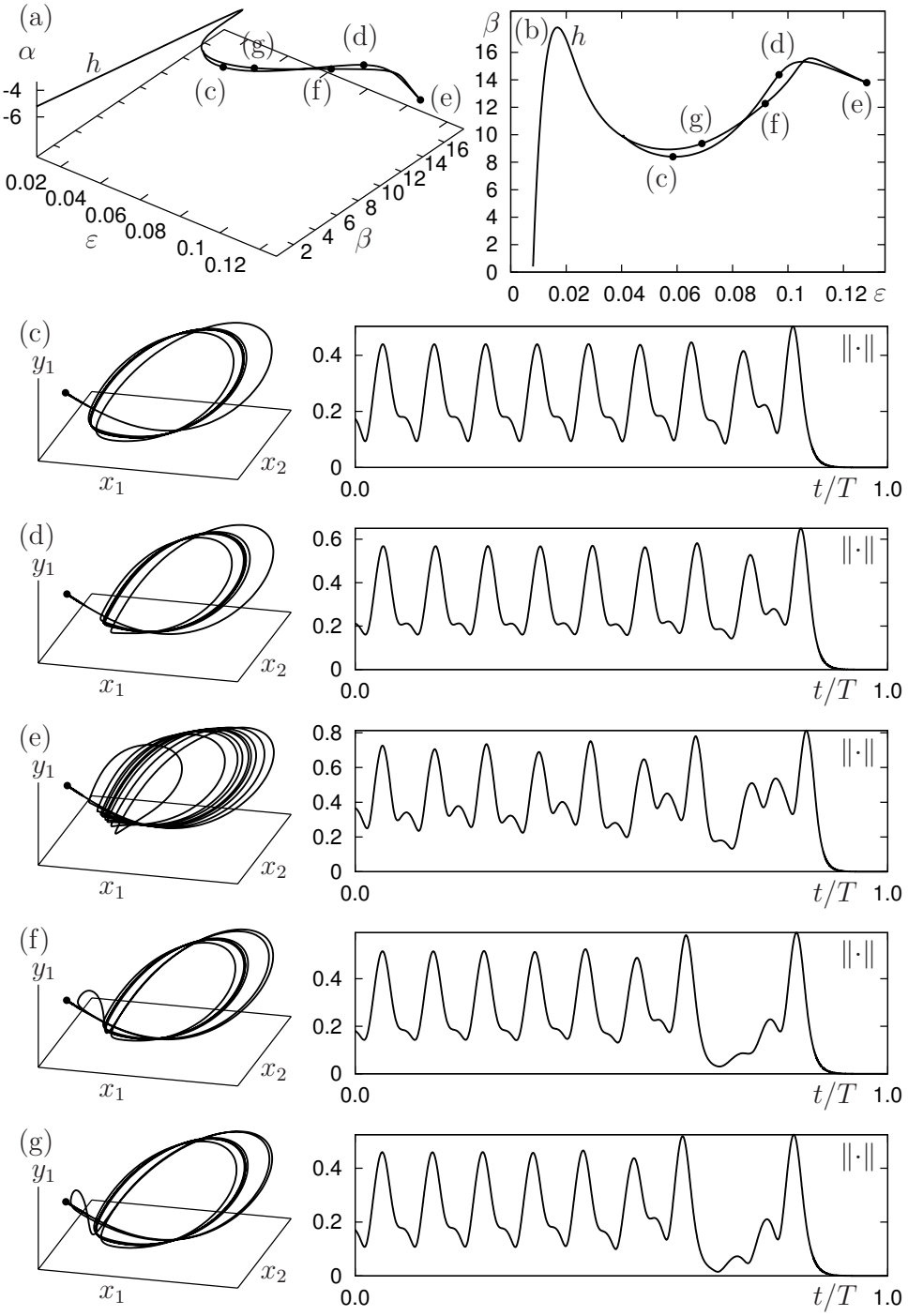

Figure 3.17: The curve h of codimension-two EtoP connections of (3.5.4) shown in $(\varepsilon, \alpha, \beta)$-space (a) and in projection onto the (ε, β)-plane (b). (c)–(g) show selected orbits, as indicated along h, in (x_1, x_2, y_1)-space and as time series of the norm; from (c) to (g) $(\varepsilon, \alpha, \beta)$ has the values $(0.0584877, -3.51797, 8.40132)$, $(0.0967731, -4.25440, 14.3715)$, $(0.128392, -4.59897, 13.7927)$, $(0.0918179, -3.71152, 12.2683)$ and $(0.0689425, -3.46446, 9.36032)$.

to the boundary conditions

$$u^-(0) = u^1_\gamma(0) + \sum_{i=1}^{k-1} \varepsilon_i u^1_i(0), \tag{3.6.1}$$

$$u^+(1) = u^2_\gamma(0) + \sum_{i=1}^{l-1} \delta_i u^2_i(0), \tag{3.6.2}$$

$$\left\langle u^-(1) - p_\Sigma, n_\Sigma \right\rangle = 0, \tag{3.6.3}$$

$$(u^+(0) - u^-(1)) = \sum_{i=1}^{d} \eta_i(\lambda) z_i, \tag{3.6.4}$$

where the vectors z_i are again a basis of a suitably chosen d-dimensional Lin space; the numerical representations of Γ_1 and Γ_2 are denoted by u^1_γ and u^2_γ, respectively, the representations of the associated unstable and stable eigenfunctions are denoted by u^1_i and u^2_i.
The geometry of a PtoP connection is very similar to that of an EtoP connection, and we strongly believe that the equivalent statement of theorem 2.2.1 can be proved for PtoP connections. While technical details need to be checked to prove this conjecture, it appears quite clear that the two orbit segments are uniquely determined by choosing a d-dimensional Lin space. In other words, the general setup given by (3.6.1)–(3.6.4), in combination with the continuation of u^1_γ with its unstable eigenspace u^1_i and of u^2_γ with its stable eigenspace u^2_i, constitutes a well-defined boundary value problem. In particular, closing the test functions $\eta_i(\lambda)$ one by one provides a systematic way of finding a codimension-d PtoP connection.
We remark that it is not at all straighforward to find a numerical example of a codimension-d PtoP connection for $d \geq 1$. Even identifying a candidate vector field among models from applications is quite a task, as it requires finding two saddle periodic orbits with the correct dimensions of their stable and unstable manifolds. Therefore, we now discuss the problem of continuing a robust PtoP connection of codimension zero. In Section 3.5.1 and in Section 3.5.2 we have actually already seen two examples, namely for the case that the connection is a homoclinic orbit from a periodic orbit Γ back to itself. As was explained in Section 3.4.5, an initial homoclinic PtoP connection can be found from the concatenated data of an EtoP heteroclinic cycle consisting of a codimension-one and a codimension-zero EtoP connection. The homoclinic PtoP can then be continued imposing projection boundary conditions (3.4.39) and (3.4.40) at Γ at both ends of the connecting orbit segment u.
Consider now a codimension-zero PtoP connection between two different saddle periodic orbits Γ_1 and Γ_2 of periods T_1 and T_2, respectively. Indeed it is possible to approximate this PtoP connection also with a single orbit segment u subject to projection boundary conditions at both Γ_1 and Γ_2, which is the approach taken in [DR04b]. The problem is that for PtoP connections there is no simple way to construct an initial approximate connecting orbit segment. As an alternative we propose the following geometric approach. We assume that the codimension-zero PtoP connection is generic, which means that $l+k = n+1$, the Lin space is trivial, and $d = 0$ in (3.6.4). We fix the system parameter λ and, as for the general method above, perform step 1 of constructing the orbits segments u^- and u^+ by continuation in the integration time T, so that $u^-(1) \in \Sigma$ and $u^+(0) \in \Sigma$. This means that u^- and u^+

satisfy (3.6.1)–(3.6.3), but not (3.6.4) since $u^+(0) - u^-(1) \neq 0$. Recall that the Lin space is trivial, so that the difference $u^+(0) - u^-(1)$ can be chosen to be zero without changing the system parameter λ. To achieve this, we set $z_0 := (u^+(0) - u^-(1))/\|u^+(0) - u^-(1)\|$ and define the one-dimensional subspace $Z_0 := \text{span}\{z_0\}$. Replacing condition (3.6.4) by

$$(u^+(0) - u^-(1)) \;=\; \eta\, z_0 \tag{3.6.5}$$

ensures that the difference $u^+(0) - u^-(1)$ remains restricted to Z_0. As a result, the overall boundary problem given by (3.6.1)–(3.6.3), (3.6.5), together with the respective formulations for Γ_1 with its unstable eigenspace and of Γ_2 with its stable eigenspace, is well-posed, meaning that T_1, T_2, ε_i, δ_j, and η are uniquely defined. Hence, $\eta = \eta(T_1, T_2, \varepsilon_i, \delta_j)$ is a well-defined test function, so that a continuation run in the direction of decreasing η allows us to find the codimension-zero PtoP connection as a zero of η.

3.6.1 Codimension-zero PtoP connection in a four-dimensional vector field

As an example of a system with a codimension-zero PtoP connection we consider the four-dimensional system considered in [DR04b]. It is given by

$$\left\{\begin{array}{rcl} \dot{x} &=& (1-w)y + wx\,(1-x^2)\,, \\ \dot{y} &=& (1-w)\,(-x + \lambda(1-x^2)y) + w\,(z-3-\lambda)\,, \\ \dot{z} &=& (1-w)z\,(z^2 - (4+\lambda)^2) \\ && +w\,(-y+3+\lambda+\lambda\,(1-(y-3-\lambda)^2)\,(z-3-\lambda))\,, \\ \dot{w} &=& w(1-w), \end{array}\right. \tag{3.6.6}$$

where the parameter λ is set to $\lambda = 0.5$. System (3.6.6) can be interpreted as a homotopy from $w = 0$ to $w = 1$ between two planar systems in the (x, y)-plane and in the (y, z)-plane, respectively. In each of the two planes the system resembles a Van der Pol oscillator with an attracting periodic orbit. We denote the periodic orbit in the (x, y)-plane by Γ_1 and the one in the (y, z)-plane by Γ_2. Since $\dim W^u(\Gamma_1) = 2$ and $\dim W^s(\Gamma_2) = 3$ one expects a codimension-zero PtoP connection from Γ_1 to Γ_2. In [DR04b] this PtoP connection was found with difficulties by using a shooting technique and then continued in λ.
We choose the cross-section to be $\Sigma = \{w = 0.5\}$ which clearly separates the two periodic orbits. As base points on Γ_1 and Γ_2 we use

$$g_1 = \begin{pmatrix} 0.0 \\ 5.28342 \\ 4.60521 \\ 1.0 \end{pmatrix}, \quad g_2 = \begin{pmatrix} -0.0131541 \\ 2.03745 \\ 0.0 \\ 0.0 \end{pmatrix}.$$

Furthermore, we compute the (fixed) Floquet vectors at these points for the definition of the projection boundary conditions (3.6.1) and (3.6.2). After computing the orbit segments u^- and u^+ up to Σ, we construct the one-dimensional space Z_0 from $u^+(0) - u^-(1)$ and find that the distance η in (3.6.5) is $\eta = 3.76668$; see Figure 3.18(a). Continuation of the overall boundary value problem in T_1, T_2, ε_1, δ_1, δ_2 and η then detects the codimension-zero PtoP connection shown in Figure 3.18(b) as a zero of η.

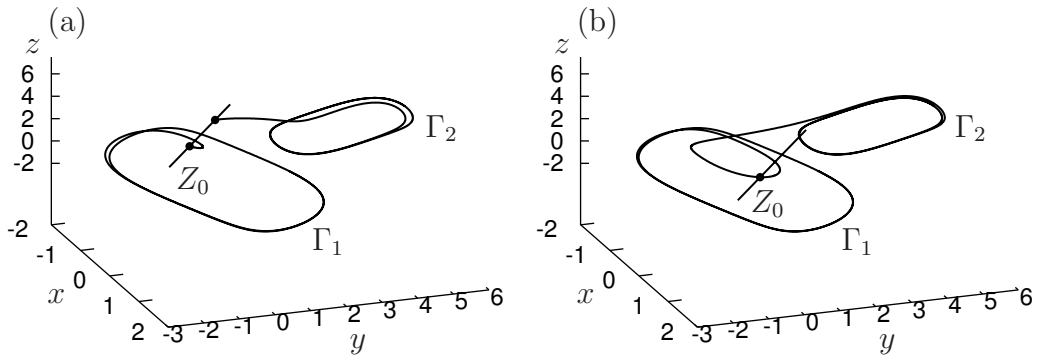

Figure 3.18: Orbit segments $u^- \subset W^u(\Gamma_1)$ and $u^+ \subset W^s(\Gamma_2)$ up to the section $\Sigma = \{w = 0.5\}$ of (3.6.6) for $\lambda = 0.5$. Their end points $u^-(1), u^+(0) \in \Sigma$ are restricted to lie in the direction Z_0. The gap η is initially nonzero (a) and is then closed by a continuation run to reveal a codimension-zero PtoP connection (b). Note that only Z_0 of the section Σ appears in the panels due to the chosen projection.

CHAPTER 4

Discussion and conclusions

This thesis provides a contribution to the bifurcation analysis of heteroclinic EtoP connections. We first present theoretical considerations that extend the well-known Lin's method to EtoP cycles. To do this extension, we use a hybrid system that consists of a continuous dynamical system and a discrete dynamical system, which is given by the Poincaré map and describes the dynamics near the periodic orbit. Then we prove that there are unique solutions of these two systems that satisfy specific projection boundary conditions within the Poincaré section. Using these solutions we show that for given transition times there is a unique Lin orbit that stays close to the EtoP cycle for all times and has discontinuities only in prescribed directions.

The derived estimates for the size of the jumps (discontinuities) of the Lin orbit are then used to discuss bifurcation equations for several types of orbits. In particular, bifurcating homoclinic orbits to the equilibrium and homoclinic orbits to the periodic orbit are considered. We find that the results about the existence of such orbits are in agreement with geometrical considerations as well as with numerical results as presented in this thesis.

However, we restrict our considerations to bifurcation equations of homoclinic orbits (to either p or Υ). We emphasize that the results of the jump estimates allow to formulate bifurcation equations for any kind of orbit that stays near the EtoP cycle for all times. For example, it is possible to consider N-homoclinic orbits, periodic orbits or even orbits that are neither homoclinic nor periodic. A complete discussion of these orbits is non-trivial and beyond the scope of this thesis, but certainly worth to consider in the future. Namely, as done for example in [KLW07] for the T-point situation, we expect to find infinitely many periodic orbits that stay near the EtoP cycle. Then it is possible to select two of these periodic solutions and construct a solution that follows either one of the periodic solutions, determined by a prescribed sequence of two symbols. We expect the dynamics to be conjugated to a shift on the sequence of two symbols which is a well-known example for chaotic dynamics.

Another challenge for future research is a complete understanding of the snaking behaviour of certain homoclinic orbits to the equilibrium near the EtoP cycle. The results in [BKL$^+$08] suggest that it is possible to explain the snaking in more detail than we discuss here.

Finally, we present a method based on the previous theoretical considerations that allows to find a generic codimension-d EtoP connection from a saddle equilibrium to a saddle periodic orbit. The key idea is to set up an overall boundary value problem that defines two separate orbit segments up to a specified cross-section, whose end points lie in a well-defined d-dimensional space. The two orbit segments exist in an entire region of parameter space (and not just at the heteroclinic connection), so that they give rise to d smooth test functions, known as the Lin gaps. Closing the Lin gaps in consecutive continuation runs allows to find codimension-d EtoP connections in a systematic way. The EtoP connection and related global objects, such as homoclinic orbits of the periodic orbit, then can be continued in system parameters. With three examplary vector fields we demonstrate how our method of finding EtoP connections can be used to investigate quite complicated bifurcation phenomena.
The study of EtoP connections in other vector field models from applications is an obvious direction for future research; interesting candidates are laser models [WK05], models from cell dynamics [CKK$^+$07], or models for voltage collapse in power systems [AWA$^+$93].
We also present a general setup for finding codimension-d PtoP connections. While the underlying statement of Lin's method has not been proven, geometrical arguments strongly suggest that the respective Lin gaps are regular test functions. Furthermore, with the example of a vector field in $\mathbb{R}^4$, we show how a generic codimension-zero PtoP connection can be found in practice. The demonstration of the method for codimension-d PtoP connections for $d > 0$ remains a challenge for the future, not in the least due to the difficulty of finding vector fields with PtoP connections.

APPENDIX A

Appendix

A.1 Exponential dichotomies and trichotomies

In this section we introduce the concept of exponential dichotomies and exponential trichotomies for linear non-autonomous continuous or discrete systems. The exponential dichotomies and trichotomies are important properties of variational equations along special solutions (for example connecting orbits) in dynamical systems. They provide many useful estimates that are exploited in some of the proofs in Chapter 2. Here we only present the important results that are used throughout the thesis, we refer to the literature (for example [Cop78, HL86, Pal00]) for the proofs and for more (detailed) information about exponential dichotomies/trichotomies.

A.1.1 Continuous systems

Here we give the definitions and some properties of exponential dichtomies and exponential trichotomies for continuous systems.
We consider a linear homogeneous system

$$\dot{x} = A(t)x, \quad x \in \mathbb{R}^n, \quad A(\cdot) \in C(I, \mathbb{R}^{n\times n}) \tag{A.1.1}$$

for an interval $I \subset \mathbb{R}$ and we denote the transition matrix of this system by $\Phi(\cdot,\cdot)$.
First we give a definition of an exponential dichotomy on an interval I (typically $I = \mathbb{R}^+$, $I = \mathbb{R}^-$ or $I = \mathbb{R}$).

Definition A.1.1 *The system* (A.1.1) *has an* exponential dichotomy on I *if there are projections* P *and* $(\mathrm{id} - P)$ *on* $\mathbb{R}^n$ *such that*

$$\begin{aligned} \Phi(t,\tau)P(\tau) &= P(t)\Phi(t,\tau), \\ \Phi(t,\tau)(\mathrm{id}-P)(\tau) &= (\mathrm{id}-P)(t)\Phi(t,\tau), \quad \forall t,\tau \in I, \end{aligned} \tag{A.1.2}$$

and there are constants $K, \delta^s, \delta^u > 0$ *such that the following estimates hold:*

$$\begin{aligned} \|\Phi(t,\tau)P(\tau)\| &\leq Ke^{-\delta^s(t-\tau)}, \quad t \geq \tau, \\ \|\Phi(t,\tau)(\mathrm{id} - P(\tau))\| &\leq Ke^{-\delta^u(\tau-t)}, \quad \tau \geq t. \end{aligned} \tag{A.1.3}$$

For more information about exponential dichotomies in continuous systems, see [Cop78], [LL00] or [Pal00]. The concept of an exponential dichotomy can be seen as a replacement for the concept of invariant stable or unstable manifolds for non-autonomous linear systems. An important property of exponential dichotomies is the so-called roughness property; that means that if a system has an exponential dichotomy, also (small) perturbations have an exponential dichotomy, and the projections and constants are close to the corresponding projections and constants of the unperturbed system. We again refer to [Pal00] for roughness theorems for dichotomies, see also Theorem A.1.3 below.
The main application of exponential dichotomies in this thesis are variational equations along orbits in the stable or unstable manifold of a hyperbolic equilibrium. Let μ^s and μ^u denote the (simple) leading stable and unstable eigenvalue, then the linearised equation at the equilibrium has an exponential dichotomy with exponents $\mathrm{Re}\mu^s < \delta^s < 0 < \delta^u < \mathrm{Re}\mu^u$. The roughness property provides that also the variational equation along an orbit in the stable (or unstable) manifold has an exponential dichotomy, the exponents can be chosen arbitrarily close to the exponents of the unperturbed system. In particular, we find that $\mathrm{Re}\mu^s < -\delta^s = \bar{\mu}^s < 0 < \delta^u = \bar{\mu}^u < \mathrm{Re}\mu^u$ is possible, cf. Hypothesis (H 2.1) and Hypothesis (H 2.2). Moreover, the images of the projections P and $(\mathrm{id} - P)$ are the tangent spaces of the respective stable and unstable manifolds at the respective point on the orbit under consideration, see [Kla06].
In this thesis we also deal with variational equations along orbits that are in the stable (unstable) manifold of a hyperbolic periodic orbit. These variational equations have a so-called exponential trichotomy as defined below.

Definition A.1.2 *The system* (A.1.1) *has an* exponential trichotomy on I *if there are projections* Q_s, Q_u *and* $Q_c = \mathrm{id} - Q_s - Q_u$ *on* $\mathbb{R}^n$ *such that*

$$\Phi(t,\tau)Q_{s/c/u}(\tau) = Q_{s/c/u}(t)\Phi(t,\tau), \quad \forall t, \tau \in I, \tag{A.1.4}$$

and there are constants $K > 0$ *and* $\bar{\delta}^s, \bar{\delta}^u > \bar{\delta}^c \geq 0$ *such that the following estimates hold:*

$$\begin{aligned} \|\Phi(t,\tau)Q_s(\tau)\| &\leq Ke^{-\bar{\delta}^s(t-\tau)}, \quad t \geq \tau, \\ \|\Phi(t,\tau)Q_c(\tau)\| &\leq Ke^{\bar{\delta}^c(t-\tau)}, \quad t \geq \tau, \\ \|\Phi(t,\tau)Q_c(\tau)\| &\leq Ke^{-\bar{\delta}^c(t-\tau)}, \quad \tau \geq t, \\ \|\Phi(\tau,t)Q_u(t)\| &\leq Ke^{-\bar{\delta}^u(t-\tau)}, \quad t \geq \tau. \end{aligned} \tag{A.1.5}$$

We use the abbreviations $Q_{sc} = Q_s + Q_c$ *and* $Q_{cu} = Q_c + Q_u$.

One of the main features of exponential trichotomies is the roughness property:

Theorem A.1.3 *Let* (A.1.1) *have an exponential trichotomy on I with projections Q_s, Q_c and Q_u, constant $K > 0$ and exponents $\bar{\delta}^s$, $\bar{\delta}^c$ and $\bar{\delta}^u$ as in Definition* A.1.2. *Furthermore, let $B \in C(\mathbb{R}, \mathbb{R}^{n\times n})$ with $\|B(t)\| < Ce^{-\eta t}$ for some $0 < \eta < \min\{\bar{\delta}^s - \bar{\delta}^c, \bar{\delta}^u - \bar{\delta}^c\}$.*
Then the perturbed system

$$\dot{x} = [A(t) + B(t)]\, x$$

has an exponential trichotomy on I with exponents $\tilde{\delta}^s, \tilde{\delta}^u > \tilde{\delta}^c \geq 0$ and projections $\tilde{Q}_s$, $\tilde{Q}_c$, $\tilde{Q}_u$. The exponents $\tilde{\delta}^{s/c/u}$ can be chosen arbitrarily close to $\delta^{s/c/u}$. Moreover, if $\dim \mathrm{im} Q_c(t) = 1$ holds, then it is possible to choose $\tilde{\delta}^c = \delta^c$.
$\left\|\tilde{Q}_i(t) - Q_i\right\| \leq Ke^{-\eta t}$, *$i = s, c, u$ holds.*

This roughness theorem follows from general roughness theorems for shifted exponential dichotomies (i.e. generalized dichotomies where the exponents δ^s and δ^u may have different signs, see [HL86] and also [San93]), a proof can be found in [Bey94].
The main application of the exponential trichotomy is for variational equations along solutions in the stable (or unstable) manifold of a hyperbolic periodic orbit Υ. Let μ^s_Υ and μ^u_Υ denote the leading stable and unstable Floquet multipliers of the periodic orbit, then the variational equation along Υ has an exponential trichotomy with exponents $\bar{\delta}^s, \bar{\delta}^c$ and $\bar{\delta}^u$ such that $|\mu^s_\Upsilon| < e^{-\bar{\delta}^s} < e^{\bar{\delta}^c} = 1 < e^{\bar{\delta}^u} < \mu^u_\Upsilon$, see again [Bey94] for a proof that in this case $\bar{\delta}^c = 0$ is possible. A variational equation along an orbit in the stable or unstable manifold of Υ then has an exponential trichotomy as well, and the exponents can be chosen such that $|\mu^s_\Upsilon| < e^{-\bar{\delta}^s} < e^{\bar{\delta}^c} = 1 < e^{\bar{\delta}^u} < |\mu^u_\Upsilon|$ holds (see Theorem A.1.3), cf. Hypothesis (H 2.1) and Hypothesis (H 2.2). Moreover, the images of the projections Q_{cs} and Q_{cu} are the tangent spaces of the respective stable and unstable manifolds at the respective point on the orbit under consideration, see [Kla06] and [Rad04].

A.1.2 Discrete systems

The concept of exponential dichotomies for discrete dynamical systems is analogous to the above considerations of dichotomies of continuous systems. Nonetheless we give a seperate introduction to provide the notation that is used in Chapter 2.
We consider a discrete dynamical system in $\mathbb{R}^l$

$$y(n+1) = A(n)y(n), \quad y \in \mathbb{R}^l, \quad A(\cdot) \in \mathbb{R}^{l\times l}. \tag{A.1.6}$$

The transition matrix of (A.1.6) is denoted by $\Phi(\cdot,\cdot)$.

Definition A.1.4 *The system* (A.1.6) *has an* exponential dichotomy on $I \subset \mathbb{Z}$ *if there are projections R and* $(\mathrm{id} - R)$ *on $\mathbb{R}^l$ such that*

$$\begin{aligned} \Phi(n,m)R(m) &= R(n)\Phi(n,m), \\ \Phi(n,m)(\mathrm{id} - R)(m) &= (\mathrm{id} - R)(n)\Phi(n,m), \quad \forall n, m \in I, \end{aligned} \tag{A.1.7}$$

and there are constants $K, \hat{\delta}^s, \hat{\delta}^u > 0$ such that the following estimates hold:

$$\begin{aligned} \|\Phi(n,m)R(m)\| &\leq Ke^{-\hat{\delta}^s(n-m)}, \quad n \geq m, \\ \|\Phi(n,m)(\mathrm{id} - R)(m)\| &\leq Ke^{-\hat{\delta}^u(m-n)}, \quad m \geq n. \end{aligned} \tag{A.1.8}$$

Again, the exponential dichotomy has the roughness property and thus a theorem similar to Theorem A.1.3 applies.
The main application of exponential dichotomies in this thesis is for variational equations along solutions in the stable (or unstable) manifolds of hyperbolic equilibria. In accordance with the notation used throughout this thesis, let μ^s_Υ and μ^u_Υ denote the leading stable and unstable eigenvalues of the linearisation of the hyperbolic equilibrium. First we observe that the linearised equation at the equilibrium point has an exponential dichotomy, then the exponents $\hat{\delta}^s$ and $\hat{\delta}^u$ are such that $|\mu^s_\Upsilon| < e^{-\hat{\delta}^s} < 1$ and $1 < e^{\hat{\delta}^u} < |\mu^u_\Upsilon|$. The roughness property of the dichotomy then provides that a solution along an orbit in the stable (or unstable) manifold of the equilibrium also has an exponential dichotomy, the exponents can be chosen such that $|\mu^s_\Upsilon| < e^{-\hat{\delta}^s} = \bar{\mu}^s_\Upsilon < 1$ and $1 < e^{\hat{\delta}^u} = \bar{\mu}^u_\Upsilon < |\mu^u_\Upsilon|$ holds, cf. Hypothesis (H 2.1) and Hypothesis (H 2.2). Moreover, the images of the projections R^+ and R^- are the tangent spaces of the respective stable and unstable manifolds at the respective point on the orbit under consideration, see [Kla06].
For more information about exponential dichotomies for discrete systems, we refer to [Kno04], [Pal00] and references therein, in particular [Pal84] and [Pal88].

A.2 Consequences of Condition (C6)

We show that from (1.2.5) follows that $\dim(W^s(p) \cap W^u(\Upsilon)) = d$.

Lemma A.2.1 *Consider system* (1.2.1) *and assume that Conditions* (C1)–(C6) *hold. Then*

$$\dim(W^s(p) \cap W^u(\Upsilon)) = n - k - l + 1 =: d.$$

Proof. Let $g \in W^s(p) \cap W^u(\Upsilon)$. Then there is a function $F^s : \mathbb{R}^n \to \mathbb{R}^k$ with $\mathrm{rank} DF^s(g) = k$ such that, locally around g, $W^s(p)$ is given by

$$F^s(x) = 0.$$

Then $T_g W^s(p) = \ker DF^s(g)$.
Similarly, there is a function $F^u : \mathbb{R}^n \to \mathbb{R}^{l-1}$ with $\mathrm{rank} DF^u(g) = l - 1$ such that, locally around g, $W^u(\Upsilon)$ is given by

$$F^u(x) = 0.$$

Then $T_g W^u(\Upsilon) = \ker DF^u(g)$.
The intersection $W^s(p) \cap W^u(\Upsilon)$ is then given by

$$F(x) := (F^s(x), F^u(x)) = 0, \quad F : \mathbb{R}^n \to \mathbb{R}^k \times \mathbb{R}^{l-1} \cong R^{k+l-1}.$$

$DF(g) = (DF^s(g), DF^u(g))$ holds and hence

$$\ker DF(g) = \ker DF^s(g) \cap DF^u(g).$$

Due to Condition (C6) $\dim\ker DF(g) = d = n-(k+l-1)$ and thus $\dim\mathrm{im}DF(g) = n-d = k+l-1$ (note that $DF(g) \cong \mathbb{R}^n/\ker DF(g)$). Therefore $\mathrm{rank}DF(g) = k+l-1$ and $F(x) = 0$ can be solved near g by means of the Implicite Function Theorem for

$$(x_1, \cdots, x_{k+l-1}) = (x_1, \cdots, x_{k+l-1})(x_{k+l}, \cdots, x_n)$$

(up to renumeration). Hence $\dim W^s(p) \cap W^u(\Upsilon) = d$. □

A.3 Transformations

We give justifications for the technical Hypothesis (H 2.6) and (H 2.8) in this section.

Justification of Hypothesis (H 2.6)
The following considerations are taken from [Rie03] and modified to apply to the presented setting in $\mathbb{R}^n$.
For some of the estimates in this thesis, it is convenient to use a transformation of the vector field $f(x,\lambda)$ such that for $\lambda \neq 0$ the periodic orbit as well as the vector field along the periodic orbit coincide with the periodic orbit at $\lambda = \lambda^*$ and the vector field along that orbit.
In the following we denote the perturbed periodic solution by $p_\lambda(\cdot)$ and the unperturbed solution by $p(\cdot)$.
We do this transformation in several steps:
First we use a transformation of the time such that the minimal period T of the periodic solution $p_\lambda(\cdot)$ is the same as for the unperturbed periodic solution $p(\cdot)$.
Then we define two-dimensional discs $D_\delta(p(t))$ in $\mathbb{R}^n$ such that the centre of each disc is $p(t)$ for some $t \in [0,T)$ and each disc is perpendicular to the vector field direction at the centre. Moreover, we demand that $p_\lambda(t)$ is contained in the disc and that none of the discs intersect each other. This construction is always possible if we only choose the radius of the discs small enough. To justify this construction, we consider a coordinate change such that the periodic orbit Υ is a circle in a plane and then choose the discs such that each of them points towards the centre of the circle. Clearly, none of them intersect (if the radius is small enough) and the union of all those circles forms a 'tubular neighbourhood' of Υ, see [Hir93].
The following transformation takes place in the coordinates defined by $t \in S^1$ (each t determines one disc $D_\delta(p(t))$) and $\tilde{x} \in D_\delta(p(t)) \subset \mathbb{R}^{n-1}$. Thus we look for a transformation $\mathcal{T}_{loc}(\cdot,\cdot) : S^1 \times \mathbb{R}^{n-1} \to S^1 \times \mathbb{R}^{n-1}$ that acts on these coordinates.
Now we change coordinates on each disc $D_\delta(p(t))$ such that $p_\lambda(t)$ is moved to the origin (which is $p(t)$) of the disc. This local transformation can be expressed by $\mathcal{T}_{loc}(t,\tilde{x}) := (t, \tilde{x} - (\tilde{p}_\lambda(t) - p(t)))$. The $p(t)$ is given by the ODE, the $\tilde{p}_\lambda(t)$ if defined by $\tilde{p}_\lambda(t) := \Upsilon_\lambda \cap D_\delta(p(t))$. It is obvious that this transformation $\mathcal{T}_{loc}(\cdot,\cdot)$ is close to the identity transformation and thus we can write $\mathcal{T}_{loc}(t,\tilde{x}) = \Big(t, \tilde{x} + \tilde{\mathcal{T}}(t)\Big)$ where $\tilde{\mathcal{T}}(t) := \tilde{p}_\lambda(t) - p(t)$.
We see that $\mathcal{T}_{loc}$ is indeed a smooth transformation by looking at the Jacobian $D\mathcal{T}_{loc}$:

$$D\mathcal{T}_{loc} = \begin{pmatrix} 1 & 0 \\ D_1\tilde{\mathcal{T}} & 1 \end{pmatrix}.$$

This Jacobian is indeed regular for all $(t, \tilde{x}) \in S^1 \times \mathbb{R}^{n-1}$ and thus $\mathcal{T}_{loc}(\cdot,\cdot)$ is a smooth transformation.
To perform a globalisation of this transformation, we use a C^∞-smooth cut-off function $\chi(\cdot)$ acting on $[0,1] \subset \mathbb{R}$ defined as follows:

$$\chi(x) = \begin{cases} 1 \text{ if } x \leq \frac{1}{3}, \\ 0 \text{ if } x \geq \frac{2}{3}. \end{cases}$$

Using $\chi(\cdot)$ we can define $\chi_\delta(\cdot,\cdot) : S^1 \times \mathbb{R}^{n-1} \to \mathbb{R}$:

$$\chi_\delta(t, \tilde{x}) := \chi\left(\frac{\|\tilde{x} - p(t)\|}{\delta}\right).$$

Now we can use $\chi_\delta(\cdot,\cdot)$ to globalise the transformation $\mathcal{T}_{loc}(\cdot,\cdot)$ to the tubular neighbuorhood in the following way:

$$\mathcal{T}(t, \tilde{x}) = \left(t, \tilde{x} + \chi_\delta(t, \tilde{x})\tilde{\mathcal{T}}(t)\right).$$

Finally we examine the Jacobian of $\mathcal{T}(\cdot,\cdot)$:

$$D\mathcal{T} = \begin{pmatrix} 1 & 0 \\ D_1\mathcal{T} & 1 + D_2\chi_\delta(t,\tilde{x}) \cdot \tilde{\mathcal{T}}(t) \end{pmatrix}.$$

Considerations similar to those in [Van89] show that $\sup_{x \in D_\delta(p(t))} \left\| D_2\chi_\delta(t,\tilde{x}) \cdot \tilde{\mathcal{T}}(t) \right\| \to 0$ as $\delta \to 0$. Thus the Jacobian is everywhere regular and so this global transformation $\mathcal{T}(\cdot,\cdot)$ provides a smooth transformation of the perturbed periodic orbit onto the unperturbed periodic orbit. Note that we have to choose $\|\lambda\|$ sufficiently small such that the points of the perturbed orbit $p_\lambda(t)$ lie in the inner third of each of the discs with radius δ, this is due to the choice of the cut-off function. Also note that $\mathcal{T}(\cdot,\cdot)$ is in fact dependent on λ, thus in the following we write $\mathcal{T}_\lambda(\cdot,\cdot)$.
Now we consider $\mathcal{T}_\lambda(\cdot)$ as a transformation in $\mathbb{R}^n$ that consists of the transformation $\mathcal{T}_\lambda(\cdot,\cdot)$ for points that are in the tubular neighbuorhood of Υ (and thus can be described by coordinates $(t,\tilde{x})$) and of the identity for all other points. In terms of the vector field, the transformation $\mathcal{T}_\lambda(\cdot)$ preserves the vector field direction along $p(\cdot)$, but does not necessarily preserve the vector length. We denote the transformed vector field by $\tilde{f}$:

$$\tilde{f}(\mathcal{T}_\lambda x, \lambda) = D\mathcal{T}_\lambda(x) f(x,\lambda).$$

To achieve the preserving of the length of each vector along the periodic orbit, we use one final transformation on the fibres of the tangent bundle of $\mathbb{R}^n$. We denote the tubular neighbourhood that we defined by the construction as described above by $U_\delta(\Upsilon)$. Moreover, we denote the cut-off function that transforms to the tubular coordinates $(t,\tilde{x})$ and then applies $\chi_\delta(t,\tilde{x})$ by $\chi_\delta(\cdot)$. Then we can define the final transformation by

$$\bar{f}(x,\lambda) := \begin{cases} \chi_\delta(x)\frac{\|f(x,0)\|}{\left\|\tilde{f}(x,\lambda)\right\|}\tilde{f}(x,\lambda) + (1 - \chi_\delta(x))\,\tilde{f}(x,\lambda) & , x \in U_\delta(\Upsilon), \\ \tilde{f}(x,\lambda) & , x \notin U_\delta(\Upsilon). \end{cases}$$

It remains to check that $\tilde{f}(x,\lambda) \neq 0$ for $x \in U_\delta(\Upsilon)$. Because of the properties of the periodic solutions, $\tilde{f}(x,\lambda) \neq 0$ for $x \in \Upsilon$, and thus we can find a $\delta > 0$ such that this holds for all $x \in U_\delta(\Upsilon)$.
With both transformations combined the final result is that we can transform the vector field in such a way that the periodic orbit and the vector field along the periodic orbit do not change as the parameter λ changes.

Justification of Hypothesis (H 2.8)
The following lemma gives a justification of Hypothesis (H 2.8).

Lemma A.3.1 *There is a smooth function $K : \mathbb{R}^n \to \mathbb{R}$, $K(x) \neq 0$, such that all solutions of the scaled ODE*

$$\dot{x} = K(x)f(x) \tag{A.3.1}$$

that start sufficiently close to $\gamma_1(0)$ in Σ_1, need the same time to reach the Poincaré section Σ_Υ.

Proof. We set $K(x) = (1 + k(x)b(x))$ where $b(x)$ is an arbitrary (but smooth) cut-off function with the following properties:

(i) $b(x) = 0$ for all $d(x,\Sigma_1) \leq \epsilon_1$ and $d(x,\Sigma_\Upsilon) \leq \epsilon_2$,

(ii) $b(x) = 0$ for all $x \in \Gamma_1$,

(iii) $b(x) = 1$ for all $\frac{2}{5} \leq d(x,\Gamma_1) \leq \frac{3}{5}$ and

(iv) $b(x) = 0$ for all $d(x,\Gamma_1) \geq \frac{4}{5}$.

We denote the flow of (A.3.1) by $\psi(t,\cdot;k)$.
In the following, t_{x_0} denotes the time that the solution starting in $x_0 \in \Sigma_1$ needs to hit Σ_Υ.
The goal is to choose k such that $\psi(\tilde{t},x,k) \in \Sigma_\Upsilon$ for all $x \in \Sigma_1$, where $\tilde{t}$ is fix.
We define a projection $P : \mathbb{R}^n \to \Sigma_\Upsilon^\perp$ which projects along Σ_Υ. Obviously, the goal is to find k such that $P\psi(t_{x_0},x,k) = 0$. It is easy to see that $P\psi(t_{x_0},\cdot,\cdot) : \mathbb{R}^{n-1} \times \mathbb{R} \to \mathbb{R}$, $P\psi(t_{x_0},x_0,0) = 0$. If $D_k(P\psi(t_{x_0},x_0,0)) \neq 0$, then we can use the Implicite Function Theorem to solve for $k = k(x)$ and thus we have $\psi(t_{x_0},x,k(x)) \in \Sigma_\Upsilon$ for all $x \in \Sigma_2$.
In order to show that we consider $\dot{x} = a(x)f(x)$ and let $\psi(t,x) := \varphi(T(t,x),x)$. Now we have to find conditions for T such that ψ is a solution:

$$\dot{\psi} = \dot{\varphi}(T(t,x),x) \cdot \dot{T}(t,x) = f(\varphi(T(t,x),x)) \cdot \dot{T}(t,x).$$

So we have

$$\dot{T}(t,x) = a(\varphi(T(t,x),x)), \quad T(0,x) = 0$$

or a shorter notation

$$\dot{T} = a(\varphi(T,x)), \quad T(0) = 0$$

as an ODE for T.
For $a(x) = 1 + kb(x)$ the ODE is as follows:

$$\dot{T} = 1 + kb(\varphi(T,x)), \quad T(0) = 0.$$

A Appendix

We denote the solution by $T = T(t, x, k)$.
Plugging this in we get

$$\begin{aligned}\psi(t, x, k) &= \varphi(T(t, x, k), x),\\ \psi(t_{x_0}, x, k) &= \varphi(T(t_{x_0}, x, k), x)\end{aligned}$$

and

$$\begin{aligned}D_k\psi(t_{x_0}, x_0, 0) &= \dot{\varphi}(T(t_{x_0}, x_0, 0), x_0) \cdot D_kT(t_{x_0}, x_0, 0)\\ &= f(\varphi(T(t_{x_0}, x_0, 0)), x_0) \cdot D_kT(t_{x_0}, x_0, 0)\\ &= f(\varphi(t_{x_0}, x_0)) \cdot D_kT(t_{x_0}, x_0, 0).\end{aligned}$$

Thus we have

$$D_kP\psi(t_{x_0}, x_0, 0) = P\left(f(\varphi(t_{x_0}, x_0))D_kT(t_{x_0}, x_0, 0)\right).$$

It remains to show that $D_kT(t_{x_0}, x_0, 0) \neq 0$.
Consider $(D_kT)^{\cdot} = b(\varphi(T, x)) + kb(\varphi(T, x)) \cdot \dot{\varphi}(T, x) \cdot D_kT$. For $k = 0$ this reduces to $(D_kT)^{\cdot} = b(\varphi(T, x))$. Integrating gives $D_kT(t_{x_0}, x_0, 0) - D_kT(0, x_0, 0) = \int_0^{t_{x_0}} b(\varphi(T(t, x_0, 0)))dt$ and thus $D_kT(t_{x_0}, x_0, 0) > 0$. □

Acknowledgements

I would like to thank everybody who supported me during the creation of this thesis. In particular, I am deeply grateful to my supervisors Jürgen Knobloch and Bernd Krauskopf for their dedication and many insightful discussions, and I thank the referees Bernd Marx and Eusebius Doedel for helpful comments. Part of my research was supported by the two-year scholarship of the 'Landesgraduiertenförderung des Landes Thüringen', which I acknowledge. Moreover, I thank Klaus Zimmermann from the Department of Mechanical Engineering at the TU Ilmenau, whose support made it possible to complete this thesis. Also, I appreciate the support and hospitality of the Bristol Centre for Applied Nonlinear Mathematics (BCANM) during several long research visits.
I thank my parents and grandparents for their patience and support throughout the years. Last but not least I thank my charming wife Nicole for her love and her support.

Table of notations

Chapter 1

EtoP	Connecting orbit/cycle between a hyperbolic equilibrium and a hyperbolic periodic orbit (regardless of the direction of the flow)
PtoP	Connecting orbit/cycle between two (not necessarily distinct) hyperbolic periodic orbits
d	codimension of the EtoP connection/cycle
$f(\cdot, \lambda)$	family of vector fields
$\lambda \in \mathbb{R}^m$	family parameter
λ^*	critical parameter value, usually $\lambda^* = 0$
p	hyperbolic equilibrium
Υ	hyperbolic periodic orbit
$W^s_\lambda(p)$	stable manifold of p
$W^s(p)$	stable manifold of p for $\lambda = \lambda^*$
$W^u(p)$	unstable manifold of p for $\lambda = \lambda^*$
$T_{\gamma_1(0)}W^s(\Upsilon)$	tangent space of the stable manifold of Υ at $\gamma_1(0)$
Γ_1, $\gamma_1(\cdot)$	orbit and associated solution of the heteroclinic connection between p and Υ (for $\lambda = \lambda^*$)
Γ_2, $\gamma_2(\cdot)$	orbit and associated solution of the robust heteroclinic connection between Υ and p (for $\lambda = \lambda^*$)

Chapter 2

$\gamma_1^-(\lambda)(\cdot)$	solution in the unstable manifold of p near $\gamma_1(\cdot)$
$\gamma_1^+(\lambda)(\cdot)$	solution in the stable manifold of Υ near $\gamma_1(\cdot)$
$\gamma_2^-(\vartheta, \lambda)(\cdot)$	solution in the unstable manifold of Υ near $\gamma_2(\cdot)$
$\gamma_2^+(\vartheta, \lambda)(\cdot)$	solution in the stable manifold of p near $\gamma_2(\cdot)$

$D_i f$	partial derivative of f with respect to the ith argument
$D_x f$	derivative of f with respect to variable x
q	hyperbolic equilibrium of the discrete dynamical system
$\gamma^+(\lambda)(\cdot)$, $\gamma^-(\vartheta,\lambda)(\cdot)$	solutions in the stable/unstable manifold of q (discrete system)
ϑ	element in U that provides uniqueness of the solutions
α	variable that describes the projection boundary condition in Σ_Υ for the continuous system
β	variable that describes the projection boundary consition in Σ_Υ for the discrete system
P^+, P^-	projections of the dichotomies on $\mathbb{R}^+$ and $\mathbb{R}^-$ of the homogenuous variational equation along γ_2^+ and γ_1^-
Q_s^+, Q_{sc}^+, Q_u^-, Q_{cu}^-	projections of the trichotomies on $\mathbb{R}^+$ and $\mathbb{R}^-$ of the homogenuous variational equation along γ_1^+ and γ_2^-
R^+, R^-	projections of the dichotomies on $\mathbb{R}^+$ and $\mathbb{R}^-$ of the homogenuous variational equation along γ^+ and γ^- (discrete system)
$x_1^\pm$, $x_2^\pm$	solutions of the continuous system, $x_i^\pm = \gamma_i^\pm + v_i^\pm$
$y^\pm$	solutions of the discrete system, $y^\pm = \gamma^\pm + u^\pm$

Chapter 3

p	hyperbolic equilibrium
Γ	hyperbolic periodic orbit
Q	heteroclinic EtoP connection of codimension d
Q^+, Q^-, $q^+(\cdot)$, $q^-(\cdot)$	orbits and associated solutions in $W^s(\Gamma)$ and $W^u(p)$ for $\lambda \neq \lambda^*$
Σ	cross-section of Q, $\Sigma = p_\Sigma + Y$
n_Σ	normal vector of Y
Z	d-dimensional Lin space, $Z \subset Y$
u	solution of a discretised boundary value problem for the...
u_γ	...periodic orbit
u_i	...stable/unstable eigenfunctions
u^-	...orbit segment from p to Σ
u^+	...orbit segment from Σ to Γ
u_r	...codimension-zero EtoP orbit
u_h	...homoclinic orbit to Γ
η_i	Lin gaps, well-defined test functions to detect the EtoP connection

BIBLIOGRAPHY

[ARS04] P. Ashwin, A.M. Rucklidge, and R. Sturman. Two-state intermittency near a symmetric interaction of saddle-node and Hopf bifurcations: a case study from dynamo theory. *Physica D*, 194:30–48, 2004.

[AWA+93] E.H. Abed, H.O. Wang, J.C. Alexander, A.M.A. Hamdan, and H.-C. Lee. Dynamic bifurcations in a power system model exhibiting voltage collapse. *Int. Journal of Bif. and Chaos*, 3:1169–76, 1993.

[Bey90] W.-J. Beyn. The numerical computation of connecting orbits in dynamical systems. *IMA J. Numer. Anal.*, 10:379–405, 1990.

[Bey94] W.-J. Beyn. On well-posed problems for connecting orbits in dynamical systems. *Contemporary Mathematics 172 Chaotic Numerics*, pages 131–168, 1994.

[BKL+08] M. Beck, J. Knobloch, D. Lloyd, B. Sandstede, and T. Wagenknecht. Snakes, ladders, and isolas of localised patterns. *Preprint*, 2008.

[CKK+07] A.R. Champneys, V. Kirk, E. Knobloch, B.E. Oldeman, and J. Sneyd. When Shil'nikov meets Hopf in excitable systems. *SIAM J. Appl. Dyna. Syst.*, 6:663–93, 2007.

[CKS96] A.R. Champneys, Yu.A. Kuznetsov, and B. Sandstede. A numerical toolbox for homoclinic bifurcation analysis. *Int. Journal of Bif. and Chaos*, 6:867–87, 1996.

[Cop78] W.A. Coppel. *Dichotomies in Stability Theory*. Springer, 1978.

[DDF00] J.W. Demmel, L. Dieci, and M.J. Friedman. Computing connecting orbits via an improved algorithm for continuing invariant subspaces. *SIAM J. Sci. Comput.*, 22:81–94, 2000.

[Den89] B. Deng. The Sil'nikov Problem, Exponential Expansion, Strong λ-Lemma, C^1-Linearization, and Homoclinic Bifurcation. *Journal of Differential Equations*, 79:189–231, 1989.

[Der07] F. Dercole. BPcont: an Auto97 driver for the continuation of branch points of algebraic and boundary-value problems. Presented at *CRM workshop Advanced Algorithms and Numerical Software for the Bifurcation Analysis of Dynamical Systems*, July 2007.

[DF89] E.J. Doedel and M.J. Friedman. Numerical computation of heteroclinic orbits. *J. Comput. Appl. Math.*, 26:155–70, 1989.

[DKKvVa] E.J. Doedel, B.W. Kooi, Yu.A. Kuznetsov, and G.A.K. van Voorn. Continuation of connecting orbits in 3D-ODEs: (I) Point-to-cycle connections. arXiv:0706.1688v2 Preprint 12 June 2007.

[DKKvVb] E.J. Doedel, B.W. Kooi, Yu.A. Kuznetsov, and G.A.K. van Voorn. Continuation of connecting orbits in 3D-ODEs: (II) Cycle-to-cycle connections. arXiv:0804.0179v1 Preprint 1 April 2008.

[DKO06] E.J. Doedel, B. Krauskopf, and H.M. Osinga. Global bifurcations of the Lorenz manifold. *Nonlinearity*, 19:2947–2972, 2006.

[Doe07] E.J. Doedel. Lecture notes on numerical analysis of nonlinear equations. In: Numerical Continuation Methods for Dynamical Systems, B. Krauskopf, H.M. Osinga and J. Galán-Vioque (ed.), Springer, p. 1–49, 2007.

[DPC+00] E.J. Doedel, R.C. Paffenroth, A.R. Champneys, T.F. Fairgrieve, Yu.A. Kuznetsov, B.E. Oldeman, B. Sandstede, and X.J. Wang. Auto 2000: Continuation and bifurcation software for ordinary differential equations. Technical report, Concordia University, Montreal, 2000.

[DPC+06] E.J. Doedel, R.C. Paffenroth, A.R. Champneys, T.F. Fairgrieve, Yu.A. Kuznetsov, B.E. Oldeman, B. Sandstede, X.J. Wang, and C. Zhang. Auto-07p: Continuation and bifurcation software for ordinary differential equations. Technical report, Concordia University, Montreal, 2006.

[DR04a] L. Dieci and J. Rebaza. Erratum: Point-to-periodic and periodic-to-periodic connections. *BIT Numerical Mathematics*, 44:617–18, 2004.

[DR04b] L. Dieci and J. Rebaza. Point-to-periodic and periodic-to-periodic connections. *BIT Numerical Mathematics*, 44(1):41–62, 2004.

[EKO05] J.P. England, B. Krauskopf, and H.M. Osinga. Computing one-dimensional global manifolds of Poincaré maps by continuation. *SIAM J. Appl. Dynam. Syst.*, 4:1008–41, 2005.

[FD93] M.J. Friedman and E.J. Doedel. Computational methods for global analysis of homoclinic and heteroclinic orbits: A case study. *J. Dyn. Diff. Equ.*, 5:37–57, 1993.

[FSFRL02] F. Fernández-Sánchez, E. Freire, and A.J. Rodríguez-Luis. T-points in a $\mathbb{Z}_2$-symmetric electronic oscillator. (I) Analysis. *Nonlinear Dynamics*, 28(1):53–69, 2002.

[GH83] J. Guckenheimer and P. Holmes. *Nonlinear Oscillations, Dynamical Systems, and Bifurcations of Vector Fields*, volume 42 of *Applied Mathematical Sciences*. Springer, 1983.

[GS86] P. Glendinning and C. Sparrow. T-points: A codimension two heteroclinic bifurcation. *Journal of Statistical Physics*, 43(3–4):479–488, 1986.

[Hir93] M.W. Hirsch. *Differential Topology*. Springer, 1993.

[HK93] P. Hirschberg and E. Knobloch. Šil'nikov-hopf bifurcation. *Physica D*, 62:202–16, 1993.

[HL86] J.K. Hale and X.-B. Lin. Heteroclinic orbits for retarded functional differential equations. *Journal of Differential Equations*, 65:175–202, 1986.

[KK03] J. Klaus and J. Knobloch. Bifurcation of homoclinic orbits to a saddle-center in reversible systems. *Int. Journal of Bif. and Chaos*, 13(9), 2003.

[Kla06] J. Klaus. *Bifurcations from Homoclinic Orbits to a Saddle-Centre in Reversible Systems*. PhD thesis, TU Ilmenau, 2006.

[KLW07] J. Knobloch, J.S.W. Lamb, and K.N. Webster. Shift dynamics near T-point heteroclinic cycles. Preprint, 2007.

[Kno04] J. Knobloch. Lin's Method for Discrete and Continuous Dynamical Systems and Applications. Habilitationsschrift, TU Ilmenau, 2004.

[KO06] B. Krauskopf and B.E. Oldeman. Bifurcations of global reinjection orbits near a saddle-node hopf bifurcation. *Nonlinearity*, 19:2149–2167, 2006.

[KOGV07] B. Krauskopf, H.M. Osinga, and J. Galán-Vioque, editors. *Numerical Continuation Methods for Dynamical Systems*. Springer, 2007.

[KR08] B. Krauskopf and T. Rieß. A Lin's method approach to finding and continuing heteroclinic connections involving periodic orbits. *Nonlinearity*, to appear, 2008.

[KTL98] B. Krauskopf, N. Tollenaar, and D. Lenstra. Tori and their bifurcations in an optically injected semiconductor laser. *Optics Communications*, 156:158–69, 1998.

[Kuz98] Yu.A. Kuznetsov. *Elements of Applied Bifurcation Theory*, volume 112 of *Applied Mathematical Sciences*. Springer, 1998.

[Lin90] X.-B. Lin. Using Melnikov's method to solve Shilnikov's problems. In *Proc. Roy. Soc. Edinburgh 116A*, pages 295–325, 1990.

[LK80] M. Lentini and H.B. Keller. Boundary value problems on semi-infinite intervals and their numerical solution. *SIAM J. Num. Anal.*, 17:577–604, 1980.

[LL00] Z. Lin and Y. Lin. *Linear Systems Exponential Dichotomy and Structure of Sets of Hyperbolic Points*. World Scientific, 2000.

[Lor63] E. N. Lorenz. Deterministic nonperiodic flows. *J. Atmospheric Sci.*, 20:130–41, 1963.

[Lus01] K. Lust. Improved numerical Floquet multipliers. *Int. Journal of Bif. and Chaos*, 11:2389–410, 2001.

[LX03] W. Li and P. Xu. The existence of Silnikov's orbits in four-dimensional Duffing's systems. *Acta Mathematicae Applicatae Sinica, English Series*, 19(4):677–690, 2003.

[OCK03] B.E. Oldeman, A.R. Champneys, and B. Krauskopf. Homoclinic branch switching: a numerical implementation of Lin's method. *Int. Journal of Bif. and Chaos*, 13:2977–99, 2003.

[Pal84] K. Palmer. Exponential dichotomies and transversal homoclinic points. *J.Diff.Eqns.*, 55:225–256, 1984.

[Pal88] K. Palmer. Exponential dichotomies, the shadowing lemma and transversal homoclinic points. *Dynamics Reported*, 1:265–306, 1988.

[Pal00] K. Palmer. *Shadowing in Dynamical Systems - Theory and Applications*. Kluwer Academic Publishers, 2000.

[Pam01] T. Pampel. Numerical approximation of connecting orbits with asymptotic rate. *Numerische Mathematik*, 90:309–48, 2001.

[Poi90] H. Poincaré. Sur le problème des trois corps et les équations de la dynamique (Mémoire couronné du prise de S. M. le roi Oscar de Suède). *Acta Math.*, 13:1–270, 1890.

[Rad04] J.D. Rademacher. *Homoclinic Bifurcation from Heteroclinic Cycles with Periodic Orbits and Tracefiring of Pulses*. PhD thesis, University of Minnesota, 2004.

[Rad05] J.D. Rademacher. Homoclinic orbits near heteroclinic cycles with one equilibrium and one periodic orbit. *Journal of Differential Equations*, 218:390–443, 2005.

[Rie03] T. Rieß. Using Lin's method for an almost Shilnikov problem. Diploma Thesis, TU Ilmenau, 2003.

[Rob99] C. Robinson. *Dynamical Systems*. CRC Press, 1999.

[San93] B. Sandstede. *Verzweigungstheorie homokliner Verdopplungen*. PhD thesis, Universität Stuttgart, 1993.

[Spa82] C. Sparrow. *The Lorenz Equations: Bifurcations, Chaos and Strange Attractors*, volume 41 of *Applied Mathematical Sciences*. Springer, 1982.

[SSTC98] L.P. Shilnikov, A.L. Shilnikov, D.V. Turaev, and L.O. Chua. *Methods of qualitative theory in nonlinear dynamics, part 1*. World Scientific, 1998.

[SSTC01] L.P. Shilnikov, A.L. Shilnikov, D.V. Turaev, and L.O. Chua. *Methods of qualitative theory in nonlinear dynamics, part 2*. World Scientific, 2001.

[Str94] S. Strogatz. *Nonlinear Dynamics and Chaos: With Applications to Physics, Biology, Chemistry and Engineering*. Addison-Wesley, 1994.

[Van89] A. Vanderbauwhede. Centre manifolds, normal forms and elementary bifurcations. *Dynamics Reported*, 2:89–169, 1989.

[VF92] A. Vanderbauwhede and B. Fiedler. Homoclinic period blow-up in reversible and conservative systems. *Z. angew. Math. Phys.*, 43:292–318, 1992.

[Vit03] R. Vitolo. *Bifurcations of attractors in 3D diffeomorphisms: a study in experimental mathematics*. PhD thesis, University of Groningen, 2003.

[Wig90] S. Wiggins. *Introduction to Applied Nonlinear Dynamical Systems and Chaos*. Springer, 1990.

[WK05] S.M. Wieczorek and B. Krauskopf. Bifurcations of n-homoclinic orbits in optically injected lasers. *Nonlinearity*, 18:1095–120, 2005.

[WKSL05] S.M. Wieczorek, B. Krauskopf, T.B. Simpson, and D. Lenstra. The dynamical complexity of optically injected semiconductor lasers. *Physics Reports*, 416:1–128, 2005.

[Yew01] A.C. Yew. Multipulses of nonlinearly coupled Schrödinger equations. *J. Diff. Eq.*, 173:92–137, 2001.

[ZNS01] M. Zimmermann, M. Natiello, and H. Solari. Global bifurcations in a laser with injected signal: beyond Adler's approximation. *Chaos*, 11:500–13, 2001.